Role of the CCL17/CCL22-CCR4-axis in the barrier organs skin and gut

Dissertation

zur

Erlangung des Doktorgrades (Dr. rer. nat.)

der

Mathematisch-Naturwissenschaftlichen Fakultät

der

Rheinischen Friedrich-Wilhelms-Universität Bonn

vorgelegt von

Marlene Gottschalk

aus

Köln

Bonn, Februar 2024

Angefertigt mit Genehmigung der Mathematisch-Naturwissenschaftlichen Fakultät

der Rheinischen Friedrich-Wilhelms-Universität Bonn

Erstgutachterin: Prof. Irmgard Förster

Zweitgutachter: Prof. Günter Mayer

Tag der Promotion: 24.04.2024

Erscheinungsjahr: 2024

Table of contents

List of publications

Parts of this thesis are included in the following publication:

Jonczyck A*, **Gottschalk M***, Mangan MSJ, Majlesain Y, Thiem MW, Burbaum L, Weighardt H, Latz E, Mayer G, Förster I. Topical application of a CCL22-binding aptamer suppresses contact allergy. 2024 Sept, 35(3): 102254. doi: 10.1016/j.omtn.2024.102254. Epub June 2024 17.

*shared first authorship.

Additional publications:

Shin H, Prasad V, Lupancu T, Malik S, Achuthan A, Biondo M, Kingwell BA, Thiem M, **Gottschalk M**, Weighardt H, Förster I, de Steiger R, Hamilton JA, Lee KM. The GM-CSF/CCL17 pathway in obesity-associated osteoarthritic pain and disease in mice. Osteoarthritis Cartilage. 2023 Oct;31(10):1327-1341. doi: 10.1016/j.joca.2023.05.008. Epub 2023 May 22. PMID: 37225052.

Graelmann FJ, Gondorf F, Majlesain Y, Niemann B, Klepac K, Gosejacob D, **Gottschalk M**, Mayer M, Iriady I, Hatzfeld P, Lindenberg SK, Wunderling K, Thiele C, Abdullah Z, He W, Hiller K, Händler K, Beyer MD, Ulas T, Pfeifer A, Esser C, Weighardt H, Förster I, Reverte-Salisa L. Differential cell type-specific function of the aryl hydrocarbon receptor and its repressor in diet-induced obesity and fibrosis. Mol Metab. 2024 Jul;85:101963. doi: 10.1016/j.molmet.2024.101963. Epub 2024 May 29. PMID: 38821174; PMCID: PMC11214421

Abstract

The chemokines C-C motif chemokine ligand 17 (CCL17) and C-C motif chemokine ligand 22 (CCL22) are ligands of the C-C Motif chemokine receptor 4 (CCR4). They are mainly secreted by dendritic cells (DC) and macrophages to recruit CCR4-expressing T cells in physiological processes, and notably during disease. Although both chemokines bind the same receptor, they possess different affinities to CCR4, with CCL22 being the dominant ligand. Moreover, they are known to exert different immune functions. While CCL17 expression often occurs during inflammation, CCL22 is rather involved in regulatory processes, preferably recruiting regulatory T cells (Treg) over conventional T cells. Both chemokines are known to be involved in inflammatory diseases of barrier organs, such as skin and the gastrointestinal tract (GI-tract). Increased protein levels of CCL17 and CCL22 can be found in patients suffering from atopic dermatitis (AD) and mRNA transcripts are elevated in the mucosa of Morbus Crohn (MC) patients.

In this PhD thesis the role of the CCL17, CCL22 and their receptor CCR4 in development of diseases affecting the barrier organs skin and GI-tract was investigated by pharmacological inhibition of the chemokines, or using mice deficient for different components of the CCL17/CCL22-CCR4-axis in mouse models for allergic contact dermatitis (ACD), AD and inflammatory bowel diseases (IBD).

First, a previously generated CCL17-specific RNA aptamer was used in contact hypersensitivity (CHS) experiments, the mouse model for ACD, to further assess its therapeutic efficacy, as we observed that CCL17- or CCL22 deficiency reduced allergic reactions in CHS effectively by reducing the ear swelling and the migration of activated T-cells. Testing of different injection time-points revealed that the duration of action was likely in the range of 12 h–24 h. Furthermore, we could show that, although less effective, the CCL17-specific aptamer still displayed suppressive functions when applied at a later time-point, however, the suppressive capacity did not persist for a second allergen challenge.

Additionally, to test the role of CCL22 in CHS and to investigate CCL22 as a potential target for therapy of ACD, CCL22-specific DNA aptamers, newly generated by Anna Jonczyk, were tested functionally *in vitro* and *in vivo* for inhibition of T cell migration and suppression of allergic symptoms in CHS. The most promising aptamer candidate AJ102.29m was additionally applied topically in a cream during a CHS experiment to investigate the potential of a non-invasive

aptamer-aided treatment for ACD. Intraperitoneal as well as topical application of AJ102.29m could effectively suppress ear swelling during CHS and decreased T cell migration into the ears. These experiments provided proof-of-principle that topical application of an aptamer represents a possibility for development of a non-invasive local ACD treatment.

The last part of the thesis covers the analysis of the CCL17/CCL22-CCR4-axis in development of inflammatory bowel disease (IBD) by employing the dextran sodium sulfate (DSS)-induced colitis model. While similar colitis symptoms could be observed for $CCL17^{E/E}$ and wild type mice, $CCL22^{-/-}$ and to a lesser degree CCL17- and CCL22-double deficient mice (DKO), as well as $CCR4^{-/-}$ mice were protected from severe colitis induced symptoms. Their mesenteric lymph nodes contained significantly more T cells and the mice displayed less severe weight loss, colon-shortening and immune cell infiltration into the colon. The results confirmed the importance of CCL22 in the development of colitis and hint towards the existence of a fourth player in the CCL17/CCL22-CCR4-axis.

List of Abbreviations

ACD	Allergic contact dermatitis
ACKR	Atypical chemokine receptor
AD	Atopic dermatitis
AMP	Antimicrobial peptides
APC	Antigen presenting cell
BCR	B cell receptor
CCL	C-C motif chemokine ligand
CCR	C-C chemokine receptor type
cDC	Conventional dendritic cells
CHS	Contact hypersensitivity
CTLA4	Cytotoxic T-lymphocyte-associated protein 4
DAMPs	Danger associated molecular patterns
DC	Dendritic cells
Der. f.	Dermatophagoides farina
DETC	Dendritic epidermal T cells
DNFB	1-Fluoro-2,4-dinitrobenzene
DSS	Dextran sodium sulfate
EMP	Erythro-myeloid progenitor
EpCam	Epithelial cell adhesion molecule
FAE	Follicle-associated epithelium
FoxP3	Forkhead box P3
GALT	Gut associated lymphoid tissue
GI-tract	Gastrointestinal tract
GM-CSF	Granulocyte-macrophage colony-stimulating factor
i.p.	intraperitoneal
IBD	Inflammatory bowel disease
ICAM-1	Intercellular adhesion molecule 1
ICD	Irritant contact dermatitis
IEL	Intraepithelial lymphocyte
IFNγ	Interferon γ
Ig	Immunoglobulin

IL	Interleukin
ILC	Innate lymphoid cell
ILF	Isolated Lymphoid Follicles
LC	Langerhans cell
Ly6C	Lymphocyte antigen 6 family complex
Ly6G	Lymphocyte antigen 6 family member C1
M cell	Microfold cell
MC	Morbus crohn
MHC	Major histocompatibility complex
mLN	Mesenteric lymph nodes
NK cell	Natural killer cell
OVA	Ovalbumin
PAMPs	Pathogen associated molecular patterns
pDC	Plasmacytoid dendritic cell
PEG	Polyethylenglycol
PRR	Pattern recognition receptor
RAG	Recombination-activating genes
Rorγt	RAR-related orphan receptor gamma
ROS	Reaktive oxygen species
S.aureus	Staphylococcus aureus
SCID	Severe combined immunodeficiency
Sirp1α	Signal regulatory protein 1 α
SNP	Single nucleotide polymorphism
T cells	Thymocytes
Tbet	T-box transcription factor
TCR	T Cell receptor
TGFβ	Tumor growth factor β
Th	T helper
TNBS	2,4,6-trinitrobenzene sulfonic acid
TNF	Tumor necrosis factor
Treg	Regulatory T cells
T_{RM}	Tissue resident memory T cell

TSLP	Thymic stromal lymphopoietin
UC	Ulcerative colitis
UV	Ultraviolet
WT	Wild type
XCR1	X-C motif chemokine receptor 1

Table of Figures

Table of Tables

1. Introduction

1.1. The immune system

The recent Covid pandemic brought to light how important an understanding of the immune system is. While this knowledge is not only required for the development of vaccines and protection from foreign diseases, it also helps to comprehend every day threats the human body encounters. With exposure to the environment contact to pathogens is inevitable. To fight infections, the immune system evolved mechanisms to eradicate invading pathogens and fight abnormal self-structures.

The first obstacle for pathogens to enter the body are barrier organs like the skin, the gastrointestinal tract or the lungs that are anatomically built to prevent entry (Murphy & Weaver, 2017). Additionally, chemical barriers exist at the site of the organ such as a low pH on the skin or the mucus in the gastrointestinal tract which contains glycoproteins that bind pathogens (Cornick et al., 2015; Proksch, 2018). If both of these barriers are overcome, the innate immune system as part of the immunological barrier is activated. The innate immune system is evolutionary conserved in all species and offers a protection against a broad spectrum of pathogens with a limited range of specificity (Buchmann, 2014). Here, pathogen-associated-molecular-patterns (PAMPs) and danger-associated molecular patterns (DAMPs) are recognized by pattern recognition receptors (PRRs) on cell surfaces and intracellularly leading to the activation of specific transduction pathways and release of effector molecules. Activated innate immune cells like granulocytes (neutrophils, basophils, eosinophils), macrophages, mast cells, innate lymphoid cells (ILC) and dendritic cells (DC) secrete soluble immune factors such as antimicrobial peptides (AMP), cytokines and chemokines. Chemokines are small chemotactic cytokines which facilitate the recruitment or homing of immune cells (Zlotnik et al., 2006). Furthermore, acute phase proteins and proteins of the complement system enhance pathogen recognition and clearance. In addition, some immune cells such as macrophages, neutrophils and DC are able to phagocytose pathogens and digest the proteins to generate pathogen specific peptides and in case of macrophages, neutrophils and mast cells to kill the evading pathogen (Murphy & Weaver, 2017). The pathogen-specific peptides are linkers to activate the adaptive immune system. Particularly, DC are professional in sampling proteins with their dendrites and in the generation of peptides which are presented on major histocompatibility complex (MHC) molecules to stimulate the adaptive immune system. As antigen presenting cells (APC) DC can migrate out of the site of infection into lymphoid organs.

Here the peptide/MHC complexes are presented and can be recognized by the T cell receptor (TCR) on the surface of T cells. T cells are adaptive immune cells that develop in the thymus and are highly specific against a certain type of antigen. $CD8^+$ T cells recognize antigenic peptides in the context of MHC class I (MHC I) and are also called cytotoxic T cells as they release granzymes to kill pathogens directly. In contrast, $CD4^+$ T cells are selected for the recognition of peptide/MHC class II (MHC II) complexes and can differentiate into different T helper (Th) subset. Thus, they clear the threat efficiently by creating a pathogen specific micromilieu with secretion of T helper subset specific cytokines (Murphy & Weaver, 2017). Th1 cells execute the defense against intracellular pathogens like viruses and bacteria during type I immune infections, whereas Th2 cells differentiate in case of type II infections e.g., parasite infection or during allergies. Th17 cells participate in removal of type III infections by supporting the immune response against fungi and extracellular bacteria (Luckheeram et al., 2012). Moreover, a certain set of $CD4^+$ T cells called regulatory T cells (Treg) exhibit suppressive functions that are required to turn down immune responses and, thus, contribute to homeostasis. Apart from conventional T cells, during thymic development double negative thymocytes can also give rise to a T cell population called $\gamma\delta$ T cells which express a γ chain and δ chain combination in their TCR instead of an α and a β chain found in the conventional T cells. $\gamma\delta$ T cells are not MHC restricted, often home to mucosal and epithelial sites of the body and can fulfill innate immune functions (Holtmeier & Kabelitz, 2005). Following a chemokine gradient, activated T cells can migrate to sites of infection to fulfill their effector functions locally. B cells form a second major branch of the adaptive immune system. Once activated, the highly variable membrane-bound B cell receptor (BCR) can also be secreted as an antibody. Antibodies are an essential part of the humoral immune response and can opsonize and neutralize pathogens effectively. A subset of T cells as well as B cells can gain memory cell functions with longevity so that they can quickly respond towards re-exposure to previously encountered pathogens to rapidly provide large numbers of effector T cells. Thereby, they ensure long-lasting immunity against certain threats, such as viruses or bacteria, but can also propagate inappropriate responses, such as allergies or autoimmune responses (Murphy & Weaver, 2017).

1.2. Immunity in the skin

As a barrier organ, the skin is constantly confronted with environmental challenges, such as ultraviolet (UV) light, chemicals, or pathogens. To protect the body from harm, the skin can

exert a highly evolved set of immune functions. Its structure can mainly be divided into three layers, epidermis, dermis and subcutis.

The basal layer of the epidermis that separates the epidermis from the dermis comprises undifferentiated keratinocytes that frequently proliferate to replenish keratinocytes in the stratum granulosum, stratum lucidum and the surface-facing stratum corneum, where they terminally differentiate to corneocytes (Tay et al., 2013). Water loss and pathogen penetration is hindered by tight junctions and desmosomes between keratinocytes as well as through a dense network of keratins (Ovaere et al., 2009; Tay et al., 2013). The basal epidermal layer also harbors Langerhans cells (LC) and tissue-resident memory $CD8^+$ T cells (T_{RM}) (Ho & Kupper, 2019; Pasparakis et al., 2014). LC are specialized APC of the skin, functionally similar to DC, with the ability to take up antigens, generate peptides and present antigens in the context of MHCII to induce an immune response. Furthermore, they migrate to skin-draining lymph nodes (Collin & Milne, 2016). They arise from early erythro-myeloid progenitors (EMP) emerging in the yolk sac, as well as from a second wave c-myb^+ EMP subset that gives rise to fetal liver monocytes and colonizes the skin before birth (Hoeffel et al., 2015). Under homeostatic conditions LC have a self-renewal capacity independent of the bone marrow. Interestingly, it has been shown that in case of inflammation, bone-marrow derived monocytes can replenish LC that emigrated out of the skin (Ferrer et al., 2019; Martínez-Cingolani et al., 2014; Milne et al., 2015). In mice, the relatively thin epidermis contains a unique immune cell population of dendritic epidermal T cells (DETC) important for tissue integrity and homeostasis (MacLeod & Havran, 2011; Ovaere et al., 2009; Ribot et al., 2020). This unconventional $\gamma\delta$ T cell population is in close contact to keratinocytes to promote homeostatic proliferation but also senses keratinocyte derived antigens and induces wound healing upon cellular stress (Thelen & Witherden, 2020). Furthermore, DETC play an important role during contact allergies where they become indirectly activated through their intense communication with keratinocytes and produce cytokines in response to allergens (Mraz et al., 2020). In both species, humans and mice, most immune cells reside in the dermal layer that is lined with vessels and fibroblasts. Here, innate immune cells like dermal DC, macrophages and ILC as well as different types of T cells populate the dermis such as $CD4^+$ T cells and $\gamma\delta$ T cells that are termed dermal $\gamma\delta$ T cells in mice (O'Brien & Born, 2015). The DC network in the skin can be further divided into subpopulation based on their function and surface marker expression. Plasmacytoid DC (pDC) are dedicated to antiviral response and secrete large amounts of type I

interferons but are only sparsely located in the skin (Reizis et al., 2011). While all dermal DC share the expression of CD11c and MHC II, migratory conventional DC (cDC) can be further separated based on their CD11b expression. $CD11b^+$ cDC type 2 (cDC2) are the most abundant dermal DC subset (Malissen et al., 2014). They are specialized in antigen presentation towards $CD4^+$ T cells and shape Th17 and Th2 driven immune responses (Y. Gao et al., 2013; Murakami et al., 2013). $CD11b^-$ cDC type 1 (cDC1) additionally express XC-motif chemokine receptor 1 (XCR1), while lacking Sirpα expression and can be further divided into $CD103^+$ and $CD103^-$ cDC1. These $CD103^+$ cDC1 excel in cross presenting antigens to $CD8^+$ T cells and both $CD103^-$ and $CD103^+$ cDC1 initiate Th1 immune responses (Henri et al., 2010). Additionally, $CD11b^-$ XCR1- double negative cDC (DN cDC) populate the dermis, and like cDC2 initiate type 2 immune responses. Dermal DC can be distinguished from LC not only by the faster turnover, as they are constitutively replenished by bone marrow derived precursors, but also by the lack of epithelial cell adhesion molecule (EpCAM) expression (Clausen & Stoitzner, 2015). Moreover, DC undergo homeostatic maturation and frequently migrate to the skin-draining lymph nodes (Malissen et al., 2014). Remarkably, monocytes can also give rise to DC that are then termed monocyte-derived DC which, in contrast to the other DC subsets, express lymphocyte antigen 6 family member C1 (Ly6C) (Kashem et al., 2017; Malissen et al., 2014). The subcutis is composed of adipose and connective tissue. Its main function is insulation and protection against mechanical trauma (Brüggen & Stingl, 2020). In addition to subdermal fat and subcutaneous fat mice possess an extensive layer of striated muscle beneath the subdermal fat that allows rapid skin contractions independent from deeper muscles.

1.2.1. Allergic contact dermatitis

Contact dermatitis can be separated into allergic contact dermatitis (ACD) and irritant contact dermatitis (ICD). Around 20% of the population in industrialized countries are affected by this occupational disease (Alinaghi et al., 2019; Bergmann et al., 2016; Diepgen et al., 2016). While ICD describes a prolonged contact to an irritant leading to destruction of epidermal cells inducing an immune response, ACD is caused by a delayed type of hypersensitivity, classified as type IV hypersensitivity reaction according to Gell and Coombs (Marwa & Kondamudi, 2023). Here, low molecular weight chemicals called haptens that become immunogenic by binding carrier molecules such as endogenous or exogenous proteins lead to an allergic skin reaction. Haptens form covalent bonds to nucleophilic centers on endogenous or exogenous proteins thereby creating an immunogenic neo-antigen that then elicits an antigen-specific T

cell response. Only upon a second contact the already formed memory T cells become activated and initiate a strong immune response within a couple of days – the allergic reaction **(Figure 1.1)**. Examples for haptens are nickel, components of hair dyes or urushiol that is contained in poison ivy.

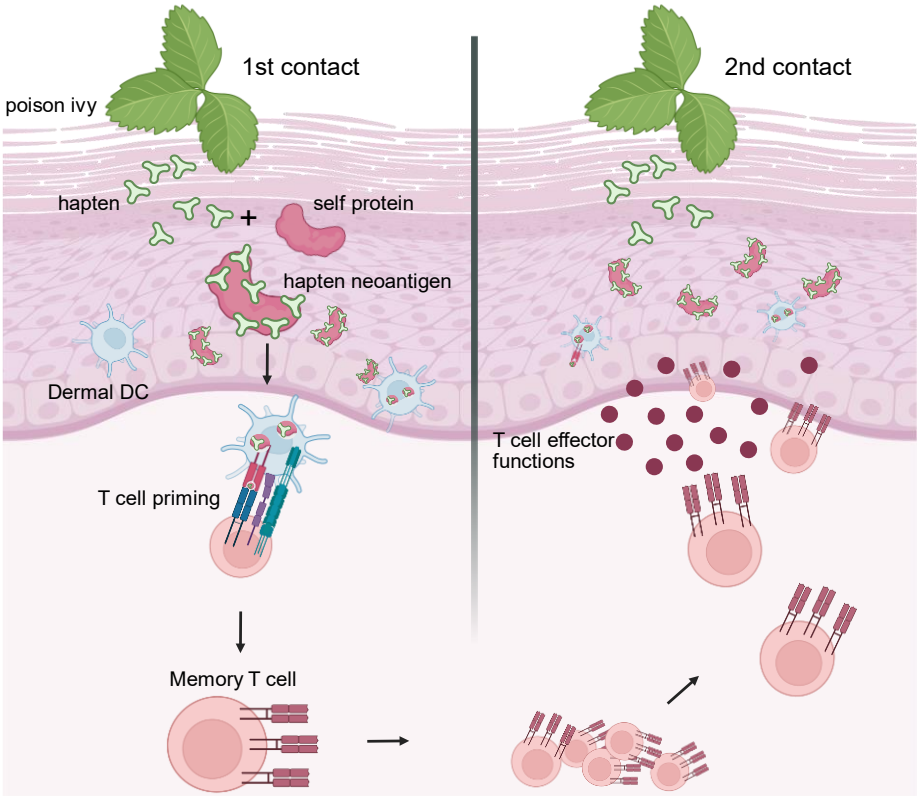

Figure 1.1 | Simplified immune mechanism of contact dermatitis.
Contact to a hapten like in poison ivy leads to formation of a hapten neoantigen by binding to a carrier protein. Subsequently the hapten neoantigen is recognized by the immune system. Dendritic cells prime specific T cells. Activated T cells become memory T cells that can quickly react upon a second contact to the hapten.

There are many different immune events taking place from recognition of the hapten-modified neoantigen to the allergic skin reactions. In experimental models frequently used haptens are oxalozone or 1-fluoro-2,4-dinitrobenzene (DNFB) (Kaplan et al., 2012). Before induction of the antigen-specific immune response towards DNFB, inflammasome activation and generation of DAMPs lead to reactive oxygen species (ROS) production and Interleukin 1 (IL-1)/Interleukin 18 (IL-18) activation (Antonopoulos et al., 2001; Esser et al., 2012). Furthermore, DNFB drives maturation of DC via the unfolded protein response (Luís et al., 2014). Activated dermal DC and LC migrate to skin-draining lymph nodes and prime T cells to become effector T cells recognizing hapten-modified neoantigens in complex with MHC molecules. Effector T cells then traffic back to the site of inflammation to eliminate haptenized cells bearing the same neopeptide/MHC complexes on their surface and/or home to the skin as $CD8^+$ T_{RM} to prepare

for a second encounter. In mice, CD8 T_{RM} displace DETC in the skin after exposure to allergen. Although it has been suggested earlier that during sensitization DETC emigrate out of the skin to the lymph nodes Gadsbøll et al postulate that tissue-resident $CD8^+$ T cells outcompete DETC likely because of their bioenergetic advantage (Gadsbøll et al., 2020; Nielsen et al., 2014). Clearly DETC and $CD8^+$ T cells play a crucial role in contact hypersensitivity (CHS) development (Funch et al., 2022; Sølberg et al., 2019). Nevertheless, once memory T cells are formed, another contact to the hapten leads to the symptoms associated with skin allergy - rash, swelling, redness and pain.

1.2.1.1. Mouse model for allergic contact dermatitis

A frequently used and reliable mouse model for ACD is CHS. CHS can be divided into two phases, the sensitization phase in which the immune response is initiated and the effector phase leading to allergic symptoms. A commonly used sensitizer in CHS is the lipophilic compound DNFB. In CHS 0.25% DNFB in an acetone/olive oil solution is applied on day -5 and on day -4 to induce sensitization **(Figure 1.2)**. 4 days later the effector phase is initiated by epicutaneous application of 0.3% DNFB on the right ear, whereas the left ear is treated with vehicle only. Ear swelling can be assessed the following days and compared to baseline thickness on day 0 as a measure for the strength of the allergic response.

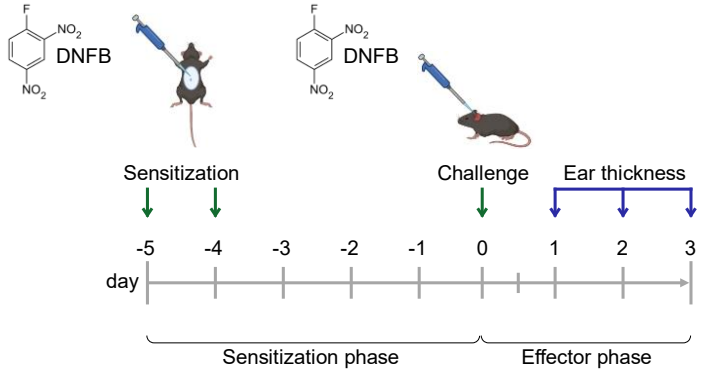

Figure 1.2 | Timeline of a contact hypersensitivity assay.
On day -5 and day -4 mice become sensitized with 0.25 % DNFB in acetone/olive oil on the shaved belly. On day 0 mice are challenged with 0,3 % DNFB or vehicle on the ear. Ear swelling is measured on day 0 to day 3, so that ear swelling can be calculated.

1.2.2. Atopic dermatitis

Atopic dermatitis (AD) is one of the most common chronic skin diseases with a prevalence of 2.2 % in adults and 20.4 % in children and adolescents in Germany (Barbarot et al., 2018; Silverberg et al., 2021). Its hallmarks are oozing erythematous patches and papules leading to excoriation. In later phases these skin lesions become chronic, turn dull and lichenified. They occur classically at symmetrical flexural regions, face, neck, hands and trunk, manifesting based on the onset, age, and severity (Facheris et al., 2023). An immune dysregulation or a genetic disorder such as mutation in the filaggrin gene, together with environmental triggers such as allergens or chemical irritants lead to skin barrier dysfunction (Guttman-Yassky et al., 2009; Irvine et al., 2011; J. Kim et al., 2019; Leung et al., 2020; Paller et al., 2019). This can lead to damaging of keratinocytes, failure of keratinocyte differentiation, lipid abnormalities and changes in microbial composition (Leung et al., 2020). Subsequently, cytokines and chemokines such as IL-1β, IL-33 or C-C motif chemokine ligand 17 (CCL17) and C-C motif chemokine ligand 22 (CCL22), get secreted, initiating an immune response or directly activating LC due to the barrier integrity malfunction (Didovic et al., 2016; Vestergaard et al., 2000; Yano et al., 2015). Dermal DC, LC and ILC become activated, migrate to the draining lymph nodes to prime T cells, while they themselves release soluble mediators. These secreted cytokines are thereby forcing T cells to become Th2 cells during the acute phase of AD. Thus, initially, type II cytokines are released that create an inflammatory milieu **(Figure 1.3)**.

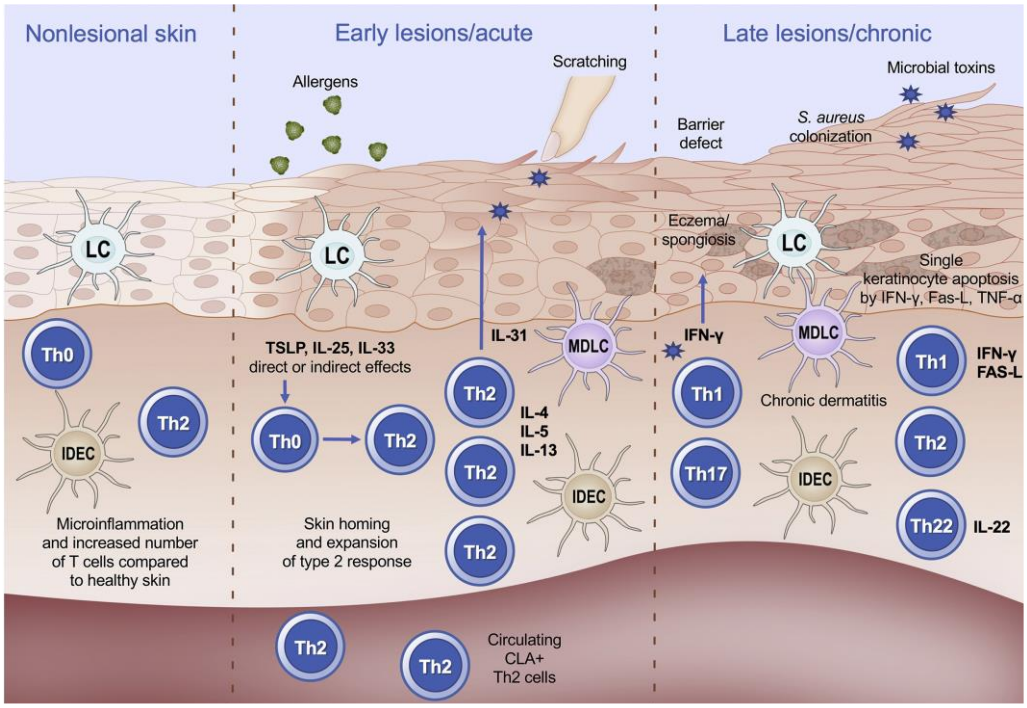

Figure 1.3 | Schematic overview of the progression of atopic dermatitis.
In an acute phase of atopic dermatitis nonlesional skin develops early lesions in which Th2 cells are induced by the cytokine released by keratinocytes as a consequence of allergen exposure. Th2 cells secrete type II cytokines and this leads to epidermal thickening and itching. In the chronic phase the skin can be populated by Staphylococcus aureus, further thickening of the epidermis and spongiosis is occurring. The former type II immune profile can change to favour Th1 and Th17 cells. Figure taken from Sugita et al. (Sugita & Akdis, 2020)

Moreover, due to stronger proliferation and less pronounced differentiation of the keratinocytes the epidermis thickens, and because of lower lipid contents and an increased water loss, the skin becomes dry and itchy, so that eczemas are forming (Guttman-Yassky et al., 2009; J. Kim et al., 2019; Leung et al., 2020). As a result of immune dysregulation, barrier defects and reduced AMP production in the Th2 environment, the skin can be colonized by *Staphylococcus aureus* (*S. aureus*) during the chronic phase of AD shifting the immune response from type II to a type I and type III response, so that Interferon -γ (IFNγ) and Tumor necrosis factor (TNF) are released inducing Th1 and Th17 cells. Additionally, keratinocyte apoptosis and spongiosis can be observed (J. Kim et al., 2019; Sugita & Akdis, 2020). Nevertheless, AD is an immensely heterogenous disease with different phenotypes based on patient age, disease duration and individual treatment requirements (Chovatiya & Silverberg, 2022). Although therapy with the anti-IL-4 antibody Dupilumab and anti-IL-13 antibody Tralokinumab successfully ameliorated allergy in patients by suppressing the type II immune response, there is still the need of ongoing research to treat AD patients with different outcomes of the disease adequately (Blair, 2022; Shirley, 2017).

1.2.2.1. Mouse model for atopic dermatitis

Although AD can be multifactorial, a frequently used mouse model with epicutaneous application of allergens has been shown to be of help in understanding the disease (G. Wang et al., 2007). In this model the back skin of mice is shaved, and tape stripped in order to cause skin barrier irritation and mechanical stress that is required for mimicking the barrier disruption typically observed in skin of AD patients (Jin et al., 2009). Then, a patch soaked with ovalbumin (OVA) in saline solution is placed on the back skin of mice for continuous antigen contact. The patch is replaced after 3 days and renewed, so the mouse is exposed to the antigen for 7 days. After a two-week break, the process is repeated until a total of three application cycles (Spergel et al., 1998). Repeated application of OVA on mouse skin leads to a mild epidermal thickening and cell infiltration into the dermis and subcutaneous tissue. C-C motif chemokine receptor 3 (CCR3)-expressing eosinophils, $CD4^+$ T cells and mast cells are recruited by the enhanced expression of eotaxin and CCL17 (Jahnz-Rozyk et al., 2005; Lloyd et al., 2000; Onoue et al., 2009). Due to the upregulated expression of type II cytokines, such as IL-4, IL-13 and IL-5 induced through Thymic Stromal Lymphopoietin (TSLP) secretion by keratinocytes and epithelial cells, $CD4^+$ T cells differentiate to Th2 cells and mast cell numbers increase significantly (Indra, 2013; Jin et al., 2009; G. Wang et al., 2007).

Next to OVA house dust mice extract is also often used as an allergen as house dust mite extract induces epidermal hyperplasia, spongiosis, and cell infiltration of skin with a skewed type II immune response (Huang et al., 2003). House dust mite extract that contains proteases and act as DAMP are known as sensitizers in AD (Trompette et al., 2009). Moreover, a combination of a house dust mite extract and OVA was observed to induce strong allergic symptoms in mice (Ogasawara et al., 2022; Shimura et al., 2016).

1.2.3. The CCL17/CCL22-CCR4-axis in allergic inflammation of the skin

Both, CCL17 and CCL22 as well as their common chemokine receptor C-C chemokine receptor type 4 (CCR4) have been associated with allergic skin diseases.

Elevated levels of CCL17 and CCL22 have been found in serum of patients suffering from AD (Shimada et al., 2004). The serum levels of these chemokines correlate with disease severity and are considered an early on biomarker for the development of AD in children (Følsgaard et al., 2012; Halling et al., 2023; Horikawa et al., 2002; Kakinuma et al., 2002). Furthermore, CCL17 can be stained in epidermal keratinocytes of lesioned skin of AD patients (Vestergaard et al., 2000). In mice, both chemokines are constitutively detectable in the skin with an enhanced expression upon inflammation (Kusumoto et al., 2007). CCL17 is expressed by cutaneous DC and required for their emigration from the skin (Alferink et al., 2003; Stutte et al., 2010). Furthermore, it also enhances responsiveness towards C-C motif chemokine ligand 19/20 (CCL19/20) and C-X-C motif chemokine ligand 12 (CXCL12) (Stutte et al., 2010). Moreover, it is known that CCL17 deficiency ameliorates the CHS response in mice (Alferink et al., 2003; Fülle, Steiner, et al., 2018). Additionally, CCL17 is thought to play an important role in immunosurveillance of the skin by recruiting CCR4-positive T cells. Confocal immunofluorescence analysis confirmed a colocalization of the adhesion molecules E-selectin and Intercellular Adhesion Molecule 1 (ICAM) with CCL17 on blood vessels (Chong et al., 2004; Reiss et al., 2001). Furthermore, mice overexpressing CCL17 demonstrated an increased type II immune response in homeostatic and allergic conditions (Tsunemi et al., 2006). Interestingly, although CCL22 is also expressed in the skin (Horikawa et al., 2002; Karlsson et al., 2021; Katou et al., 2001; Thul et al., 2017; Uhlén et al., 2015; Uhlen et al., 2017; Yano et al., 2015) and binds to CCR4, different signaling pathways are used by CCL17 and CCL22 (Lim et al., 2021; Santulli-Marotto et al., 2013, 2015). CCL17 engagement induces only G protein activation, whereas CCL22 binding favors β-arrestin signaling, while also activating the G protein signal pathway. In addition, CCL22 unlike CCL17 provokes quick receptor internalization (Lin et al., 2018; Mariani et al., 2004). Moreover, CCL22 has a higher potency, can bind both conformational states of CCR4 and in contrast to CCL17 desensitizes the receptor for the other chemokine (Cronshaw et al., 2006; Viney et al., 2014). This phenomenon has also been detected for other chemokine – chemokine receptor interactions and was termed biased agonism (C. A. Anderson et al., 2016; Eiger et al., 2021). In addition to the difference in intracellular signaling, CCL22 has been primarily associated with recruitment of Treg and is thought to exert

suppressive functions (Hao et al., 2016; Rapp et al., 2019) in contrast to CCL17 that is mainly connected to inflammation with a preference of induction of Th2 cell migration (Heiseke et al., 2012; Lieberam & Förster, 1999; Shin et al., 2023). Thus, as CCL22 controls Treg migration, it may play a role in Treg homing to the skin (Eby et al., 2015). Furthermore, Rapp et al. discovered that CCL22 is essential for regulating T cell - DC contacts in lymph nodes and facilitating Treg-DC communication (Rapp et al., 2019).

As CCR4 is expressed by Th2 cells, mast cells and eosinophils it is not unexpected that CCR4 plays a role in allergic diseases, too (Matsuo et al., 2016). Using *in vivo* microscopy in mice, it was proven that CCR4-expressing T cells are recruited into the skin after induction of an ACD (X. Wang et al., 2010). In addition, an increase of CCR4-expressing $CD4^+$ T cells in blood and skin samples of AD patients can be observed (Nakatani et al., 2001). Also, in mice, expression of CCR4 is found on skin homing T cells (J. J. Campbell et al., 1999). Although an improvement of allergic symptoms in AD upon CCR4 blocking is observed in some studies (Matsuo et al., 2018; Sato et al., 2023), no defect in cutaneous DC migration and no improvement of AD-like symptoms was detected by Stutte et al (Stutte et al., 2010). Unexpectedly, CCR4-deficient mice also exhibited a stronger immune response compared with wild-type (WT) mice in an oxazolone CHS experiment (Lehtimäki et al., 2010). Furthermore, it has been reported that treatment with Mogamulizumab – a monoclonal antibody against CCR4 – as therapy for T-cell lymphoma, Sézary syndrome or Mycosis fungoides led to severe adverse skin disorders (Duvic et al., 2015; Ogura et al., 2014; Suzuki et al., 2019). Thus, in contrast to the absence of its ligands CCL17 and CCL22, lack of CCR4 appears to cause an enhanced allergic skin response. In summary, all components of the CCL17/CCL22-CCR4-axis are strongly involved in allergic diseases, but the mechanisms behind that are not fully understood so far. Hence, there is still ongoing research about the exact mode of action and whether other players, like a second receptor or other ligands, might be involved.

1.3. Immunity in the gastrointestinal tract

The gastrointestinal tract (GI tract) represents the largest compartment of the immune system and comes into contact with the exterior constantly (Mowat & Agace, 2014). It reaches from mouth over pharynx and esophagus into stomach and intestinal tract. The small intestine is structured into duodenum, jejunum and ileum starting from stomach to large intestine. It is characterized by large villi reaching into the lumen and crypts which enlarge the surface to support digestive functions, uptake of metabolites, facilitate immunological functions. The

large intestine comprises the colon with caecum and appendix. In contrast to the small intestine, the colon has no villi, and the crypts are much smaller **(Figure 1.4)**. Here, water reabsorption takes place. Mucus is produced by goblet cells in the epithelial layer as a biochemical barrier to pathogens (Cornick et al., 2015). Apart from enterocytes that are frequently replenished by stem cells located at the bottom of the crypts, specialized T cells called intraepithelial lymphocytes (IEL) that can quickly react upon antigen recognition can be found in the epithelium. Furthermore, paneth cells, microfold cells (M-cells) and enteroendocrine cells are located there (Mowat & Agace, 2014). Most immune cells of the mucosa are located in the lamina propria below the epithelium (Mason et al., 2008). Additionally, the gut-associated lymphoid tissue (GALT) includes Peyer's Patches at the distal Ileum, mesenteric lymph nodes (mLN) draining the intestine and mature lymphoid aggregates of B cells, DC, and ILC covered by follicle-associated epithelium (FAE) termed isolated lymphoid follicles (ILF). A thin muscle layer called muscularis mucosae separates the lumen facing mucosa from the submucosa and lower muscle layers (Mowat & Agace, 2014). As barrier organ, the GI tract has distinct features to defend the body from pathogens. The mucus contains a large number of commensal bacteria that contribute to homeostasis and barrier integrity by induction of mucosal and systemic immune maturation (Hayes et al., 2018). Additionally, AMP like alpha-defensins secreted by paneth cells are in the mucus that bind to bacterial surfaces and disrupt the membrane integrity (Bevins & Salzman, 2011). Furthermore, Immunoglobulin A (IgA) is secreted into the mucus by plasma cells to neutralize threats before entering the body (Pabst & Slack, 2020). The epithelial layer serves as a second barrier for entering pathogens. Moreover, M-Cells in the FAE of ILF and Peyers' Patches sample the mucus for antigens and present them to T and B cells in the lamina propria or in ILF (Kanaya et al., 2020). In addition to various T and B cells, DC, ILC and macrophages are present in the lamina propria. ILF much like Peyers' Patches are primarily filled with B cells surrounded by T cells to form a germinal center once APC, such as DC, present antigens (Pabst et al., 2005). The mLN that in mice are 4-5 individual lymph nodes positioned as a chain draining the whole intestine, are the largest lymph nodes of the body. With these various immunological structures and barrier mechanisms the gut efficiently protects the body from pathogens and maintains homeostasis.

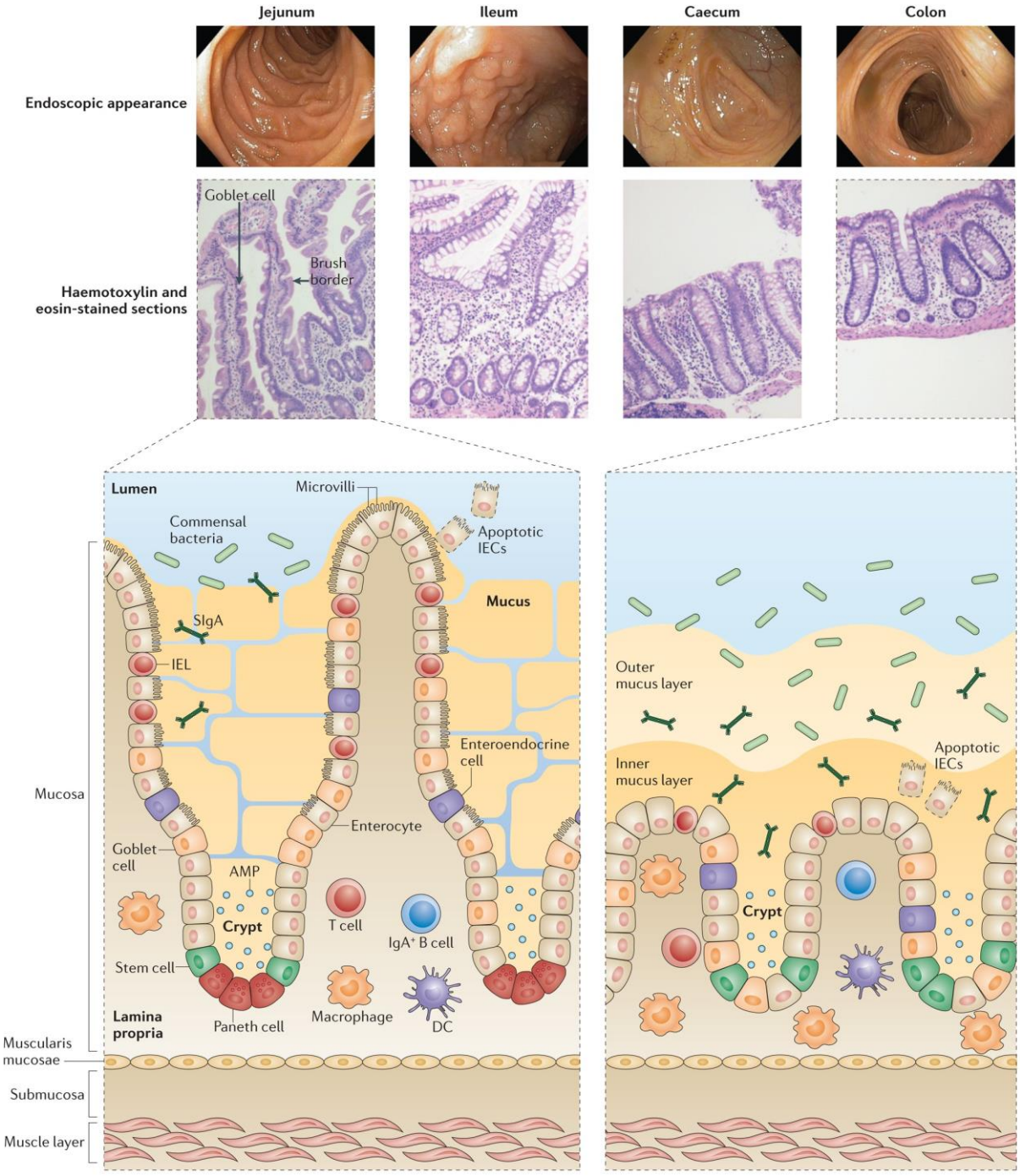

Figure 1.4 | Structure of the small and large intestine.
Endoscopic appearance, histological staining and cellular structure of the small intestine (left) and large intestine (right). The small intestine has large villi and crypts and the enterocytes possess microvilli structures to enlarge the surface to facilitate nutrient uptake. The large intestine has no villi, an extensive layer of mucus and no microvilli structures on the cell surface. The epithelial layer consists in both locations of enterocytes, intraepithelial lymphocytes (IEL), mucus producing goblet cells, antimicrobial peptide (AMP) secreting paneth cells, enteroendocrine cells and microfold cells (M-cells). The lamina propria is below the epithelium and contains Immunoglobulin A (IgA) producing plasma cells, B cells, T cells, macrophages and dendritic cells (DC).
Picture taken from Mowat et al.(Mowat & Agace, 2014).

1.3.1. Immune cells of the gut-associated lymphoid tissue

Besides protecting the host from invading pathogens, a major role of the gut immune system is to induce tolerance to commensals and diet components. Therefore, the immune cells of the gut associated lymphoid tissue (GALT) have distinct properties to fulfill both, regulatory and effector immune functions.

Major classes of APC in the gut are monocytes, macrophages and DC. Intestinal macrophages express CD64, F4/80, MHC and CD11b and continuously differentiate from recently recruited $Ly6C^+$ MHC^- $CCR2^+$ monocytes of the blood that commonly are classified by their Ly6C expression as well as increasing MHC expression upon maturation (Joeris et al., 2017) . Monocytes are the main source of proinflammatory cytokines, such as IL-1, IL-6, TNF, IL-23, and of ROS (Dunay & Sibley, 2010; Seo et al., 2015; B. Weber et al., 2011). In contrast, intestinal macrophages are sessile and rather associated with anti-inflammatory functions, such as IL-10 production, and thus are important for maintaining homeostasis (Bain et al., 2013; Cerovic et al., 2014). Intestinal DC display various functions based on their expression profile. cDC1 express XCR1 and CD103 but lack CD11b expression, whereas cDC2 express Sirpα and CD11b. $Sirpα^+$ cDC2 can be further divided into two subpopulations, depending on whether they are $CD103^+$ or $CD103^-$ (Cerovic et al., 2014; Stagg, 2018). $Sirpα^+$ $CD11b^+$ $CD103^-$ cDC2 can give rise to $Sirpα^+$ $CD11b^+$ $CD103^+$ cDC2 upon Transforming Growth Factor (TGFβ) stimulation (Bain et al., 2017). The rarest population of DC, mostly located in Peyer's Patches and ILF, are DN DC lacking the expression of CD11b and CD103 (Cerovic et al., 2013). As also observed in other organs, the intestinal cDC1 are characterized by their ability of cross-presentation of soluble antigens priming $CD8^+$ T cells (Schlitzer et al., 2013). They are important for Treg induction and Th1 polarization in the mLN (Esterházy et al., 2016; Luda et al., 2016). Whereas the cDC1 depend on Interferon Regulatory Factor 8 (IRF8), the $CD103^+$ $CD11b^+$ cDC2 are interferon regulatory factor 4 (IRF4) dependent (Luda et al., 2016). A lack of this subpopulation leads to a reduction in Th17 cells and might also influence Treg induction (Bain et al., 2017; Persson et al., 2013). The functions of $CD103^-$ $CD11b^+$ cDC2 are heterogenous. Under TGFβ stimulation they can differentiate into $CD103^+$ $CD11b^+$ cDC, whereas they can also fulfil similar functions as intestinal macrophages, i.e., sampling antigens through the epithelium with their dendrites (Bain et al., 2017; Bogunovic et al., 2009; Luciani et al., 2022; Varol et al., 2009). The least abundant population of DN DC likely shares the FMS-like tyrosine kinase 3 (FLT3) ontogeny with other DC subsets and induces IL-17 production of $CD4^+$ T cells *in vitro* (Cerovic et al., 2013,

2014). Nevertheless, all intestinal cDC subsets are migratory and can migrate in a CCR7 specific manner via afferent lymphatics to lymph nodes (Mowat & Agace, 2014). pDC have been identified in the lamina propria as cells expressing B220, Ly6C, MHCII and intermediate levels of CD11c. In contrast to cDC, intestinal pDC do not migrate to the lymph nodes.

Intestinal DC have the ability to imprint a gut-homing tolerogenic profile on T cells and induce the differentiation of Treg. One distinct feature of intestinal DC to facilitate this function is the expression of aldehyde dehydrogenase (ALDH) enzymes that turn vitamin A into retinoic acid (RA) (Coombes et al., 2007; Johansson-Lindbom et al., 2005; Worthington et al., 2011). RA enhances the expression of the integrin α4β7 and C-C chemokine receptor type 9 (CCR9) on T cells that are essential for CC-chemokine ligand 25 (CCL25) dependent migration and homing to the gut (Iwata et al., 2004). It is further believed that induction of a tolerogenic profile on developing T cells is supported by a variety of local factors like TSLP secretion by epithelial cells (Rimoldi et al., 2005). Treg are defined by the expression of the master transcription factor forkhead-box protein P3 (FoxP3) (Hori et al., 2017; Savage et al., 2020). Remarkably, Treg occur naturally and can be induced later in life in the presence of TGFβ (W. J. Chen et al., 2003). While the former happens during T cell development in the thymus as a result of strong TCR-binding by a self-antigen to escape host immunity, the latter can occur in several pro- and anti-inflammatory scenarios (Hori et al., 2017; Savage et al., 2020; Shevach & Thornton, 2014; Yadav et al., 2013). Many induced Treg are located in the gut to mediate homeostasis by suppressing proinflammatory immune responses against harmless antigens from commensals and food (Luu et al., 2017). This is indirectly accomplished by extensive binding of IL-2 via their abundant expression of the interleukin 2 receptor α-chain (IL-2Rα; CD25) on Treg and thus depleting IL-2 from the surrounding and reducing its availability for other T cell populations (Chinen et al., 2016). Furthermore, secretion of IL-10 and TGFβ creates an anti-inflammatory milieu (Bollrath & Powrie, 2013; Safinia et al., 2015; Schmidt et al., 2012; Whibley et al., 2019). But Treg can also directly inhibit DC maturation via cytotoxic T-lymphocyte-associated protein 4 (CTLA4) and are able to kill T cells via release of perforins (D. J. Campbell & Koch, 2011; Cao et al., 2007; Watanabe et al., 2016). Activated Treg can be recognized by the expression of Killer Cell Lectin Like Receptor G1 (KLRG1) (X. Yuan et al., 2014). Naïve T cells differentiate to different T helper subsets based on the micromilieu. While T-box expressed in T cells (T-bet) expressing Th1 cells provide protection against intracellular pathogens such as viruses and bacteria by secretion of IFNγ, TNF, IL-12, and IL-6, GATA binding protein 3 (GATA3) expressing

Th2 cells in the gut mediate an immune response against intestinal parasite infection. However, Th17 cells, marked by RAR-related orphan receptor γ (RORγt) expression, are important for the defense against extracellular pathogens (Imam et al., 2018). Thus, Th17 cells are very abundant in the gut and account for 30-40 % of memory $CD4^+$ T cells in the lamina propria (Imam et al., 2018). They produce the cytokines IL-17 and IL-22 which are essential for the protection against bacterial invasion as they stimulate the production of AMP and contribute to the formation of tight junctions in the epithelium (Langrish et al., 2005; Ma et al., 2019). $CD8^+$ T cells are also present as gut homing IEL. These include αβ and γδ T cells expressing a α-chain/α-chain homodimer of the CD8 molecule which are involved in immune surveillance and regulation as well as T cells expressing a CD8 α-chain/β-chain heterodimer which are associated with barrier integrity (Gui et al., 2022; Lambolez et al., 2007; Poussier et al., 2002). Furthermore, conventional $CD8^+$ T cells are located in the lamina propria or in the lymphoid-associated tissue and also participate in microbial clearance by their effector mechanisms. In conclusion, the GALT is a complex system that is keeping effector and regulatory functions in balance for a healthy life. Dysregulation in any direction can harm this sensitive equilibrium.

1.3.2. Inflammatory bowel diseases

Inflammatory bowel disease (IBD) is a term for chronic inflammation of the gastrointestinal tract including the two conditions Morbus Crohn (MC) and Ulcerative Colitis (UC). It is a permanent progressive disorder with chronically recurring inflammation in the GI tract. There are several molecular processes that contribute to the disease progression of IBD. A disbalance in the micromilieu towards a more inflammatory rather than tolerogenic micromilieu is a hallmark for IBD. Another characteristic feature are defects in the intestinal epithelial barrier function affecting e.g., the AMP and mucus production (Antoni et al., 2014). Although the cause of IBD is unknown, genetic risk factors, environmental factors, as well as disturbances in the immune system or microbiota composition play a role in IBD development (Strober et al., 2007; Thompson-Chagoyán et al., 2005). For example, individuals with IBD have a lower bacterial diversity than healthy controls with a depletion of commensal bacteria belonging to the phyla of Firmicutes and Bacteroides (Wallace et al., 2014). Additionally, genome-wide association studies (GWAS) revealed genetic risk factors for IBD. Autophagy genes such as *Atg16l1* that are important for barrier integrity, NOD-like receptors controlling antimicrobial responses and microbial binding intelectins have been found to be connected to MC, whereas

loci for IL-10 and Actin Related Protein 2/3 Complex Subunit 2 (ARPC2) were associated with UC (Caruso et al., 2014; Foerster et al., 2022; Franke et al., 2008; Nonnecke et al., 2022). Furthermore, the prevalence of MC has risen upon industrialization and consumption of Western diet (Chiba et al., 2019). In Europe, the incidence is approximately 0.2 % (Zhao et al., 2021). In Germany, around 1.1 million people suffer from IBD, ca 0.6 million are diagnosed with MC, whereas 0.39 million reportedly have UC (Zhao et al., 2021).

People suffering from IBD have diarrhea, abdominal pain, bloody stool, show weight loss, and feel fatigue. Although the symptoms are quite similar, MC differs from UC in several features. MC can affect any part of the GI tract, but most commonly occurs in the distal ileum. The impacted areas are patchy, surrounded by healthy tissue and reach deeply into the tissue. UC, on the other hand, occurs in the colon only. It spreads continuously and the inflammation is strongest in the epithelium (Imam et al., 2018). APC secrete IL-12 and thereby induce differentiation of naïve T cells into Th1 cells, secreting IFNγ (Gonsky et al., 2014). Preclinical and clinical studies demonstrated that the role of IFNγ might not be exclusively detrimental as there are controversial results regarding progression and involvement of IFNγ in IBD (Franke et al., 2008; Muzaki et al., 2016; Nava et al., 2010). Whereas Nava et al reported that IFNγ-deficient mice are protected from DSS-induced colitis, an induction of an early anti-inflammatory response in intestinal epithelial cells via $CD103^+$ $CD11b^-$ DC has been described by Muzaki et al (Muzaki et al., 2016; Nava et al., 2010). Similarly, several single nucleotide polymorphisms (SNPs) in the TNF gene have been identified in IBD patients, while the effect of TNF on disease pathogenesis also differs between model systems. Because of the multifactorial nature of IBD several mouse models, such as the dextran sodium sulfate (DSS)-induced colitis or the oxalozone-induced colitis model, mimic different dysfunctions associated with the disorders. DSS destroys the epithelial barrier allowing stool components to enter the mucosa thus inducing intestinal inflammation, whereas the haptenizing agent oxalozone generates a type II immune response. Other frequently used mouse models of IBD are different adoptive T cell transfer experiments. Here, for instance, naïve $CD4^+$ T cells are intravenously injected into immunodeficient severe combined immunodeficiency (SCID) or recombination-activating genes (RAG)-deficient mice. Furthermore, it has been observed that mice lacking the IL-10 gene spontaneously develop colitis. While TNF blockade had no effect in oxazolone-treated mice, it showed significant amelioration in DSS-induced colitis (Shen et al., 2007; Stillie & Stadnyk, 2009). Furthermore, anti-TNF therapy is currently used for the treatment of MC

and UC (Adegbola et al., 2018; Genaro et al., 2021; Hanauer et al., 2006). The cytokine IL-17, that is mainly secreted by Th17 cells, is elevated in patients with MC (Sakuraba et al., 2009). Mice deficient for the IL-17 receptor were protected in 2,4,6-trinitrobenzene sulfonic acid (TNBS)-induced colitis (Z. Zhang et al., 2006). However, treatment of MC with a human anti-IL-17A monoclonal antibody surprisingly enhanced the disease (Hueber et al., 2012). The second main cytokine of Th17 cells namely IL-23 supports IBD progression. This was shown in adoptive transfer experiments where IL-23R-deficient donor cells were transferred as well as in experiments using neutralizing antibodies for IL-23 (Ahern et al., 2010; Elson et al., 2007). Interestingly, it was demonstrated that oral therapeutic delivery of an inhibitor of the master transcription factor of Th17 cells, Rorγt, could significantly reduce IBD in different experimental models (Withers et al., 2016). Moreover, Risankizumab, an antibody binding IL-23, is used in MC therapy (D'Haens et al., 2022). Whereas the antibody Ustekinumab that binds the IL-12p40 subunit that IL-23 shares with IL-12, was used in first generation anti-IL-23 therapy, second and third generation drugs target solely IL-23 (McDonald et al., 2022). Type II cytokines like IL-4, IL-5 or IL-13 primarily released by Th2 cells may also influence the IBD progression. Treatment of mice with IL-4 antibodies during oxazolone-induced colitis prevent the disease to some extent (Boirivant et al., 1998; Mizoguchi et al., 1999). Moreover, analysis of cytokine transcripts in UC and MC revealed an increase in IL-5 and IL-13 mRNA levels compared to control patients (Nemeth et al., 2017). Additionally, treatment of UC patients with the IL-13 antibody Tralokinumab resulted in improved clinical remission rates and mucosal healing though this effect was not significant compared to the placebo group (Danese et al., 2015). Besides $CD4^+$ T cells, also $CD8^+$ T cells contribute to IBD pathogenesis by formation of fistulas in MC and in UC, and can trigger tissue destruction by the secretion of TNF (Bruckner et al., 2021; Corridoni et al., 2020).

In summary, IBD is a complex disease involving different immune processes with unclear etiology. Thus, there is still a need to understand the pathogenesis of these diseases and to find new treatment options.

1.3.2.1. Mouse model for inflammatory bowel disease

Although IBD is a multifactorial disease with unidentified cause, as already mentioned above, several mouse models are used to study the pathogenesis of IBD. A frequently used model employs DSS, a toxic sulfated polysaccharide that induces damages in the epithelial layer and compromises barrier integrity (Kiesler et al., 2015). This facilitates the entry of luminal antigens

initiating strong inflammation. The molecular weight of DSS varies strongly between 5-1400 kDA. Induction of a severe murine colitis using 40 – 50 kDA DSS resembles human UC most closely (Okayasu et al., 1990). DSS usually is solved in water and administered via the drinking water.

Depending on the administration of DSS it is possible to induce acute colitis or chronic colitis. Whereas in the acute colitis model 2-5 % DSS is given for a period of 4-9 days continuously, in the chronic colitis model lower DSS concentrations (2 % or less) are administered in alternating cycles of DSS and water treatment for several weeks. Clinical symptoms in the acute phase are weight loss, diarrhea, occult blood in stool and anemia (Perše & Cerar, 2012). Especially in the early acute phase the inflammation depends on innate immune activation. Another hallmark of DSS-induced colitis is shortening of the colon length caused by intestinal inflammation that correlates with disease severity (Chassaing et al., 2014). Histologically one can observe mucin depletion, goblet cell loss, epithelial degeneration, immune cell infiltration into the lamina propria and submucosa, as well as crypt abscesses (Perše & Cerar, 2012). Additionally, the progression of the disease is reflected by an increase in inflammatory mediators such as, TNF, IL-1β, IFNγ, IL-10 and IL-12, in the circulation (Alex et al., 2009; Y. Yan et al., 2009). As for human IBD, the microbiota plays an important role in disease progression in mouse models. Thus, Nell et al could show that DSS-induced colitis cannot be observed in gnotobiotic mice (Nell et al., 2010). Furthermore, immunodeficient SCID mice, which are germ-free, develop only minor colitis symptoms also proving the importance of the induction of inflammation in the context of colitis (Hudcovic et al., 2001). In conclusion, the DSS-induced colitis model is a widely used model to understand the pathogenic mechanisms behind IBD.

1.3.3. The CCL17/CCL22-CCR4-axis in inflammatory bowel disease

Chemokine – chemokine receptor interactions in the GI tract are essential for immune cell infiltration and activation of immune cells, but also to coordinate homeostasis (Kulkarni et al., 2017). This also applies for the CCL17/CCL22-CCR4-axis. mRNA of CCL17 and CCL22 was identified in intestinal mucosa of MC and UC patients (Günaltay et al., 2015; Jugde et al., 2001). Furthermore, transcripts of both chemokines are elevated in affected areas of MC patients compared to unaffected mucosa (Jugde et al., 2001). CCL22 was additionally detected in isolated mononuclear cells of mucosa and peripheral blood of MC and UC patients. Here, CCL22 protein in PBMC was increased compared to healthy controls (Jugde et al., 2001). Moreover, CCR4 is significantly upregulated on peripheral blood memory $CD4^+$ T cells in MC

patients and increases with stronger disease activity, whereas CCR4 levels decrease with treatment (Jo et al., 2003). Furthermore, there is a constitutive production of CCL22 by the intestinal epithelium (Cecilia Berin et al., 2001). Also, in a human intestinal epithelial cell line, the CCL22 production is upregulated in response to inflammatory stimuli like TNF and induces migration of CCR4-expressing T cells (Cecilia Berin et al., 2001). In line with these data, the human protein atlas shows high expression of CCL17 and in particular of CCL22 in the GI tract (Karlsson et al., 2021; Thul et al., 2017; Uhlén et al., 2015; Uhlen et al., 2017). In mice, CCL17 and CCL22 levels are significantly increased in the induction phase of colitis (Scheerens et al., 2001). Also, the mRNA levels of CCR4 are significantly increased in inflamed colons of IL-10-deficient mice (Scheerens et al., 2001). Heiseke et al tested CCL17-deficient mice in a DSS-induced colitis mouse model as well as with adoptive transfer of T cells into $Rag1^{-/-}$ mice and observed a protection from severe colitis symptoms (Heiseke et al., 2012). This was not due to a reduced recruitment of $CCR4^{+}$ T cells to the colonic mucosa, but rather was connected to a diminished production of proinflammatory cytokines and a Treg expansion in the mLN. However, CCR4-deficient mice also showed a protection in the model of T cell transfer colitis, whereas lack of CCR4 expression on transferred T cells did not protect from colitis induction (Heiseke et al., 2012). In contrast to these findings, Yuan et al reported that CCR4-dependent recruitment of Treg cells to the mLN is required to rescue the effects of colitis induction in the T cell transfer model (Q. Yuan et al., 2007). Although there are a lot of hints of a copious connection between IBD and the CCL17/CCL22-CCR4-axis, the exact role of these chemokines in the context of colitis is not fully understood yet (Rapp et al., 2019).

1.4. Aptamers as potential therapeutic agents

Aptamers are short RNA or DNA oligonucleotides that bind specifically to a target by folding into a three-dimensional structure. Their structures can include loops, bulges, hairpins, pseudoknots, triplexes or quadruplexes with which they bind a wide range of potential targets, starting with metal ions, small molecules, proteins up to single molecules in target mixtures or even whole organisms such as bacteria and cells (Famulok & Mayer, 1999; Göringer et al., 2003). Binding mainly occurs through stacking of aromatic rings, electrostatic and van der Waals bonds, as well as hydrogen bonds (Mayer, 2009). The commonly used selection process in which aptamers are generated is called Systematic Evolution of Ligands by EXponential enrichment (SELEX), in which with several enrichment cycles the sequences with highest affinity within a large library can be identified (Tuerk & Gold, 1990). Automatization made it

possible to accelerate the procedure immensely (Breuers & Mayer, 2023; Cox & Ellington, 2001; Eulberg et al., 2005; Wochner et al., 2007). Though some target characteristics like the isoelectric point might influence success or failure, it is not possible to predict from the structure of a target, whether a selection will be successful (Mayer, 2009). The process typically starts with a random oligonucleotide library of around 10^{13} – 10^{15} individual sequences (Stoltenburg et al., 2007). Target binding sequences are separated from unbound sequences and amplified. These sequences represent a new and enriched pool of oligonucleotides as basis for the next selection cycle. By iteration of the steps the library condenses to an oligonucleotide pool of sequences with high affinity and specificity to the targets revealing certain binding motifs (Stoltenburg et al., 2007). After identification of individual enriched sequences by next generation sequencing, possible aptamer candidates will be compared regarding affinity, specificity, and functionality. Furthermore, it is possible to modify aptamers to enhance stability, improve binding or add fluorescent moieties. A common modification is a change at the C5-position of uridine and deoxyuridine to increase resistance against exonucleases. Also, the 2´hydroxyl group of the ribose sugar in the RNA aptamer can be exchanged with a 2´fluorine to increase stability or even affinity (Z. Chen et al., 2023; S. Gao et al., 2016). PEGylation, i.e. addition of a polyethylene glycol moiety is often used to prevent renal clearance of aptamers designed for *in vivo* use as it reportedly increases half-time *in vivo* (Amero et al., 2021). Additionally, aptamers are often truncated such that the structures relevant for binding are preserved while removing unnecessary nucleotides (S. Gao et al., 2016). Each post-SELEX modification, however, requires additional tests to confirm binding, affinity and functionality. In recent years, aptamers have been considered as an alternative to small molecules and antibodies in therapeutics and diagnostics (Haßel & Mayer, 2019; Kaur et al., 2018). Aptamers bind with affinities as high as antibodies, while they have a shorter and less cost-intensive generation time, no batch-to batch variability, higher modifiability, and thermal stability (Y. Zhang et al., 2019). Hence, it is not surprising that several aptamers have successfully entered clinical studies like Pegaptanib, an aptamer specific for vascular endothelial growth factor (VEGF) which is the first aptamer-based drug approved by the FDA and is in use for treatment of macular degeneration (Ng et al., 2006). Moreover, aptamers are used in diagnostics to identify rare forms of lung cancer or ovarian cancer by biomarkers early on (Kaur et al., 2018). However, prior to therapeutic use, immunogenicity of the aptamers has to be tested, as the aptamer could induce an adverse immune reaction by activation of PRR on

immune cells (Maier & Levy, 2016). In summary, aptamers offer a wide range of applications from the use in research to diagnostics and therapy.

1.4.1. Aptamers directed against CCL22

CCL22-specific aptamers were newly generated by Anna Jonczyk (AG Mayer) to be tested *in vitro* and *in vivo* in CHS experiments to evaluate CCL22 as a potential target for ACD treatment. Nine possible CCL22 aptamer candidates were identified after 10 selection cycles in the SELEX process: AJ1, AJ4, AJ21, AJ25, AJ78, AJ81, AJ82, AJ102, AJ104 **(Figure 1.5 H)**. With increasing selection cycles, the binding efficiency to CCL22 increased, whereas the number of unique sequences and the diversity of the nucleic acid library decreased **(Figure 1.5 A-D)**. The starting library contained an equal nucleotide ratio, whereas the ratio changed in cycle 10 to G-rich sequences **(Figure 1.5 E, F),** which likely influences the secondary and tertiary aptamer structure (Roxo et al., 2019). Interestingly, among the nine candidates identified three different conserved sequence motifs were observed **(Figure 1.5 G, I)**. AJ81 and AJ82 contained motif 1, while motif 2 was found in AJ1, AJ25 and AJ104 and motif 3 was detected in AJ21 and AJ102. The sequence of AJ78 is free of any of the three motifs. The enrichment of conserved motifs during selection suggests that these regions are involved in target binding. Post SELEX analysis of the capacity of the aptamer candidates to bind murine CCL22 **(Figure 1.5 J)** revealed that all aptamer candidates, except AJ4, bound CCL22. AJ4 was likely carried through the SELEX process due to an easily amplifiable sequence. Therefore, AJ4 was not tested in further experiments. In the following thesis the eight residual candidates as well as further truncated and modified versions of the candidates were functionally evaluated and tested.

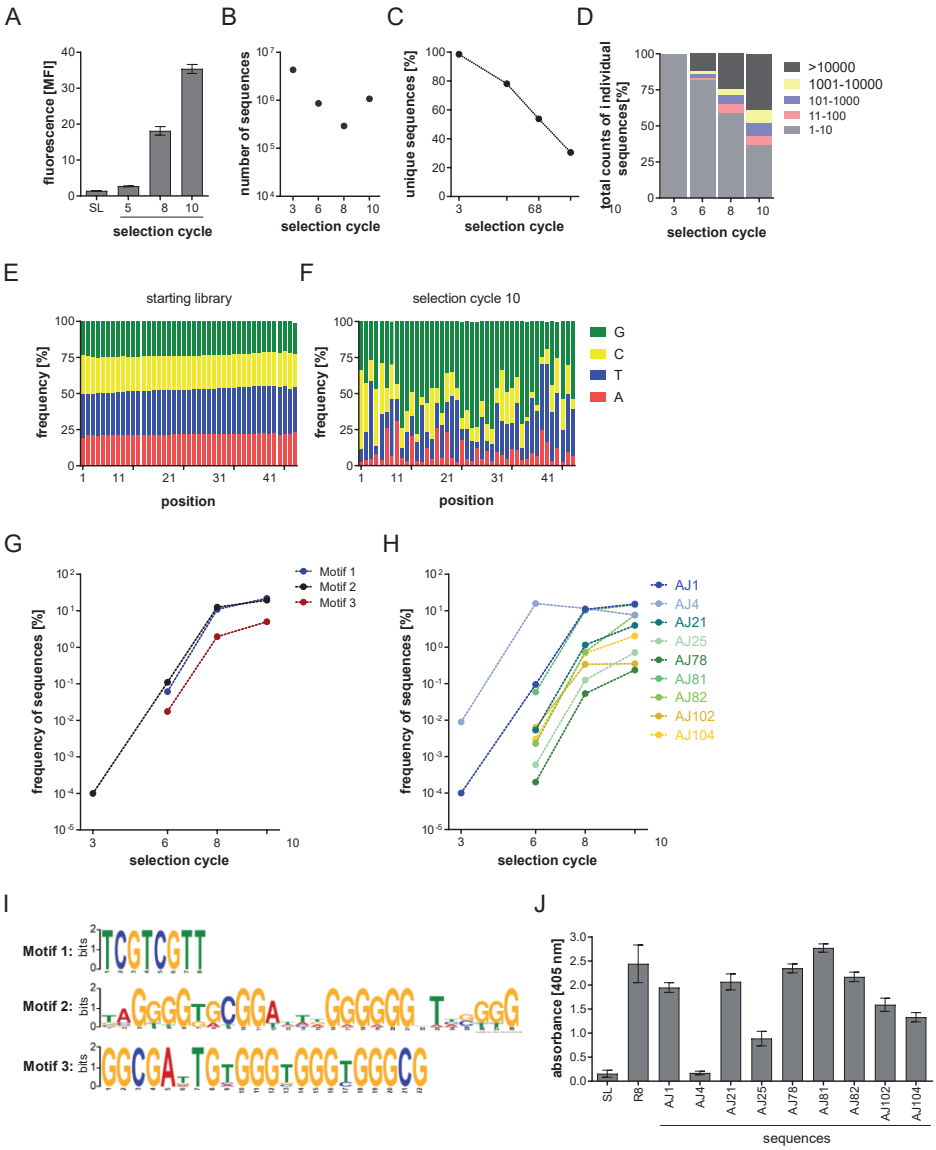

Figure 1.5 | SELEX for generation of CCL22 aptamers.
(A) Flow cytometry-based interaction analysis of enriched DNA libraries from the starting library and selection cycles 5, 8 and 10 to murine CCL22. (B) Number of sequences obtained by next-generation sequencing analysis per selection cycle. (C) Frequency of unique sequences in selection cycles 3, 6, 8 and 10. The frequency was calculated by dividing the overall number of sequences by the number of unique sequences. (D) Fraction of sequences in the DNA population from selection cycles 3, 6, 8 and 10 sharing the indicated copy numbers. (E and F) Nucleotide distribution at the different positions of the random region of the starting library and the final selection cycle 10. (G) Frequency of three motifs common among the most enriched sequences. Motif 1 is found in AJ81 and AJ82. Motif 2 is found in AJ1, AJ25 and AJ104 and motif 3 is found in AJ21 and AJ102. (H) Frequency of the most enriched sequences in selection cycle 3, 6, 8 and 10. Missing data points indicate that the sequence could not be detected in the next-generation sequencing data of the respective round. (I) Sequences of the motifs. (J) DNA sequences identified by next-generation sequencing were analyzed for binding to murine CCL22 in an enzyme-linked oligonucleotide assay (ELONA) (n = 2, mean ± SD).
Data from Anna Jonczyk (AG Mayer)

2. Aim of the thesis

A dysregulation of the CCL17/CCL22-CCR4-axis has been related to immune disorders in barrier organs including skin and GI tract. In order to understand the underlying mechanisms, mouse lines deficient for one of the two chemokines, both chemokines, or the receptor CCR4 were analyzed in mouse models of diseases with barrier integrity malfunctions.

The first part of the thesis aimed to evaluate the function of CCL17, CCL22 and CCR4 in models of skin allergy, such as CHS and AD. Our group observed a reduction in allergic symptoms associated with CHS in CCL17 and CCL22-deficient mice, whereas CCR4 deficiency led to an aggravation of the disease. Based on these findings, CCL17 and CCL22 were considered as promising targets for treatment of skin allergies. In this thesis, previously published CCL17-specific aptamers were used in CHS experiments to get further insight into potential application time points, effectiveness and underlying mechanisms of amelioration of symptoms by aptamer blockade. In addition, CCL22-specific aptamers, newly generated by Anna Jonczyk in the group of Prof. Günter Mayer, were tested *in vitro* and *in vivo* as a possible therapeutics for ACD. Here, especially the potential of topical application should be investigated. Secondly, the role of the chemokines and their receptor in AD, which in contrast to CHS represents a Th2-driven allergy, was studied.

The second part of the thesis focuses on the role of the CCL17/CCL22-CCR4-axis in DSS-induced colitis as a model for IBD. Here, earlier studies hinted at the importance of CCL17, CCL22 and CCR4 in maintaining intestinal homeostasis. Therefore, another aim of this thesis was to understand the mechanisms of IBD development that are connected to the CCL17/CCL22-CCR4-axis.

In summary, in this thesis the role of CCL17, CCL22, and CCR4 in CHS, AD and DSS-induced colitis was assessed, while these chemokines also should be evaluated as possible new targets to treat diseases involving barrier defects. Here, the potency of newly generated CCL22-specific aptamers for the treatment of CHS in a preclinical model was particularly assessed.

3. Material and Methods

3.1. Materials

3.1.1. Equipment

Table 3.1 | Equipment

Equipment	**Article – (Company)**
Automatic tissue processor	Leica ASP300 (Leica Microsystems, Wetzlar, Germany)
Cell Counting Chamber	Neubauer improved (La Fontaine via Labotec, Göttingen, Germany)
Centrifuge Concentrator	Concentrator plus (Eppendorf, Hamburg, Germany)
Centrifuges	5415R (Eppendorf, Hamburg, Germany) 5810R (Eppendorf, Hamburg, Germany) Allegra® X-15R Centrifuge (Beckman Coulter, Brea, USA)
Cryostat	Leica CM3050 S (Leica Microsystems, Wetzlar, Germany)
Dewar Carrying Flasks	26B (KGW-Isotherm, Karlsruhe, Germany)
Electrophoresis Power Supply	Power SourceTM 300V (VWR International, Radnor, USA)
Electrophoresis System	XCell SureLock (Invitrogen, Waltham, USA)
ELISA washer	CAPP wash 12 (CAPP, Odense, Germany)
Flow Cytometer	BD LSR II Flow (BD Biosciences, Heidelberg, Germany) BD FACS Symphony TM (BD Biosciences, Heidelberg, Germany)
Forceps	FV126-115, vedena® feine anatomische Pinzette SEMKEN, 155 mm (6‘‘) (Medical Highlights Germany GmbH, Rohrdorf, Germany)

Franz diffusion cell	Unjacketed 2mm flat joint 5mm orifice diameter Franz diffusion cell (PermeGear, Hellertown,USA)
Freezer (-20 °C)	Comfort (Liebherr, Biberach, Germany)
Freezer (-80 °C)	New Brunswick Ultra-Low Temperature Freezer (Eppendorf, Hamburg, Germany)
Fridge (+4 °C)	MediLine LKUexv1610 (Liebherr, Biberach, Germany)
Fume Hood	System DELTA 30 laboratory fume cupboards (Wesemann International GmbH, Wangen im Allgäu, Germany)
Gel documentation system	Odyssey (Li-Cor Bioscience, Bad Homburg, Germany)
Gel electrophoresis	PerfectBlue Gel System (Peqlab, Erlangen, Germany)
Heating devices	TS1 Thermo Shaker (Biometra, Göttingen, Germany) Heating block Thermostat TH21 (HLC BioTech, Bovenden, Germany)
Ice machine	Scotsman Flockeneisbereiter AF200 (Hubbard Systems, Birmingham, USA)
Incubator	CB 150 (Binder, Tuttlingen, Germany) ECOCELL (MMM Group, Planegg/München, Germany) Memmert INE 500 (Memmert GmbH + Co.KG, Schwabach, Germany) ECOCELL (MMM Group, Planegg/München, Germany)
Incubator shaker	New Brunswick Innova® 44/44R (Eppendorf, Hamburg, Germany) Stuart orbital incubator SI500 (Cole-Parmer, Stone, UK)

Isoflurane Vaporizer	Combi-vet® system (Rothacher Medical, Berne, Switzerland)
Laminar flow workbench	BDK Laminar Flow (BDK, Sonnenbrühl, Genkingen, Germany)
Magnetic stirrer	IKA RCT basic (IKA-Werke GmbH & Co. KG, Staufen, Germany)
Microscope	BZ 9000 Keyence (KEYENCE DEUTSCHLAND GmbH, Neu-Isenburg, Germany) Olympus BX50 (Olympus Corporation, Tokyo, Japan)
Microtome	Leica RM2255 (Leica Microsystems, Wetzlar, Germany)
Microwave	Leica RM2255 (Leica Microsystems, Wetzlar, Germany)
Multichannel pipette	DV8-10, DV12-50, DV8-300 (HTL Lab Solutions, Warsaw, Poland)
Paraffin Embedding Station	Leica EG1150 H (Leica Microsystems, Wetzlar, Germany)
pH meter	FiveEasy FE20-Basic (Mettler Toledo, Columbus, USA)
Pipettes	10 µl, 20 µl, 100 µl, 200 µl, 1000 µl (Eppendorf, Hamburg, Germany)
Real-Time PCR Detection System	TCFX96 Touch™ Real-Time PCR Detection System (BioRad, Hercules, USA)
Rocking Shaker	Duomax 1030 (Heidolph Instruments GmbH & Co.KG, Schwabach, Germany)
Scales	440-35A (Kern & Sohn, Balingen, Germany) ABJ 220-4M (Kern & Sohn, Balingen, Germany)

Scissors	EV107-110, Vedena® Feine Schere IRIS, spitz-spitz, gerade, 110 mm (Medical Highlights Germany GmbH, Rohrdorf, Germany) EV118-115, Vedena® chirurgische Schere, spitz-stumpf, gerade, 115 mm (Medical Highlights Germany GmbH, Rohrdorf, Germany)
Spectrophotometer	NanoDropTM ND-1000 (NanoDrop Products, Wilmington, USA) EL 800 (BioTek, Winooski, USA) infinite M200 (Group Ltd., Männedorf, Switzerland
Thermal Cycler	T100TM (BioRad, Hercules, USA) T1 Thermocycler (Biometra, Göttingen, Germany)
Tissue homogenizer	IKA® T10 basic (IKA®-Werke GmbH & Co.KG, Staufen, Germany)
Tissue Homogenizer	Precellys®24 (Bertin Instruments, Montigny-le-Bretonneux, France)
Transilluminator	Biostep Dark Hood DH-40/50 (biostep, Burkhaltsdorf, Germany)
Vortex shaker	Vortex Genie 2 (Scientific Industries, New York, USA)
Water bath	Leica HI1210 (Leica Microsystems, Wetzlar, Germany)

3.1.2. Consumables

Table 3.2 | Consumables

Item	**Company**
BD Plastipak 1ml Sub-Q	BD Medical, Le Pont de Claix Cedex, France
Cell culture flasks (T25, T75, T175)	Greiner Bio-One, Kremsmünster, Austria
Cell strainer nylon (40µm, 70µm, 100µm)	VWR, Radnor, USA
CellTrics®	Partec, Meckenheim, Germany
Corning® HTS Transwell® cell culture plates	Corning, New York, Vereinigte Staaten
Cover slips	Roth, Karlsruhe, Germany
CryoPure Tube 1.8 ml	Sarstedt, Nümbrecht, Germany
Culture plates (6-well/ 24-well/ 48-well/ 96well, flat bottom)	Greiner, Frickenhausen, Germany
Disposal bags	Roth, Kalsruhe, Germany
ELISA plate (half-area, 96 K)	Greiner, Kremsmünster, Austria
Embedding cassettes	Carl Roth GmbH + Co.KG, Karlsruhe, Germany
Eppendorf Tubes® 5ml	Eppendorf, Hamburg, Germany
Filter tips	Sarstedt, Nümbrecht, Germany
Flow cytometry tubes	Sarstedt, Nümbrecht, Germany
Glass beads	Roth, Kalsruhe, Germany
Glass Pasteur pipette	Roth, Kalsruhe, Germany
Glass Reagent/Media Bottles (10 ml, 50 ml, 200 ml, 500 ml)	VWR International, Radnor, USA
Gloves	Semperit Technische Produkte GmbH, Wien, Austria
Hard-shell PCR plates	Bio-Rad, München, Germany
Measuring pipettes (5ml, 10ml, 25ml)	Greiner, Kremsmünster, Austria
Micro tube 1.1ml Z-Gel	Sarstedt, Nümbrecht, Germany
Micro tube 2ml + screw cap	Sarstedt, Nümbrecht, Germany
Microplate, 96well (F/U)	Greiner, Frickenhausen, Germany
Microscope slides (Superfrost plus)	Thermo Scientific, Waltham, USA

Multiply® µStrip Pro mix.colour	Sarstedt, Nümbrecht, Germany
Parafilm®	American National Cam, Greenwich, USA
PCR tubes	Sarstedt, Nümbrecht, Germany
Petri dishes	Greiner, Kremsmünster, Austria
Precision wipes	Kimberly-Clark, Reigate, United Kingdom
Reaction tubes (15ml, 50ml)	Greiner, Frickenhausen, Germany
Reagent reservoirs	Thermo Scientific, Waltham, USA
Safe seal reaction tubes (0,5, 1.5ml, 2.0ml)	Sarstedt, Nümbrecht, Germany
Serological pipettes (5 ml, 10 ml, 25 ml)	Greiner, Kremsmünster, Austria
Sterican needles	Braun, Melsungen, Germany
Sterile filters (Filtropur S 0.45)	Braun, Melsungen, Germany
Surgical disposable scalpel	Braun, Tuttlingen, Germany
Syringe filtration unit (Filtropur S0.2/0.45)	Sarstedt, Nümbrecht, Germany
Syringes Inject® (2ml, 5ml, 10ml, 20ml)	Braun, Tuttlingen, Germany
Syringes Inject-F Tuberkulin (1ml)	Braun, Tuttlingen, Germany
Tegaderm® 1624W	3 M Medica, Neuss
Tissue freezing medium	Leica, Nussloch, Germany
Tissue-Tek® Cryomold (15x15mm, 25x20mm)	Sakura Finetek, Torrance, USA
Venofix® A 21G	Braun, Tuttlingen, Germany
Weighing pans	Roth, Karlsruhe, Germany

3.1.3. Chemical reagents and recombinant proteins

Table 3.3 | Chemical reagents and recombinant proteins

Chemical/ reagent	**Company**
100 bp DNA Ladder	New England BioLabs, Ipswich, USA
10x TAE buffer	Invitrogen, Carlsbad, USA
1-Fluoro-2,4,-dinitrobenzene (DNFB)	Sigma-Aldrich, St. Louis, USA
2-Propanol >99.5 %	Roth, Karlsruhe, Germany
Acetic acid 100 %	Roth, Karlsruhe, Germany
Acetone	VWR, Darmstadt, Germany
Albumin Bovine Fraction V, pH=7.0	SERVA Electrophoresis GmBH, Heidelberg, Germany
Ampuwa	Fresenius Kabi, Bad Homburg, Germany
B-27™ supplement (50X)	Gibco by Life technologies, Carlsbad, USA
Collagenase D	SERVA Electrophoresis GmbH, Heidelberg, Germany
completeTM Protease inhibitor tablets	Roche, Basel, Switzerland
CountBright™ absolute counting beads	Life technologies, Carlsbad, USA
CpG ODN 1668	TIB Molbiol, Berlin, Germany
Deoxynucleotide (dNTP) Solution Mix	Peqlab, Erlangen, Germany
Dextran Sulfate Sodium Salt, Colitis Grade	MP Biomedicals, Solon, USA
Diphteria Toxin (Unnicked)	Calbiochem by Merck, Darmstadt, Germany
Dithiothreitol (DTT) Molecular Grade	Promega, Fitchburg, USA
DNase I	Merck, Darmstadt, Germany
DNase/RNase-Free Water	Zymo Research, Irvine, USA
Dulbecco's PBS	Sigma-Aldrich, St. Louis, USA
Dulbecco's Modified Eagle Medium (DMEM)	ThermoFisher, Waltham, USA
Entellan	Merck, Darmstadt, Germany
Eosin	Sigma-Aldrich, St. Louis, USA
Ethanol 70% (methylated)	Roth, Karlsruhe, Germany
Ethanol absolute for molecular biology	AppliChem, Darmstadt, Germany
Ethanol Rotipuran >99.8 %	Roth, Karlsruhe, Germany

Ethylenediaminetetraacetic acid (EDTA)	Sigma-Aldrich, St. Louis, USA
Euparal	Roth, Karlsruhe, Germany
FACS Clean Solution	BD Bioscience, Franklin Lakes, USA
FACS Rinse Solution	BD Bioscience, Franklin Lakes, USA
Fetal Bovine Serum	ThermoFischer, Waltham, USA
Fixable Viability Dye eFluor 450/780	eBioscience, San Diego, USA
Hair removal Veet®	Reckitt Benckiser Group plc, Slough, England, UK
Hank's Balanced Salt Solution (HBSS) (10x)	Gibco by Life Technologies, Carlsbad, USA
Hemalaun solution	Sigma-Aldrich, St. Louis, USA
HEPES	Sigma-Aldrich, St. Louis, USA
Human recombinant cytokines (CCL17, CCL22, IL-2)	Peprotech, New York, USA
Hydrochloric acid 37 %	Roth, Karlsruhe, Germany
Ionomycin	Sigma-Aldrich, St. Louis, USA
Laminin	Sigma-Aldrich, St. Louis, USA
L-Glutamine	Gibco by Life Technologies, Carlsbad, USA
Liberase™	Merck, Darmstadt, Germany
LPS, E. coli 0111:B4	Sigma-Aldrich, St. Louis, USA
Mowiol	Sigma-Aldrich, St. Louis, USA
Murine recombinant chemokines (CCL17, CCL22)	Peprotech, New York, USA
Oligo $(dT)_{12\text{-}18}$ primer	ThermoFisher, Waltham, USA
Olive oil	Sigma-Aldrich, St. Louis, USA
OneComp / UltraComp eBeads™	Thermo Fisher, Waltham, USA
Ovalbumin	Sigma-Aldrich, St. Louis, USA
Paraffin	Leica Biosystems, Nußloch, Germany
Paraformaldehyde (PFA)	Merck, Darmstadt, Germany
Penicillin-Streptomycin	Gibco by Life Technologies, Carlsbad, USA
peqGOLD Universal Agarose	Peqlab, Erlangen, Germany

Percoll	GE healthcare life science, Chalfont St Giles, Buckinghamshire, GB
Phosphate buffered saline (PBS)	Merck, Darmstadt, Germany
Poly-D-lysine	Invitrogen, Carlsbad, USA
Polyinosinic:polycytidylic acid (poly (I:C))	Invivogen, San Diego, USA
Precision Count beadsTM	Biolegend, Fell, German
QIAzol Lysis Reagent	Qiagen, Hilden, Germany
Reverse transcription buffer (5X)	Peqlab, Erlangen, Germany
Roswell Park Memorial Institute Medium (RPMI) 1640	Thermo Fisher Scientifc, Waltham, USA
Sucrose	Sigma-Aldrich, St. Louis, USA
Sulfuric acid (H_2SO_4)	Roth, Karlsruhe, Germany
SYBR® DNA Gel Stain	Invitrogen, Carlsbad, USA
Tissue Freezing Medium	Leica Biosystems, Nussloch, Germany
Toluidine Blue O	VWR, Darmstadt, Germany
TritonX-100	ThermoFisher, Waltham, USA
Trypan Blue	Sigma-Aldrich, St. Louis, USA
Trypsin	Gibco by Life technologies, Carlsbad, USA
Tween-20	Roth, Karlsruhe, Germany
UltraPureTM Distilled Water	Invitrogen, Waltham, USA
Xylol	Roth, Karlsruhe, Germany

3.1.4. Kits and assays

Table 3.4 | Kits and assays

Kits/assays	**Company**
DuoSet® ELISA Mouse CCL17/TARC	R&D Systems, Minneapolis, USA
DuoSet® ELISA Mouse CCL22/MDC	R&D Systems, Minneapolis, USA
DuoSet® ELISA Mouse IL-10	R&D Systems, Minneapolis, USA
DuoSet® ELISA Mouse IL-13	R&D Systems, Minneapolis, USA
DuoSet® ELISA Mouse IL-5	R&D Systems, Minneapolis, USA
DuoSet® ELISA Mouse TNF	R&D Systems, Minneapolis, USA
eBioscience™ Foxp3 / Transcription Factor Staining Buffer Set	eBioscience, Inc., San Diego, USA
LEGENDplex™ Mouse Inflammation Panel (13-plex)	Biolegend, Fell, Germany
MojoSort™ Human CD4 T Cell Isolation Kit	Biolegend, Fell, German
Mouse IgE ELISA Kit	Merck, Darmstadt, Germany
MyTaq™ HS Red DNA Polymerase	Bioline, London, UK
Pierce™ BCA Protein Assay Kits	ThermoFisher, Waltham, USA
T Cell Activation/Expansion Kit, human	Miltenyi Biotec, Bergisch-Gladbach, Germany
Direct-zol RNA Miniprep Kit	Zymo Research, Irvine, USA

3.1.5. Solutions and buffers

Table 3.5 | Solutions and buffers

Solutions/buffers	**Ingredients**
BW5147.3 media	RPMI 1640 10 % heat-inactivated FCS 2 mM L-glutamine 100 U/ml penicillin 100 µg/ml streptomycin 1.43 µM mM 2-mercaptoethanol
BW5147.3 starvation medium	RPMI 1640 0.5 % heat-inactivated FCS 100 U/ml penicillin 100 µg/ml streptomycin
DAC cream	Gycerolmonostearat Cetylalkohol Middle chain triglycerides White vaseline Macrogol- 20- glycerolmonostearat Propylenglycol water
Digestion buffer (back skin)	RPMI 1640 5 % FCS 0.625 U/ml DNAse I 120 g/ml
Digestion buffer (ear skin)	PBS 1:10 Liberase (Merck) 0.25 U/ml DNAse I
Digestion buffer (lymph nodes)	1:10 Liberase (Merck)
ELISA stopping solution	25 % H_2SO_4 in H_2O
ELISA wash buffer	0.05 % Tween-20 in PBS
FACS buffer	PBS 2 mM EDTA 0.5 % heat-inactivated FCS

Lysis buffer (tail lysis)	5 mM EDTA, pH8.0 0.2 % SDS 200 mM NaCl 0.1 mg/ml proteinase K
Mowiol mounting solution	2.4 g mowiol 6 g glycerol 12 ml Tris (0.2 M, pH 8.5) 2.5 % DABCO
PFA (4 %)	4 g PFA in 100 ml PBS, pH 7.4

3.1.6. Antibodies

Table 3.6 | Antibodies

Antigen	Clone	Conjugate	Dilution	Company
B220	RA3-6B2	APC-Cy7	200	Biolegend
CCR2	SA203G11	AlexaFluor647	200	Biolegend
CCR4	2G12	BV421	100	Biolegend
CD103	M290	BV421	200	BD Bioscience
CD11b	M1/70	BV605	200	Biolegend
CD11b	M1/70	BUV395	300	BD Bioscience
CD11c	N418	Alexa700	200	Biolegend
CD11c	N418	BV605	200	Biolegend
CD172α	P84	BUV395	300	BD Bioscience
CD24	M1/69	PE	200	eBioscience
CD25	PC61	PE-Cy7	200	Biolegend
CD26	H194-112	PE-Cy7	200	Biolegend
CD3	145-2C11	APC-Cy7	200	Biolegend
CD326/Epcam	G8.8	AlexaFluor700	200	Biolegend
CD4	GK1.5	BUV563	200	BD Bioscience
CD44	IM7	BV570	300	Biolegend
CD45	30-F11	BV510	200	Biolegend
CD62L	MEL-14	APC-R700	200	BD Bioscience
CD64	X54-5/7.1	PerCP-Cy5.5	200	Biolegend
CD69	H1.2F3	BV711	200	Biolegend
CD8β	YTS156.7.7	PerCP-Cy5.5	400	Biolegend
F4/80	BM8	APC-Cy7	200	Biolegend
FoxP3	FJK-16s	PE	100	eBioscience
GATA3	L50-823	PE-CF594	50	BD Bioscience
KLRG1	2F1	BUV395	100	BD Bioscience
Ly6C	HK1.4	BV711	200	Biolegend
Ly6G	1A8	PE-Dazzle	200	BD Bioscience
Ly6G	1A8	BUV563	200	BD Bioscience

MHC/I-A/I-E	M5/114.15.2	APC-Cy7	200	Biolegend
MHC/I-A/I-E	M5/114.15.2	PerCP	400	Biolegend
RORγt	B2D	APC	100	eBioscience
TCRγδ	GL3	BV605	200	Biolegend
TCRβ	H57-597	BUV737	200	Biolegend
XCR1	ZET	BV421	200	Biolegend
Zombie Fixable Viability Dye		APC-Cy7	1000	Biolegend

3.1.7. Software

Table 3.7 | Software

Software	**Company**
BioRender	BioRender, Toronto, Canada
BZ-II Analyzer	Keyence, Montabaur, Germany
Explore Q Exactive Plus Tune	Thermo Fisher Scientific, Waltham, USA
FACS Diva	BD, Franklin Lakes, USA
FlowJo 10.5.3	TreeStar, Inc., Ashland, USA
GraphPad Prism 9.2.0	GraphPad, La Jolla, USA
ImageJ (Fiji)	Rasband, W.S., ImageJ, U. S. National Institutes of Health, Bethesda, USA
Mendeley Software	Elsevier, Amsterdam, Netherlands
Microsoft Office 2016	Microsoft, Redmond, USA
Bio-Rad qPCR analysis software	BioRad, Hercules, USA

3.2. Methods

3.2.1. Animal Experiments

3.2.1.1. Mouse housing conditions

All mice were kept in the animal facility of the LIMES Institute, University of Bonn under specific pathogen-free conditions in individually ventilated cages (12h/12h light/dark cycle, 22°C) with *ad libitum* access to food and water. The experiments were performed with female 8- to 12-week-old mice. Genotypes were defined through polymerase-chain reaction (PCR).

Table 3.8 | Mouse lines

Mouse line	**Genetic background**	**Reference**	**Supplier**
C57BL/6JRccHsd	C57BL/6JRcc	-	Envigo, Rossdorf, Germany, LIMES-GRC
$CCL17^{E/E}$	C57BL/6JRcc	(Alferink et al., 2003)	LIMES-GRC
$CCL22^{-/-}$	C57BL/6JRcc	(Shin et al., 2023)	LIMES-GRC
$CCL17^{E/E}$ $CCL22^{-/-}$	C57BL/6JRcc	I.Förster (unpublished)	LIMES-GRC
CCR4-/-	C57BL/6JRcc	(Chvatchko et al., 2000)	LIMES-GRC

3.2.1.2. Contact hypersensitivity

Mice were sensitized with 70 µl 0.25 % DNFB in acetone/olive oil (5:1) on the shaved abdomen at day -5 and day -4. At day 0 mice were anesthetized to measure the baseline ear thickness using a gauge caliper. Following, the animals were challenged with 10 µl 0.3 % DNFB in acetone/olive oil on the dorsal and ventral side of the right ears. The left ears were treated with the vehicle only. The ear thickness was measured blinded 24 h (day 1), 48 h (day 2), and 72 h (day 3) after application of DNFB and the swelling was calculated by subtraction of the individual baseline thickness (day 0) at the end of the experiment. Immune cell composition in the ears of the mice was analyzed at the end of the experiment (day 3) after DNFB challenge, if not stated otherwise.

3.2.1.2.1. Contact hypersensitivity with two challenges

Mice were sensitized with 70 µl 0.25 % DNFB in acetone/olive oil (5:1) on the shaved abdomen at day -5 and day -4. At day 0 mice were anesthetized to measure the baseline ear thickness using a gauge caliper. At this day and additionally on day 6 the animals were challenged with 10 µl 0.3 % DNFB in acetone/olive oil (4:1) each on the dorsal and ventral side of the right ears. The left ears were treated with the vehicle only. The ear thickness was measured blinded 24 h

(day 1, day 7), 48 h (day 2, day 8), and 72 h (day 3, day 9) after application of DNFB and the swelling was calculated by subtraction of the individual baseline thickness (day 0) at the end of the experiment.

3.2.1.2.2. Aptamer injections during contact hypersensitivity

Contact hypersensitivity assay was performed as described above. For the aptamer treatment, 5 nmol or 10 nmol of the CCL17-specific or CCL22-specific aptamer was administered intraperitoneally in PBS at the time of the challenge and 12 h post DNFB challenge, or 24 h post DNFB challenge as described in the respective figure legends.

3.2.1.2.3. Administration of aptamer in cream during contact hypersensitivity

DAC cream (90 – 100 mg) was mixed with the aptamer at the desired concentration under sterile conditions. The aptamer cream was applied with a clean spatula on the dorsal and ventral site of the ear while mice were kept under anesthesia for 15 minutes to ensure absorption of the cream. Application time points were at the time of the challenge and 12 h post DNFB challenge.

3.2.1.3. Atopic dermatitis-like skin inflammation

The back of the mice was shaved, tape-stripped and a patch soaked with either OVA (100 µg; 100 µl of a 0.1 % solution in 0.9 % NaCl), OVA and Dermatophagoides farina (Der.f.) extract (100 mg in 0.9 % NaCl) or NaCl alone was applied and fixed with a Tegaderm plaster. Tape-stripping was performed by repeated application and quick removal of a Tegaderm plaster. Antigen application was done two times per week, so that the skin had contact with the antigen for 7 days. This procedure was repeated three times with treatmentfree breaks of two weeks.

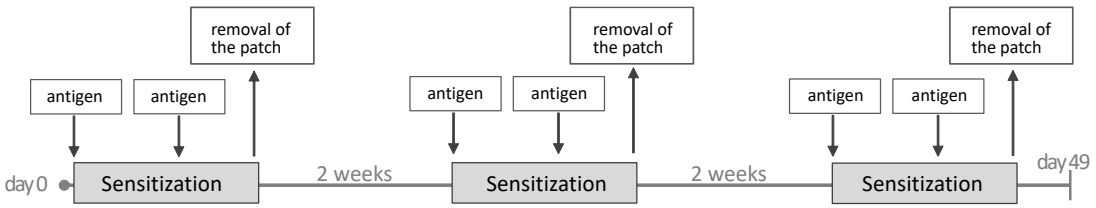

Figure 3.1 | Timeline of the experimental model for atopic dermatitis-like skin inflammation.

3.2.1.4. DSS-induced colitis

DSS colitis was induced in aged-matched female mice by adding 3 % DSS (w/vol) to the drinking water for 7 days. The health of the mice was monitored daily using a disease score including general behavior, posture, stool consistency, and body weight. At the end of the experiment serum was separated for analysis of inflammatory cytokines or markers. Moreover, colons

were removed and the colon length was determined. Parts of the colon were used for histological analysis or semi quantitative PCR.

3.2.2. Histology

3.2.2.1. Organ treatment and fixation

After removal, organs were transferred into 4 % PFA for preservation of structures. They were kept in PFA-solution for 4 h at room temperature.

3.2.2.2. Preparation of tissue for paraffin sections

PFA-fixed tissue samples were transferred into plastic cassettes and further processed with a Tissue Processor that incubates the samples in a series of ascending ethanol concentrations (70 % 2 h, 80 % 2 h, 90 % 1 h, 96 % 1 h, 100 % 2 h) for dehydration, followed by Xylene incubation (2 h) and ends with paraffin incubation (2 h). Then, tissue samples were embedded into paraffin blocks, cooled down and stored at room temperature. Subsequently, paraffin embedded tissue samples were sectioned with a rotary microtome to obtain 5 µm sections. These sections were transferred to a warm water bath (40°C) and pulled onto microscope slides.

3.2.2.3. Preparation of tissue for cryosectioning

The tissue was dehydrated with sucrose in PBS at rising concentrations (5 %, 10 %, 20 %). Therefore, organs were kept for 1 h in each solution or alternatively in the 20 % sucrose solution overnight. Afterwards, tissue samples were embedded in cryomedium and frozen using dry ice. Subsequently, samples were stored at -80°C until cryosectioning. Using a cryostat, tissue sections of 7 to 10 µm were produced and mounted on a microscope slide. Sections were air dried before staining. Slides were stored at -80°C.

3.2.2.4. H&E Staining

Hematoxylin and eosin staining (H&E staining) was performed to analyze tissue structure. Paraffin sections were treated with xylol, a series of decreasing ethanol concentrations for rehydration and water followed by staining of nuclei with hematoxylin and positively charged cytoplasm components using eosin. After staining, dehydration and preparation for embedding was performed by repeating the rehydration steps in reverse order before embedding with Entellan and drying overnight at room temperature.

Table 3.9 | H&E staining protocol

Steps	Treatment	Time
1	Xylol	10 min
2	Xylol	10 min
3	100 % EtOH	10 min
4	96 % EtOH	5 min
5	90 % EtOH	5 min
6	80 % EtOH	5 min
7	70 % EtOH	5 min
8	Hemalaun	3 min
9	H_2O	2 min (Rinse)
10	Eosin	3 min
11	H_2O	1 min (Rinse)

3.2.2.5. Toluidin blue staining

Paraffin sections were heated in a 65°C oven for 30 min to eliminate paraffin from the sections, followed by two times incubation in xylol for 5 min each. Subsequently, the sections were incubated in ethanol (99 %, 95 %, 90 %, 80 %,70 %) and water for 5 min each for rehydration of the sections. Slides were then stained in 0.01 % Toluidine Blue solution for 10 min. Afterwards, the sections were washed in water 3x for 5 min and air-dried before they were mounted with Euparal and dried overnight and kept at room temperature until microscopic analysis.

3.2.2.6. Microscopy

Microscopy and analysis of H&E or, Toluidin blue stainings were performed with the BZ-9000 (Keyence) microscope using 4x, 10x and 20x magnification. Microscopy and analysis of Franz assay sections were performed with the BZ-9000 (Keyence) or Zeiss LSM 780 confocal microscope.

3.2.2.7. Image analysis

Images were processed using Fiji software ImageJ.

3.2.3. Flow cytometry

3.2.3.1. Preparation of single cells – lymph nodes

Connective and fat tissue was removed from lymph nodes. Then, lymph nodes were transferred to a 48-well plate with 200 µl PBS with 1:10 Liberase, cut two times and incubated in the shaking incubator at 150 rpm for 10 min to mildly digest the connective tissue and release all lymph node cells. Subsequently, the solution was transferred onto a 70 µm strainer using blunted tips and mashed with the plunger of a syringe. The strainer was washed with 10 ml PBS. Afterwards the cell suspension was centrifuged at 400 g for 5 min at 4 °C. The cell pellet was resuspended and transferred to a 96 well U-bottom plate for staining.

3.2.3.2. Preparation of single cells – ear skin

For the isolation of single cells from the ears, ears were harvested and stored in PBS at 4 °C. Then, the dorsal and ventral side of the ear were separated using forceps and subsequently cut into small pieces in a 12-well plate followed by addition of digestion buffer. The minced tissue was digested in a shaking incubator (100 rpm) at 37 °C for 90 min in 500 µl of digestion buffer. After incubation, the tissue was further dissociated by pipetting the suspension with a blunted tip onto a 100 µm filter that was previously equilibrated with 1 ml FCS and the residual tissue on the filter was mashed using a syringe plunger. The filter was washed with 10 ml PBS, and the single cell solution was filtered a second time through a 70 µm cell strainer. Finally, the suspension was centrifuged at 4000 rpm for 10 min at 4 °C, the cell pellet was resuspended and transferred to a 96 well U-bottom plate for staining.

3.2.3.3. Preparation of single cells – back skin

For the isolation of single cells form the back skin, an adapted protocol of Broggi et al. (Broggi et al., 2016) was used. In brief, the shaved skin was freed from fat and connective tissue using forceps. 500 µl of back skin digestion buffer was added to the chopped skin tissue in a 48- or 24-well plate and incubated for 90 min at 140 rpm at 37°C for 90 min in an incubating shaker. Digested samples were filtered through a 70 µm strainer, equilibrated with 1 ml FCS into a 50 ml falcon tube. The strainer was washed with 5 ml RPMI and residual tissue was mashed with a syringe plunger. Afterwards the filter was washed with another 20 ml RPMI and the cell solution centrifuged at 4000 rpm for 10 min at 4°C. The cell pellet was resuspended and transferred to a 96 well U-bottom plate for staining.

3.2.3.4. Staining procedure

Cell surface staining was performed in V- or U-bottom plates. Cells were washed with 100 µl PBS and centrifuged at 400 g 5 min 4 °C. After discarding of the liquid, 50 µl of the prepared surface antibody mix were added to the cells and incubated for 30 min at 4 °C in the dark. When CCR4 was stained, a separate antibody mixture was prepared and cells were stained for 20 min at 37 °C, washed with 100 µl PBS, centrifuged at 400 g 5 min 4 °C before the surface staining was performed. Unspecific binding was avoided by addition of Fc-Block™. Subsequently, 100 µl PBS were added and cells were centrifuged at 400 g for 5 min at 4 °C. Before cell acquisition, 5 µl counting beads were added for calculation of total cell counts.

3.2.3.5. Intracellular staining of transcription factors

Intracellular staining was performed after staining of surface markers. Cells were fixed and permeabilized using the eBioscience™ FoxP3/transcription factor staining kit according to manufacturer's instructions. Antibodies were stained overnight in 50 µl permeabilization buffer shaking at 4°C. The following day, cells were washed using 100 µl permeabilization buffer at 400 g for 5 min at 4°C and then using PBS 400 g for 5 min at 4°C. For the measurement, cells were resuspended in 100 µl or 200 µl PBS and 5 µl counting beads were added for calculation of total cell counts.

3.2.4. Cell culture

3.2.4.1. Human Peripheral blood mononuclear cells (PBMC) isolation

Peripheral blood mononuclear cells (PBMCs) were isolated from peripheral blood of healthy volunteers by Ficoll density gradient centrifugation 400 g for 5 min at 4 °C, counted and kept on ice in FACS buffer until magnetic isolation of T cells.

3.2.4.2. Magnetic Activated Cell Sorting (MACS) T cells

Primary $CD4^+$ T cells were isolated using the MojoSort™ Human CD4 T Cell Isolation Kit from Biolegend according to manufacturer's instructions. Isolated cells were kept in cell culture in complete RPMI for up to 14 days.

3.2.4.3. Activation of primary T cells

Primary isolated $CD4^+$ T cells were activated using the T Cell Activation/Expansion Kit human form Miltenyi Biotec according to manufacturer's instructions. Activated cells were split and supplemented with fresh IL-2 every 3-4 days.

3.2.4.4. BW5147.3 cells culture

BW5147.3 cells were kept in complete RPMI and split based on confluency.

3.2.4.5. Human Mac1 cells culture

Mac1 cells were kept in complete RPMI and split based on confluency. Mac1 cells were kindly provided by M.E. Kadin. (Davis et al., 2010; Su et al., 1988)

3.2.4.6. Transwell migration assay with BW5147.3 cells/Mac1 cells

Cells were thawed one day prior to the assay and cultured in RPMI complete medium. On the day of the assay, cells were starved for 3.5 h in starvation medium at 37°C, 5 % CO_2. Lower chambers of 96-well transwell plates were filled with 235 µl starvation medium and supplemented with recombinant chemokines. When analyzing aptamer-dependent inhibition of migration, the bottom chamber was supplemented with murine CCL22 [12.8 nM] or CCL17 [12.6 nM] and aptamer or the matching aptamer control in 1:10 molar ratio [1.28 nM/1.28 nM], equimolar ratio [12.8 nM/ 12.6 nM] and 10:1 molar ratio [128 nM/ 126 nM]. The starved cells were adjusted to a concentration of 5 x 10^4 cells/ml, and 100 µl cell suspension were filled into the upper chambers. After a migration period of 2.5 h at 37°C ,5 % CO_2 the transmigrated cells in the lower chamber were harvested and quantified using flow cytometry.

3.2.4.7. Transwell migration assay with primary human $CD4^+$ T cells

Activated primary human CD4 T cells were starved for 3.5 h in starvation medium at 37°C 5 % CO_2. Lower chambers of 96-well transwell plates were filled with 235 µl starvation medium and supplemented with recombinant chemokines. When analyzing aptamer-dependent inhibition of migration, the bottom chamber was supplemented with human CCL22 [12.8 nM] or CCL17 [12.6 nM] and aptamer or the matching aptamer control in 1:10 molar ratio [1.28 nM/1.28 nM], equimolar ratio [12.8 nM/ 12.6 nM] and 10:1 molar ratio [128 nM/

126 nM]. The starved cells were adjusted to a concentration of 5 x 10^4 cells/ml, and 100 µl cell suspension were filled into the upper chambers. After a migration period of 2.5 h at 37°C 5 % CO_2 the transmigrated cells in the lower chamber were harvested and quantified using flow cytometry.

3.2.5. Protein isolation from ear tissue

Ears were snap frozen in liquid nitrogen after organ harvest and stored in cryotubes at -80°C until protein isolation. For isolation, the skin was thawed on ice and the connective and fat tissue was removed using forceps. Subsequently, the ears were cut into smaller pieces and transferred to a screw cap tube filled with glass pearls and 200 µL of 1x RIPA buffer with 1x protease inhibitor. Next, the skin tissue was disrupted at 6500 3 x 30 s using the Precellys®24 tissue homogenizer and lysates were transferred to a fresh tube. The tube was washed with another 200 µL of 1x RIPA buffer with protease inhibitor and lysates were centrifuged at 16,000 g for 15 min at 4°C to clear proteins from residual tissue.

3.2.6. Determination of protein concentration

Protein concentration of isolated protein solution of tissue was determined using Pierce™ BCA Protein Assay Kits from ThemoFisher according to manufacturer's instructions.

3.2.7. Enzyme-linked immunosorbent assay (ELISA)

Chemokine or cytokine concentration was measured by Enzyme Linked Immunosorbent Assay (ELISA) according to the manufacturer's instructions.

3.2.8. Real Time Quantitative PCR (qPCR)

3.2.8.1. RNA isolation

To isolate whole RNA, colons were cleaned from intestinal content and fat. Then, samples were transferred into glass bead tubes and snap frozen in liquid nitrogen and subsequently stored at -80°C until further usage. 600µl of QIAzol Lysis Reagent were added to the tissue samples immediately before thawing. Tissue lysis and homogenization was performed with a tissue homogenizer at 6000 rpm (3x20 s). RNA was isolated using the Zymo Research Directzol MiniPrep kit according to the manufacturer's instructions. RNA was eluted with 50µl of DNase/RNase free water and RNA concentration was determined using the NanoDrop1000 Photospectrometer. The RNA was stored at -80°C for further procedures.

3.2.8.2. cDNA synthesis

RNA was transcribed into complementary DNA (cDNA) by reverse transcriptase. The RNA was diluted to the desired concentration in DNase/RNase free water. A maximum volume of 10 µl RNA was used. RNA was mixed with 3 µl Oligo(dT)12-18 primer for hybridization to the poly(A) tail. The mixture was incubated for 10 minutes at 72°C to unfold and denature the RNA and allow the primers to anneal to the RNA. Then the samples were cooled down on ice and a master mix was added. After an incubation of 1 h at 42°C a final step of 5 min incubation at 95°C to inactivate the reverse transcriptase was performed.

Table 3.10 | cDNA sythesis protocol

	Volume (1 reaction)
DEPC water	9 µl
5 x RT buffer	8 µl
dNTP (10nM)	4 µl
DTT (100mM)	4 µl
Ribolock (40 U/µl)	1 µl
RT (200 U/µl)	1 µl
	27 µl

3.2.8.3. qPCR protocol

The cDNA was used as a template for amplification via PCR. To the SYBR Green Mix that contains SYBR Green I dye and Thermo-Start DNA Polymerase the cDNA and primers were added. By emission of green light by the SYBR dye newly synthesized double-stranded DNA can be measured. 15 µl qPCR mix contained 7.5 µl qPCR SYBR Green Mix, 0.3 µl forward primer (10 µmol/l), 0.3 µl reverse primer (10 µmol/l), 1.9 µl water and 5 µl cDNA.

Table 3.11 | qPCR protocol

	Step	**Temperature**	**Time interval**
	Initial denaturation	95°C	15 min
Repetition 40 times	Denaturation	95°C	15 sec
	Annealing	60°C	60 sec
	Melting curve measurement	65°C - 95°C by steps of 0,5°C	5 sec per step

3.2.8.4. Analysis of qPCR

For analysis, first the quality of the qPCR was evaluated by checking the water control, comparing technical replicates, and visualizing the melting points of the produced amplicons. Afterwards the ΔΔCt method was performed for relative quantification of gene expression. For this, the mean cycle threshold (Ct) value between technical replicates was calculated and all mean Ct values obtained were normalized against the housekeeping gene. Afterwards, these ΔCt values were normalized against the untreated naive colon controls to obtain the respective ΔΔCt value. To obtain relative expression differences, the log2-scaled ΔΔCt values were shown as negative power of two.

3.2.9. Franz diffusion cell

3.2.9.1. Franz diffusion cell assay

After sacrifice, ears of the mice were tape-stripped ten times, incubated for 1 min in antibiotic/antimycotic reagent and separated into dorsal and ventral halves. The dorsal side was put on the lower chamber of an unjacketed Franz-diffusion cell (2 ml volume, 5 mm pore) with the dermal side facing the receptor chamber. DAC cream with or without fluorescently labeled AJ102.29 or AJ102.29ctrl [10 pmol/mg] was applied on the epidermal side of the skin. Donor and receptor chamber were tightly sealed with a clamp. The receptor chamber was filled with 2 ml complete RPMI. After a 24 h incubation period on a magnetic stirrer at 37°C 5 % CO_2 the Franz-diffusion cell was disassembled. The skin was gently wiped with a HBSS drained tissue to remove excess of cream. Subsequently the skin piece was embedded into cryo freezing medium and 10 µm slices were prepared for staining.

3.2.9.2. Franz diffusion cell kinetic

Before and during the Franz diffusion cell assay probes of the media in the bottom chamber were taken via the sampling port and frozen until further use. Then, samples were used in a qPCR assay to quantify penetration of the skin by the aptamer. 1 µl of the qPCR master mix containing specific primers for the aptamer used, were added to 6.9 µl of the 1:5.9 diluted full-medium samples. Triplicates or quadruplicates of samples from each Franz cell assay at each time point were measured. For quantification, a dilution series of the aptamer (5 pmol/ml top standard) was added. For analysis of the qPCR the quality was evaluated by checking the water and medium control, comparison of technical replicates and visualization of the melting points of the generated amplicons. Ct values were further analyzed by calculating the mean between the technical replicates and by subtracting the mean Ct-value of each sample from the mean

Ct-value of the full-medium control. Concentrations were calculated using linear regression of the standard dilution series.

Table 3.12 | Franz assay qPCR protocol

	Step	**Temperature**	**Time interval**
	Initial denaturation	95°C	15 min
Repetition 40 times	Denaturation	95°C	15 sec
	Annealing	59°C	60 sec
	Melting curve measurement	65°C - 95°C by steps of 0.5°C	5 sec per step

3.2.10. Multiplex assay to determine concentrations of inflammatory mediators in mouse sera

To determine the concentration of various inflammatory cytokines and chemokines the LEGENDplex™ Mouse Inflammation Panel from Biolegend was used according to manufacturer's instructions.

3.2.11. Statistical analysis

All statistical analyses were performed with GraphPad Prism 9.2.0. The statistical tests used are indicated in each figure legend. P-values were calculated to determine statistical significance. A p-value of ≤ 0.05 was considered significant (*p=0.01-0.05, **p=0.001-0.01, ***p<0.001, ****p<0.0001). Data are represented as mean values ± standard deviation or standard error of the mean as indicated in the figure legends.

4. Results

4.1. Pharmacological blockage of the CCL17/CCL22-CCR4-axis using aptamers in the context of contact hypersensitivity

The CCL17/CCL22-CCR4-axis is known to play a role in the pathogenesis of allergic diseases such as allergic asthma, AD and ACD (Matsuo et al., 2019; Nakatani et al., 2001; Quoc et al., 2022; Sebastiani, Albanesi, De Pità, et al., 2002; Sebastiani, Albanesi, Nasorri, et al., 2002; Staples et al., 2012). Remarkably, increased levels of CCL17 and CCL22 have been detected in sera of patients suffering from contact allergies (Shimada et al., 2004). Moreover, a relation between CCL17/CCL22 expression and immigration of T cells into inflamed skin has been demonstrated (Jinquan & Thestrup-Pedersen, 1995; Matsuo et al., 2018; Sebastiani, Albanesi, De Pità, et al., 2002; Stutte et al., 2010; Vestergaard et al., 2000).

Our group previously also investigated the role of the CCL17/CCL22-CCR4-axis in CHS, a mouse model for ACD. There, it has been shown that lack of either CCL17 or CCL22 or both CCL17 and CCL22 can suppress allergic symptoms in CHS, whereas the lack of the receptor CCR4 led to an increased allergic reaction. Furthermore, it was possible to show that pharmacological blockage of CCL17 by RNA aptamers efficiently ameliorated CHS symptoms (Fülle, Steiner, et al., 2018). In the current work, duration of action and application times and -routes of the CCL17-specific aptamer MF35.47m were investigated in the context of CHS to further analyze their therapeutic efficacy.

To understand the role of CCL22 in ACD as well as to elucidate the potential of blocking CCL22 action *in vivo,* we tested newly generated CCL22-specific DNA aptamers in WT mice next to $CCL22^{-/-}$ mice. To test the efficiency of the aptamers we used transwell migration assays as well as the CHS. In the CHS model, mice are sensitized with DNFB at day -5 and -4 and are challenged with DNFB on day 0. In the following days the allergic reaction is measured by ear swelling caused by immune cell infiltration into the ears (Zemelka-Wiacek et al., 2022). At last, in order to translate our research to human allergic dermatitis, we generated aptamers against human CCL17 and CCL22.

4.1.1. Analysis of the therapeutic efficacy of CCL17-specific aptamers

To get better insight into the duration of action of the CCL17-specific RNA aptamer MF35.47m *in vivo*, a series of experiments changing the time point of treatment and the timing of the biological readout were performed (Fülle, Steiner, et al., 2018). In these experiments it was assessed how long a suppressive effect of aptamers persists, as well as whether the suppressive effects of aptamer application were effective also for a second challenge, and whether application at a later time point than 1 h prior and 12 h post DNFB challenge would also lead to a reduction in allergic symptoms in CHS. These results are of relevance to estimate the time window of therapeutic efficacy of the aptamer for treatment of contact allergies. For this purpose, the CCL17-specific aptamer MF35m was used (Fülle, Steiner, et al., 2018).

4.1.1.1. Testing the duration of action of CCL17-specific aptamers in CHS

To investigate the perseverance of the suppressive effects of the CCL17-blocking RNA aptamer MF35.47m, WT mice received MF35.47m intraperitoneally 48 h, 24 h and 1 h before the DNFB challenge. Ear swelling and T cell infiltration into the ears was analyzed on day 3 after challenge and were compared to CCL17$^{E/E}$ mice and WT mice that received the matching scrambled aptamer control **(Figure 4.1)**.

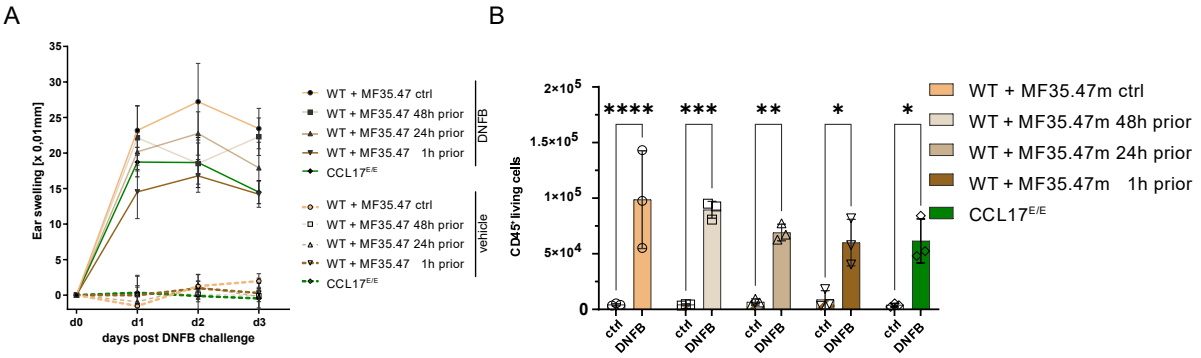

Figure 4.1 | Duration of action of CCL17-specific aptamer MF35.47m tested in a contact hypersensitivity.
WT and CCL17$^{E/E}$ mice were sensitized with DNFB on day −5 and day −4. On day 0, WT mice were i.p. injected with 5 nmol MF35.47m and MF35.47m ctrl 48 h, 24 h, and 1 h before DNFB challenge. (A) Ear swelling of WT and CCL17$^{E/E}$ mice 24 h (day 1), 48 h (day 2), and 72 h (day 3) after application of DNFB (solid lines) or vehicle (dashed lines) Statistical significance was tested using two-way ANOVA with Bonferroni post hoc test for multiple comparisons (n = 3 per group, mean±SEM, *p=0.01-0.05, **p=0.001-0.01, ***p<0.001, ****p<0.0001).(B) Flow cytometric analysis of the immune cell infiltrate of the ears. At day 3, mice were sacrificed, and cells of the ears were isolated and stained for flow cytometry. Absolute numbers of CD45$^+$ were determined by flow cytometry. Statistical significance was tested using two-way ANOVA with Bonferroni post hoc test for multiple comparisons (n = 3 per group, mean ± SEM, *p=0.01-0.05, **p=0.001-0.01, ***p<0.001, ****p<0.0001).

Although changes were not significant, the ear swelling of CCL17$^{E/E}$ mice and mice that received the aptamer 1h before challenge were lowest, whereas the mice that received the scrambled control demonstrated the strongest ear swelling followed by the mice treated with the aptamer 48h prior to the challenge **(Figure 4.1 A)**. These results were also consistent with

the numbers of infiltrated immune cells into the DNFB-treated ears **(Figure 4.1 B)**. As expected, the DNFB challenged ears of CCL17$^{E/E}$ mice contained the least CD45^{+} lineage^{-} cells together with the mice that received the aptamer 1 h before challenge, followed by the cohorts in which the aptamer got injected 24 h and 48 h before challenge. Interestingly, the mice that received the aptamer 48h before the DNFB challenge had almost as high numbers of immune cells as the control mice. Hence, with increasing time span between injection of the aptamers and the DNFB challenge the suppressive effect of the aptamers decreased, which is most likely due to degradation, renal excretion, or absorption of the aptamer in tissues. Additionally, early administration of the aptamer could also interfere with the sensitization.

For the analysis of T cell infiltration, immune cells were further separated into T cell subsets and frequencies and cell numbers were compared between cohorts **(Figure 4.2)**.

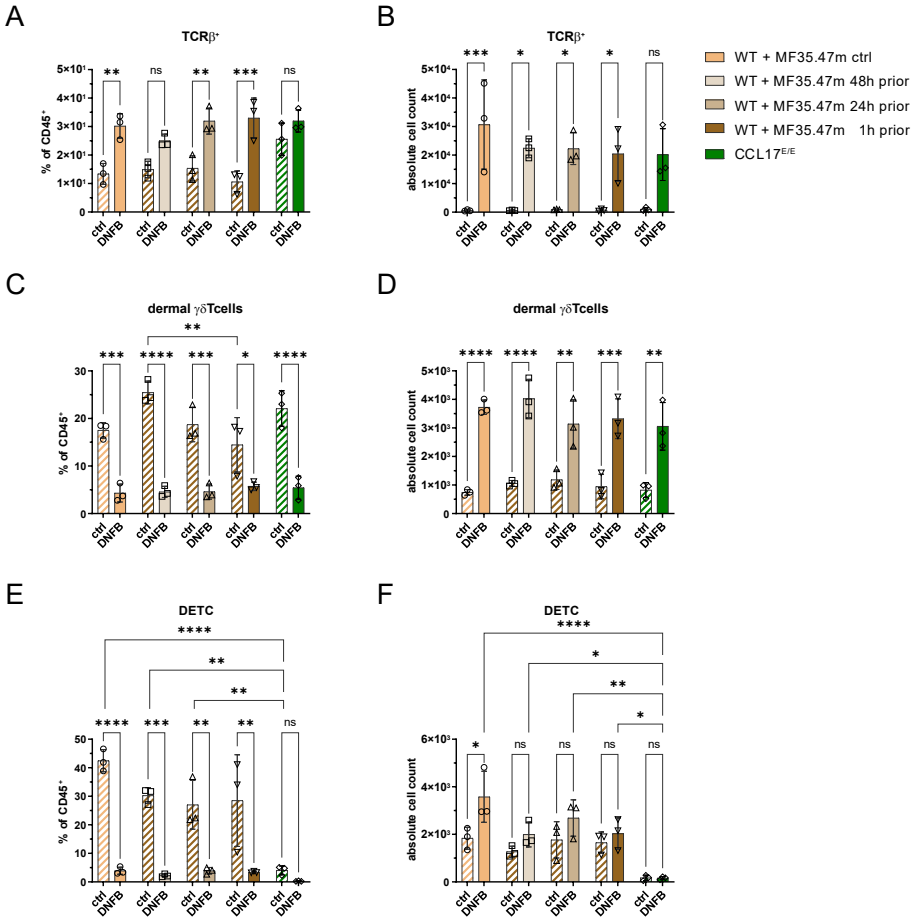

Figure 4.2 | Frequencies and absolute cell counts of T cell subsets in the ears of mice after induction of CHS with application of CCL17-specific aptamers.
WT and CCL17$^{E/E}$ mice were sensitized with DNFB on day −5 and day −4. On day 0, WT mice were i.p. injected with 5 nmol MF35.47m and MF35.47m ctrl 48 h, 24 h, and 1 h before DNFB challenge. Depicted are the frequencies and absolute cell counts of (A, B) TCRβ^{+} T cells, (C, D) dermal γδ T cells and (E, F) Dendritic Epidermal T Cells (DETC) isolated from ear skin after CHS induction and analyzed by flow cytometry. Statistical significance was tested using two-way ANOVA with Bonferroni post hoc test for multiple comparisons (n = 3 per group, mean ± SEM, *p=0.01-0.05, **p=0.001-0.01, ***p<0.001, ****p<0.0001).

While the frequency of conventional T cells did not differ strongly between cohorts, the cell numbers were lowest in CCL17$^{E/E}$ mice, followed by the mice injected with the aptamer 1h, 24 h and 48 h respectively. **(Figure 4.2 A, B)**. As observed in the other CHS experiments, dermal γδ T cells decreased in percentage after challenge, whereas their cell counts increased in every cohort **(Figure 4.2 C, D)**. Correspondingly, the absolute dermal γδ T cells numbers in DNFB-treated ears were lowest in the CCL17$^{E/E}$ mice, while the ears of the control cohort as well as the 48 h cohort contained most γδ T cells. Also, the percentage of DETC declined after DNFB application in every cohort **(Figure 4.2 E)**. Interestingly, the percentage as well as absolute cell numbers of DETC in CCL17$^{E/E}$ mice was already significantly lower in vehicle-treated ears compared to the other cohorts. Similarly, the DNFB-treated ears of CCL17$^{E/E}$ contained only very low numbers of DETC thereby being significantly lower than the other cohorts when comparing the allergic ears **(Figure 4.2 F)**.

To assess the effect of the treatment on individual T cell subsets, conventional T cells were further separated into CD4$^+$ T cells, CD8$^+$ T cells and Treg **(Figure 4.3)** using the previously established gating strategy **(Figure 4.17)**.

For the CD4 and CD8$^+$ T cell subsets the same tendencies as for the total T cell population could be observed. The percentage of CD8$^+$ T cells did not differ between cohorts **(Figure 4.3 A)**. With decreasing time between aptamer injection and challenge, however, less CD8$^+$ T cells infiltrated the DNFB-treated ears, while the DNFB-treated ears of CCL17$^{E/E}$ contained the fewest CD8$^+$ T cells **(Figure 4.3 B)**. Neither for the frequencies, nor for the cell numbers of CD4$^+$ T cells large differences between cohorts were visible **(Figure 4.3 C, D)**. Notably, the number of infiltrated Treg decreased significantly in the DNFB-treated ears with decreasing time distance between the aptamer treatment and DNFB challenge. In line, ears of DNFB-challenged CCL17$^{E/E}$ mice contained the least Treg **(Figure 4.3 F)**. This was also reflected in the numbers of activated Treg **(Figure 4.3 H)**. Furthermore, the CCL17$^{E/E}$ mice had significantly enhanced frequencies of activated Treg in the vehicle-treated ears compared to the WT mice that received the aptamer 1 h before challenge **(Figure 4.3 G)**.

Taken together, the finding that with increasing time between aptamer injection and DNFB challenge more T cells infiltrate the ears holds true for conventional T cells, CD8$^+$ T cells, and Treg whereas the overall CD4$^+$ T cells are less affected.

Conclusively, the effectiveness of aptamer application increases the closer the application to the DNFB challenge indicating a duration of action between 12.

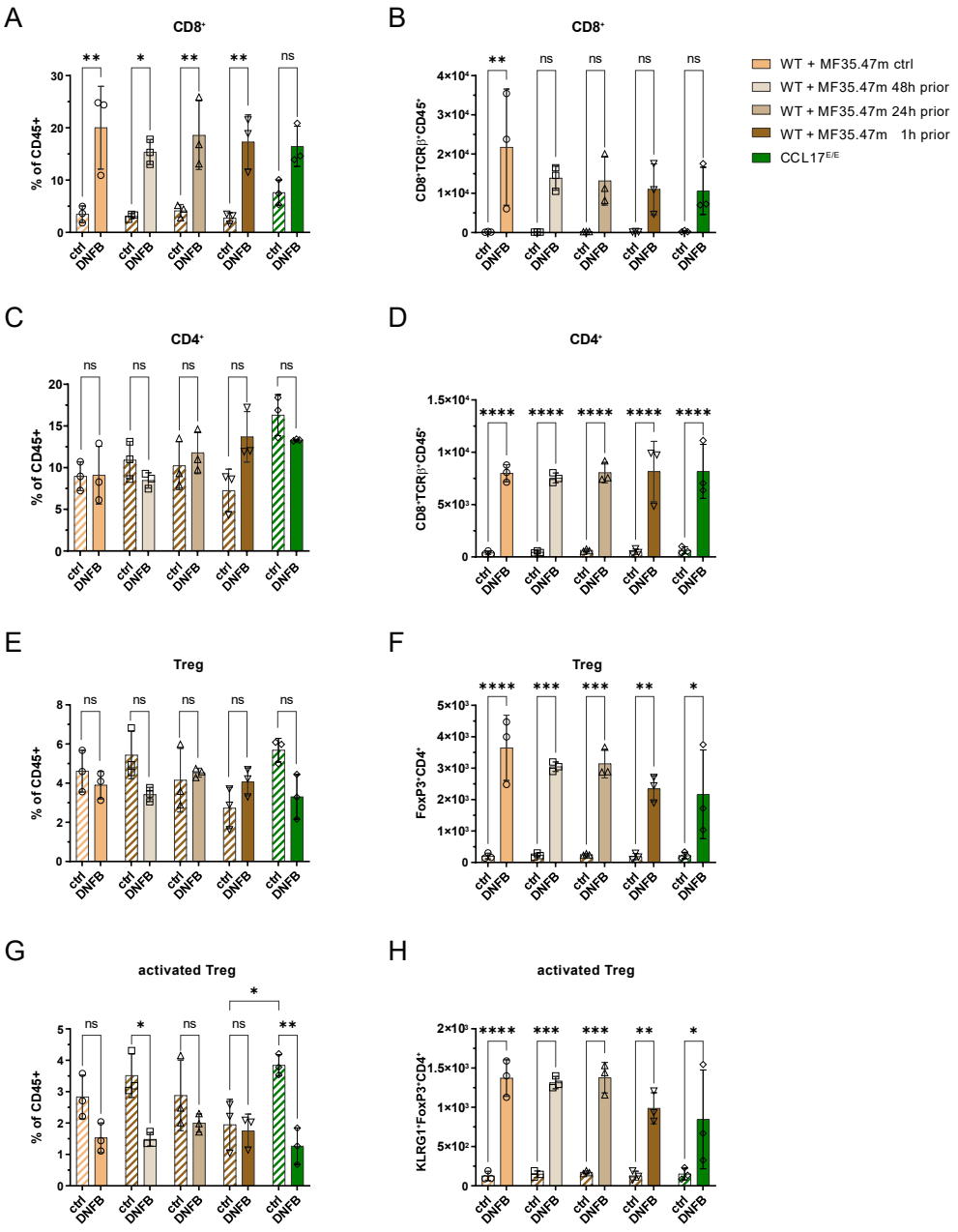

Figure 4.3 | Frequencies and absolute cell counts of conventional T cell subsets in the ears of mice after induction of CHS with application of CCL17-specific aptamers.
WT and CCL17$^{E/E}$ mice were sensitized with DNFB on day −5 and day −4. On day 0, WT mice were i.p. injected with 5 nmol MF35.47m and MF35.47m ctrl 48 h, 24 h, and 1 h before DNFB challenge. Depicted are the frequencies and cell count of (A, B) CD8$^+$ T cells, (C, D) CD4$^+$ T cells, (E, F) FoxP3$^+$ Treg and (G, H) KLRG1$^+$ Treg isolated of the ear skin after an contact hypersensitivity. Statistical significance was tested using two-way ANOVA with Bonferroni post hoc test for multiple comparisons (n = 3 per group, mean ± SEM, *p=0.01-0.05, **p=0.001-0.01, ***p<0.001, ****p<0.0001).

4.1.1.2. Assessment of duration of CCL17 inhibition after repeated challenge with DNFB

In order to find out whether application of aptamers once would lead to possible long-term effects in terms of amelioration of allergic symptoms, the CCL17 aptamer MF35.47m was applied during the first but not the second challenge in a 14 day-long CHS experiment similar to the model from Gaffal and colleagues (Gaffal et al., 2013).

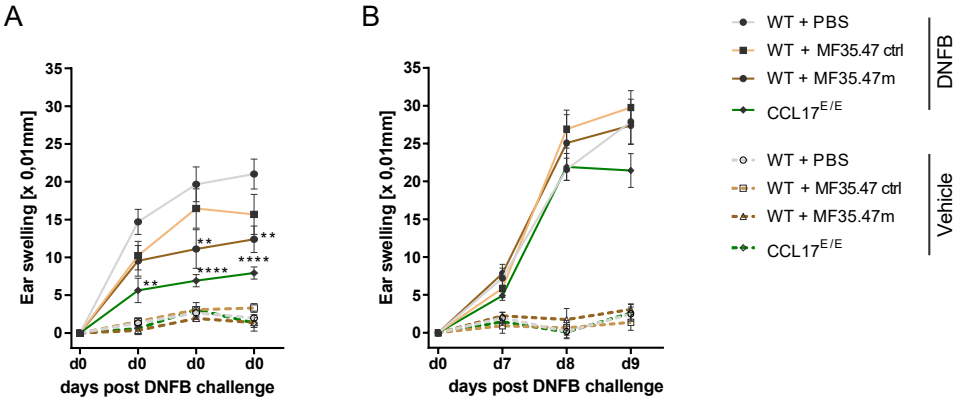

Figure 4.4 | Long-term effects of application of the CCL17-specific aptamer MF35 after repeated challenge with allergen
WT and CCL17$^{E/E}$ mice were sensitized with DNFB on day −5 and day −4. On day 0, WT mice were i.p. injected with 5 nmol MF35.47m and MF35.47m ctrl or PBS 12 h before and 1 h after the first DNFB challenge on day 0, but not at the second challenge on day 6. (A) Ear swelling response of WT and CCL17$^{E/E}$ mice 24 h (day 1), 48 h (day 2), and 72 h (day 3) after first application of DNFB (solid lines) or vehicle (dashed lines) and (B) on day 7, day 8 and day 9 after the challenge with DNFB or vehicle (n = 3 per group, mean ± SEM Statistical significance was tested using two-way ANOVA with Bonferroni post hoc test for multiple comparisons, *p=0.01-0.05, **p=0.001-0.01, ***p<0.001, ****p<0.0001).

Ear swelling measurements after both challenge time points revealed a significant reduction of ear thickness in the aptamer-treated mice compared to WT mice treated with PBS only after the first DNFB challenge **(Figure 4.4 A)**. As shown in previous experiments the CCL17$^{E/E}$ mice demonstrated the least swelling of ears, while the mice that were treated with the scrambled control had a similar ear swelling response as WT control mice. In contrast, after the second DNFB challenge no amelioration of ear swelling was observed for the aptamer-treated mice **(Figure 4.4 B)**. Of note, even the ear thickness of CCL17$^{E/E}$ mice was not significantly reduced compared to the control mice, though still showing the least swelling.

T cell status in the ears was measured by flow cytometry 3 days after the second challenge **(Figure 4.5)**. An increase in CD45^{+} lineage^{-} cells that migrated into the ears upon DNFB stimulation was still measurable in all cohorts but did not show differences in frequency or cell counts between the different cohorts **(Figure 4.5 A, B)**. A similar finding was also observed for the conventional T cells. The frequency of conventional T cells increased upon DNFB treatment to a similar extent in all cohorts, and cell number measurements revealed no significant differences between analyzed cohorts **(Figure 4.5 C, D).** Interestingly, aptamer control mice contained the fewest conventional T cells of all cohorts analyzed. Whereas the percentage of

dermal γδ T cells decreased in all cohorts, the number of dermal γδ T cells increased in the DNFB-treated ears compared to the respective control ears **(Figure 4.5 E, F)**, which is different to what has been observed for one challenge CHS experiments. However, no significant alterations between the different treatment groups could be detected. The percentage of DETC was reduced in all cohorts upon DNFB stimulation, with $CCL17^{E/E}$ having the least percent of DETC **(Figure 4.5 G)**. However, $CCL17^{E/E}$ mice already had a reduced percent of DETC in the vehicle control-treated ears, similar to what was observed in the experiment before **(Figure 4.5 H)**. Additionally, the number of DETC was lowest in both ears of the $CCL17^{E/E}$ mice. In this case, the DNFB-treated ears showed a significant reduction of DETC numbers compared to the WT mice that got administered the scrambled control. Furthermore, the absolute DETC counts were lower than in previous experiments with only one DNFB challenge.

Next, $CD4^+$ T cells, $CD8^+$ T cells and Treg were further analyzed **(Figure 4.6)**.

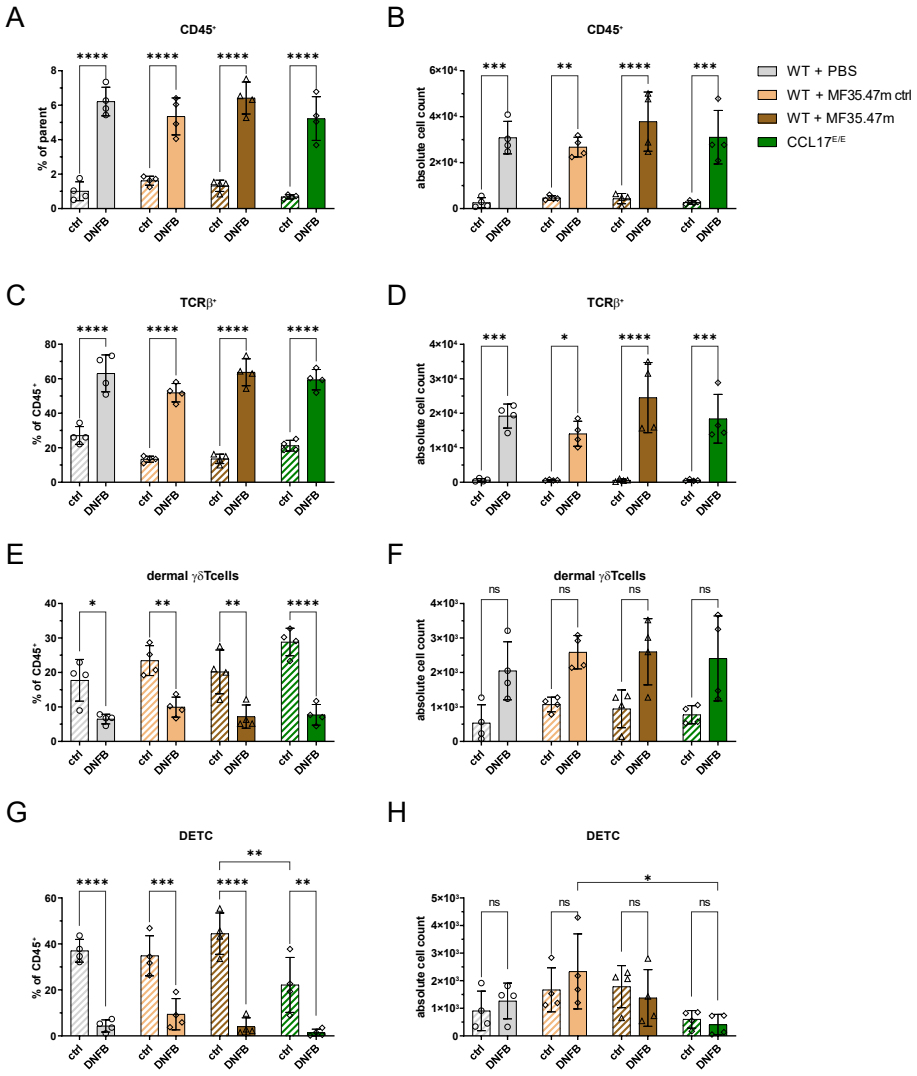

Figure 4.5 | Frequencies and absolute cell counts of T cell subsets in the ears of mice on day 3 after a second challenge during a CHS experiment with CCL17 aptamer MF35.47m application.
WT and CCL17$^{E/E}$ mice were sensitized with DNFB on day −5 and day −4. On day 0, WT mice were i.p. injected with 5 nmol MF35.47m and MF35.47m ctrl or PBS 12 h before and 1 h after the first DNFB challenge on day 0, but not at the second challenge on day 6. Depicted are the frequencies and cell count (A, B) of CD45$^+$, (C, D) TCRβ$^+$ T cells, (E, F) dermal γδ T cells and (G, H) DETC. (n = 3 per group, mean ± SEM Statistical significance was tested using two-way ANOVA with Bonferroni post hoc test for multiple comparisons, *p=0.01-0.05, **p=0.001-0.01, ***p<0.001, ****p<0.0001).

Neither in frequencies, nor in cell numbers did the CD8$^+$ T cells differ between cohorts **(Figure 4.6 A, B).** CCL17$^{E/E}$ mice that were treated with DNFB had the highest percentage of CD4$^+$ T cells and their frequency was significantly higher than that of WT control mice **(Figure 4.6 C)**. In addition, numbers of CD4$^+$ T cells increased upon DNFB stimulation compared to the respective control ears in each cohort, yet no significant differences could be detected **(Figure 4.6 D)**. While the percent of Treg significantly decreased in the DNFB-treated ears of control WT mice and CCL17$^{E/E}$ mice, the Treg number increased in all cohorts **(Figure 4.6 E, F)**. Interestingly, ears of CCL17$^{E/E}$ mice contained the most Treg, followed by the mice that received the aptamer MF35.47m. Additionally, this was also reflected in the number of

activated Treg as the most activated Treg were found in mice that received the aptamer and in CC17$^{E/E}$ mice **(Figure 4.6 H)**. Nevertheless, no differences between cohorts were detectable when analyzing the frequency of activated Treg **(Figure 4.6 G)**.

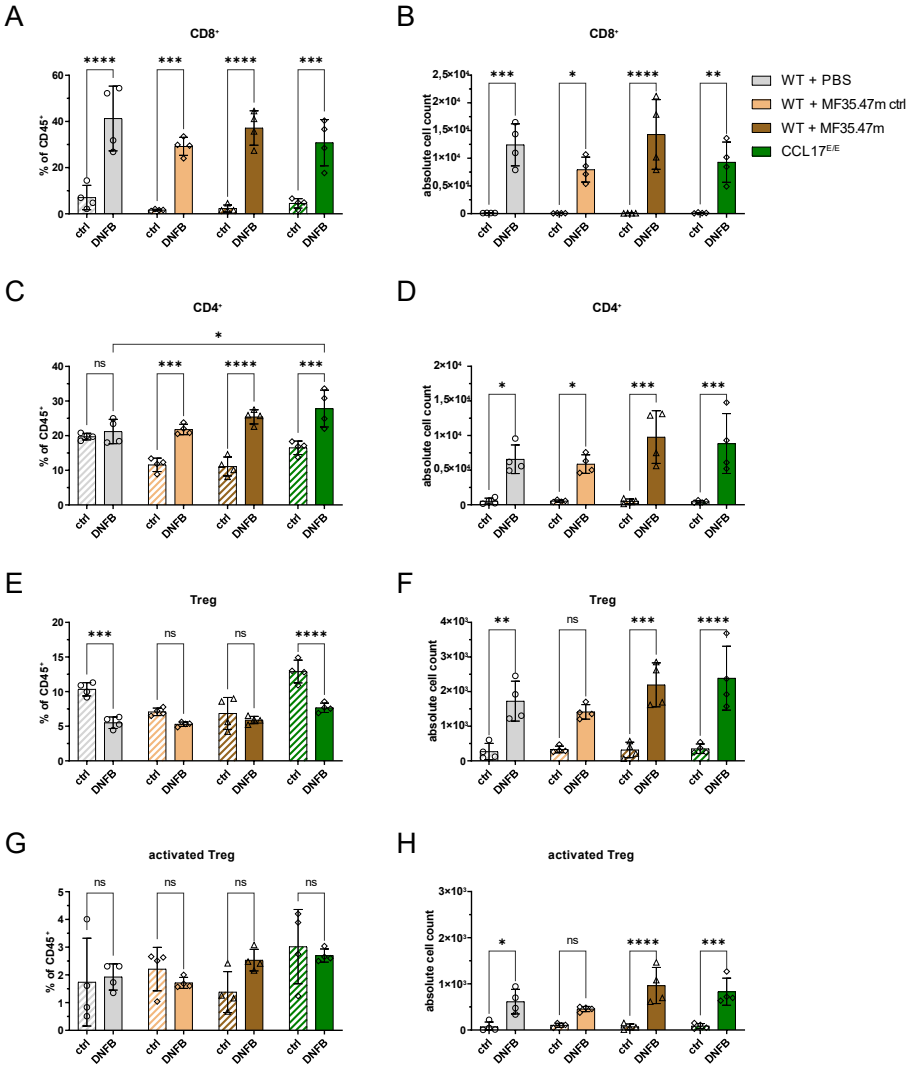

Figure 4.6 | Frequencies and absolute cell counts of conventional T cell subsets in the ears of mice on day 3 after a second challenge during a CHS experiment with CCL17 aptamer MF35 application.
WT and CCL17$^{E/E}$ mice were sensitized with DNFB on day −5 and day −4. On day 0, WT mice were i.p. injected with 5 nmol MF35.47m and MF35.47m ctrl 12 h before and 1 h after the first DNFB challenge on day 0, but not at the second challenge on day 6. Depicted are the frequencies and cell count (A, B) of CD8$^+$, (C, D) CD4$^+$, (E, F) FoxP3$^+$ Treg and (G, H) KLRG1$^+$ FoxP3$^+$ activated Treg isolated of the ear skin after an contact hypersensitivity. (n = 3 per group, mean ± SEM Statistical significance was tested using two-way ANOVA with Bonferroni post hoc test for multiple comparisons, *p=0.01-0.05, **p=0.001-0.01, ***p<0.001, ****p<0.0001).

Taken together, the decreased ear swelling response and reduced infiltration of immune cells into the ears caused by genetic CCL17 deficiency or pharmacological blocking of CCL17 using CCL17-specific aptamers, was not detectable after a second challenge in contrast to the reduction observed after primary challenge. Interestingly, the number of Treg and activated Treg were increased in aptamer-treated and CCL17-deficient mice, indicating an influence of CCL17 deficiency on the Treg count. The reduced ear swelling response in aptamer-treated

mice after the first challenge was similar to previous CHS experiments showing that the aptamers successfully ameliorated allergic symptoms and thereby T cell infiltration into the ears. However, the loss of a suppression and the change in T cell status after the second challenge compared to previous one-challenge CHS experiments might indicate that the cellular mechanisms for this two-challenge CHS model is different as the immunological state at the time of the second challenge is different to the initial state.

4.1.1.3. Effects on allergic symptoms of CCL17-specific aptamer application at a later timepoint after elicitation of contact hypersensitivity

Because therapeutic use of aptamers would likely be most relevant after a second contact with the hapten has already occurred, we compared the well-established application time points of 1h and 12h post challenge with the application of MF35.47m 24h after the DNFB challenge.

The DNFB-treated ears of mice that received the aptamers at 1 h before and 12 h after challenge, showed a significant reduction in the ear swelling response compared to WT control mice **(Figure 4.7 A)**. Interestingly, for mice that received the aptamer 24 h post DNFB challenge, the ear swelling response on day 1 was comparable to WT mice but showed a decrease in ear swelling response on the following days. No reduction in immune cell infiltration could be measured in these mice in DNFB-stimulated ears **(Figure 4.7 B)**.

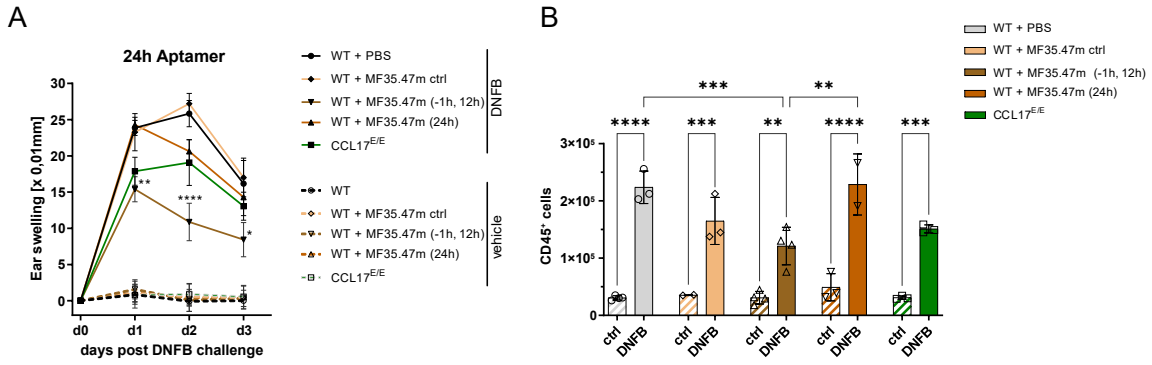

Figure 4.7 | Ear swelling and immune cell infiltrate in the ears of mice after induction of CHS with therapeutic application of CCL17-specific aptamers in DAC cream.
WT and CCL17$^{E/E}$ mice were sensitized with DNFB on day −5 and day −4. On day 0, WT mice were i.p. injected with 5 nmol MF35.47m 24 h post DNFB challenge and with MF35.47m and MF35.47m ctrl 1 h prior and 12 h post challenge. (A) Ear swelling of WT and CCL17$^{E/E}$ mice 24 h (day 1), 48 h (day 2), and 72 h (day 3) after application of DNFB (solid lines) or vehicle (dashed lines) (n = 3 per group, mean ± SEM Statistical significance was tested using two-way ANOVA with Bonferroni post hoc test for multiple comparisons, *p=0.01-0.05, **p=0.001-0.01, ***p<0.001, ****p<0.0001). (B) Flow cytometric analysis of the immune cell infiltrate of the ears. At day 3, mice were sacrificed, and cells of the ears were isolated and stained for flow cytometry. Absolute numbers of CD45^{+}were determined by flow cytometry. Statistical significance was tested using two-way ANOVA with Bonferroni post hoc test for multiple comparisons (n = 2-4 per group, mean ± SEM, *p=0.01-0.05, **p=0.001-0.01, ***p<0.001, ****p<0.0001).

Additionally, T cell subsets were analyzed based on the established gating strategy **(Figure 4.27)**. The frequencies of conventional T cells did not differ between cohorts **(Figure 4.8 A)**. In

this experiment, the number of conventional T cells was lowest in the mice that received the aptamer control and the aptamer at the established time points of 1 h prior to the challenge and 12 h post challenge. However, data varied strongly for the other cohorts **(Figure 4.8 B)**. Furthermore, no significant changes between cohorts were measured. The percentage of dermal γδ T cells did not show differences either **(Figure 4.8 C)**. Nevertheless, different to one challenge CHS experiments, the number of γδ T cells increased upon hapten stimulation and was significantly higher in the WT control mice compared to all cohorts but the mice treated with aptamer 24 h post challenge cohort **(Figure 4.8 D)**. Of note, neither the frequency of DETC, nor the DETC count differed between the analyzed cohorts **(Figure 4.8 E, F)**. Again, the CCL17$^{E/E}$ mice demonstrated the lowest percentages and absolute cell numbers of DETC as observed in the previous experiments.

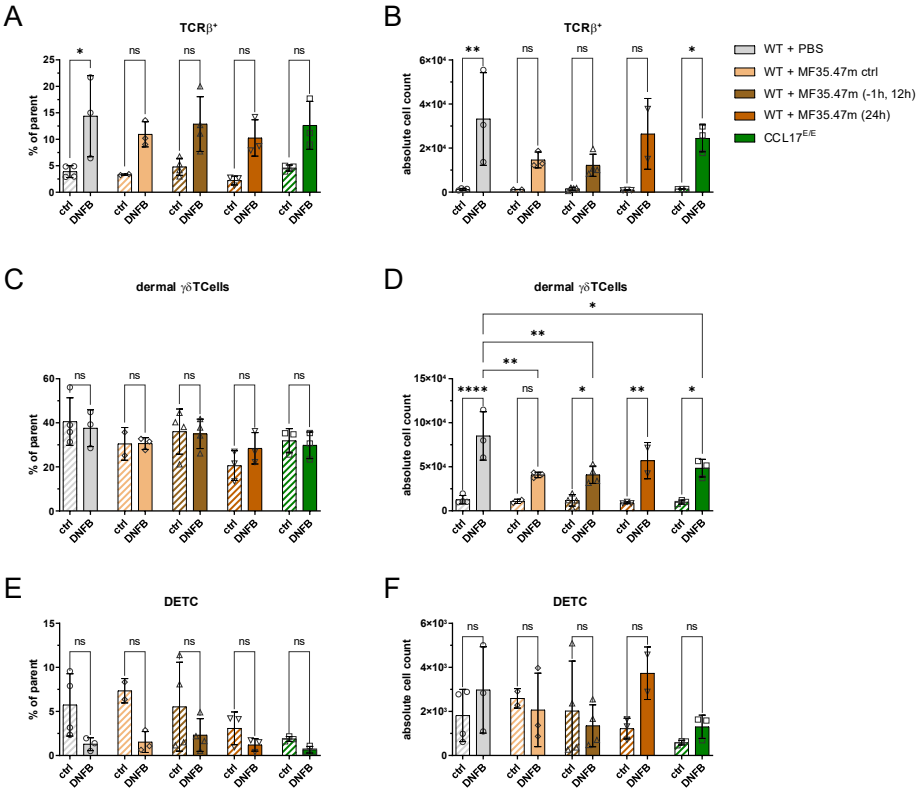

Figure 4.8 | Frequencies and absolute cell counts of T cell subsets in the ears of mice after induction of CHS with therapeutic application of CCL17-specific aptamers in DAC cream.
WT and CCL17$^{E/E}$ mice were sensitized with DNFB on day −5 and day −4. On day 0, WT mice were i.p. injected with 5 nmol MF35.47m 24 h post DNFB challenge and with MF35.47m and MF35.47m ctrl 1 h prior and 12 h post challenge. Depicted are the frequencies and cell count of (A, B) TCRβ$^+$ T cells, (C, D) dermal γδ T cells and (E, F) DETC isolated of the ear skin after a contact hypersensitivity. Statistical significance was tested using two-way ANOVA with Bonferroni post hoc test for multiple comparisons (n = 2-4 per group, mean ± SEM, *p=0.01-0.05, **p=0.001-0.01, ***p<0.001, ****p<0.0001).

Whereas the frequency of CD8$^+$ T cells did not show significant alteration between cohorts, the DNFB-treated ears of WT control mice had significantly more CD8$^+$ T cells than both aptamer- and the aptamer control-treated mice, but not CCL17$^{E/E}$ mice **(Figure 4.9 A, B)**.

Additionally, the number of $CD8^+$ T cells in the mice that received the aptamer at -1 h and 12 h post challenge was also significantly reduced compared to the $CCL17^{E/E}$ mice. In contrast, neither the frequencies nor the number of $CD4^+$ T cells demonstrated any significant alterations between treatments or cohorts **(Figure 4.9 C, D)**. Additionally, the variations between the samples were quite high. The frequency of Treg was highest in the WT control mice, whereas the mice that received the aptamer 24h post challenge showed the least rate of Treg **(Figure 4.9 E)**. Nevertheless, the lowest Treg number after DNFB application were obtained in the cohort in which the aptamer was administered at -1 h and 12 h post DNFB challenge thus showing a significant decrease compared to WT control mice **(Figure 4.9 F)**. This is also reflected in the activated Treg frequency and cell counts **(Figure 4.9 G, H)**. There, a significant increase of infiltrated activated Treg upon DNFB treatment was measured for the WT control mice only.

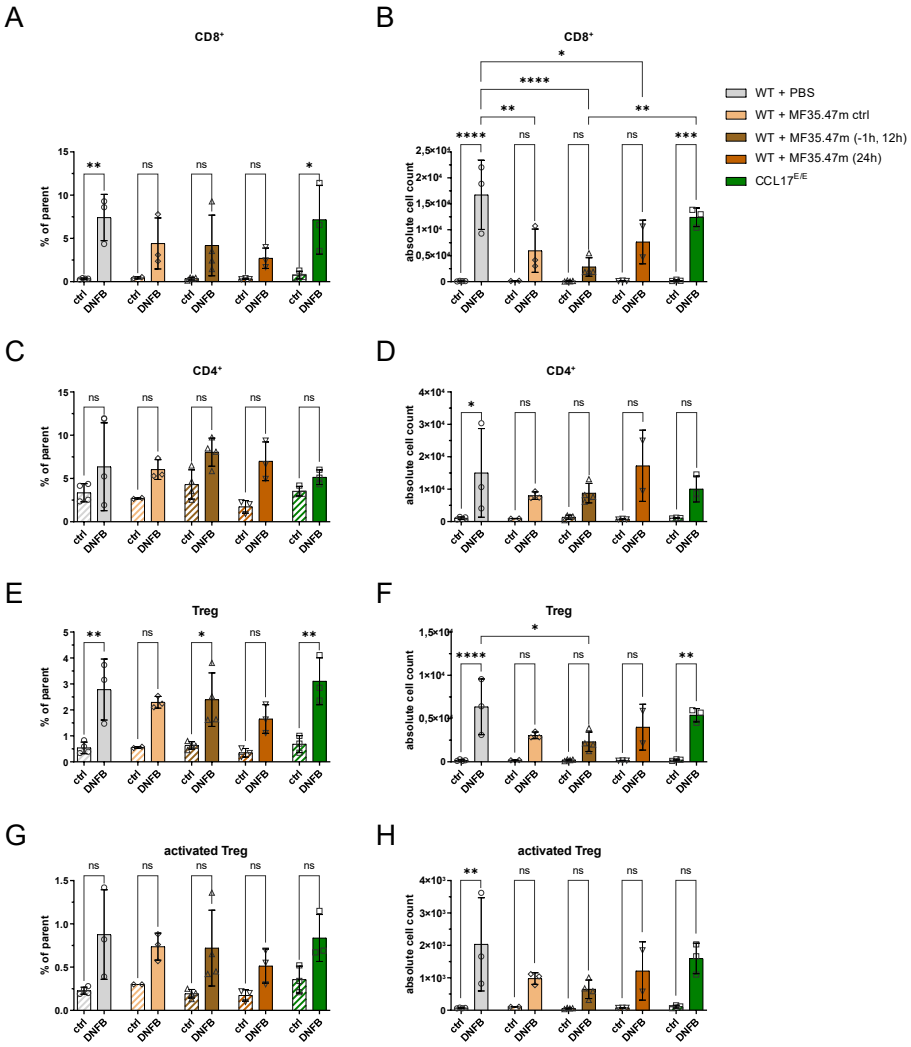

Figure 4.9 | Frequencies and absolute cell counts of conventional T cell subsets in the ears of mice after induction of CHS with therapeutic application of CCL17-specific aptamers in DAC cream.
WT and CCL17$^{E/E}$ mice were sensitized with DNFB on day −5 and day −4. On day 0, WT mice were i.p. injected with 5 nmol MF3.475m 24 h post DNFB challenge and with MF35.47m and MF35.47m ctrl 1 h prior and 12 h post challenge. Depicted are the frequencies and cell count of (A, B) CD8$^+$ T cells, (C, D) CD4$^+$, (E, F) FoxP3$^+$ Treg and (G, H) KLRG1$^+$ FoxP3$^+$ Treg isolated of the ear skin after a contact hypersensitivity. Statistical significance was tested using two-way ANOVA with Bonferroni post hoc test for multiple comparisons (n = 3 per group, mean ± SEM, *p=0.01-0,05, **p=0,001-0,01, ***p<0,001, ****p<0,0001).

All in all, application of aptamer 24 h post DNFB challenge only showed a reduced ear swelling at later time points after challenge but did not suppress the infiltration of immune cells into the ears completely. Compared to the previously used injection time points of 1 h prior and 12 h post DNFB challenge the suppressive effect was much milder. Hence, early application of aptamer blocking the CCL17/CCL22-CCR4-axis appears to be of importance to fulfill their inhibitory functions and reduce immune infiltration.

4.1.2. CCL22 is upregulated during contact hypersensitivity and CCL22 deficiency suppresses allergic symptoms similar to effects seen in CCL17 deficiency

To investigate the role of CCL22 in the development of ACD, CHS experiments were performed with WT, CCL17$^{E/E}$, CCL22$^{-/-}$ and CCR4$^{-/-}$ mice. As readout, the ear swelling response was measured **(Figure 4.10 A)** and, in addition, the CCL22 concentration in homogenized ear samples of the mice analyzed on day 3 was assessed **(Figure 4.10 B)**.

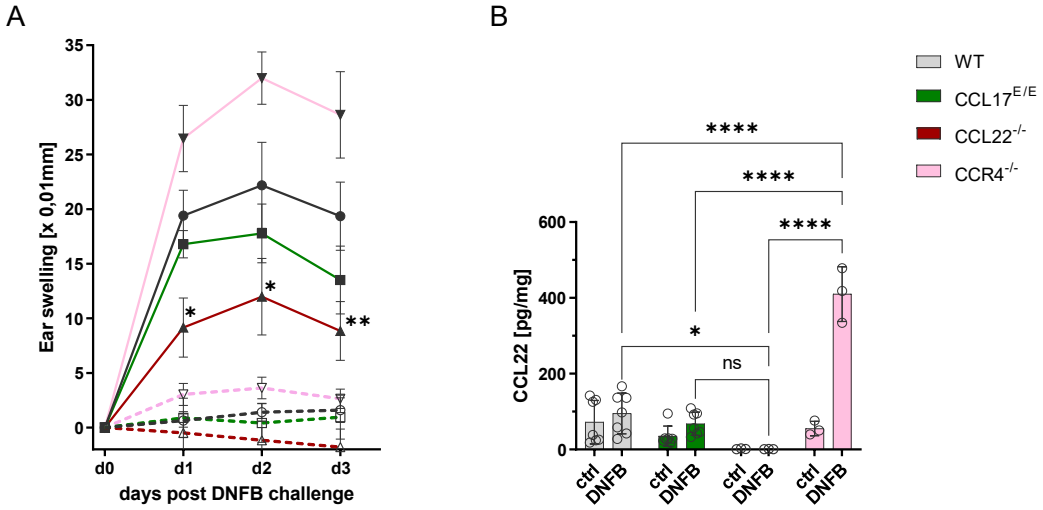

Figure 4.10 | Ear thickness of WT, CCL17$^{E/E}$, CCL22$^{-/-}$, and CCR4$^{-/-}$ mice in CHS)and CCL22 concentration in control and DNFB-treated ear samples.
Mice were sensitized with DNFB on day −5 and day −4. On day 0 mice were challenged with DNFB on the right ear. (A) Ear swelling of WT, CCL17$^{E/E}$, CCL22$^{-/-}$ and CCR4$^{-/-}$ mice is shown after 24 h (day 1), 48 h (day 2), and 72 h (day 3) after application of DNFB (solid lines) or vehicle (dashed lines). (B) The concentration of CCL22 in the ear tissue was measured using ELISA (Enzyme Linked Immunosorbent Assay) three days after DNFB challenge. Statistical significance was tested by ordinary two-way-ANOVA with post-hoc Tukey test (n = 3-8 of two independent experiments, mean±SEM, *p=0.01-0.05, **p=0.001-0.01, ***p<0.001, ****p<0.0001).

CCL22$^{-/-}$ mice demonstrated a similar phenotype as the CCL17$^{E/E}$ mice during CHS, namely they had a significantly reduced ear swelling response after the challenge. When CCL22 levels in the ear skin were analyzed 3 days after the DNFB challenge, CCL22 was detectable in both ear samples, the vehicle- and the hapten-treated ears, to a similar extent in WT and CCL17$^{E/E}$ mice. Interestingly, in CCR4$^{-/-}$ mice, an immense increase of CCL22 was observed. In contrast to the single deficient mice, CCR4$^{-/-}$ mice also showed an aggravated allergic reaction compared to WT mice **(Figure 4.10 A).**

Thus, the local CCL22 expression might play an important role in the development of CHS. Therefore, CCL22-specific aptamers were generated to investigate the pharmacological effects of a CCL22 blockade for CHS development.

4.1.3. Functional testing of newly generated CCL22-specific aptamers

To assess the therapeutic potential of CCL22 blockage in the context of contact allergies, we collaborated with the group of Prof. Günter Mayer (LIMES Institute) to generate CCL22-specific aptamers that functionally inhibit binding of CCL22 to a chemokine receptor thus preventing immune cell trafficking to the inflamed skin. These aptamers were tested functionally in *in vitro* and *in vivo* assays to understand underlying mechanisms of CCL22 blockade and to evaluate their relevance as a treatment option for contact allergies.

4.1.3.1. CCL22-specific aptamer candidates functionally inhibit migration in *in vitro* transwell assays

CCL22-specific DNA aptamers newly generated by Anna Jonczyk of Prof. Günter Mayers group, that had been shown to specifically bind CCL22 **(Figure 1.5)**, were tested functionally in *in vitro* transwell assays to assess their capacity to inhibit T cell migration. For this the CCR4 expressing T cell lymphoma line BW5147.3 that is known to migrate towards CCL17 and CCL22 in vitro was used (Fülle, Steiner, et al., 2018; Lieberam & Förster, 1999). Therefore, migration of the T cell lymphoma cell line BW5147.3 towards different concentrations of CCL17 and CCL22 was tested first to identify an optimal concentration of the chemokines for the aptamer-dependent inhibition assays, namely the lowest concentration with the strongest induction of migration, **(Figure 4.11).**

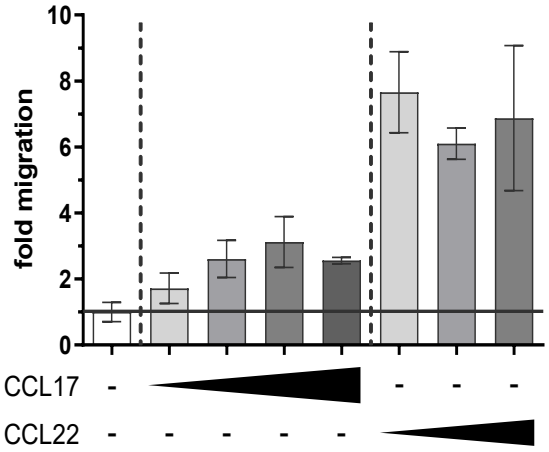

Figure 4.11 | Dose-dependent migration of BW5147.3 cells towards CCL17 and CCL22.
Dose-dependent migration to the chemokines CCL17 and CCL22 as percent of transmigrated cells normalized to the medium control and depicted as fold migration. Increasing concentrations of CCL17 (33.3 ng/ml, 100 ng/ml, 300 ng/ml, 900 ng/ml) and CCL22 (33.3 ng/ml, 100 ng/ml, 300 ng/ml) were added to the bottom compartment. Statistical significance was tested using ordinary one-way-ANOVA with post-hoc Bonferroni test (n = 3, mean±SEM, *p=0.01-0.05, **p=0.001-0.01, ***p<0.001, ****p<0.0001).

BW5147.3 cells migrated concentration-dependently towards CCL17 with a peak migration of around three times more than the medium control at 100 ng/ml. In contrast, for CCL22 already

the lowest concentration of 33.3 ng/ml led to eight times higher migration rates compared to the control, and six and seven times more for the increasing concentrations, respectively, indicating a stronger migration induction by CCL22 compared to CCL17. Thus, an optimal CCL22 concentration for the inhibition assay is 33.3 ng/ml. However, since all tested concentrations of CCL22 yielded in a strong migration of BW5147 cells, 100ng/ml CCL22 was used in all following transwell experiments to additionally keep it comparable to the data obtained for CCL17 in previous transwell experiments.

Anna Jonczyk from the group of Prof. Günter Mayer identified 8 aptamers (AJ1, AJ21, AJ25, AJ78, AJ81, AJ82, AJ102, AJ104) which specifically bound CCL22 using SELEX. To assess their inhibitory capacity each candidate was tested functionally in 1:10 molar ratio, equimolar ratio and 10:1 molar ratio to CCL22 in transwell assays **(Figure 4.12)**. Scrambled non-binding controls of each aptamer were generated and tested in an equimolar ratio to test for unspecific binding.

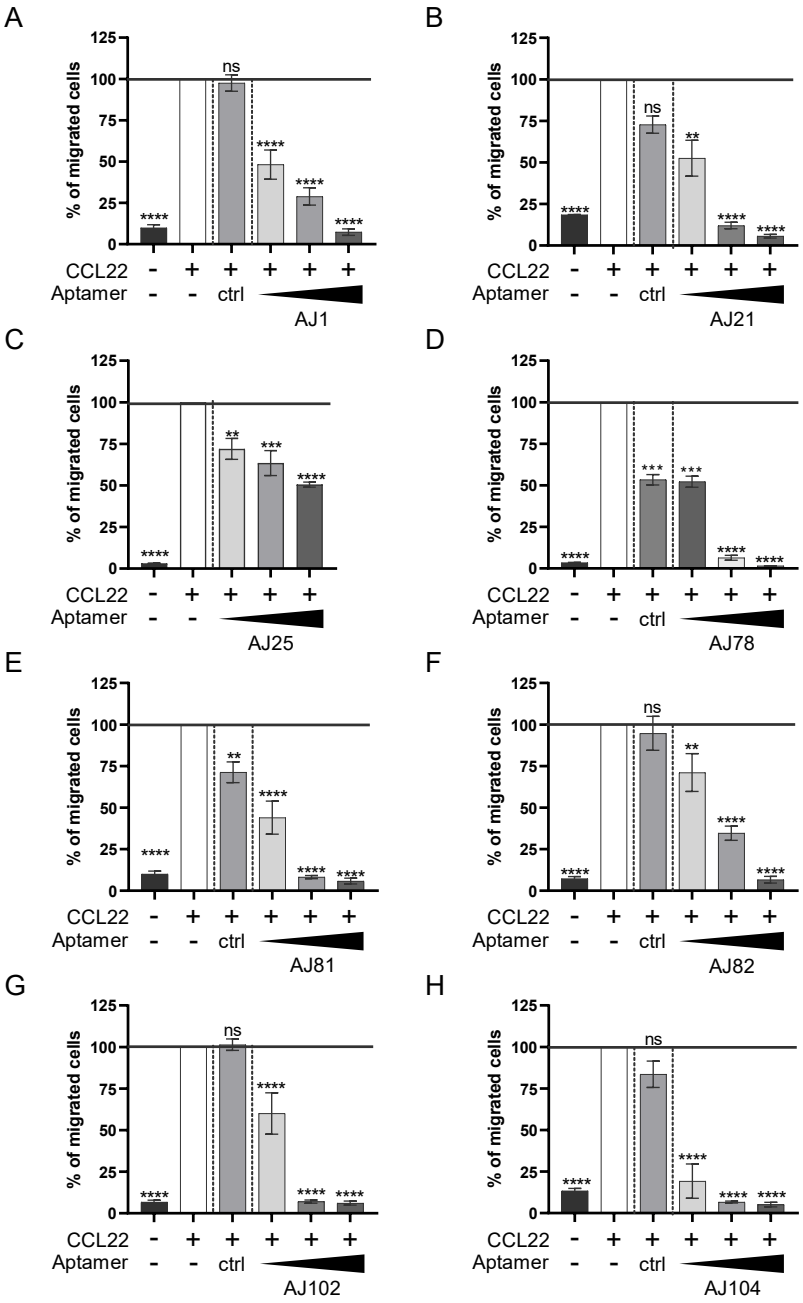

Figure 4.12 | Aptamer dependent inhibition of migration towards mCCL22 in an *in vitro* transwell migration assay.
Migration of BW5147.3 cells towards CCL22 [12,8nM] in the presence of aptamers (A) AJ1, (B) AJ21, (C) AJ25, (D) AJ78, (E) AJ81, (F) AJ82, (G) AJ102 and (H) AJ104 in 1:10 molar ratio (1.28 nmol/well), equimolar ratio (12.8 nmol/well) and 10:1 molar ratio (128 nmol/well). Scrambled versions of the aptamers were added in equimolar ratio (ctrl). Migration without the addition of CCL22 or aptamers, as well as the migration towards CCL22 alone were measured as controls. Statistical significance was tested using ordinary one-way-ANOVA with post-hoc Bonferroni test (n = 3-16, mean±SEM, *p=0.01-0.05, **p=0.001-0.01, ***p<0.001, ****p<0.0001).

All aptamers demonstrated a significant concentration-dependent inhibition of migration of BW5147.3 cells towards CCL22. The aptamer AJ1 reduced the migration of BW5147.3 cells by about 50 % in the 10:1 molar ratio, 70 % in the equimolar ratio and to levels similar to the medium control in the 10:1 molar ratio **(Figure 4.12 A)**. AJ21 performed better compared to AJ1 in the equimolar ratio and 10:1 molar ratio as it decreased the frequency of migrated cells to values lower than the medium control in both conditions **(Figure 4.12 B)**. The 1:10 molar ratio however reduced the migration only to 60 %. Additionally, the scrambled control showed a tendency to reduce the migration around 15 %, however, this was not significantly different. Although AJ25 also showed a concentration-dependent inhibition of migration, even the highest concentration of the aptamer only led to a decrease of around 40 % **(Figure 4.12 C)**. AJ78 efficiently reduced CCL22-dependent migration of T cells, but its scrambled version also demonstrated inhibitory capacity **(Figure 4.12 D)**. Similarly, AJ81 showed a significant reduction of the migration rate with increasing levels of aptamers, yet, its scrambled version also significantly decreased T cell migration **(Figure 4.12 E).** The aptamer AJ82 diminished the migration of T cells concentration-dependently, 30 % in the 10:1 molar ratio, 70 % in the equimolar ratio and to levels similar to the medium control in 10:1 molar ratio, whereas its control did not show any signs of migration inhibition **(Figure 4.12 F)**. AJ102 performed very well as it reduced migration up to 60 % of migrated cells in the 10:1 molar ratio, and up to 10% of migrated cells in the equimolar and 10:1 molar ratio that reflected similar percentages as seen in the medium control **(Figure 4.12 G)**. For the eighth aptamer AJ104 strong inhibition of migration could be observed with levels up to 25 % of transmigrated cells in the lowest aptamer condition **(Figure 4.12 H)**.

All in all, although some aptamers performed better than others, all eight candidates did not only bind CCL22 but were also able to functionally inhibit CCL22 dependent migration. The tested aptamers were categorized into three groups as next generation sequencing analysis revealed that three main sequence motifs emerged in the last selection cycle of the SELEX. Motif 1 was found in AJ81 and AJ82. Motif 2 was found in AJ1, AJ25 and AJ104 and Motif 3 was found in AJ21 and AJ102. Based on these results together with the affinity and specificity data gathered from Anna Jonczyk, we chose two aptamers for further testing. As these aptamers are DNA oligonucleotides, there is a risk that one motif is recognized by PRRs such as Toll-like receptor 9 (TLR9), cyclic GMP-AMP synthase (cGAS) – stimulator of interferon genes (STING) or absent in melanoma 2 (AIM2) (Carty et al., 2021). Hence, to maximize the chance

to find an immune-tolerant aptamer we decided to choose two aptamers bearing different motifs. Thus, we selected AJ82 with motif 1 and AJ102 bearing motif 2 as these ones also showed high inhibitory potential, whereas their scrambled controls did not lead to a reduced transmigration rate.

4.1.3.2. Truncated and modified aptamers AJ82 and AJ102 inhibit T cell migration *in vitro*

Based on the predicted 3D structures by the Mfold web server from UNAFold (Zuker, 2003) the chosen aptamers AJ82 and AJ102 were truncated to keep the necessary binding structures while removing the non-essential parts to minimize conformational polymorphisms. Conformational polymorphisms are multiple structural isoforms the aptamer folds into. In addition, to increase the half-life of the DNA aptamers *in vivo* they were modified with a 5'-polyethylenglycol (PEG) tail and a 3'-dT-cap structure as these modifications have been reported to reduce renal clearance and prolong stability, respectively (Amero et al., 2021; Healy et al., 2004; Ni et al., 2021).

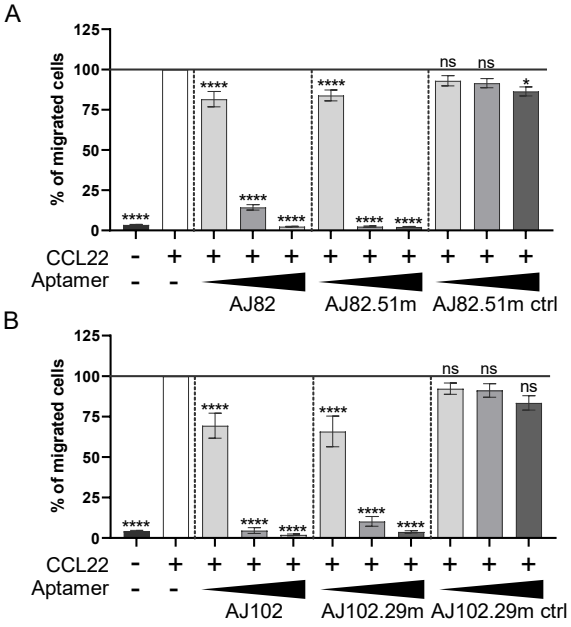

Figure 4.13 | Inhibition of CCL22-dependent cell migration by the truncated aptamers AJ82 and AJ102.
Migration of BW5147.3 cells towards CCL22 [12.8 nM] was measured in a transwell migration assay in the presence of aptamers. Full length aptamers (A) AJ82 and (B) AJ102, truncated and modified aptamers (A) AJ82.51m, (B) AJ102.29m and their scrambled controls (A) AJ82.51m ctrl and (B) AJ102.29m ctrl were tested in 1:10 molar ratio (1.28 nmol/well), equimolar ratio (12.8 nmol/well) and 10:1 molar ratio (128 nmol/well). Migration without the addition of CCL22 or aptamers, as well as the migration towards CCL22 only were measured as controls. Statistical significance was tested by using ordinary one-way-ANOVA with post-hoc Bonferroni test ((A) n = 4-23, (B) n =7-15, mean±SEM, *p=0.01-0.05, **p=0.001-0.01, ***p<0.001, ****p<0.0001).

AJ82 was modified and reduced to 51 nucleotides yielding AJ82.51m which was tested for its inhibitory capacity in transwell assays in comparison with its parent aptamer AJ82 and its equally modified and truncated scrambled control AJ82.51m ctrl **(Figure 4.13 A)**. Whereas the

values for the 10:1 molar ratio of the parent aptamer and AJ82.51m were similar, the equimolar ratio of the modified aptamer was even more effective in reducing the frequency of transmigrated cells. Thus, it diminished migration to 4 % whereas the original aptamer diminished the migration only to 15 % of the positive control. For the inhibition of T cell migration in the 10:1 molar ratio, both, the parent aptamer and its truncated version reduced migration to 3 %, which was lower than the medium control. In this case, we also tested the scrambled control in 1:10, equimolar and 10:1 molar ratio. In the first two conditions no significant decrease regarding the percentage of transmigrated cells was visible. However, the migration of the BW5147.3 cells was significantly decreased when 10 times more AJ82.51m ctrl than CCL22 was added.

The second aptamer AJ102 was modified and truncated to 29 nucleotides and was also tested in comparison with its parent aptamer and its equally modified scrambled control AJ102.29m ctrl in transwell assays **(Figure 4.13 B)**. While the original and the modified aptamer showed similar inhibition of T lymphoma cell migration in the 1:10 molar ratio, the parent aptamer performed slightly better than AJ102.29m in the equimolar and 10:1 molar ratio condition. The parent aptamer reduced the frequency of transmigrated cells to 4.5 % and 2 % respectively, whereas the truncated aptamer decreased migration to 10% in the equimolar ratio and by 3.8 % in the 10:1 molar ratio. Nevertheless, AJ102.29 effectively inhibited migration in a concentration dependent manner. Remarkably, although the values for the 10:1 ratio of the scrambled control to CCL22 were similar to the experiment with AJ82.51m ctrl, no significant reduction of migration was calculated for the AJ102.29m ctrl.

Taken together, truncation and modification of AJ82 and AJ102 led to similar degrees of inhibition of migration as the original aptamers. Thus, the truncated and modified aptamers were used in the following experiments as the reduction in size and modification diminishes structural polymorphisms, production costs, whereas *in vivo* stability is enhanced. As the scrambled control AJ82.51 ctrl demonstrated a potential to reduce migration of T cells, the AJ102.29m and its scrambled control were favored for subsequent experiments.

Furthermore, both aptamers were tested for their immunostimulatory function by Matthew Mangan from Prof. Eicke Latz group (Institute for Innate Immunity, University clinic of Bonn). This experiment revealed that AJ82.51 and its modified version AJ82.51 were indeed recognized by pattern recognition receptors and induced an immune response **(Figure 4.14)**.

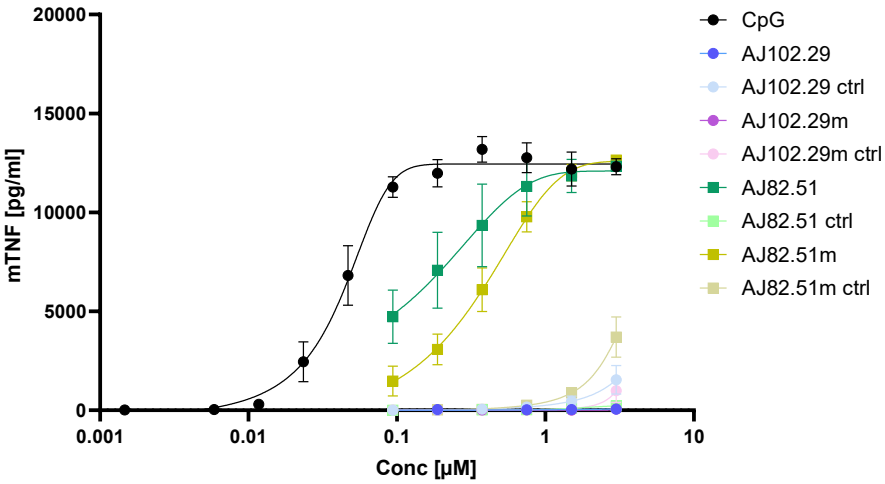

Figure 4.14 | Testing of innate immune activation by CCL22-specific aptamers .
Immortalized murine embryonic stem cell-derived macrophages were incubated with increasing concentrations of the immunostimulatory TLR9 ligand CpG along with the aptamers AJ82.51, AJ102.29 and their modified versions AJj82.51m and AJ102.29m together with their respective control sequences. After 24 h incubation the TNF secretion in the supernatant was measured.
This experiment was performed by Matthew Mangan (group of Prof Eicke Latz)

As for a potential therapeutic use for contact dermatitis this could potentially counteract the treatment, we dismissed AJ82.51m for *in vivo* testing and proceeded with AJ102.29m only.

4.1.4. AJ102.29m effectively suppresses allergic reactions in contact hypersensitivity

To test the efficacy of AJ102.29m *in vivo* the aptamer or its scrambled control were injected intraperitoneally at the time point of the challenge (day 0) and 12 h post DNFB challenge. Application of 5 nmol aptamer per injection yielded in no change of ear thickness and thus was not effective enough to see significant results **(Figure 4.15)**.

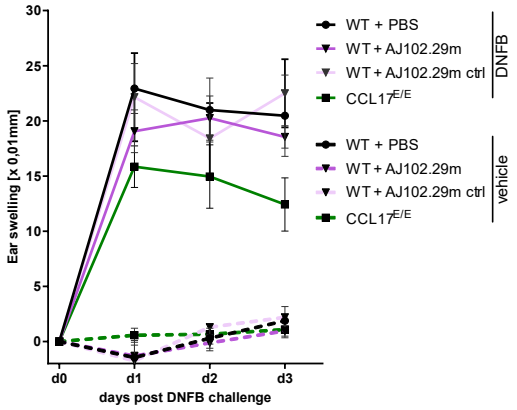

Figure 4.15 | No change in ear swelling after induction of CHS with application of 5nmol CCL22-specific aptamers.
WT and CCL17$^{E/E}$ mice were sensitized with DNFB on day −5 and day −4. On day 0, WT mice were injected i.p. with 5 nmol AJ102.29m and AJ102.29m ctrl or PBS (WT PBS) right before and 12 h after DNFB challenge. CCL17$^{E/E}$ received PBS injections. Ear swelling of WT and CCL17$^{E/E}$ mice 24 (day 1), 48 (day 2), and 72 h (day 3) after application of DNFB (solid lines) or vehicle (dashed lines). Statistical significance was tested using two-way ANOVA with Bonferroni post hoc test for multiple comparisons (n = 6 per group, mean±SEM, *p=0.01-0.05, **p=0.001-0.01, ***p<0.001, ****p<0.0001.)

Therefore, the injection dose was increased to 10 nmol aptamer per injection in order to see aptamer-dependent effects in the allergic reaction after CHS induction **(Figure 4.16)**. Ear thickness and infiltration of immune cells in ear samples of WT mice that received AJ102.29m, AJ102.29m ctrl, or PBS as a control were measured. In addition, CCL22$^{-/-}$ mice were used as control to estimate the highest possible level of protection. The mice were treated with DNFB or vehicle on the right and left ear, respectively, and were analyzed to evaluate the ability of AJ102.29m to suppress allergic symptoms in the CHS model **(Figure 4.16)**.

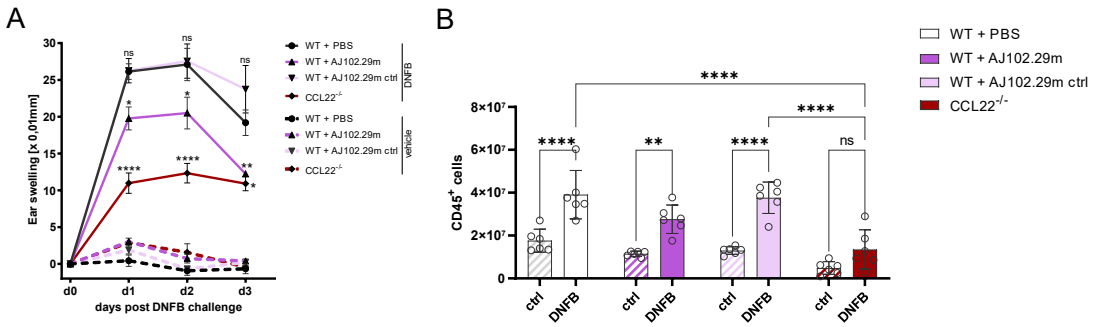

Figure 4.16 | Reduced ear swelling and immune cell infiltration into the ears after induction of CHS with application of CCL22-specific aptamers.
WT and CCL22$^{-/-}$ mice were sensitized with DNFB on day −5 and day −4. On day 0, WT mice were injected i.p. with 10 nmol AJ102.29m and AJ102.29m ctrl or PBS (WT ctrl) right before and 12 h after DNFB challenge. CCL22-/- received PBS injections. (A) Ear swelling of WT and CCL22$^{-/-}$ mice 24 h (day 1), 48 h (day 2), and 72 h (day 3) after application of DNFB (solid lines) or vehicle (dashed lines). Statistical significance was tested using two-way ANOVA with Bonferroni post hoc test for multiple comparisons (n = 6 per group, mean±SEM, *p=0.01-0.05, **p=0.001-0.01, ***p<0.001, ****p<0.0001.) (B) Flow cytometric analysis of the immune cell infiltrate. At day 3, mice were sacrificed, and cells of the ears were isolated and stained for flow cytometry. Absolute numbers of CD45^{+} cells (B) were determined by flow cytometry (n = 5-6 per group, mean±SEM, *p=0.01-0.05, **p=0.001-0.01, ***p<0.001, ****p<0.0001).

WT mice demonstrated a strong ear swelling response on day 1 and day 2 post challenge, whereas the ear thickness of CCL22$^{-/-}$ mice was 60 % lower, being significantly reduced compared to PBS-treated WT mice **(Figure 4.16 A)**. Injection of AJ102.29m ctrl led to no significant difference in the ear swelling response compared to that of DNFB challenged WT mice treated with PBS only. Strikingly, AJ102.29m treatment showed a significant decrease of the ear swelling response compared to PBS-treated WT mice. In this case, the values were 20 % lower than those measured in WT mice treated with either PBS or AJ102.29m ctrl. Nevertheless, CCL22$^{-/-}$ mice showed the strongest suppression of ear swelling. The vehicle-treated ears of all analyzed cohorts were only slightly thicker than the starting value at day 0 and appeared to be similar under all conditions.

To gain insights about the cell populations infiltrating the ears, single cell suspensions of the vehicle and DNFB-treated ear samples were analyzed by flow cytometry. The results were reflected by the absolute numbers of immune cells that infiltrated the ears **(Figure 4.16 B).** Upon DNFB challenge more CD45^{+} cells infiltrated the ears in all experimental cohorts. In WT mice treated with either PBS or AJ102.29 ctrl the numbers of cells in the DNFB-treated ears were significantly higher than in vehicle-treated ears, whereas in CCL22$^{-/-}$ mice no significant increase was detectable. In these mice, the number of CD45^{+} cells, which infiltrated into the ear was significantly lower than in PBS-treated and aptamer ctrl-treated mice. Interestingly, WT mice injected with AJ102.29m ctrl showed a significant increase of CD45^{+} cells in the hapten-treated ear compared to the other one, but to a lesser extent than the WT ctrl or

AJ102.29m ctrl mice. Thus, the highest cell infiltration was observed for the DNFB-treated ears of WT control mice and mice that received AJ102.29m ctrl, followed by the mice that received the aptamer AJ102.29m and the least infiltration was measured for the CCL22$^{-/-}$ mice. This indicates that injection of the aptamer AJ102.29m, but not its control AJ102.29m ctrl showed an effect on immune cell infiltration, but not as strong as the systemic absence of CCL22 in CCL22$^{-/-}$ mice.

As it is well documented that CD8^{+} T cells immigrate into the inflamed skin during CHS, and CCR4 is expressed on skin homing T cells, (Egawa & Kabashima, 2017; Matsuo et al., 2018; Stutte et al., 2010; Vocanson et al., 2005; X. Wang et al., 2010) we focused on the analysis of different T cell subsets **(Figure 4.17)**.

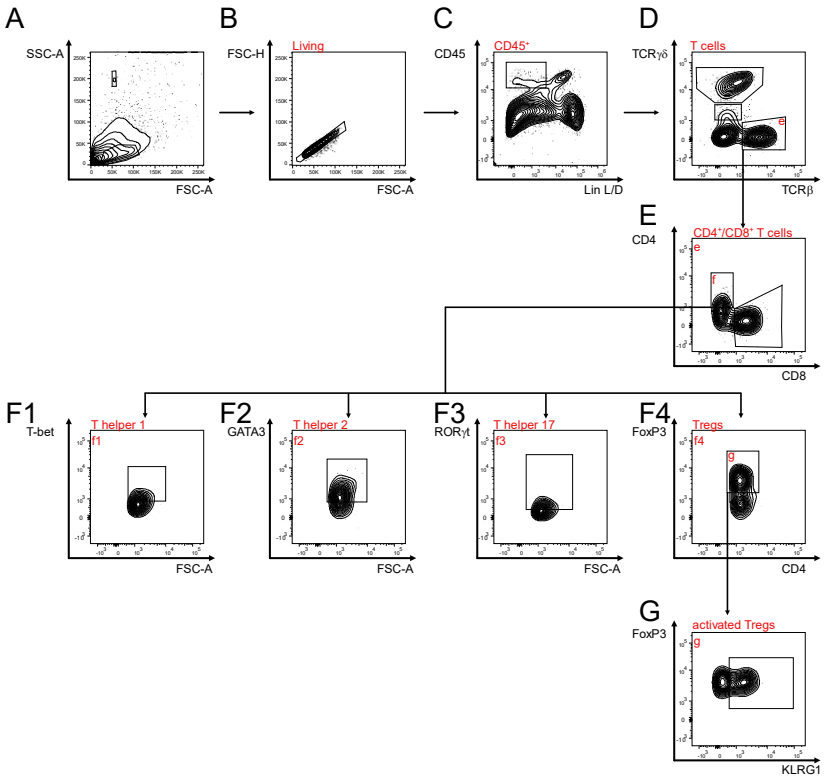

Figure 4.17 | T cell gating strategy for ear skin of mice after induction of contact hypersensitivity (CHS).
(A-C) Lineage^{-}(F480, B220) living single cells were gated on CD45 expression. (D) CD45^{+} cells were divided into TCRβ^{+} T cells, dermal γδ T cells (TCRγδ^{int}) and DETC (TCRγδ^{high}). (E) TCRβ^{+} cells were separated into CD4^{+} and CD8^{+} T cells. (F1-F4)) CD4^{+} cells were checked for master transcription factor expression of Th subtypes using FMO controls (fluorescent minus one). (G) Treg were further gated based on KLRG1 expression to identify the activated Treg.

The frequencies and absolute cell numbers of conventional T cells, as well as dermal γδ T cells and DETC were analyzed in order to find out which cell subset might be affected by the application of AJ102.29m and CCL22 deficiency **(Figure 4.18)**.

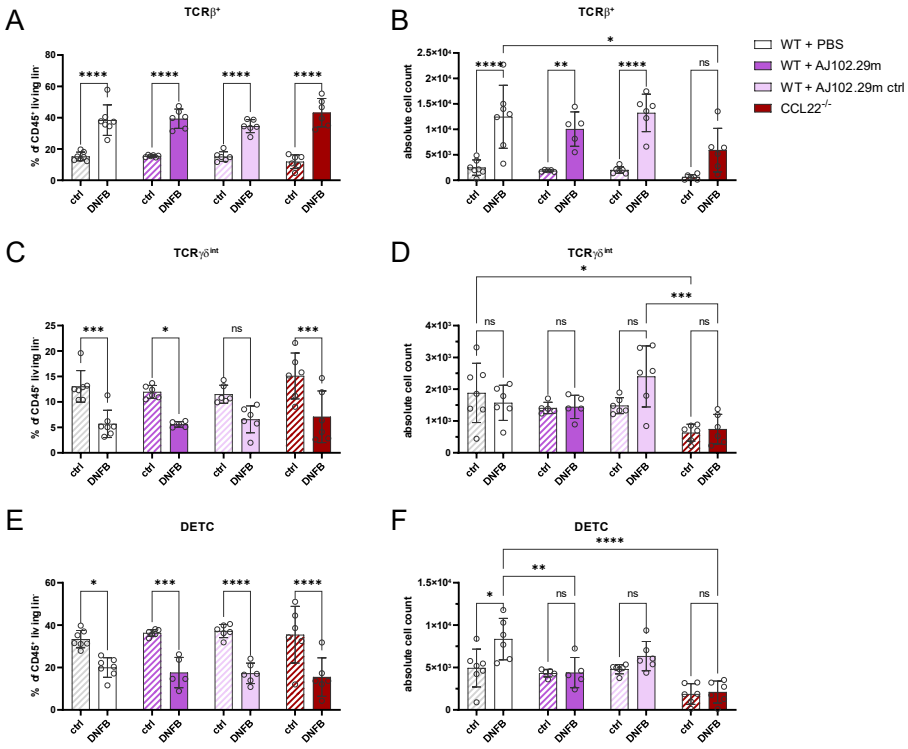

Figure 4.18 | Frequencies and absolute cell counts of different T cell subsets in ear samples of mice after induction of CHS with application of AJ102.29m during CHS.
WT and CCL22$^{-/-}$ mice were sensitized with DNFB on day −5 and day −4. On day 0, WT mice were injected i.p. with 10 nmol AJ102.29m, AJ102.29m ctrl or PBS right before and 12 h after DNFB challenge. CCL22$^{-/-}$ mice received PBS injections. Depicted are the frequencies and cell counts of (A, B) TCRβ^{+} T cells, (C, D) dermal γδ T cells and (E, F) DETC isolated from the ear skin after the induction of contact hypersensitivity. Statistical significance was tested using two-way ANOVA with Bonferroni post hoc test for multiple comparisons (n = 5-6 per group, mean±SEM, *p=0.01-0.05, **p=0.001-0.01, ***p<0.001, ****p<0.0001).

The frequencies of TCRβ^{+} cells were similar between the cohorts and increased significantly from around 20% to 40% upon DNFB treatment **(Figure 4.18 A)**. Moreover, the absolute cell counts also increased in ear samples of each cohort when treated with DNFB compared to controls **(Figure 4.18 B)**. As shown before for CD45^{+} cells, the TCRβ^{+} cell numbers of WT mice injected with PBS or AJ102.29m ctrl were highest upon DNFB treatment, followed by mice injected with AJ102.29m and lowest cell numbers were obtained in the CCL22$^{-/-}$ mice **(Figure 4.18 B)**. Here, the DNFB-treated ear of CCL22$^{-/-}$ mice contained significantly less conventional T cells than the DNFB-treated WT control ears.

The distribution of the frequencies and absolute cell numbers of dermal γδ T cells were different from the conventional T cells shown above. The frequencies in vehicle-treated ears were comparable in all cohorts and were reduced to a similar percentage in all mice analyzed.

For the WT mice injected with AJ102.29m ctrl, however, a high variability was observed. **(Figure 4.18 C)**. Although the frequencies decreased when ears were treated with the hapten, the absolute cell numbers in the ear samples stayed similar or even increased upon treatment **(Figure 4.18 D)**. This is not unexpected as dermal γδ T cells play a role in inflammatory skin disorders, but do not circulate immensely (Jiang et al., 2017). Interestingly, CCL22$^{-/-}$ mice had reduced γδ T cells in the control condition compared to WT ctrl mice and significantly reduced cell numbers in the DNFB condition when compared to the AJ102.29m ctrl mice. Furthermore, an increase in the absolute numbers of dermal γδ T cells in DNFB-treated ear samples of AJ102.29 ctrl mice was visible. However, this might be due to a high variability between analyzed mice in this cohort.

In line with the dermal γδ T cells, DETC frequencies significantly decreased upon DNFB treatment in all analyzed mice but did not differ in between cohorts. Again, this is supported by the literature as a decline in DETC upon DNFB treatment is due to loss of survival signals and emigration out of the affected areas (Gadsbøll et al., 2020; Mraz et al., 2020; Nielsen et al., 2014). For the total cell count however, the WT ctrl showed a significant increase upon DNFB treatment. Interestingly, the DETC numbers in DNFB-treated ears of CCL22$^{-/-}$ and mice that received AJ102.29m were significantly lower than in those of the WT control mice which was not noticed for the other cell types.

In conclusion, the percentages of all T cell subsets were rather similar between all cohorts, although the frequencies of γδ T cells decreased upon DNFB treatment, whereas TCRβ^{+} T cells increased. When comparing the absolute number of T cell subsets CCL22$^{-/-}$ mice had a reduction in dermal γδ T cells already in the control ear samples. Overall, less T cells immigrated into the ears of CCL22$^{-/-}$ mice upon DNFB stimulation. Additionally, the T cells, in particular the DETC but also the other subsets analyzed, were slightly reduced in numbers in the aptamer-treated mice indicating a suppressive effect on T cell immigration when blocking CCL22 with AJ102.29m, but not with its scrambled control.

The conventional T cell subset was further separated into CD4^{+} and CD8^{+} T cells. CD8^{+} T cells have a dominant function during CHS but also CD4^{+} T cell effects play important roles in the process (Vocanson et al., 2005; B. Wang et al., 2000) **(Figure 4.19)**. Additionally, the CCR4 expression on these cells was assessed.

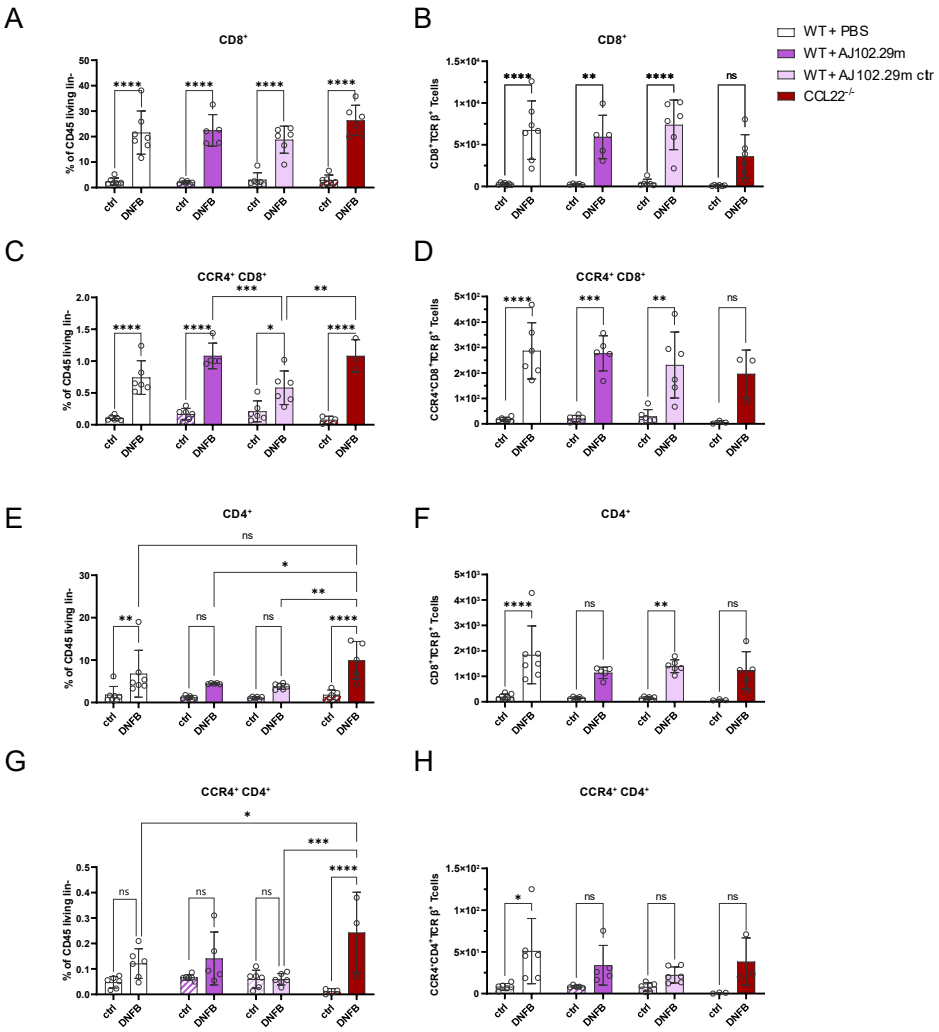

Figure 4.19 | CD4⁺ and CD8⁺ conventional T cells in ears of in the ear samples of mice after induction of CHS with application of AJ102.29m during CHS.
WT and CCL22$^{-/-}$ mice were sensitized with DNFB on day −5 and day −4. On day 0, WT mice were injected i.p. with 10 nmol AJ102.29m, AJ102.29m ctrl or PBS right before and 12 h after DNFB challenge. CCL22$^{-/-}$ mice received PBS injections. Depicted are the frequencies and cell counts of (A, B) TCRβ⁺ CD8⁺ T cells, and (E, F) TCRβ⁺ CD4⁺ T cells isolated of the ear skin after the induction of contact hypersensitivity. CCR4 expression is shown of (C, D) CD8⁺ and (G, H) CD4⁺ T cells. Statistical significance was tested using two-way ANOVA with Bonferroni post hoc test for multiple comparisons (n = 3-6 per group, mean±SEM, *p=0.01-0.05, **p=0.001-0.01, ***p<0.001, ****p<0.0001).

The frequencies of CD8⁺ T cells increased significantly in all cohorts analyzed comparing vehicle- and DNFB-treated ears **(Figure 4.19 A)**. Interestingly, in WT control and AJ102.29m ctrl-treated mice the absolute number of CD8⁺ T cells increased massively in the hapten-treated ears, whereas the increase for the mice that received the aptamer was slightly reduced compared to the WT control mice and to the mice that received AJ102.29m ctrl. In CCL22$^{-/-}$ mice DNFB treatment did not lead to a significant increase in CD8⁺ T cells **(Figure 4.19 B)**.

The percentage of CCR4-expressing CD8⁺ T cells increased in WT control, AJ102.29 treated and CCL22$^{-/-}$ mice in a similar way, whereas the frequency in ear samples of mice treated with the scrambled control were significantly decreased compared to AJ102.29m and CCL22$^{-/-}$ mice

(Figure 4.19 C). Although the numbers of $CCR4^+$ $CD8^+$ T cells increased in the DNFB-treated ears compared to control ears in all cohorts, the increase was not significantly different in $CCL22^{-/-}$ mice **(Figure 4.19 D)**.

The percentages of $CD4^+$ T cells in the ear samples are generally lower than the $CD8^+$ T cells. Additionally, the increase upon DNFB stimulation was not as pronounced for the $CD4^+$ as for $CD8^+$ T cells. Interestingly, in the hapten-treated ears of $CCL22^{-/-}$ mice the frequencies were highest compared to the other cohorts and significantly increased compared to the aptamer and aptamer ctrl-treated mice **(Figure 4.19 E)**. Nevertheless, the absolute cell numbers did not differ between cohorts **(Figure 4.19 F)**.

Interestingly, the frequency of CCR4-expressing $CD4^+$ T cells in ear samples of hapten-treated $CCL22^{-/-}$ mice was also significantly higher than in the WT control and AJ102.29m ctrl-treated mice, but not compared to the AJ102.29m-treated mice **(Figure 4.19 G)**. This was not reflected by the actual cell counts of $CCR4^+$ $CD4^+$ T cells, as no difference between cohorts was observed **(Figure 4.19 H)**.

Taken together, lower amounts of $CD4^+$ and $CD8^+$ T cells infiltrated the ears upon DNFB challenge in $CCL22^{-/-}$ and aptamer-treated mice, compared to control mice. Furthermore, the lack of CCL22, as well as the pharmacological blockage of CCL22 by AJ102.29m might influence the amount of CCR4-expressing T cells.

Additionally, the CD4$^+$ T cells were further separated into T helper subsets based on the expression of master transcription factors to access T helper cell differentiation during inflammation **(Figure 4.20, Figure 4.21)**. As CCL22 is strongly associated with Treg recruitment (Eby et al., 2015; Faget et al., 2011; Rapp et al., 2019), Treg activation was also analyzed **(Figure 4.20)**.

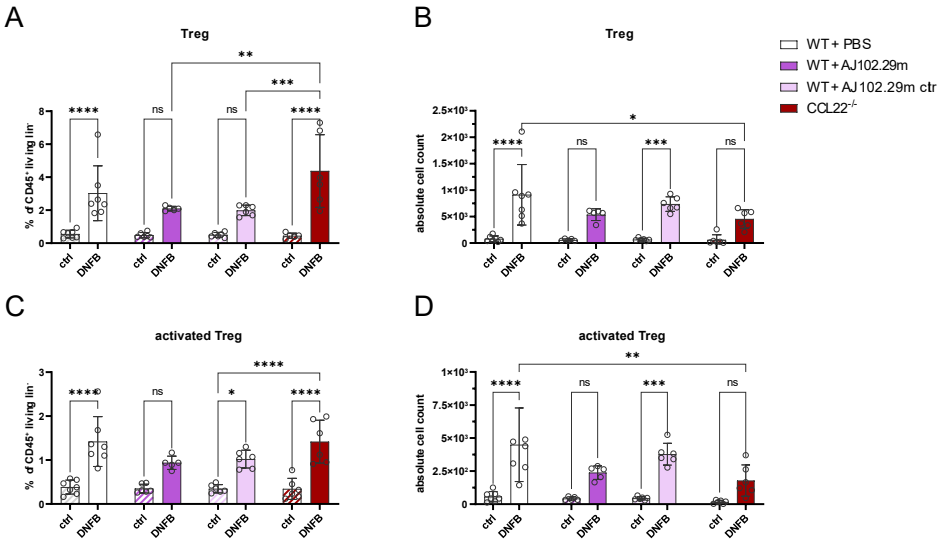

Figure 4.20 | Treg in the ear samples of mice after induction of CHS with application of AJ102.29m.
WT and CCL22$^{-/-}$ mice were sensitized with DNFB on day −5 and day −4. On day 0, WT mice were injected i.p. with 10 nmol AJ102.29m, AJ102.29m ctrl or PBS right before and 12 h after DNFB challenge. CCL22$^{-/-}$ mice received PBS injections. Depicted are the frequencies and cell count of (A, B) FoxP3$^+$ Treg, and (C, D) KLRG1$^+$ FoxP3$^+$ activated Treg isolated the ear skin after the induction of contact hypersensitivity. Statistical significance was tested using two-way ANOVA with Bonferroni post hoc test for multiple comparisons (n = 3-6 per group, mean±SEM, *p=0.01-0.05, **p=0.001-0.01, ***p<0.001, ****p<0.0001).

Here, the percentage of Treg was highest in WT control and CCL22$^{-/-}$ mice. Remarkably, the frequency of Treg in ear samples of allergic CCL22$^{-/-}$ mice was significantly higher than the frequencies found in ears of aptamer- and aptamer ctrl-treated mice **(Figure 4.20 A)**. In contrast, the absolute cell numbers of Treg in the hapten-treated ears of CCL22$^{-/-}$ mice and AJ102.29m-treated mice were lowest and no significant increase compared to the respective control ear samples was apparent **(Figure 4.20 B)**. Strikingly, in CCL22$^{-/-}$ mice the DNFB-treated ears contained significantly less Treg than the DNFB-treated ears of WT ctrl mice. The finding that the frequency increased, whereas the absolute cell number decreased might be explained by an overall lower cell infiltrate in ears of CCL22$^{-/-}$ mice.

Thus, also the Treg population might be affected by the absence or the blockage of CCL22.

Besides the Treg, Th1, Th2 and Th17 T cells were analyzed as it has been shown that T helper subsets influence CHS progression (Larsen et al., 2009; B. Wang et al., 2000) **(Figure 4.21)**.

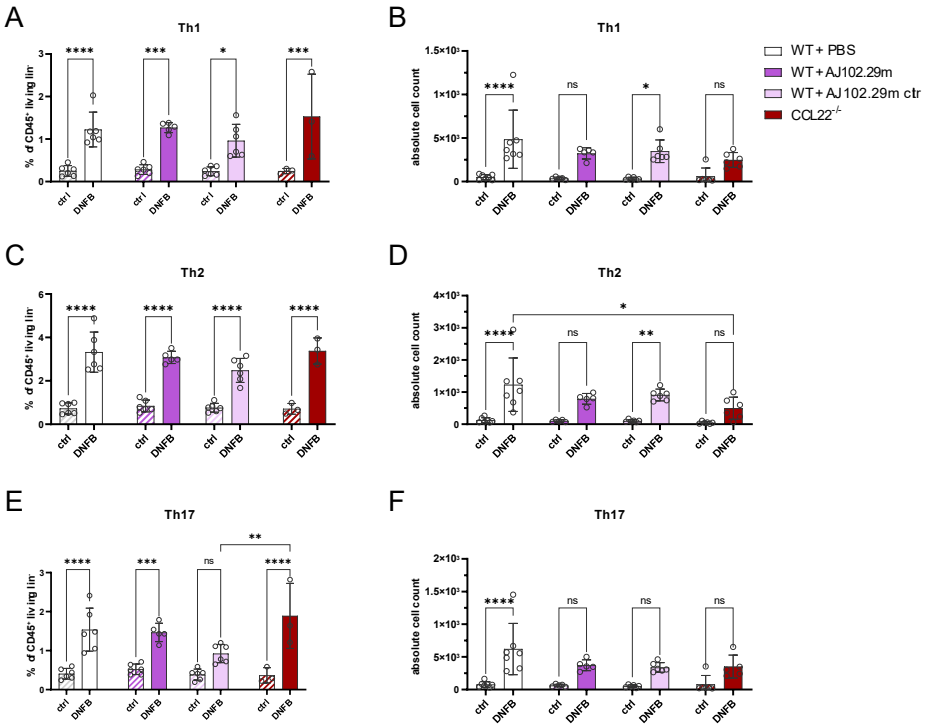

Figure 4.21 | T helper subsets in the ear samples of mice after induction of CHS with application of AJ102.29m.
WT and CCL22$^{-/-}$ mice were sensitized with DNFB on day −5 and day −4. On day 0, WT mice were injected i.p. with 10 nmol AJ102.29m, AJ102.29m ctrl or PBS right before and 12 h after DNFB challenge. CCL22$^{-/-}$ mice received PBS injections. Depicted are the frequencies and cell count of (A; B), Tbet^{+} Th1 cells, and (C, D) Gata3^{+} Th2 cells and (E, F) Rorγt^{+} Th17 cells isolated of the ear skin after the induction of a contact hypersensitivity. Statistical significance was tested using two-way ANOVA with Bonferroni post hoc test for multiple comparisons (n = 3-6 per group, mean±SEM, *p=0.01-0.05, **p=0.001-0.01, ***p<0.001, ****p<0.0001).

The percentages of Th1 T cells in the ears significantly increased after hapten application, however no significant differences between the analyzed cohorts were observed **(Figure 4.21 A)**. The absolute count of Th1 T cells only increased significantly in the WT control and AJ102.29m ctrl mice upon DNFB treatment **(Figure 4.21 B).**

Around 1 % of lineage^{-} CD45^{+} infiltrated immune cells were Th2 cells in the control ear sample, while these cells increased up to 3.5% after allergen encounter in all analyzed mice. The numbers of infiltrated Th2 cells were different between the analyzed cohorts. Whereas the absolute counts significantly increased when mice were treated with DNFB in the control cohorts, the mice that received AJ102.29m and CCL22$^{-/-}$ mice showed no significant elevation of Th2 cell numbers **(Figure 4.21 C).** In fact, the numbers in the DNFB-treated ears of the CCL22$^{-/-}$ mice were significantly lower than in the ears of the WT control mice.

The percentage of Th17 cells was comparable in all analyzed cohorts except for the ear samples of aptamer ctrl mice where the frequency was lower **(Figure 4.21 D)**. Although more Th17 cells could be detected in the ears treated with DNFB in all analyzed cohorts, a significant increase was only apparent for the WT control mice **(Figure 4.21 F)**.

All in all, the flow cytometric analysis revealed that intraperitoneal injection of AJ102.29m led to a similar effect as in CCL22$^{-/-}$ mice, although less pronounced. In both cases, less T cell infiltrate was present in the ears after allergen encounter. CD8^{+} T cells as well as CD4^{+} T cell populations, such as Treg and Th1 cells were affected, suggesting that cell trafficking of these cells was disturbed. However, no clear change in the frequency of CCR4^{+} cells was apparent.

4.1.5. Topical application of CCL22-specific aptamers for suppression of allergic reactions in contact hypersensitivity

4.1.5.1. CCL22-specific aptamers are able to penetrate skin

With the prospect of developing CCL22 aptamers as a potential therapeutic for allergic skin reactions we aimed to find more suitable application method than intraperitoneal injection. Therefore, we tested topical application in form of an easily applicable cream. For this purpose, an assay was established to first check the penetration of the skin *ex vivo*. Either AJ82.51 or AJ102.29 was applied in DAC cream – an amphiphilic basic cream preparation according to the German Drug Codex frequently used by dermatologists to apply medication topically (Gloor et al., 2003). In this Franz diffusion cell assay, the formulation was applied topically on *ex vivo* isolated mouse ears in a closed system. Subsequently, penetration of the aptamer was tested by measuring the concentration of the aptamer in the media on the dermal side of the skin as well as by microscopic analysis of the skin itself when fluorescently labelled aptamers where used **(Figure 4.22)**.

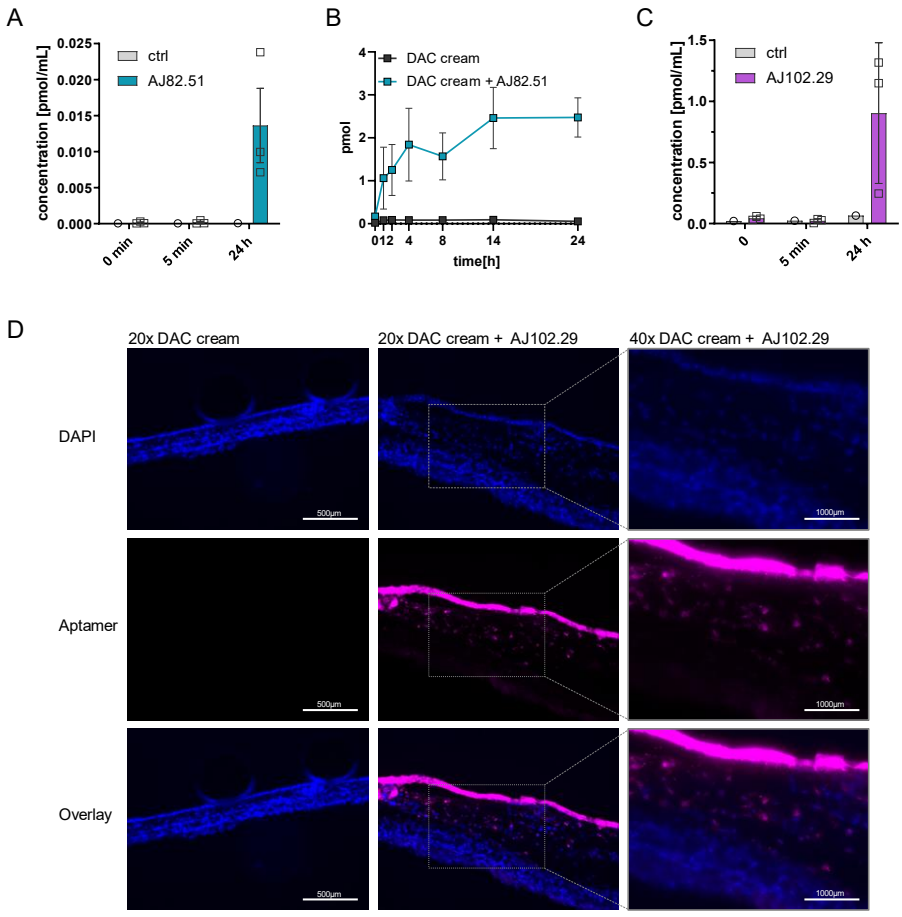

Figure 4.22 | Topically applied AJ82.51 and AJ102.29 in DAC cream penetrates the skin in an *ex vivo* skin assay.
(A, B) Amount of AJ82.51 that penetrated the skin in a Franz-diffusion cell assay at different time points. (C) Concentration of AJ102.29 that penetrated the skin in a Franz-diffusion cell assay. (D) Application of DAC cream with or without 1 nmol Atto647 labelled AJ102.29 in an *ex vivo* Franz-diffusion cell assay. Nuclei were stained with DAPI (blue). Left scale bar = 500 µm, right scale bar = 1000 µm.

Directly after assembling the assay and 5 minutes later neither AJ82.51, nor AJ102.29 could be detected within the skin. In contrast, 24 h after application, both aptamers penetrated the skin **(Figure 4.22 A, C)**. Interestingly, when comparing the two aptamers, AJ102.29 was more efficient in penetrating the skin as almost 10 times more aptamer reached the bottom chamber of the Franz cell. This might be due to its shorter length and/or differences in the skin area that was fully covered by the cream. A time course experiment revealed that AJ82.51 was able to penetrate the skin already after 1h, which increased over time until it peaked at around 14h **(Figure 4.22 B)**.

Remarkably, microscopic analysis of the skin after topical application of fluorescently labelled AJ102.29 demonstrated that the aptamer penetrated the epidermis and reached the dermis **(Figure 4.22 D).** In contrast to the control skin, where only DAPI staining was visible, in the skin sample that was treated with the aptamer topically, AJ102.29 fluorescence signals could be

detected on top of the skin, as well as in the epidermis and in the dermis. At a higher magnification AJ102.29 could be identified in the interstitial space of the dermis and deposited on cell surfaces, confirming penetration of the skin by AJ102.29. Additionally, in a Franz diffusion cell experiment with fluorescently labelled AJ102.29 and AJ102.29 ctrl, penetration could be observed for both – AJ102.29 and its scrambled control **(Figure 4.23)**.

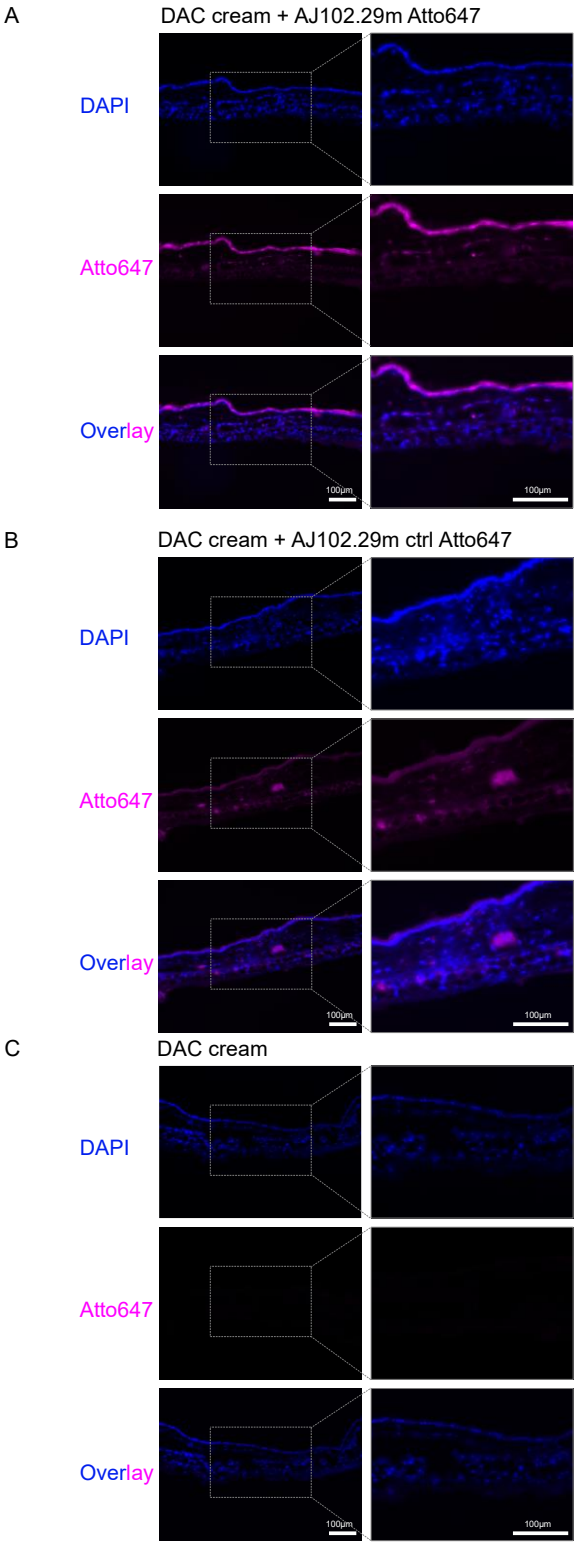

Figure 4.23 | Topically applied AJ102.29 and AJ102.29 ctrl in DAC cream penetrates the skin in an *ex vivo* skin assay. Application of 1nmol Atto647 labelled (A) AJ102.29 or (B) AJ102.29 ctrl in comparison with (C) DAC cream alone in an *ex vivo* Franz-diffusion cell assay. Nuclei were stained with DAPI (blue). scale bar = 100 µm.

4.1.5.2. Application of the DAC cream alone does not ameliorate allergic symptoms during contact hypersensitivity

Before the topical application of AJ102.29m was tested in a CHS experiment, it was investigated whether application of the cream alone already ameliorates allergic symptoms in the CHS model. For this purpose, WT mice with and without topical application of DAC cream were compared to CCL17$^{E/E}$ mice, that are known to have a milder allergic reaction to DNFB in the CHS model (Fülle, Steiner, et al., 2018)**.**

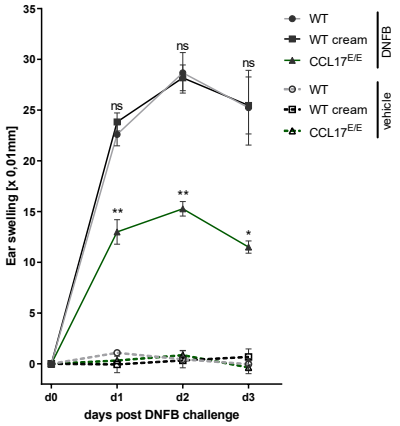

Figure 4.24 | No change in ear swelling reaction after induction of CHS with application of DAC cream alone.
WT and CCL17$^{E/E}$ mice were sensitized with DNFB on day −5 and day −4. On day 0, WT mice were treated topically with 100 µg DAC cream right before and 12 h after DNFB challenge. Ear swelling response of WT and CCL17$^{E/E}$ mice 24 h (day 1), 48 h (day 2), and 72 h (day 3) after application of DNFB (solid lines) or vehicle (dashed lines) Statistical significance was tested using two-way ANOVA with Bonferroni post hoc test for multiple comparisons (n = 4-5 per group, mean±SEM, *p=0.01-0.05, **p=0.001-0.01, ***p<0.001, ****p<0.0001).

Remarkably, the ear swelling response of WT mice treated twice with DAC cream or without DAC cream was similar, whereas the CCL17$^{E/E}$ mice displayed a reduced ear swelling response **(Figure 4.24)**. Thus, DAC cream alone did not influence the strength of the CHS reaction.

In addition to the ear swelling reaction the infiltration of T cells into the ears was analyzed using flow cytometry **(Figure 4.25)**.

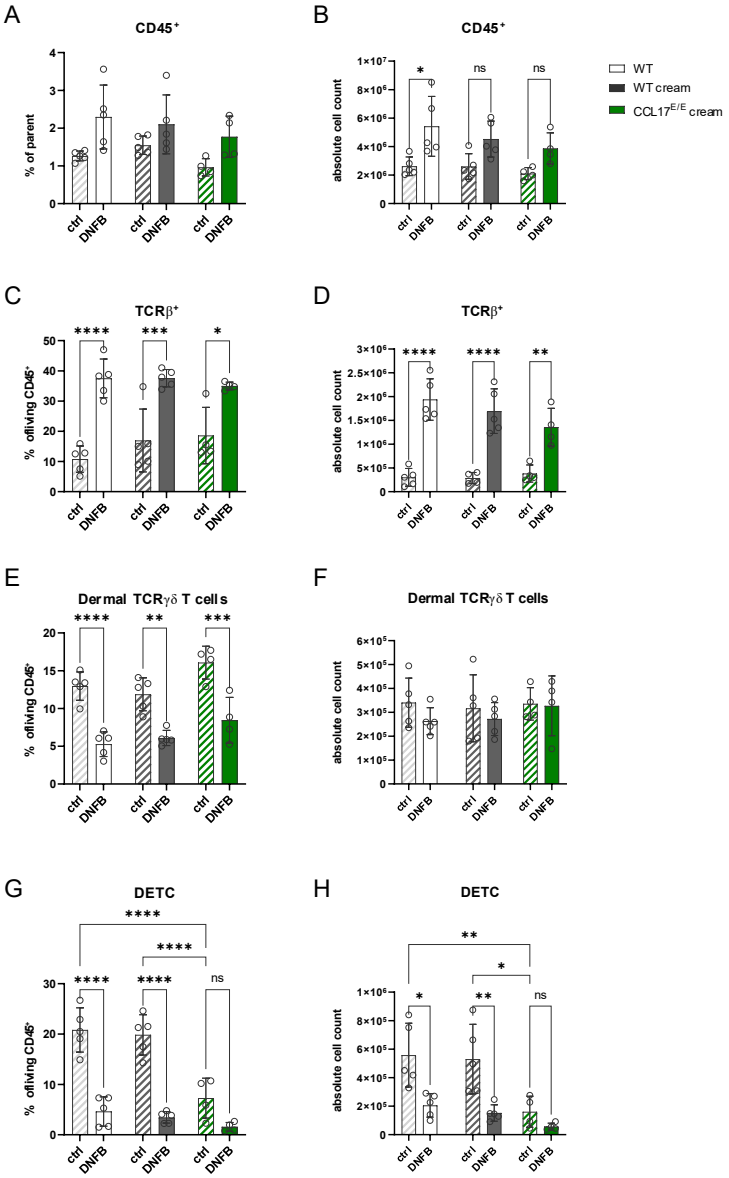

Figure 4.25 | Flow cytometric analysis of immune cell infiltration into the ears of mice after induction of CHS with DAC cream treatment.
WT and CCL17$^{E/E}$ mice were sensitized with DNFB on day −5 and day −4. On day 0, WT mice were treated topically with 100 µg DAC cream right before and 12 h after DNFB challenge. Depicted are the frequencies and cell count of (A, B) CD45$^+$, (C, D) TCRβ$^+$ T cells, (E, F) Tbet$^+$ dermal γδ T cells and (G, H) DETC. Statistical significance was tested using two-way ANOVA with Bonferroni post hoc test for multiple comparisons (n = 4-5 per group, mean±SEM, *p=0.01-0.05, **p=0.001-0.01, ***p<0.001, ****p<0.0001).

Like the ear swelling reaction, DAC cream-treated mice demonstrated comparable results to WT control mice. Expectedly, DNFB application led to an increase in frequency and absolute numbers of CD45$^+$ lineage-negative immune cells in the ears in all cohorts analyzed **(Figure 4.25 A, B)**. While WT control mice demonstrated significantly elevated numbers of CD45$^+$ cells in the allergic ear compared to the control ear, CCL17$^{E/E}$ mice had the lowest numbers of immune cells in the allergic ears. Similarly, the percentage and the absolute cell count of conventional T cells were alike in WT control mice and WT mice treated with DAC cream, while

CCL17$^{E/E}$ had the least cell infiltration **(Figure 4.25 C, D)**. For the frequency and absolute cell number of dermal γδT cells no differences between groups were apparent **(Figure 4.25 E, F)**. Notably, similar to the previous observations **(4.1.1)**, the percentage of DETC was already significantly lower in the vehicle-treated ears of CCL17$^{E/E}$ mice compared to the WT control and WT mice that received the DAC cream **(Figure 4.25 G).** Upon DNFB treatment the frequency decreased even further in WT control mice and WT mice treated with DAC cream, but not significantly in the CCL17$^{E/E}$ mice. Likewise, the number of DETC in the vehicle-treated ears is significantly decreased in the CCL17$^{E/E}$ mice compared to both WT cohorts **(Figure 4.25 H)**. The number of DETC in the DNFB-treated ears, however, decreased in all cohorts, though not significantly in CCL17$^{E/E}$ mice compared to the vehicle-treated ear. Overall, for the WT mice with and without cream application similar cell frequencies and numbers of all cell types were detected.

Thus, topical application of the DAC cream did not induce any alterations in allergic symptoms upon CHS induction and was therefore well suited to serve as vehicle for the aptamers in the following experiments.

4.1.5.3. Topical application of AJ102.29m ameliorates allergic symptoms during contact hypersensitivity

To test the efficiency of topical application of a CCL22-specific aptamer, AJ102.29m was mixed with DAC cream and applied at the same time points as for the experiments performed with intraperitoneal injections, i.e. directly after the challenge and 12 h post challenge. The ear swelling reaction and the infiltration of immune cells into the ears of mice receiving either AJ102.29m or its scrambled control were analyzed and compared to CCL22$^{-/-}$ mice **(Figure 4.26)**.

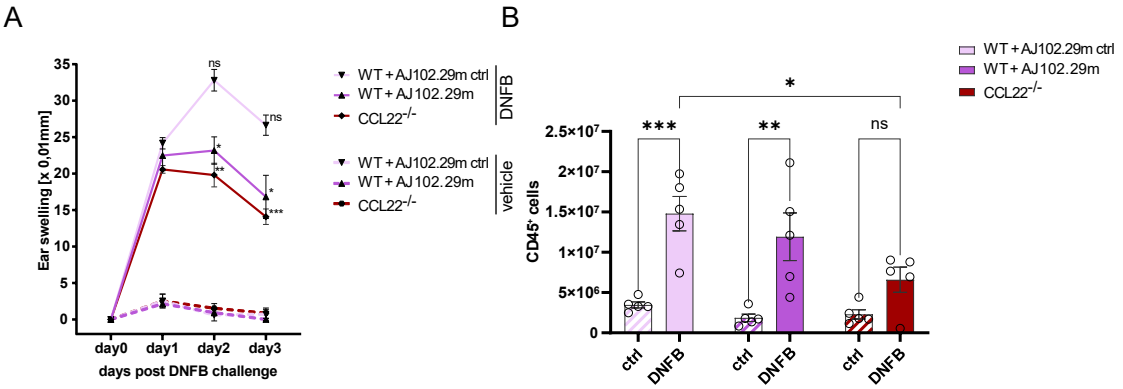

Figure 4.26 | Reduced ear swelling and leukocyte infiltration into the ears after induction of CHS with topical application of CCL22-specific aptamers in DAC cream.
WT and CCL22$^{-/-}$ mice were sensitized with DNFB on day −5 and day −4. On day 0, WT mice were treated with 10 nmol AJ102.29m and AJ102.29m ctrl in 100 mg DAC cream right before and 12 h after DNFB challenge. (A) Ear swelling of WT and CCL22$^{-/-}$ mice 24 h (day 1), 48 h (day 2), and 72 h (day 3) after application of DNFB (solid lines) or vehicle (dashed lines). Statistical significance was tested using two-way ANOVA with Bonferroni post hoc test for multiple comparisons (n = 4-5 per group, mean±SEM, *p=0.01-0.05, **p=0.001-0.01, ***p<0.001, ****p<0.0001). (B) Flow cytometric analysis of the immune cell infiltrate of the ears. At day 3, mice were sacrificed, and cells of the ears were isolated and stained for flow cytometry. Absolute numbers of CD45$^+$ cells were determined by flow cytometry. Statistical significance was tested using two-way ANOVA with Bonferroni post hoc test for multiple comparisons (n = 4-5 per group, mean±SEM, *p=0.01-0.05, **p=0.001-0.01, ***p<0.001, ****p<0.0001).

The ear thickness measurement revealed that topical application of AJ102.29 was able to suppress the ear swelling response significantly compared to control mice that received AJ102.29m ctrl **(Figure 4.26 A).** CCL22$^{-/-}$ mice, however, exhibited the lowest swelling response. In line, the frequency of CD45$^+$ lineage-negative immune cells in the allergic ears was highest in the AJ102.29m ctrl mice, whereas the number of infiltrating cells was lowest in the CCL22$^{-/-}$ mice. Nevertheless, the number of cells of AJ102.29m-treated mice was lower than in the mice that received the scrambled control.

To identify which cell populations were affected by the blockage of CCL22 after topical application of the aptamer cream, immune cell subsets were further gated using the following gating scheme **(Figure 4.27)**.

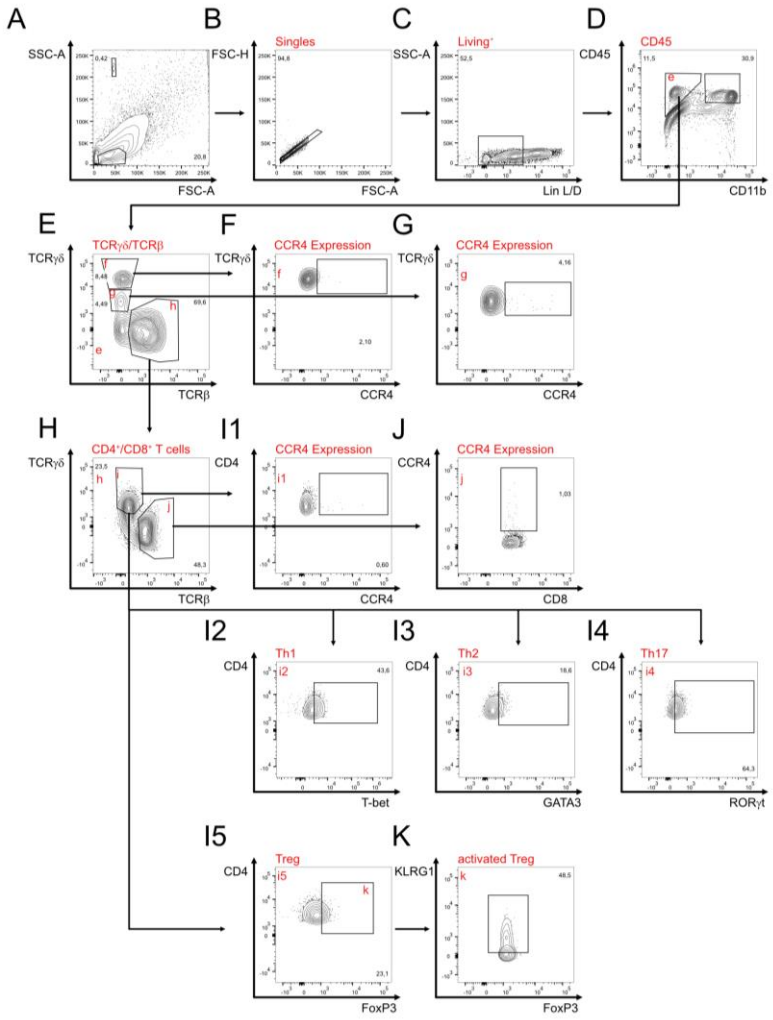

Figure 4.27 | Gating strategy for T cells in the ear skin of mice after CHS.
(A-D) Lineage$^-$ living single cells were gated for CD45 expression. (E) CD45$^+$ cells were further divided into conventional T cells, dermal γδ T cells and DETC using TCRβ and TCRγδ. (H) TCRβ$^+$ cells were gated for CD4 and CD8. Furthermore, the CCR4 expression was assessed (F, G, I1, J). (I2-I5) CD4$^+$ cells were checked for master transcription factor expression of Th subtypes using FMO controls (fluorescent minus one). (K) Treg were further gated for KLRG1 expression to identify the activated Treg.

Remarkably, the same effects for the T cell subsets as in the experiment in which AJ102.29m and its control were injected **(Figure 4.16)** were observed during this assay. Again, the percentage of TCRβ$^+$ T cells increased upon DNFB challenge but did not exhibit any differences between the cohorts. In contrast, the number of conventional T cells that infiltrated the ears upon DNFB challenge differed between groups **(Figure 4.28 A, B)**. As before, DNFB stimulation did not increase conventional T cells in ear samples of CCL22$^{-/-}$ mice and only slightly in mice that received the aptamer cream.

The frequency of dermal γδ T cells decreased in the DNFB-treated ear samples compared to the controls in all mice analyzed **(Figure 4.28 C)**. Interestingly, as observed for the CHS with aptamer injection **(Figure 4.18)** CCL22$^{-/-}$ mice had significantly higher frequencies of γδ T cells in the vehicle-treated ears compared to the other mice. In addition, the absolute number of

γδ T cells increased in all analyzed cohorts upon hapten treatment, yet, showed only a significant increase in the mice that received the aptamer cream **(Figure 4.28 D)**.

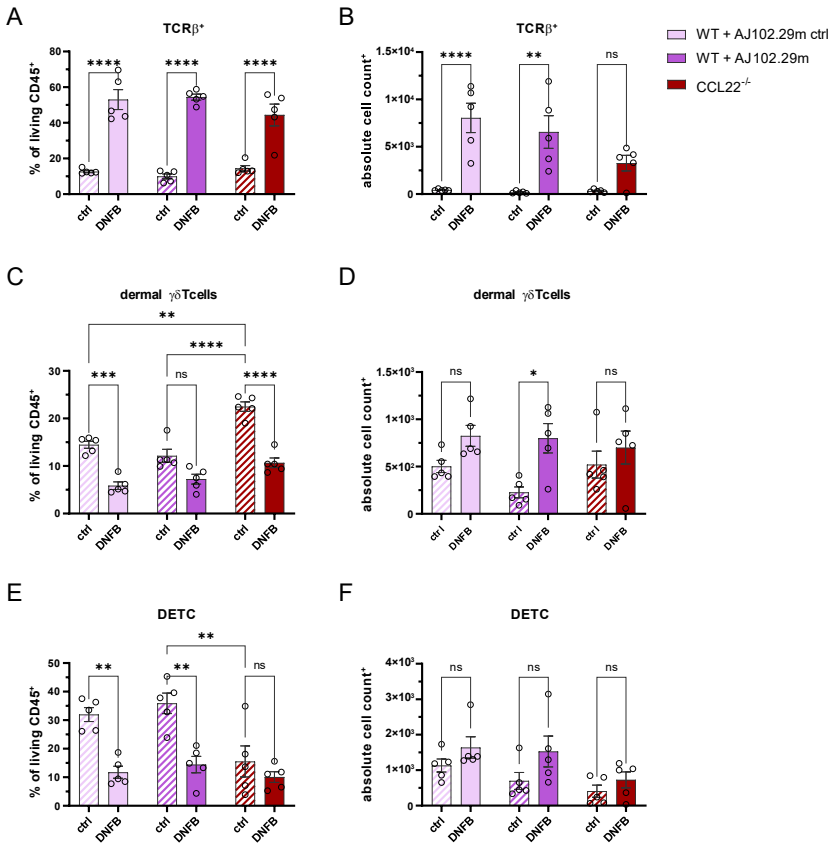

Figure 4.28 | Frequencies and absolute cell counts of T cell subsets in the ears of mice after induction of CHS with topical application of AJ102.29m in DAC cream.
WT and CCL22$^{-/-}$ mice were sensitized with DNFB on day −5 and day −4. On day 0, WT mice were treated with 10 nmol AJ102.29m and AJ102.29m ctrl in 100 mg DAC cream right before and 12 h after DNFB challenge. Depicted are the frequencies and cell count of (A, B) TCRβ^{+} T cells, (C, D) dermal γδ T cells and (E, F) DETC isolated of the ear skin after contact hypersensitivity. Statistical significance was tested using two-way ANOVA with Bonferroni post hoc test for multiple comparisons (n = 4-5 per group, mean±SEM, *p=0.01-0.05, **p=0.001-0.01, ***p<0.001, ****p<0.0001).

Whereas the frequency of DETC decreased in all cohorts when the ears were challenged with DNFB, the absolute numbers of DETC increased **(Figure 4.28 E, F).** In CCL22$^{-/-}$ mice, however, the DETC frequency only slightly increased upon DNFB stimulation. Here, similar to what has been observed before for CCL22$^{-/-}$ mice and for the CCL17$^{E/E}$ mice **(Figure 4.25),** the frequency of DETC was significantly lower in the control ears compared to WT mice. In addition, CCL22$^{-/-}$ mice had the lowest numbers of DETC in both ears compared to the other cohorts.

When analyzing the CCR4-expressing γδ T cells and DETC, no significant changes in frequencies and absolute cell count were apparent **(Figure 4.29).** Here, aptamer-treated mice showed slightly lower values than the AJ102.29 ctrl-treated mice. Interestingly, the frequency and absolute count of DETC were lowest in the control- and DNFB-treated ears of CCL22$^{-/-}$ mice when comparing all cohorts.

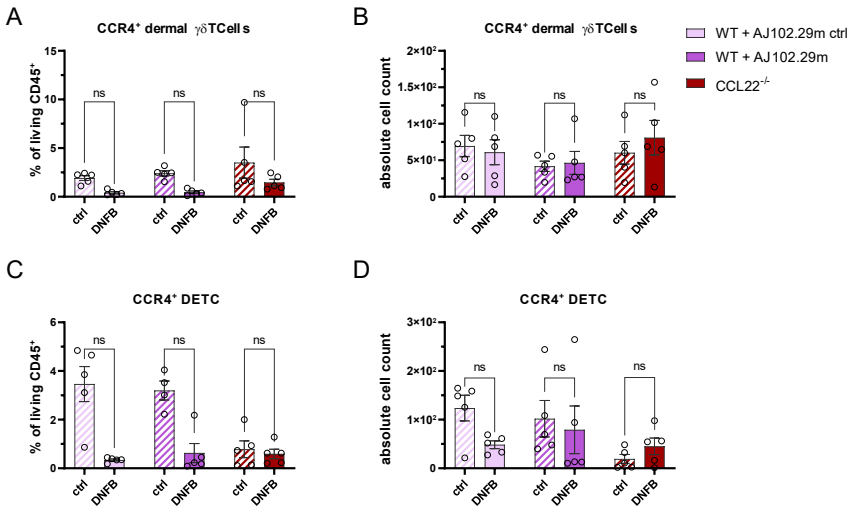

Figure 4.29 | Frequencies and absolute cell counts of CCR4 expressing γδ T cell subsets in the ears of mice after induction of CHS with topical application of AJ102.29m in DAC cream.
WT and CCL22$^{-/-}$ mice were sensitized with DNFB on day −5 and day −4. On day 0, WT mice were treated with 10 nmol AJ102.29m and AJ102.29m ctrl in 100 mg DAC cream right before and 12 h after DNFB challenge. Depicted are the frequencies and cell counts of (A, B) CCR4^{+} dermal γδ T cells and (C, D) CCR4^{+} DETC isolated of the ear skin after contact hypersensitivity. Statistical significance was tested using two-way ANOVA with Bonferroni post hoc test for multiple comparisons (n = 4-5 per group, mean±SEM, *p=0.01-0.05, **p=0.001-0.01, ***p<0.001, ****p<0.0001).

The percentage of infiltrated CD8⁺ T cells increased equally in all cohorts upon DNFB stimulation **(Figure 4.30 A)**. As in the experiments described before, the difference in numbers of CD8⁺ T cells did not reach statistical significance in CCL22$^{-/-}$ mice **(Figure 4.30 B)**. Interestingly, the increase of CD8⁺ T cells in the aptamer cream-treated mice was not as pronounced compared to control cream-treated mice. In addition, the CCR4 expression of CD8⁺ T cells did not reveal differences in frequencies or cell counts between all cohorts or upon DNFB stimulation **(Figure 4.30 C, D)**.

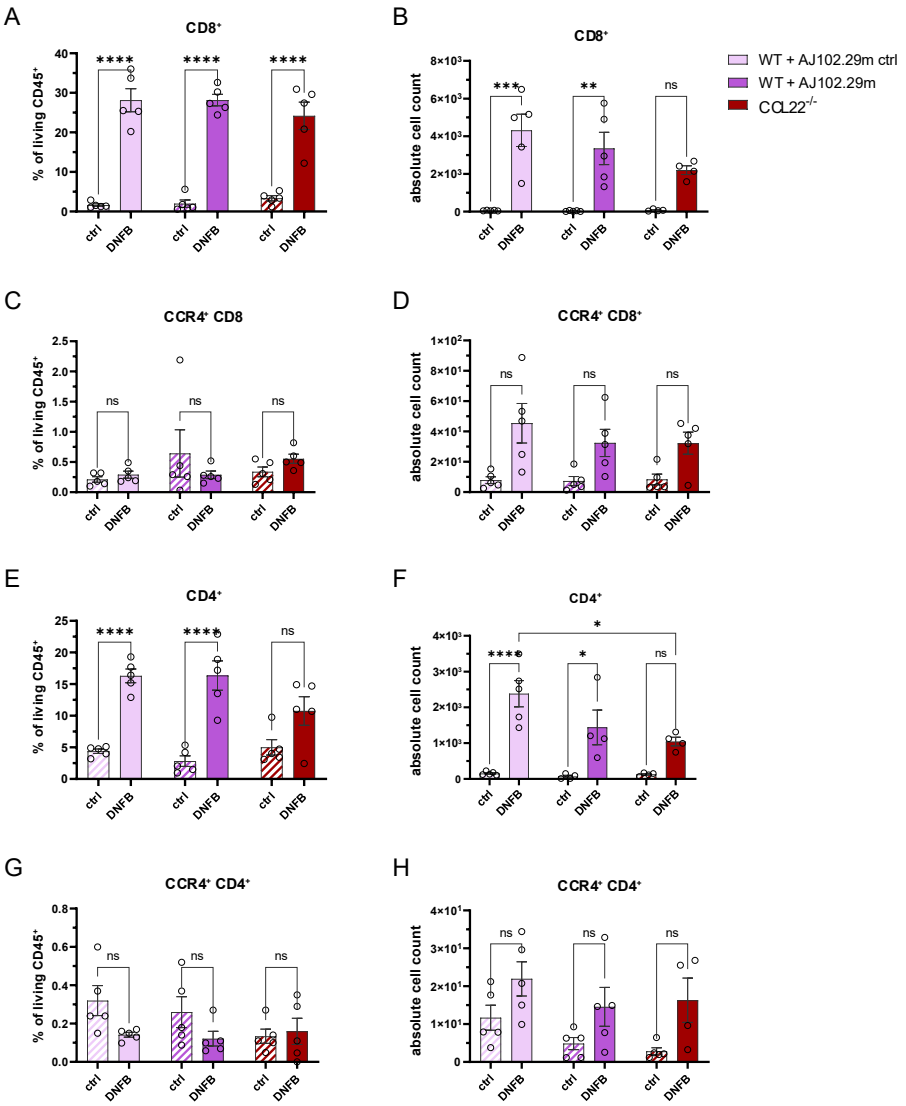

Figure 4.30 | Frequencies and absolute cell numbers of CD4⁺ and CD8⁺ T cell subsets in the ears of mice after induction of CHS with topical application of AJ102.29m in DAC cream.
WT and CCL22$^{-/-}$ mice were sensitized with DNFB on day −5 and day −4. On day 0, WT mice were treated with 10 nmol AJ102.29m and AJ102.29m ctrl in 100 mg DAC cream right before and 12 h after DNFB challenge. Depicted are the frequencies and cell count of (A, B) CD8⁺, (C, D) CCR4⁺ CD8⁺ and (E, F) CD4⁺ and (G, H) CCR4⁺ CD4⁺ T cells isolated of the ear skin after an contact hypersensitivity. Statistical significance was tested using two-way ANOVA with Bonferroni post hoc test for multiple comparisons (n = 4-5 per group, mean±SEM, *p=0.01-0.05, **p=0.001-0.01, ***p<0.001, ****p<0.0001).

Different from the aptamer injection experiment, the frequency of CD4⁺ T cells increased in the allergic ears compared to the control ears in all cohorts, but the increase was not

significantly different in CCL22$^{-/-}$ mice **(Figure 4.30 E)**. In line with the previous results, however, less CD4^{+} T cells infiltrated the ears of the DNFB challenged CCL22$^{-/-}$ mice, and CD4^{+} T cell counts were significantly lower compared to the AJ102.29m ctrl mice **(Figure 4.30 F)**. Strikingly, AJ102.29m-treated mice had less CD4^{+} T cells in the ear skin than the control mice though not significantly decreased. While the frequency of CCR4-expressing CD4^{+} T cells decreased, the absolute number increased upon DNFB stimulation in each cohort analyzed, yet no significant differences were obvious **(Figure 4.30 G, H)**.

Overall, application of AJ102.29m in DAC cream led to decreased CD8^{+} and CD4^{+} T cell numbers in DNFB-treated ears compared to the mice treated with AJ102.29m ctrl. Taken together, CD4^{+} and CD8^{+} T cell subsets reflected what the analysis of conventional T cells had already shown: inhibition of CCL22 by AJ102.29m in DAC cream reduced T cell infiltration into inflamed ears similarly to a genetic CCL22-deficiency, but not as profoundly.

As CCL22 is known to be involved in Treg recruitment (Eby et al., 2015; Faget et al., 2011; Hao et al., 2016; Rapp et al., 2019; Röhrle et al., 2020), the percentage and cell counts of Treg were analyzed **(Figure 4.31)**.

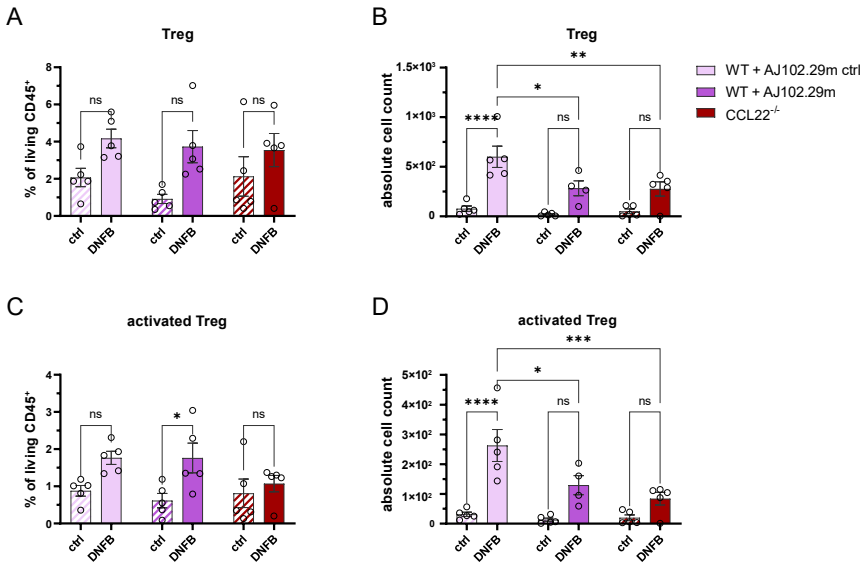

Figure 4.31 | Regulatory T cells in the ears of mice after induction of CHS with topical application of AJ102.29m in DAC cream.
WT and CCL22$^{-/-}$ mice were sensitized with DNFB on day −5 and day −4. On day 0, WT mice were treated with 10 nmol AJ102.29m and AJ102.29m ctrl in 100 mg DAC cream right before and 12 h after DNFB challenge. Depicted are the frequencies and cell count of (A, B) FoxP3$^+$ Treg and (C, D) KLRG1$^+$ FoxP3$^+$ activated Treg isolated of the ear skin after contact hypersensitivity induction. Statistical significance was tested using two-way ANOVA with Bonferroni post hoc test for multiple comparisons (n = 4-5 per group, mean±SEM, *p=0.01-0.05, **p=0.001-0.01, ***p<0.001, ****p<0.0001).

In contrast to the aptamer-treatment experiment described above, using intraperitoneal injection **(Figure 4.20),** no differences were apparent regarding the frequencies of Treg. In contrast, the absolute counts of Treg in DNFB-stimulated ear samples of mice that received AJ102.29m cream and CCL22$^{-/-}$ mice were both significantly reduced in comparison to control mice. Hence, this clearly indicates that the genetic deficiency of CCL22 and the inhibition by topical administration of CCL22-specific aptamers affected the recruitment of Treg into the skin.

Based on the expression of the master transcription factors CD4$^+$ T cells were separated into different T helper subsets **(Figure 4.32)**.

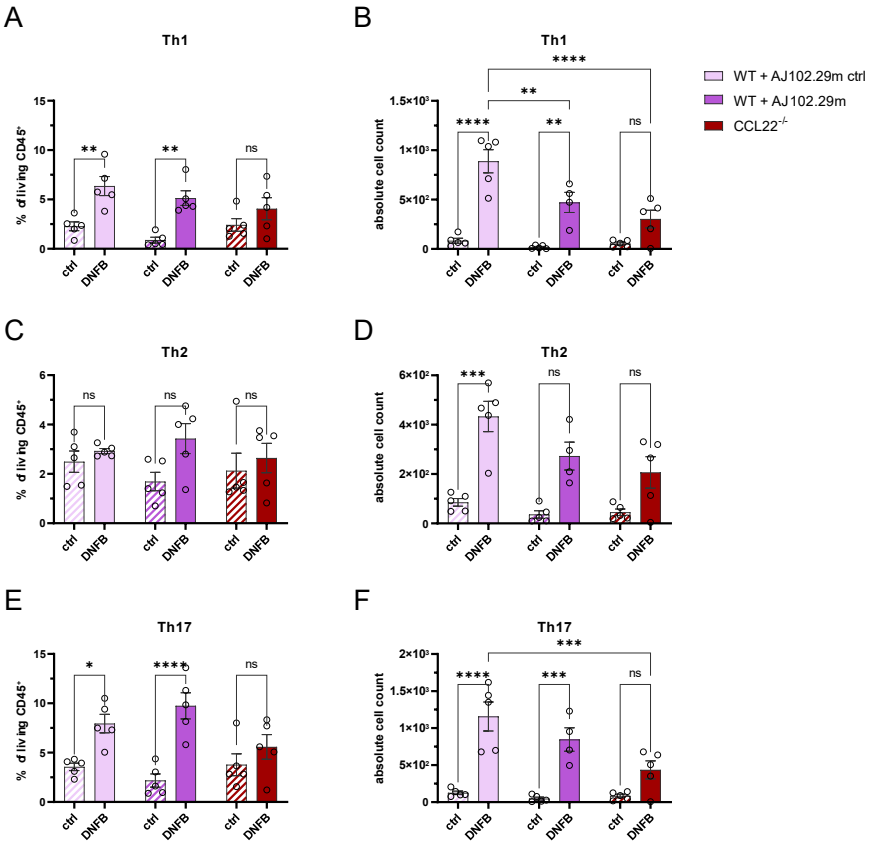

Figure 4.32 | T helper subsets in the ears of mice after induction of CHS with application of CCL22-specific aptamers. WT and CCL22$^{-/-}$ mice were treated with 10 nmol AJ102.29m and AJ102.29m ctrl in 100mg DAC cream right before and 12 h after DNFB challenge. Depicted are the frequencies and cell counts of (A, B) Tbet$^+$ Th1 cells, (C, D) GATA3$^+$ Th2 cells and (E, F) Rorγt$^+$ Th17 cells isolated from the ear skin after contact hypersensitivity induction. Statistical significance was tested using two-way ANOVA with Bonferroni post hoc test for multiple comparisons (n = 4-5 per group, mean±SEM, *p=0.01-0.05, **p=0.001-0.01, ***p<0.001, ****p<0.0001).

The results for the T helper cell subsets gained in this experiment were similar to the effects observed in the previous experiment in which the aptamer was injected intraperitoneally. In the current experiment, the mice treated with the AJ102.29m cream and CCL22$^{-/-}$ mice contained significantly less Th1 cells in DNFB-treated ears compared to mice treated with AJ102.29m ctrl **(Figure 4.32 B)**. The absolute numbers of Th2 cells infiltrating the ears increased significantly in AJ102.29m ctrl cream-treated ears after DNFB challenge, whereas there were no significant changes in the AJ102.29m-treated mice and the CCL22$^{-/-}$ mice **(Figure 4.32 D)**. Mice which received the cream with either AJ102.29m or AJ102.29m ctrl showed significantly increased frequencies of Th17 cells upon DNFB stimulation **(Figure 4.32 E)**. Regarding absolute numbers of Th17 cells, most Th17 cells infiltrated the DNFB-treated ears of mice treated with AJ102.29m ctrl, whereas CCL22$^{-/-}$ mice contained the least followed by the mice that received AJ102.29m **(Figure 4.32 F)**. In AJ102.29m-treated mice the numbers of

all three T helper subsets analyzed were lower than in the control animals, yet still not as low as in the CCL22$^{-/-}$ mice.

Overall, it could be clearly shown that topical treatment with AJ102.29m led to reduced T cell infiltration upon hapten exposure nearly in a range as in CCL22$^{-/-}$ mice. Here, especially CD4^{+} and CD8^{+} conventional T cells were affected. Also, Treg, Th1, Th2 and Th17 T cell subsets were decreased in the mice that either got AJ102.29m or lacked CCL22 systemically.

Overall, it could be clearly shown that topical treatment with AJ102.29m permits penetration of the aptamers into the skin and was able to suppress allergic symptoms of CHS almost as much as in CCL22$^{-/-}$ mice. The treatment not only reduced the ear swelling response, but also a notable reduction of T cell infiltration in the ears could be observed. Here, especially CD4^{+} and CD8^{+} conventional T cells were affected. Also, Treg, Th1, Th2 and Th17 T cell subsets were decreased in the mice that either got AJ102.29m or lacked CCL22 systemically. Hence, the experiments performed in this thesis provide proof-of-principle that non-invasive administration of CCL22-specific aptamers mixed in a cream applied to the skin could be a potential treatment option for contact allergies.

4.1.6. Functional testing of aptamers directed against human CCL17

After confirming the effects of pharmacological blockage of the CCL17/CCL22-CCR4-axis by aptamers in CHS - the murine model of ACD- the next step in the progress of evaluating the CCL17/CCL22-CCR4-axis as a target for contact allergy treatment was generating aptamers specific for human CCL17 or CCL22. So far, Anna Jonczyk selected one possible candidate binding CCL17, which was tested in this thesis for functionality.

A transwell assay with the human T cell lymphoma cell line Mac1 (Davis et al., 2010; Su et al., 1988) was used to evaluate the inhibitory capacity of the aptamer candidate hAJ78 **(Figure 4.33)**. First, concentration-dependent migration of Mac1 cells was tested using increasing concentrations of CCL17 and confirmed the CCL17-dependent migration of Mac1 cells **(Figure 4.33 A)**. Next, the inhibition of migration by hAJ78 was tested in the transwell assay **(Figure 4.33 B)**. Here, no concentration-dependent inhibition of migration by the aptamer was detectable. However, when comparing the medium control with the condition in which CCL17 only was added the difference in migration was not very high. Thus, the cell line used might not be suitable for testing the aptamer functionally. Additionally, the percentage of migrated cells slightly decreased with increasing aptamer concentrations supporting the hypothesis that the migration potential of Mac1 cells is not big enough to see the aptamer-dependent inhibition of migration.

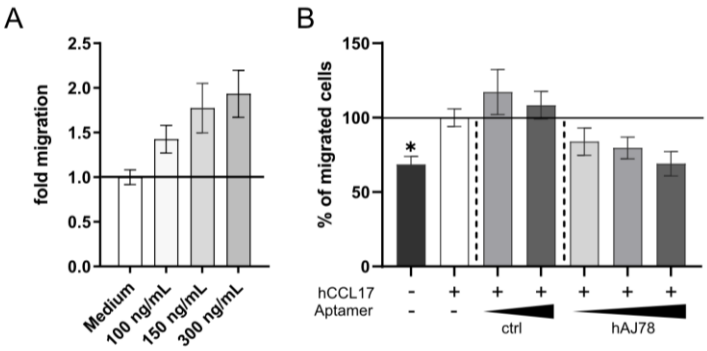

Figure 4.33 | Concentration dependent transwell migration of the human cell line Mac1 towards CCL17 in the presence of the human CCL17 aptamer candidate hAJ78.
(A) Concentration dependent migration of Mac1 cells shown as fold migration of the medium control with increasing concentrations of CCL17 (100 ng/ml, 150 ng/ml, 300 ng/ml). (B) Migration of Mac1 cells towards CCL17 [12.8 nM] was measured in a transwell migration assay in the presence of aptamers. Aptamer candidate hAJ78 was tested in 1:10 molar ratio (1.28 nmol/well), equimolar ratio (12.8 nmol/well) and 10:1 molar ratio (128 nmol/well). The scrambled control was tested in equimolar ratio (12.8 nmol/well) and 10:1 molar ratio (128 nmol/well). As control migration without the addition of CCL17 or aptamers, as well as the migration towards CCL17 only was measured. Statistical significance was tested by using ordinary one-way-ANOVA with post-hoc Bonferroni test (n = 3 per group, mean ± SEM, *p=0.01-0,05, **p=0.001-0.01, ***p<0.001, ****p<0.0001).

As an alternative approach, the inhibitory capacity of the aptamer was then tested in a transwell assay using primary human $CD4^+$ T cells isolated from PBMCs by magnetic sorting.

First, the CCR4 expression required for migration towards CCL17 was measured over a time course of 14 days during the activation period of the cells **(Figure 4.34 A)**.

CCR4 expression increased from 30 % of $CD4^+$ T cells up to 40 % of $CD4^+$ T cells over the time course. Besides CCR4 expression, the activation status was checked using CD25 staining at day 8 of the culture **(Figure 4.34 B)**. Around 70 % of $CD4^+$ T cells were positive for CD25, thus, additionally proofing the activated state of the T cells. Hence, a transwell assay with addition of hAJ78 was performed **(Figure 4.34 C)**. Although a tendency of inhibition of migration by hAJ78 was visible in previous experiments using Mac1 cells, no notable reduction in the frequency of migrated cells was observed in this experiment. Furthermore, the addition of hAJ78 lead to the same values as addition of the scrambled control, whereas for the medium control a strong decrease in percent of migrated cells compared to the CCL22 condition was obtained.

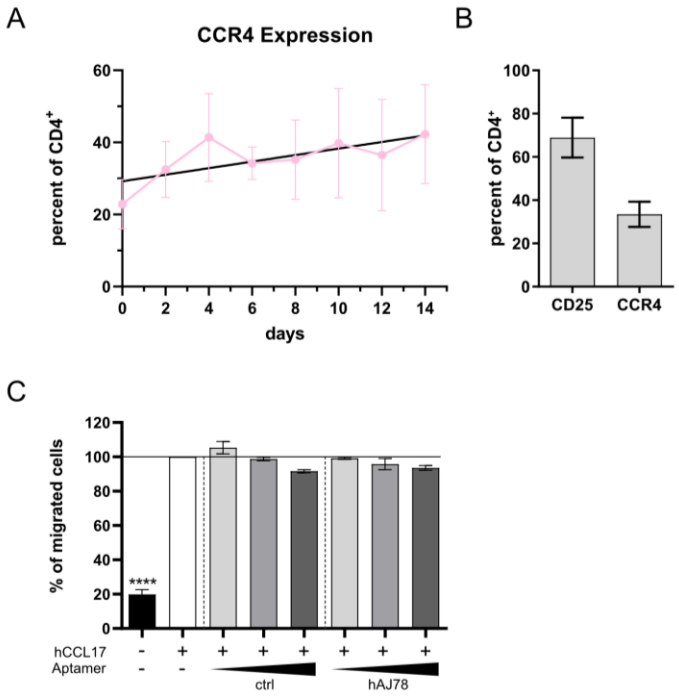

Figure 4.34 | Testing human CCL17 aptamer candidate hAJ78 with primary human T cells.
(A) CCR4 expression of activated human primary T cells in a time course of 14 days. (B) Activation status of human primary T cells on day 8 of cultivation. (C) Migration of human primary T cells towards CCL17 [12,8 nM] was measured in a transwell migration assay in the presence of human aptamer candidate hAJ78. Aptamer candidate hAJ78 and its control was tested in 1:10 molar ratio (1.28 nmol/well), equimolar ratio (12.8 nmol/well) and 10:1 molar ratio (128 nmol/well). As control migration without the addition of CCL17 or aptamers, as well as the migration towards CCL17 only was measured. Statistical significance was tested by using ordinary one-way-ANOVA with post-hoc Bonferroni test (n = 2 (A-B) n = 3 (C), *p=0.01-0,05, **p=0,001-0,01, ***p<0,001, ****p<0,0001).

Taken together, while the human T cell lymphoma cell line was not sufficient to test the inhibitory capacity of the aptamer, transwell assays with primary human T cells isolated from

PBMCS, magnetically sorted for $CD4^+$ T cells were well suited for functional testing of the aptamer. However, hAJ78 specific for human CCL17 did not inhibit CCL17-dependent migration.

4.2. The CCL17/CCL22-CCR4-axis in atopic dermatitis-like skin inflammation

After highlighting the importance of the CCL17/CCL22-CCR4-axis in contact allergies, the role of the chemokines and chemokine receptor with AD was of interest, because AD is caused by a different type of allergy representing a Type II immune response (Auriemma et al., 2013; J. Kim et al., 2019; F. T. Liu et al., 2011; G. Wang et al., 2007). Additionally, a former publication demonstrated that CCL17 plays a role in AD, as CCL17 deficiency in the BALB/c genetic background led to suppressed allergic symptoms and impaired DC migration in the pathogenesis of AD (Stutte et al., 2010). Moreover, elevated levels of CCL17 and CCL22 have been identified in AD patients and are regarded as biomarkers for progression of AD in children (Halling et al., 2023; Kakinuma et al., 2001; Shimada et al., 2004).

Hence, mice lacking either CCL17 or CCL22, or both, as well as CCR4-deficient mice were compared to WT mice in the AD mouse model. In this model, mice undergo three treatment cycles with two weeks pause in between. Each treatment cycle consists of two treatments in which the back of the mice is shaved and tape stripped to disrupt the skin barrier and then a patch with ovalbumin is taped on the backs for allergen exposure. After seven weeks, histological features of the skin, IgE levels in the serum, cytokine production of OVA-restimulated immune cells, as well as immune cell analysis of the skin tissue can be investigated to evaluate the symptoms of allergy.

4.2.1. More Type II cytokine production by immune cells and higher levels of IgE in serum after induction of atopic dermatitis-like skin inflammation.

First, it was tested whether the experimental model led to signs of Type II inflammation. Therefore, WT C57BL/6J mice were either treated with OVA or NaCl as a control and the IgE serum levels as well as cytokine production of restimulated immune cells from skin-draining lymph nodes were compared **(Figure 4.35)**. The lymph node cells were restimulated with OVA, αCD3/αCD28 as positive control or medium as negative control for 24 h and afterwards the supernatant was harvested to measure IL-5 and IL-13 concentrations using ELISA **(Figure 4.35 A, B)**.

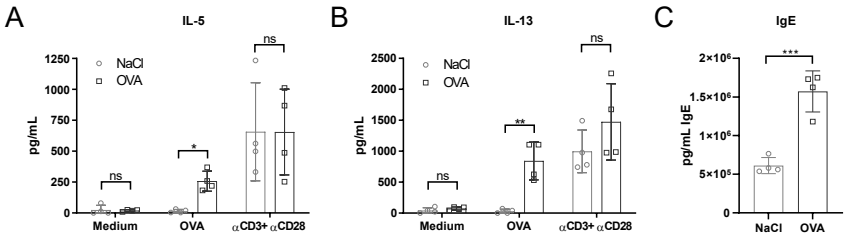

Figure 4.35 | Cytokine secretion of restimulated brachial lymph node cells and serum IgE levels after induction of AD-like skin inflammation in WT mice.
Brachial lymph node cells were seeded and stimulated with OVA (100 µg/mL), αCD3/αCD28 (3 µg/mL,2 µg/mL) or media as control for 5 days. (A) IL-5 and (B) IL-13 were measured in the supernatant of the restimulated cells using an ELISA. (C) Serum levels of IgE in WT mice after induction of AD-like skin inflammation were measured using ELISA. Statistical significance was tested using a two-way-ANOVA with post-hoc Sidak test with (n = 4, mean±SEM, *p=0.01-0.05, **p=0.001-0.01, ***p<0.001, ****p<0.0001).

Whereas addition of medium lead to no IL-5 or IL-13 secretion, T cell receptor activation by αCD3/αCD28 strongly induced IL-5 and IL-13 production in the lymph node cells of mice treated with OVA and NaCl. OVA stimulation, in contrast, only increased cytokine production in cells from OVA-treated mice, but not NaCl-treated mice, confirming the presence of OVA-specific T cells. IL-5 and IL-13 were significantly increased in OVA-treated mice when restimulated with OVA compared to NaCl-treated mice. Additionally, IgE concentration in the serum of mice was measured using ELISA **(Figure 4.35 C).** In mice that received the OVA patches almost three times more IgE antibodies were obtained indicating that the OVA treatment led to plasma cell formation and OVA-specific IgE antibodies.

Taken together, these experiments proved that the experimental procedure in the mouse model of AD induced signs of Type II inflammation in WT mice.

4.2.2. Influence of the CCL17/CCL22-CCR4-axis on the course of atopic dermatitis-like skin inflammation

4.2.2.1. Allergy induced serum IgE levels and cytokine production were not significantly altered when comparing CCL17$^{E/E}$, CCl22$^{-/-}$ and WT mice

Next, mice lacking different components of the CCL17/CCL22-CCR4-axis were compared in AD experiments. Here, additionally to OVA patches, a cohort of WT-, CCL17$^{E/E}$- and CCL22$^{-/-}$ mice was treated with patches containing a combination of OVA and a crude extract of Dermatophagoides farina, house dust mite protein (Der.f.). Lymph node cells were restimulated with OVA, αCD3/αCD28 or medium only and cytokine secretion was measured using ELISA **(Figure 4.36)**.

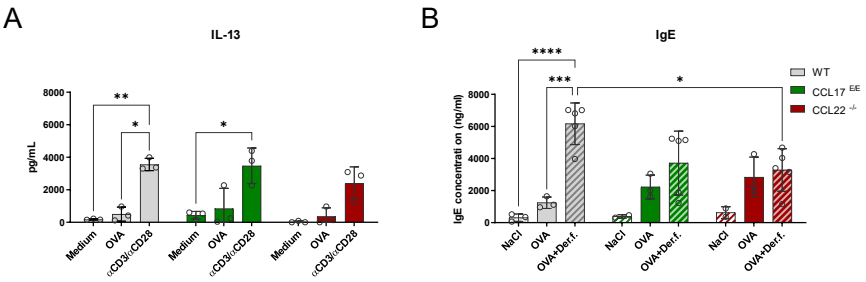

Figure 4.36 | Cytokine secretion of brachial lymph node cells of WT, CCL17$^{E/E}$ and CCL22$^{-/-}$ mice after restimulation with OVA and OVA/Der.f. after induction of AD-like skin inflammation in WT mice.
Brachial lymph node cells of OVA-treated WT, CCL17$^{E/E}$ and CCL22$^{-/-}$ mice were seeded and stimulated with OVA (100 µg/mL), αCD3/αCD28 (3 µg/mL, 2 µg/mL) or media as control for 5 days. (A) IL-13 and (B) IgE were measured in the supernatant of the restimulated cells using an ELISA. WT, CCL17$^{E/E}$ and CCL22$^{-/-}$ mice treated with either NaCl, OVA or OVA/Der.f. after induction of AD-like skin inflammation were measured using ELISA Statistical significance was tested by using a two-way-ANOVA with post-hoc Sidak test (n = 4, mean±SEM, *p=0.01-0.05, **p=0.001-0.01, ***p<0.001, ****p<0.0001).

WT mice showed a significant increase in IL-13 production from comparing medium- and OVA stimulation to the positive control **(Figure 4.36 A)**. Lymph node cells of CCL17$^{E/E}$ mice also significantly increased IL-13 secretion upon αCD3/αCD28 treatment compared to the negative control. Remarkably, in all tested conditions, lymph node cells of CCL22$^{-/-}$ mice had the lowest amount of IL-13. Nevertheless, no significant differences were obtained for the different stimulations of CCL22$^{-/-}$ lymph node cells. Furthermore, the cohorts demonstrated no differences between each other.

The IgE serum levels in the cohorts increased in the mice that received OVA or OVA/Der.f. **(Figure 4.36 B)**. While OVA treatment led to highest IgE levels in CCL22$^{-/-}$, followed by CCL17$^{E/E}$ mice, OVA/Der.f. treatment increased IgE levels most strongly in WT mice. Nevertheless, no significant changes were observed. Of note, some technical issues might have influenced the results as the values are lower in comparison to what has been observed in previous experiments in our group.

4.2.2.2. No major differences between genotypes in skin histology in the atopic dermatitis model

Additionally, histological sections of the atopic skin were compared to analyze epidermal and dermal thickness, as well as mast cell count. For this purpose, the skin was fixed, paraffin embedded and 10µm slices were stained with H&E **(Figure 4.37)** or Toluidine blue **(Figure 4.38)**.

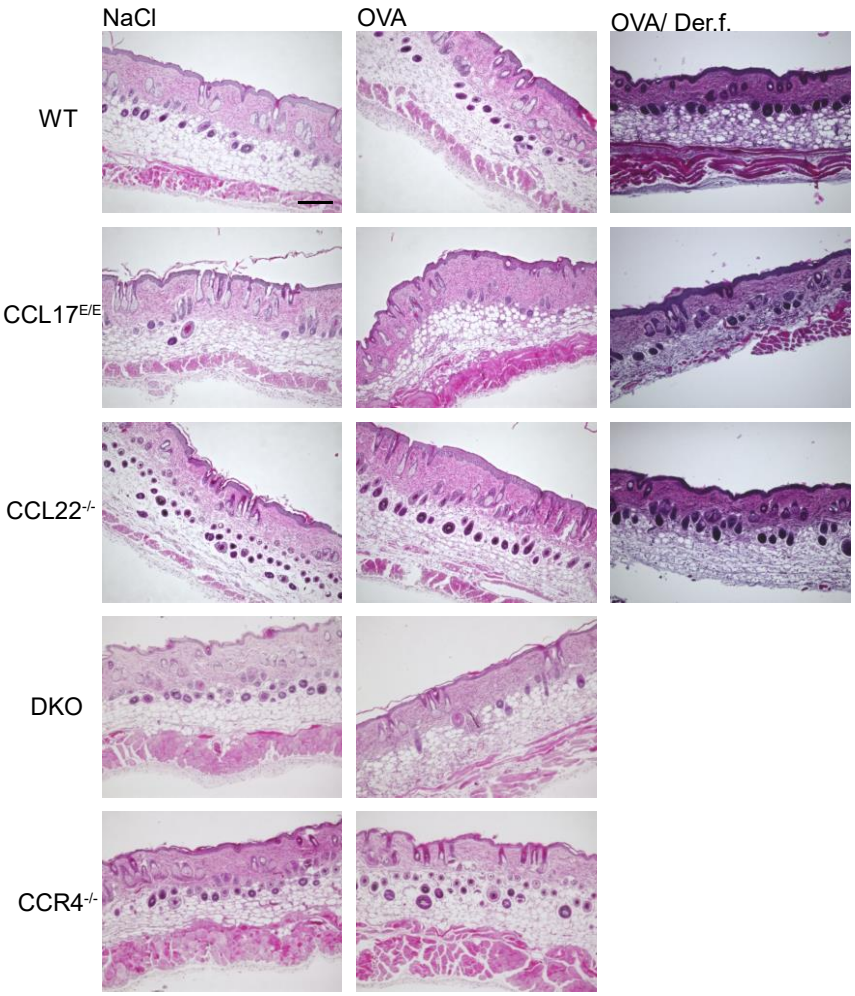

Figure 4.37 | H&E staining of back skin of WT, CCL17$^{E/E}$, CCL22$^{-/-}$, DKO and CCR4$^{-/-}$ mice after induction of AD-like skin inflammation.
Depicted are representative pictures of NaCl, OVA and OVA/Der.f. treated animals after induction of AD-like skin inflammation. Sections were stained with H&E. 10x magnification scale=200 µm

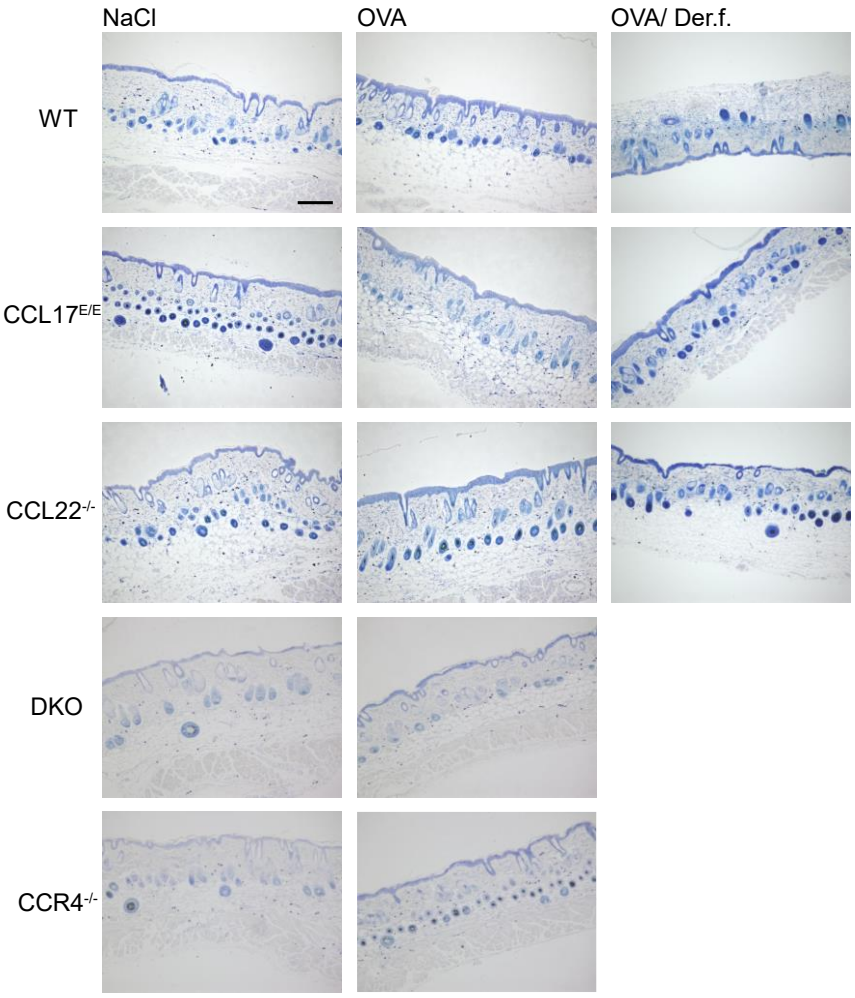

Figure 4.38 | Toluidine blue staining of back skin of WT, CCL17$^{E/E}$, CCL22$^{-/-}$, DKO and CCR4$^{-/-}$ after induction of AD-like skin inflammation.
Depicted are representative pictures of NaCl, OVA and OVA/Der.f. treated animals after induction of AD-like skin inflammation. Sections were stained with toluidine blue. 10x magnification scale = 200 µm

All parameters were measured blinded and afterwards quantified and depicted as a bar graph **(Figure 4.39)**.

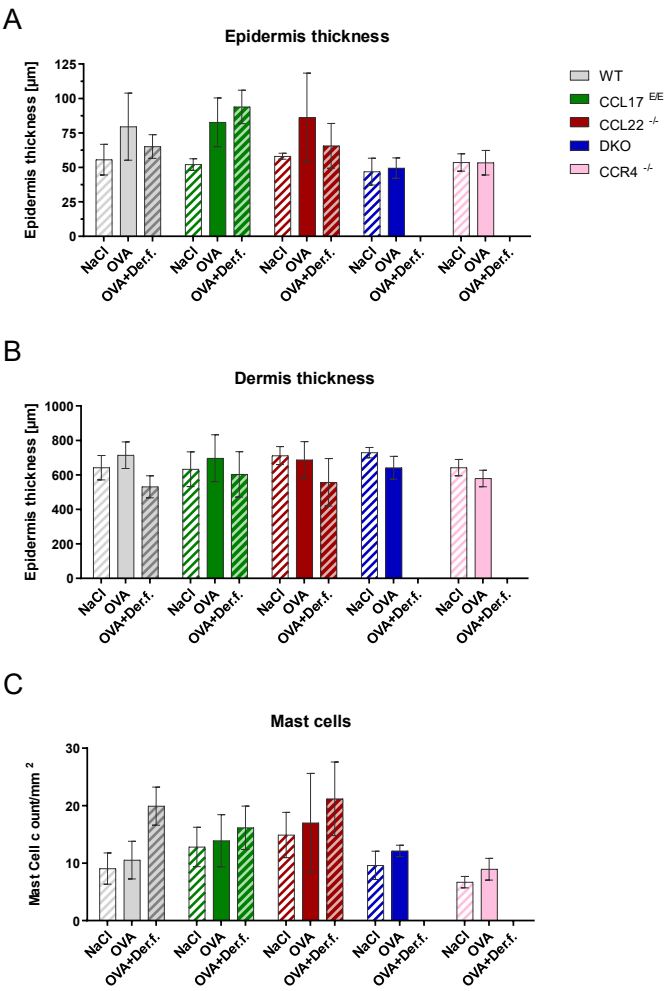

Figure 4.39 | Analysis of histological features of WT, CCL17$^{E/E}$, CCL22$^{-/-}$, DKO and CCR4$^{-/-}$ mice after induction of AD-like skin inflammation.
Three positions of three individual pictures of each mouse were analyzed blinded for (A) epidermis and (B) dermis thickness. In three individual pictures of toluidine blue stained back skin of each mouse mast cell count was calculated (C). Statistical significance was tested by using a two-way-ANOVA with post-hoc Sidak test with n = 3-9 (mean±SEM, *p=0.01-0.05, **p=0.001-0.01, ***p<0.001, ****p<0.0001).

Generally, only slight differences between allergen treatment and the respective NaCl control in all analyzed cohorts were obtained. DKO and CCR4$^{-/-}$ mice were treated only with NaCl and OVA and not a combination of OVA and Der.f.. While in WT-, CCL17$^{E/E}$- and CCL22$^{-/-}$ mice epidermal thickness mildly increased upon OVA or OVA/Der.f. treatment, the effect of the OVA treatment was barely visible for DKO and CCR4$^{-/-}$ mice **(Figure 4.39 A)**. Additionally, no alteration in epidermal and dermal thickness between genotypes were apparent **(Figure 4.39 B)**.

Mast cells normally accumulate in allergic tissue (Liu et al., 2011; Wang et al., 2007b). In the present experiment, the mast cell counts increased upon allergy induction in all cohorts when compared to the respective NaCl control. Interestingly, treatment with OVA/Der.f. led to higher mast cell counts than OVA alone. However, in DKO- and CCR4$^{-/-}$ mice, fewer mast cells were

counted already in NaCl-treated mice and were also reduced in OVA-treated mice compared to WT-, CCL17$^{E/E}$- and CCL22$^{-/-}$ mice. Overall, lower mast cell numbers were obtained in allergic skin in this experiment in comparison with previous experiments performed in our lab. Nevertheless, no significant changes between treatment conditions and cohorts were observed, indicating either that NaCl treatment already induced thickening of the skin and mast cell accumulation or that the effect of the allergen treatment was not sufficiently effective.

4.2.2.3. Flow cytometric analysis of the skin and skin-draining lymph nodes did not reveal differences between cohorts

In addition to the histological features of the skin, the back skin was analyzed via flow cytometry: First the T cell compartment was analyzed **(Figure 4.40)** to investigate a possible change of T cell composition after allergy induction.

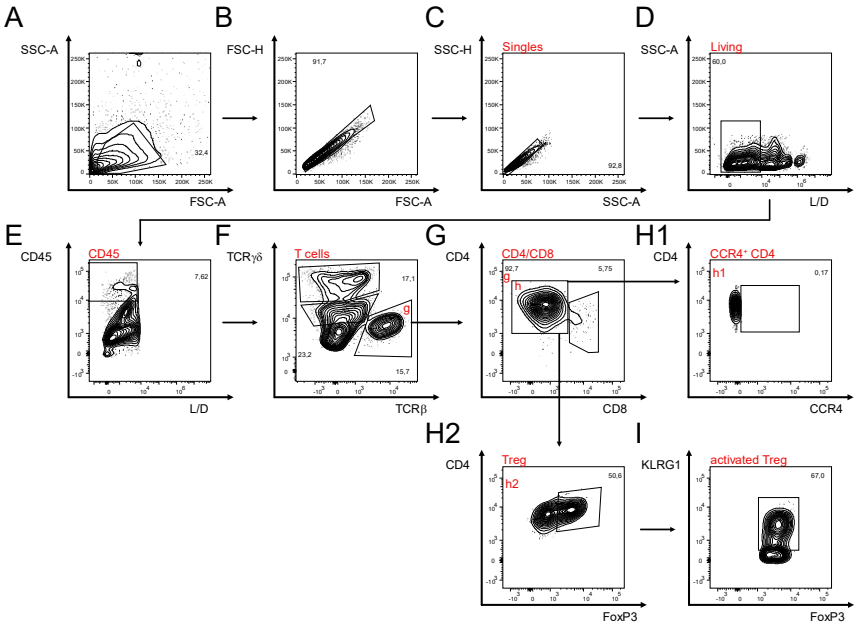

Figure 4.40 | T cell gating strategy for analysis of back skin samples.
(A-D) Lineage$^-$(F480, MHCII, B220) living single cells were gated, (E) CD45$^+$ cells were selected and (F) divided into DETC (TCRγδ^{hi}), dermal γδ T cells (TCRγδ^{int}) and conventional T cells (TCRβ$^+$). (G) TCRβ$^+$ cells were further gated on CD4$^+$ and CD8$^+$ cells. Furthermore, the CCR4 expression was assessed (H1). (H2) CD4$^+$ T cells were gated on FoxP3 expression for Tregs (FoxP3$^+$). (I) Tregs were then gated on KLRG1 to identify activated Tregs.

Although a change in T cell composition was expected, no change between treatments or cohorts occurred, indicating again a technical issue that prevented proper induction of allergic symptoms.

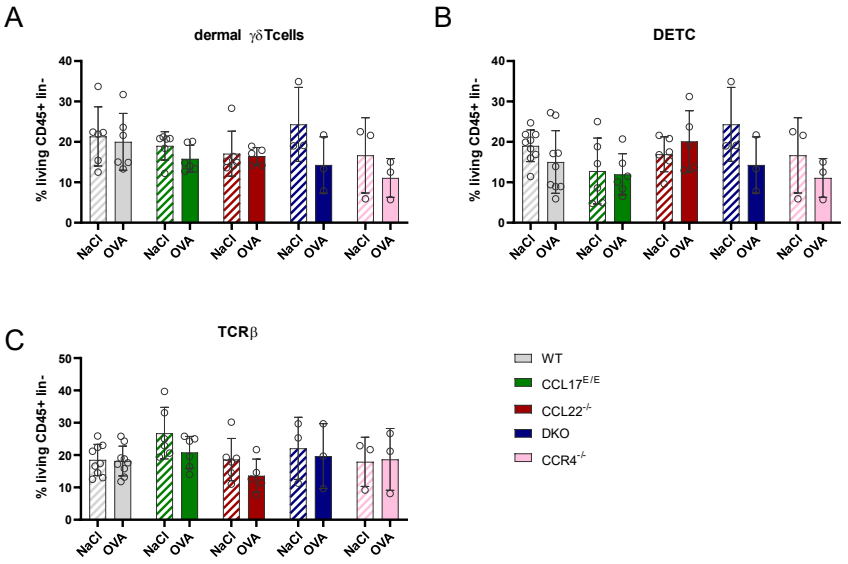

Figure 4.41 | Percentage of different T cell subsets in the back skin of NaCl and OVA treated WT, CCL17$^{E/E}$, CCL22$^{-/-}$, DKO, CCR4$^{-/-}$ mice after induction of AD-like skin inflammation.
Depicted are the percentages of (A) dermal γδ T cells, (B) DETC and (C) conventional T cells from the back skin processed and stained for flow cytometry. Statistical significance was tested by using ordinary two-way-ANOVA with post-hoc Dunnett test (n = 3-6, mean±SEM, *p=0.01-0.05, **p=0.001-0.01, ***p<0.001, ****p<0.0001).

Moreover, the skin-draining lymph nodes were analyzed via flow cytometry for T cell and myeloid cell composition as cell trafficking of myeloid cells from skin into the lymph node or T cells from lymph node into skin could be affected after induction of AD-like symptoms (Auriemma et al., 2013; Koch et al., 2006; Ogg, 2009; Ohl et al., 2004; Stutte et al., 2010).

T cells were gated based on a gating strategy published by Bouladoux et al (Bouladoux et al., 2017) **(Figure 4.42)**.

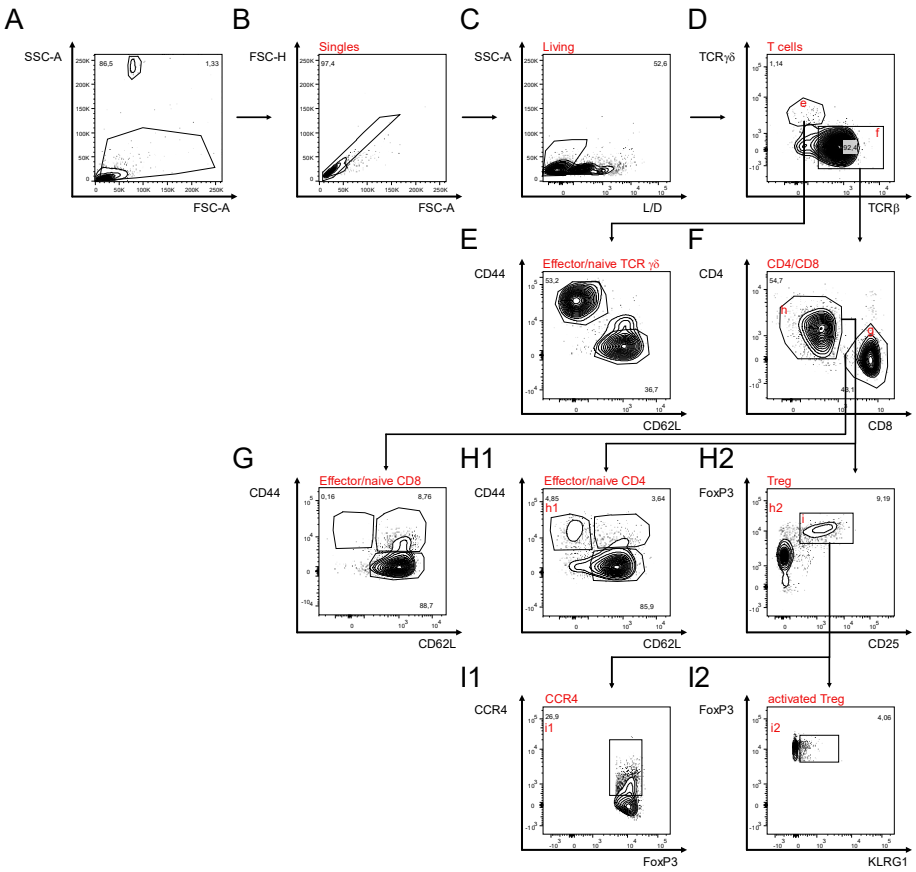

Figure 4.42 | T cell gating strategy of skin-draining lymph nodes.
(A-C) Lineage$^-$ (MHCII, F4/80, B220) living single CD45$^+$ cells were gated, (D) CD45$^+$ cells were separated into TCR γδ and conventional T cells (TCRβ$^+$). (E) To assess effector and naïve state of TCR γδ cells, cells were further gated based on their expression of CD44 and CD62L and divided into naïve (CD62L$^+$ CD44$^-$), effector (CD62L$^-$ CD44$^+$) and central memory (CD62L$^+$ CD44$^+$) T cells. (F) TCRβ$^+$ cells were further checked for their expression of CD4 and CD8. (G, H1) CD4$^+$ and CD8$^+$ cells were analyzed for effector T cells (CD44$^+$ CD62L$^-$), central memory T cells (CD44$^+$ CD62L$^+$) and naïve T cells (CD44$^-$ CD62L$^+$). (H2) CD4$^+$ T cells were gated based on the expression of FoxP3 for Treg (FoxP3$^+$). (I2) Treg were then checked for KLRG1 expression to identify activated Treg. Furthermore, the CCR4 expression was assessed (I1).

Here, only the frequencies of conventional T cells and γδ T cells are shown **(Figure 4.44)**. However, in line with the previous results no significant differences between treatment or cohorts were obtained.

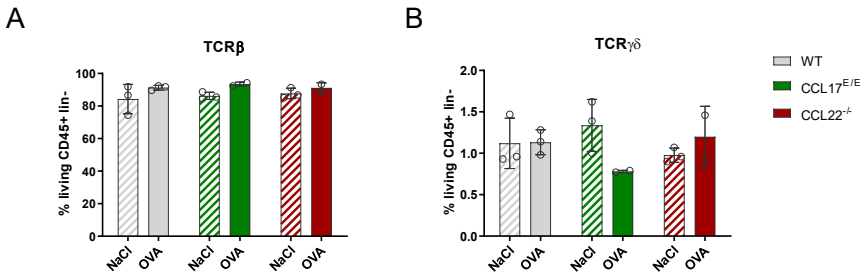

Figure 4.44 | Frequencies of different T cell subsets in skin-draining lymph nodes of NaCl and OVA treated WT, CCL17$^{E/E}$, CCL22$^{-/-}$ mice after induction of AD-like skin inflammation.
Depicted are the frequencies of (A) γδ T cells and (B) conventional T cells of inguinal lymph nodes after induction of an AD experiment of WT, CCL17$^{E/E}$, CCL22$^{-/-}$ mice. Statistical significance was tested using ordinary two-way-ANOVA with post-hoc Dunnett test with n = 3-6 (mean±SEM, *p=0.01-0.05, **p=0.001-0.01, ***p<0.001, ****p<0.0001).

For myeloid cells a gating strategy modified from Bouladoux et al and Malosse et al was used to identify monocytes, DC and macrophages (Bouladoux et al., 2017; Malosse & Henri, 2016) **(Figure 4.43)**.

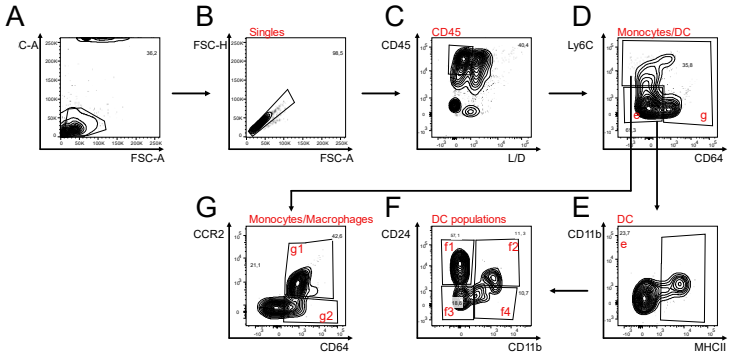

Figure 4.43 | Gating strategy for myeloid cells of skin-draining lymph nodes.
Lineage^{-} (CD3, B220) living single CD45^{+} cells were gated (A-C) and further separated based on the expression of Ly6C and CD64 to distinguish DC and monocytes (D). To identify DC, cells were separated based on their MHCII expression (E) and then separated into four DC populations distinguished by their expression of CD24 and CD11b (F). Monocytes were divided into CCR2^{+} monocytes and CD64 expressing macrophages (G).

Similar to what was observed before, neither the treatment nor different genetic deficiencies led to significant changes in myeloid cell composition **(Figure 4.45)**. Here, the frequencies measured had a large standard deviation. Furthermore, in WT-, CCL17$^{E/E}$- and CCL22$^{-/-}$ mice the percentage of CD45^{+} cells was lower in the OVA-treated mice compared to the NaCl-treated mice supporting the hypothesis that technical issues influenced the outcome of the experiments. Additionally, the percentage of CD45^{+} cells was much larger in DKO and CCR4$^{-/-}$ mice that showed less inflammation in the histological analysis compared to WT-, CCL17$^{E/E}$- and CCL22$^{-/-}$ mice suggesting a possible batch effect as the DKO-, CCR4$^{-/-}$ mice together with another cohort of WT mice were analyzed in a second experiment.

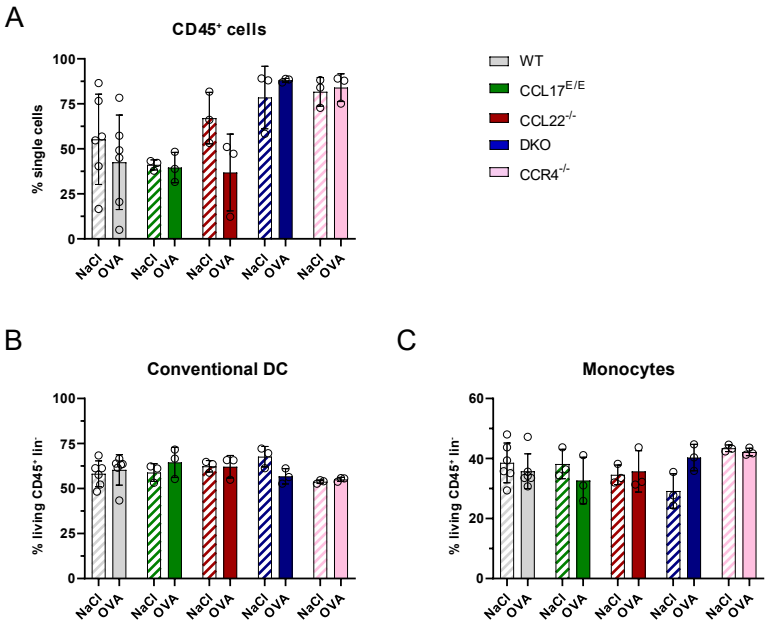

Figure 4.45 | Flow cytometric analysis of DC and monocytes in skin-draining lymph nodes of WT, CCL17$^{E/E}$, CCL22$^{-/-}$, DKO and CCR4$^{-/-}$ mice after induction of AD-like skin inflammation.
Shown are percentages of (A) CD45^{+} cells, (B) conventional DC and (C) monocytes of inguinal lymph nodes in WT, CCL17$^{E/E}$, CCL22$^{-/-}$, DKO and CCR4$^{-/-}$ mice. Statistical significance was tested by using ordinary two-way-ANOVA with post-hoc Dunnett test (n = 3-6, mean±SEM, *p=0.01-0.05, **p=0.001-0.01, ***p<0.001, ****p<0.0001)

All in all, although a first experiment had proven the effectiveness of the experimental procedure, later experiments comparing mice lacking different components of the CCL17/CCL22-CCR4-axis did not demonstrate strong effects of the OVA- or OVA/Der.f. treatment thus influence of the CCL17/CCL22-CCR4-axis on AD induction could not really be analyzed. This might be due to technical issues, such as not properly analyzing the affected skin area, duration of expiration of OVA caused by early removal of the patch by the mice themselves and batch effects between the two experiments pooled. In addition, many AD experiments are performed using mice of BALB/c background instead of C57BL/6J background as we did here. It is known that the cellular and molecular effects in allergic reactions are not so striking in C57BL/6J mice (Atochina et al., 2003; Kelada et al., 2011; Kodama et al., 2010; Whitehead et al., 2003), making it more difficult to observe differences and evaluate the influence of the CCL17/CCL22-CCR4-axis.

4.3. Influence of the CCL17/CCL22-CCR4-axis on DSS-induced Colitis

CCL17 and CCL22 have already been associated with IBD such as Morbus Crohn and Ulcerative Colitis (Francescone et al., 2015; Heiseke et al., 2012; Jugde et al., 2001; Rapp et al., 2019). Moreover, both chemokines have been identified to be expressed in the intestinal mucosa of humans under steady state (Cecilia Berin et al., 2001; Uhlén et al., 2015), as well as under pathological conditions in Crohns disease and Ulcerative Colitis patients (Günaltay et al., 2015; Jugde et al., 2001). Although both chemokines bind the chemokine receptor CCR4, different roles in DSS-induced colitis have been reported for each ligand. Previous findings showed that CCL17-deficient mice were protected from severe symptoms in a DSS-induced colitis model by promoting activation of Th1 cells while reducing the expansion of Treg (Heiseke et al., 2012). In contrast, CCL22 deficiency has been related to higher susceptibility to chronic colitis due to the ability of CCL22 to favor DC-Treg contacts (Rapp et al., 2019). Furthermore, treatment of mice with recombinant CCL22 has been shown to alleviate the symptoms of DSS-induced colitis (D. Wang et al., 2017).Expression of CCR4 on Treg, is required for Treg trafficking to peripheral tissues and facilitating suppressive functions to inhibit colitis development (Q. Yuan et al., 2007).

To shed further light on the involvement of CCL17, CCL22 and their receptor CCR4 in the context of IBD, CCL17 and CCL22 single- and double-deficient mice, as well as CCR4-deficient mice were investigated in a model of acute DSS-induced colitis. For this, the drinking water of mice was supplemented with 3 % DSS for 7 days to disrupt the epithelial barrier and induce inflammation of the colon. Histological features and cytokine expression of the colonic tissue, as well as cell composition in the mesenteric lymph nodes and serum cytokine levels were investigated to evaluate the role of each component in the CCL17/CCL22-CCR4-axis in DSS-induced colitis.

4.3.1. Lack of CCL22 leads to less severe symptoms of DSS-induced colitis

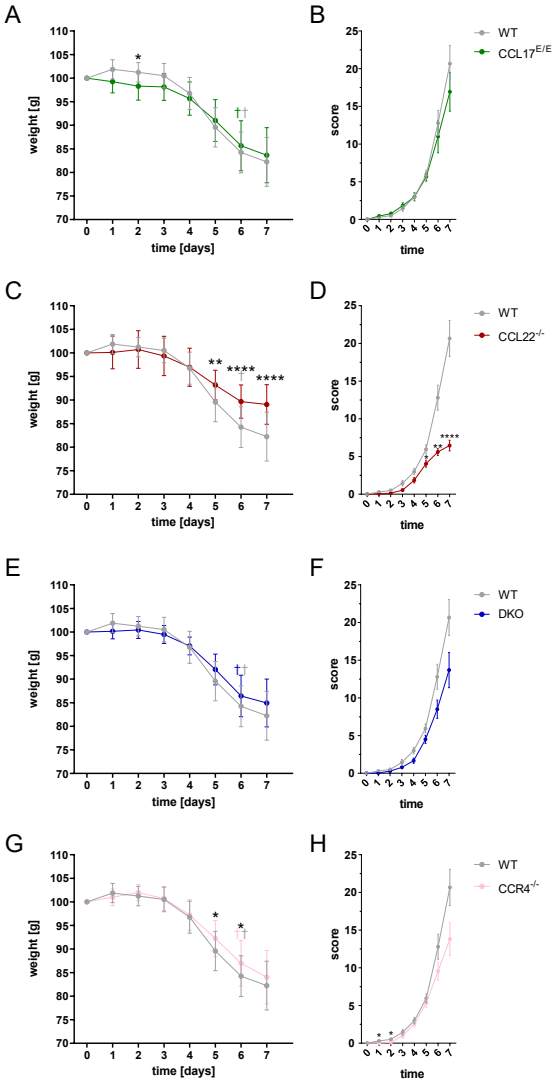

Figure 4.46 | Weight curves and disease score of CCL17$^{E/E}$, CCL22$^{-/-}$, DKO and CCR4$^{-/-}$ mice during a 7 day DSS (Dextran Sodium Sulfate) induced colitis in comparison with WT mice.
3 % DSS was supplemented into the drinking water of WT, CCL17$^{E/E}$, CCL22$^{-/-}$, DKO, CCR4$^{-/-}$ mice for 7 days. Mice were weighed and scored daily. Percent of start weight after colitis induction from day 0 to day 7 of (A) CCL17$^{E/E}$, (C) CCL22$^{-/-}$, (E) DKO and (G) CCR4$^{-/-}$ mice each in comparison with WT mice (grey). Statistical significance was tested by using a mixed-effects analysis with post-hoc Dunnett test for multiple comparison (n = 16-20, mean±SD, *p=0.01-0.05, **p=0.001-0.01, ***p<0.001, ****p<0.0001). The colored crosses mark animals that had been taken out of the experiment due to a high disease score. Disease scores that evaluate the weight, general appearance, posture, stool and behavior of the mice over the course of the experiment of (B) CCL17$^{E/E}$, (D) CCL22$^{-/-}$, (F) DKO and (H) CCR4$^{-/-}$ mice each in comparison with WT mice (grey). Statistical significance was tested by using a mixed-effects analysis with post-hoc Dunnett test for multiple comparisons (n = 18-20 of 5 independent experiments, mean±SEM, *p=0.01-0.05, **p=0.001-0.01, ***p<0.001, ****p<0.0001).

To monitor the disease progression of the mice over a 7-day DSS-induced colitis course, weight, general appearance, posture, stool consistence and behavior of the mice were assessed daily and summed up to an overall disease score **(Figure 4.46 B, D, F, H)**. All mice lost weight over the course of the experiment, though only the weight loss of CCL22$^{-/-}$ mice was significantly lower than that of WT mice from day 5 until day 7 **(Figure 4.46 C)**. Whereas WT mice lost 17 % of their starting weight, CCL22$^{-/-}$ mice lost only 10 % of their start weight. Furthermore, the

weight reduction of DKO mice on day 7 and CCR4$^{-/-}$ mice on day 6 and 7 was also lower compared to WT mice **(Figure 4.46 E, G)**. DKO mice and CCR4$^{-/-}$ mice lost 15 % of their starting weight. CCL17$^{E/E}$ mice showed a significantly reduced weight on day 1 but behaved similarly to the WT mice from day 2 on **(Figure 4.46 A)**. The disease score that includes weight, general appearance, posture, stool consistence and behavior was significantly lower on day 1 and 2 in CCR4$^{-/-}$ mice **(Figure 4.46 H)**. Notably, CCL22$^{-/-}$ mice did not exceed an overall score of 7 and were less affected than WT mice **(Figure 4.46 D)**. Hence, the loss of CCL22 only leads to milder symptoms during the DSS-induced colitis compared to WT mice. Although the DKO mice and CCR4$^{-/-}$ mice lost significantly more weight and had a lower disease score than WT mice, the mice solely deficient for CCL22 were most strongly protected from the disease.

As a hallmark of DSS-induced colitis the colon length is massively reduced due to destruction of mucosal architecture by edema formation, and loss of circular smooth muscle architecture (Kawada et al., 2007; Kimball et al., 2005). Furthermore, loss of villi and crypt architecture in line with a loss of goblet cells, as well as lymphocyte infiltration into the colonic tissue can be detected during DSS-induced colitis (Koelink et al., 2018).

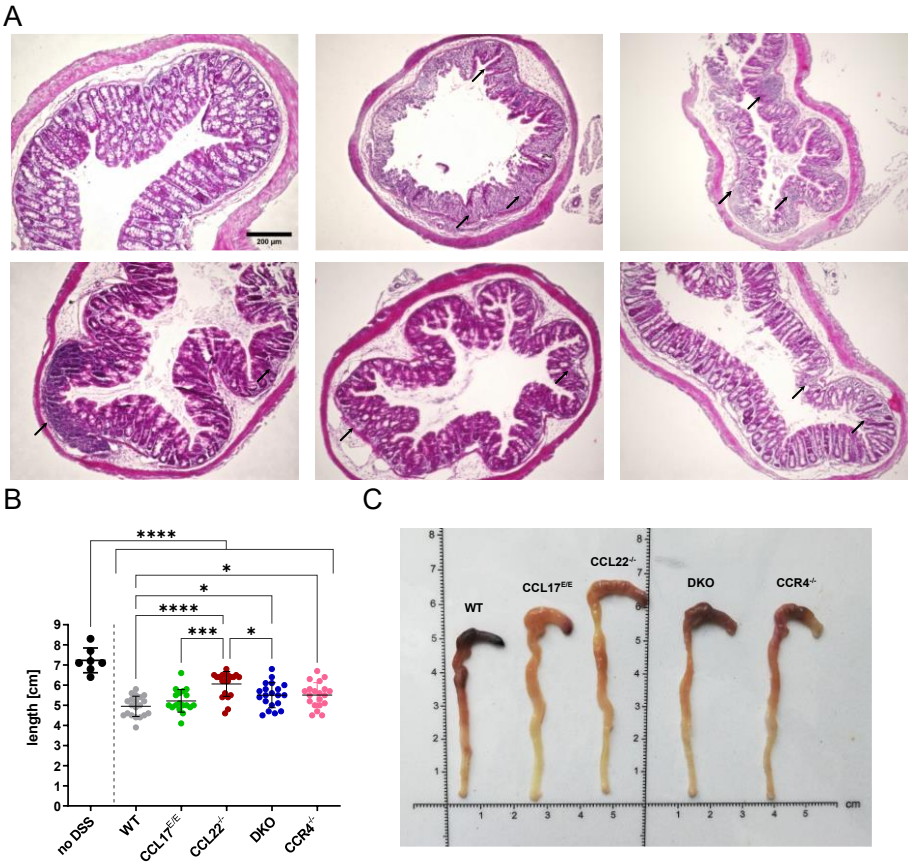

Figure 4.47 | Histological features of the colon and colon length of DSS-treated mice in comparison with naive WT mouse. (A) Representative H&E staining of transverse sections of colon adjacent to the caecum from naive WT mice (top left), 7 day DSS (3 %) treated WT mice (top center), 7 day DSS (3%) treated CCL17$^{E/E}$ mice (top right), 7 day DSS (3 %) treated CCL22$^{-/-}$ mice (bottom left), 7 day DSS (3 %) treated DKO mice (bottom center) and 7 day DSS (3 %) treated CCR4$^{-/-}$ mice (bottom right). Black arrows indicate immune cell infiltration. (B) Colon length in cm of naive WT and 7 days DSS treated WT, CCL17$^{E/E}$, CCL22$^{-/-}$, DKO, and CCR4$^{-/-}$. (C) Representative photograph of the colon after 7 days DSS treated WT, CCL17$^{E/E}$, CCL22$^{-/-}$, DKO and CCR4$^{-/-}$. Statistical significance was tested by ordinary one-way-ANOVA with post-hoc Tukey test (n = 18-20 of five independent experiments (n = 8 for no DSS), mean±SEM, *p=0.01-0.05, **p=0.001-0.01, ***p<0.001, ****p<0.0001).

To analyze morphological changes, transverse sections of the colons were generated and additionally colon length was measured on day 7 after DSS treatment (**Figure 4.47**). Compared to naïve WT mice increased immune cell infiltrates, and a loss of goblet cells could be detected in all genotypes analyzed (**Figure 4.47 A arrows**). The architectural structure with villi and crypts was maintained best in CCL22$^{-/-}$ and DKO mice, whereas it was completely disrupted in WT mice (**Figure 4.47 A**). A significant decrease in colon length compared to naïve WT mice was also observed for all genotypes. Compared to the DSS-treated WT group, however, the reduction in colon length was significantly less in CCL22$^{-/-}$, DKO and CCR4$^{-/-}$ mice, with the CCL22$^{-/-}$ mice maintaining the longest colon of all groups analyzed with a mean length of 6 cm (**Figure 4.47 B**). The colon length of CCL22$^{-/-}$ mice was not only significantly longer compared to WT mice, but also compared to the CCL17$^{E/E}$ and DKO mice. CCL17$^{E/E}$ mice had a colon length comparable to the WT mice with 5.2 cm and 5 cm. respectively.

Taken together, CCL22$^{-/-}$ mice were least affected by colon shortening and histological features after colitis induction such as immune cell infiltration and goblet cell loss in colonic tissue. Nevertheless, colitis symptoms were also lower in DKO mice and CCR4$^{-/-}$ mice compared to WT mice.

These results indicate that especially the CCL22-CCR4 interaction plays a role in the development of colitis symptoms in the acute DSS colitis model.

4.3.2. Reduced upregulation of inflammatory cytokines production in the colon of CCL22 deficient mice after DSS treatment

To evaluate the importance of the chemokine production in the colonic tissue, expression of CCL17 and CCL22 was analyzed in the colon of WT, CCL17$^{E/E}$, CCL22$^{-/-}$, DKO and CCR4$^{-/-}$ mice at day 7 after the start of DSS treatment **(Figure 4.48 A, B)**. As expected, no CCL17 mRNA could be detected in samples of CCL17$^{E/E}$ mice, and CCL22 mRNA was absent in CCL22$^{-/-}$ mice. No differences between CCL17 or CCL22 mRNA expression could be detected when comparing the

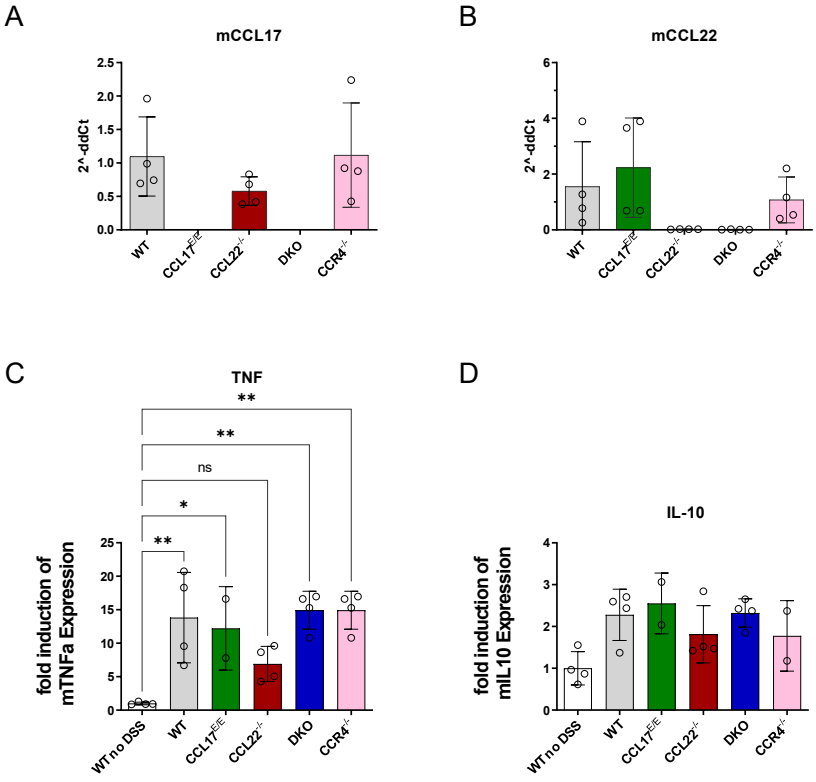

Figure 4.48 | Semi-quantitative analysis of CCL17, CCL22, TNF and IL-10 expression in the colon after a 7day DSS-induced colitis of WT, CCL17$^{E/E}$, CCL22$^{-/-}$, DKO, and CCR4$^{-/-}$ mice.
Depicted are the expression levels of (A) CCL17 and (B) CCL22 and the fold change of (C) TNF and (D) IL-10 expression in the colon 7 days after colitis induction of WT, CCL17$^{E/E}$, CCL22$^{-/-}$, DKO and CCR4$^{-/-}$ mice. Statistical significance was tested by ordinary one-way-ANOVA with post-hoc Tukey test (n = 16-20 (n = 8 for no DSS), mean±SEM, *p=0.01-0.05, **p=0.001-0.01, ***p<0.001, ****p<0.0001).

other cohorts, thus making it unlikely that CCL17 or CCL22 expression in the colon is the sole reason for differences in disease severity between different genotypes analyzed here.

Secretion of proinflammatory cytokines such as IL-1β, IL-23 or TNF can have an impact on disease progression by disrupting the intestinal barrier and inducing immune cell activation (Neurath & Chiriac, 2019; Sewell & Kaser, 2022; Xiao et al., 2016). TNF for instance is known to promote inflammation by activation of lamina propria T cells via macrophages (Kamada et al., 2008; Neurath & Chiriac, 2019). Hence, anti-TNF antibodies are frequently used biologicals to treat Morbus Crohn and Colitis Ulcerosa (Adegbola et al., 2018; Genaro et al., 2021). Thus, expression levels of TNF in the colons were checked in WT, CCL17$^{E/E}$, CCL22$^{-/-}$, DKO and CCR4$^{-/-}$ mice 7 days after colitis induction and compared to TNF expression levels of naïve mice **(Figure 4.48 C)**. A clear significant increase in TNF expression could be observed up to 13-15-fold over the expression levels in naïve WT mice for CCL17$^{E/E}$, DKO and CCR4$^{-/-}$mice. Interestingly, the increase in TNF expression during DSS-induced colitis was much lower in CCL22$^{-/-}$ mice.

IL-10 expression in the colon was also analyzed as IL-10 is not only a cytokine usually expressed by regulatory T cells that are known to be responsive towards CCL22 (Eby et al., 2015; Rapp et al., 2019), but is also associated with protection from the development of colitis (Kühn et al., 1993). In all genotypes analyzed, an increase of IL-10 expression compared to the naïve WT cohort could be observed **(Figure 4.48 D)**, although the levels were not significantly enhanced. Nonetheless, no genotype specific differences were detected indicating that IL-10 secretion in the colon is presumably not the reason for the observed differences in symptom severity of colitis.

4.3.3. Flow cytometric analysis of mesenteric lymph nodes after colitis induction reveals differences in frequencies and cell numbers of T cells

In the process of IBD, barrier disruption occurs and is followed by first innate and then adaptive immune cell inflammation. Especially, T cells migrate into the intestinal tissue further amplifying the inflammation (Giuffrida & Di Sabatino, 2020; Neurath, 2019; J. Bin Yan et al., 2020). As the priming of the T cells occurs in the mesenteric lymph nodes, the T cell composition of the mesenteric lymph nodes was analyzed. Here, we aimed to elucidate the influence of CCL17, CCL22 and CCR4 for these processes.

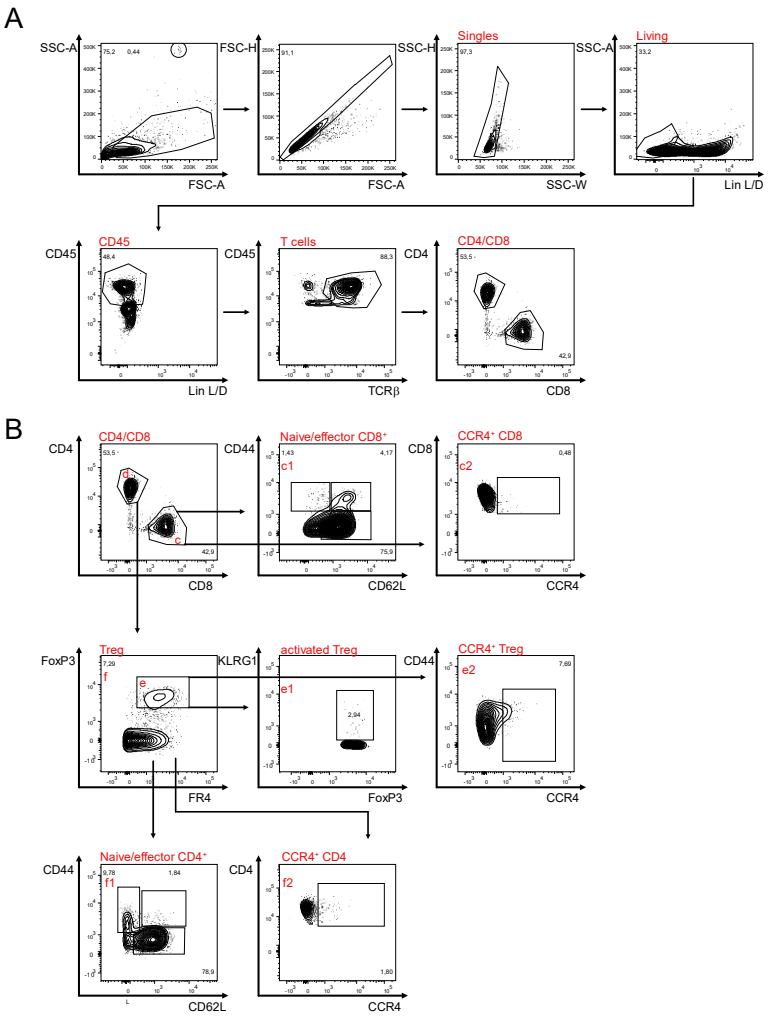

Figure 4.49 | T cell gating strategy of mesenteric lymph nodes.
(A) The upper panel was gated on lineage$^-$ living single cells and further on CD45$^+$ TCRβ$^+$ cells that could be divided into CD4$^+$ and CD8$^+$ cells. (B) CD8$^+$ T cells were further gated for expression of CD44 and CD62L to assess T_{em} (Effector Tcells) (CD44$^+$ CD62L), T_{cm} (central memory T cells) (CD44$^+$ CD62L$^+$) and naive (CD44$^-$ CD62L$^+$) cells. Furthermore, CCR4 expression was assessed. CD4$^+$ T cells were gated for FoxP3 expression identifying Treg (FoxP3$^+$). Treg were further gated for KLRG1 and CCR4. CD4$^+$ FoxP3^{+-} T cells were separated based on the expression of CD44 and CD62L expression to identify T_{em}, T_{cm} and naive T cells. Further the CCR4 expression was assessed.

The frequencies and cell numbers of T cells of the mesenteric lymph nodes were analyzed using flow cytometry at day 7 after colitis induction **(Figure 4.49)**. Conventional CD4 and CD8 cells were analyzed according to the gating strategy depicted in **Figure 4.49**. Although the frequency of T cells did not change between genotypes, the absolute cell counts of T cells in CCL22$^{-/-}$ mice were significantly higher than in WT mice and CCL17$^{E/E}$ mice **(Figure 4.50 A, B)**. Though not significantly different, mesenteric lymph nodes of CCL17$^{E/E}$, DKO and CCR4$^{-/-}$ mice also contained more T cells compared to those of WT mice **(Figure 4.50 A, B)**. When divided into CD4$^+$ and CD8$^+$ T cell populations the same overall tendency applies **(Figure 4.50 D, F)**. CCL22$^{-/-}$ mice possessed the highest numbers of CD4$^+$ T cells in the mesenteric lymph node and particularly had significantly higher numbers compared to the WT mice, CCL17$^{E/E}$ mice and

CCR4$^{-/-}$ mice. In addition, lymph nodes of CCL22$^{-/-}$ mice also contained the most CD8^{+} T cells namely 1x10^{6} which was five times more than in WT mice and 2.5 times higher than in CCL17$^{E/E}$ mice. Thus, CD8^{+} T cells in CCL22$^{-/-}$ were significantly elevated compared to the WT and CCL17$^{E/E}$ mice.

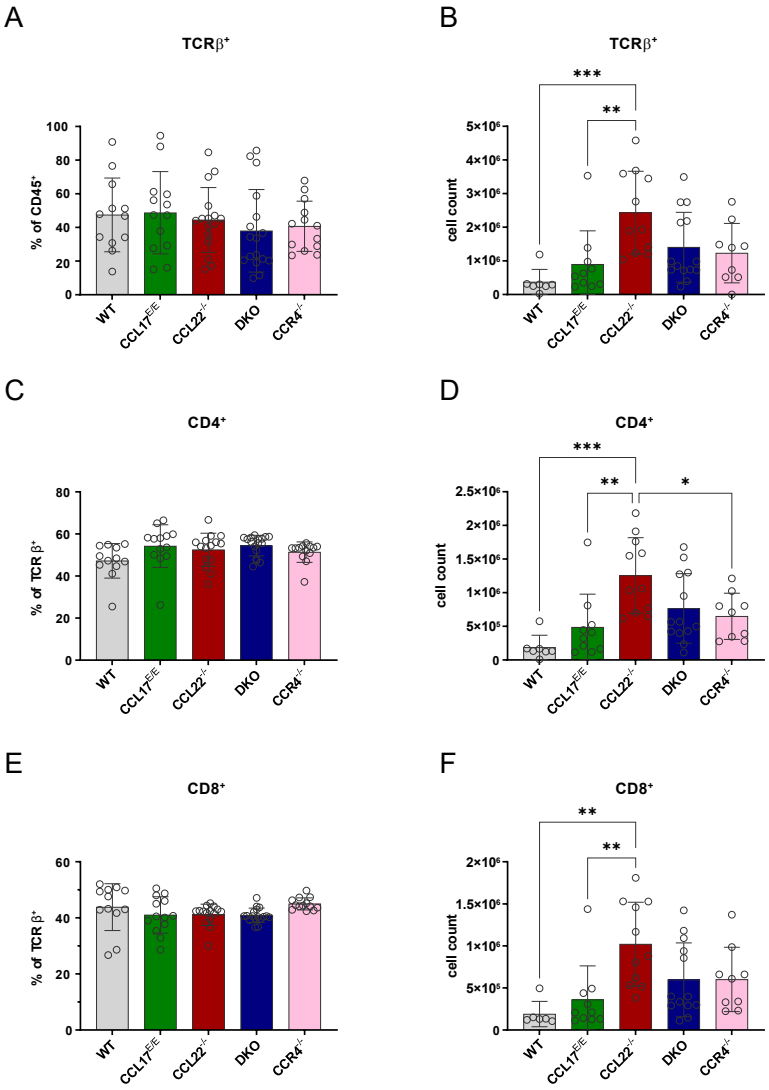

Figure 4.50 | Flow cytometric analysis of T cells in the mesenteric lymph nodes of WT, CCL17$^{E/E}$,CCL22$^{-/-}$, DKO and CCR4$^{-/-}$ mice 7 days after colitis induction.
(A, B) TCRβ^{+} cells are depicted as percent of single cells and the absolute cell count. (C, D) CD4^{+} T cells as the percent of TCRβ^{+} cells and the absolute cell count. (E, F) CD8^{+} T cells as percent of TCRβ^{+} cells and as absolute cell count. Statistical significance was tested by ordinary one-way-ANOVA with post-hoc Tukey test (n = 7-17, mean±SD, *p=0.01-0.05, **p=0.001-0.01, ***p<0.001, ****p<0.0001).

To investigate the influence of deficiencies in the CCL17/CCL22-CCR4-axis on CD8⁺ T cell subsets during DSS colitis in more depth, CD8⁺ T cells were further divided into naïve T cells, effector T cells (T_{em}) and central memory T cells T_{cm} based on the expression of CD44 and CD62L **(Figure 4.49)**.

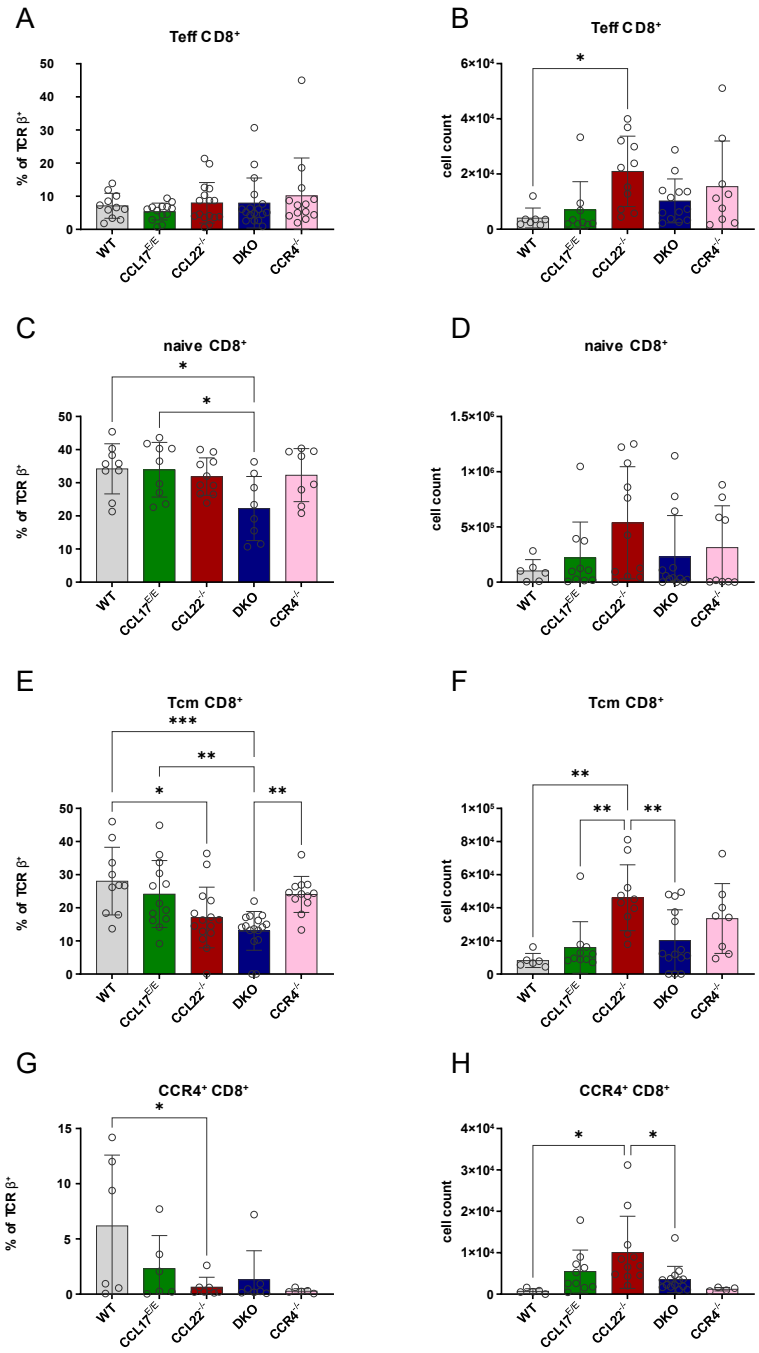

Figure 4.51 | Flow cytometric analysis of CD8⁺ T cells in the mesenteric lymph nodes of WT, CCL17$^{E/E}$, CCL22$^{-/-}$, DKO and CCR4$^{-/-}$ mice 7 days after colitis induction.
Depicted are percentages and cell numbers of (A, B) CD8⁺ T_{em}, (C, D) naïve CD8⁺ T cells, (E, F) CD8⁺ T_{cm} and (G, H) CCR4 expression of CD8⁺ cells. Statistical significance was tested by ordinary one-way-ANOVA with post-hoc Tukey test with n = 6-17 mean±SD, *p=0.01-0.05, **p=0.001-0.01, ***p<0.001, ****p<0.0001).

The effector T cells increased significantly in CCL22$^{-/-}$ mice in numbers compared to WT mice, whereas the frequencies were comparable in all genotypes **(Figure 4.51 A, B)**. The frequencies of naïve CD8^{+} T cells differed in DKO mice compared to WT and CCL17$^{E/E}$ mice as they had a significantly lower percentage of naïve CD8^{+} T cells **(Figure 4.51 C)**. Nevertheless, absolute cell numbers of naïve T cells showed the same tendency as observed for total conventional T cells with CCL22$^{-/-}$ containing the highest cell number and significantly elevated cell counts compared to WT mice, as well as a moderate overall increase in cell numbers in CCL17$^{E/E}$, DKO, and CCR4$^{-/-}$ mice compared to WT mice **(Figure 4.51 D)**. The frequencies of central memory CD8^{+} T cells were significantly decreased in CCL22$^{-/-}$- compared to WT mice **(Figure 4.51 E)**. DKO mice demonstrated significantly lower frequencies of central memory T cells compared to WT, CCL17$^{E/E}$, and CCR4$^{-/-}$ mice. The numbers of central memory T cells were, however, significantly increased in CCL22$^{-/-}$ mice compared to WT, CCL17$^{E/E}$ and DKO mice **(Figure 4.51 F)**. These results are in line with the overall increased cell numbers of CD8+ T cells described before **(Figure 4.50)**.

Interestingly, the percentage of CCR4^{+} CD8^{+} T cells was decreased in all genotypes compared to WT mice, but only in CCL22$^{-/-}$ mice the difference was significant **(Figure 4.51 G)**. In contrast, the cell counts of CCR4^{+} CD8^{+} T cells were elevated in CCL22$^{-/-}$ mice compared to WT and DKO mice **(Figure 4.51 H)**.

All in all, the chemokine- or chemokine receptor-deficient mice contained more cells than the WT mice with CCL22$^{-/-}$ mice containing the most cells in all CD8 T cell subsets. However, the frequencies of especially central memory T cells and CCR4^{+} T cells were decreased in CCL22$^{-/-}$ mice. Taken together, activated T cells (T_{em}, T_{cm} and CCR4^{+} T cells) were all significantly expanded in CCL22$^{-/-}$ mice indicating an inverse correlation between the presence of CCL22 and antigen-experienced T cells.

The CD4⁺ T cell subset in the mesenteric lymph nodes was also investigated to understand the impact of the CCL17/CCL22-CCR4 axis on the activation status, accumulation, and proliferation CD4⁺ T cells.

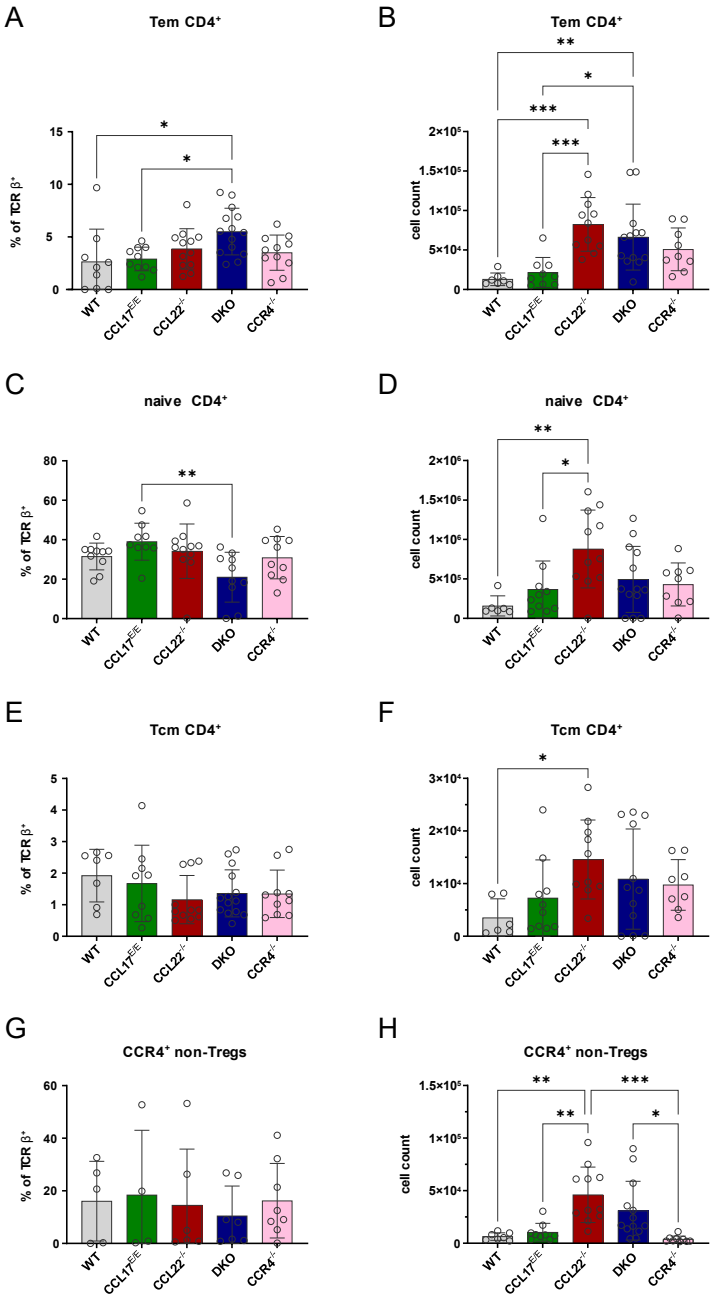

Figure 4.52 | Flow cytometric analysis of CD4⁺ T cells in the mesenteric lymph nodes of WT, CCL17$^{E/E}$, CCL22$^{-/-}$, DKO and CCR4$^{-/-}$ mice 7days after colitis induction.
Depicted are percentages and cell numbers of (A, B) effector CD4⁺ T cells, (C, D) naïve CD4⁺ T cells, (E, F) central memory T cells and (G, H) CCR4 expression of CD4⁺ cells. Statistical significance was tested by ordinary one-way-ANOVA with post-hoc Tukey test with n = 6-17 mean±SD, *p=0.01-0.05, **p=0.001-0.01, ***p<0.001, ****p<0.0001).

Interestingly, the CD4⁺ T cells subsets of CCL22$^{-/-}$ mice were strongly increased while the frequencies were rather unaffected as also seen for the overall CD4⁺ T cells **(Figure 4.50)**.

The effector T cell numbers were significantly increased in CCL22$^{-/-}$ and DKO mice compared to WT and CCL17$^{E/E}$ mice **(Figure 4.52 B)**. The percentage was only significantly elevated in DKO mice compared to WT mice **(Figure 4.52 A)**. Naïve T cell numbers were higher in all genotypes compared to WT mice, but only showed a significant increase for the CCL22$^{-/-}$ mice compared to WT and CCL17$^{E/E}$ mice **(Figure 4.52 D)**. In contrast, the frequencies were decreased in DKO mice compared to WT mice **(Figure 4.52 C)**. Central memory T cells demonstrated no differences in frequencies, but the cell numbers were significantly increased in CCL22$^{-/-}$ mice compared to WT mice **(Figure 4.52 E, F)**.

In contrast to the corresponding CD8^{+} T cell subset, the frequencies of CCR4-expressing CD4^{+} T cells were comparable among all mouse strains analyzed **(Figure 4.52 G)**. Nevertheless, the cell numbers were significantly increased in CCL22$^{-/-}$ and DKO mice compared to WT and CCR4$^{-/-}$ mice **(Figure 4.52 H)**. In this case, the CCL22$^{-/-}$ and DKO mice contained 10-fold and 7-fold more CCR4^{+} T cells than the CCR4$^{-/-}$ mice, respectively.

In conclusion, lack of CCL22 also leads to major differences in the CD4 T cell compartment, whereas the other components of the CCL17/CCL22-CCR4 axis appeared to play a minor influence on the accumulation of different CD4 T cell subsets in the mesenteric lymph nodes.

4.3.4. Influence of the CCL17/CCL22-CCR4 axis on Treg accumulation in DSS-induced colitis

Treg are key factors to keep the intestinal immune system in balance (Asseman et al., 2012; L. Wang et al., 2015; J. Bin Yan et al., 2020), and also play a crucial role in the progression of IBD by restraining inflammatory responses and facilitating tissue growth and wound healing (Asseman et al., 2012; Boehm et al., 2012; Laukova & Glatman Zaretsky, 2023; Mayne & Williams, 2013; Q. Yuan et al., 2007). For this reason, we investigated the frequency and the activation status of Treg cells 7 days after colitis induction.

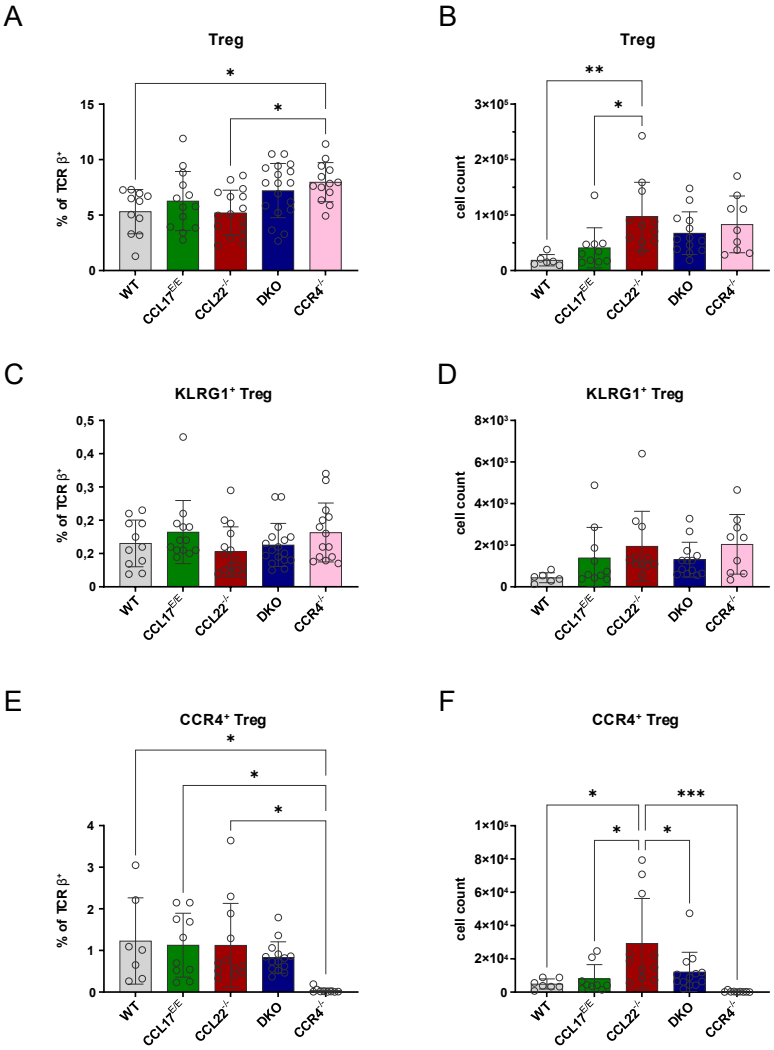

Figure 4.53 | Flow cytometric analysis of regulatory T cells in the mesenteric lymph nodes of WT, CCL17$^{E/E}$,CCL22$^{-/-}$, DKO and CCR4$^{-/-}$ mice 7 days after colitis induction.
Depicted are the percentages and absolute numbers of (A, B) Treg (TCRβ$^+$ CD4$^+$ Foxp3$^+$) and (C, D) KLRG1$^+$ Treg. (E) CCR4 expression is shown as percentage and (F) absolute cell count. Statistical significance was tested by ordinary one-way-ANOVA with post-hoc Tukey test with n=6-17 mean±SD, *p=0.01-0.05, **p=0.001-0.01, ***p<0.001, ****p<0.0001).

The frequencies of Treg were around 10 % of all TCRβ$^+$ T cells in the mesenteric lymph nodes of all mouse lines analyzed **(Figure 4.53 A)**. CCR4$^{-/-}$ mice had a significantly higher percentage of Treg compared to WT and CCL22$^{-/-}$ mice. In contrast the absolute cell counts were significantly increased in CCL22$^{-/-}$- compared to WT- and CCL17$^{E/E}$ mice **(Figure 4.53 B)** in line

with the overall increased T cell numbers in CCL22$^{-/-}$ mice observed before**.** Remarkably, these alterations in frequencies and total Treg numbers were not reflected in the frequencies or cell numbers of activated KLRG1^{+} Treg **(Figure 4.53 C, D)**.

Around 1% of Treg cells expressed CCR4, except, as expected, in CCR4$^{-/-}$ mice **(Figure 4.53 E)**. While frequencies were not altered, the cell count of CCR4^{+} T cells were again highest in CCL22$^{-/-}$ mice and significantly increased in in CCL22$^{-/-}$ compared to all other mouse strains analyzed **(Figure 4.53 F)**.

In sum, the Treg cell populations in the mesenteric lymph nodes of mice after a 7-day DSS colitis were primarily higher in CCL22- and CCR4-deficient mice supporting the correlation between CCR4^{+} Treg numbers in the mesenteric lymph nodes and the severity of symptoms in DSS colitis.

Overall, cell numbers of all analyzed T cell populations of the mesenteric lymph nodes of mice after colitis induction were massively increased in CCL22$^{-/-}$ mice and to a lesser extent in DKO and CCR4$^{-/-}$ mice. CCL17$^{E/E}$ mice, in contrast, demonstrated only small changes compared to the WT mice. These findings hint to a strong effect of the CCL22-CCR4 interaction in T cell trafficking and or differentiation during DSS-induced colitis.

4.3.5. Flow cytometric analysis of mesenteric lymph nodes 7 days after colitis induction reveals differences in the representation of myeloid subsets

CCL17 and CCL22 are mainly secreted by myeloid cells such as DC in the barrier organs like gut, lungs and skin, as well as in lymph nodes and spleen recruiting CCR4-expressing T cells and facilitating different functions such as induction of DC emigration from the skin by CCL17 or maintenance of immune homeostasis in the case of CCL22 (Alferink et al., 2003; Hao et al., 2016; Lieberam & Förster, 1999; Rapp et al., 2019; Stutte et al., 2010). In addition, CCL22 influences the ratio of conventional T cell – DC contacts and Treg – DC contacts (Rapp et al., 2016). Thus, we investigated the impact of the chemokines on frequencies and activation status of myeloid subsets in the mesenteric lymph node after induction of DSS-induced colitis **(Figure 4.55)**. For that we used a gating scheme to distinguish between different DC subsets, monocytes and neutrophils based on the publication by Scott and colleagues (Scott et al., 2011) **(Figure 4.54).**

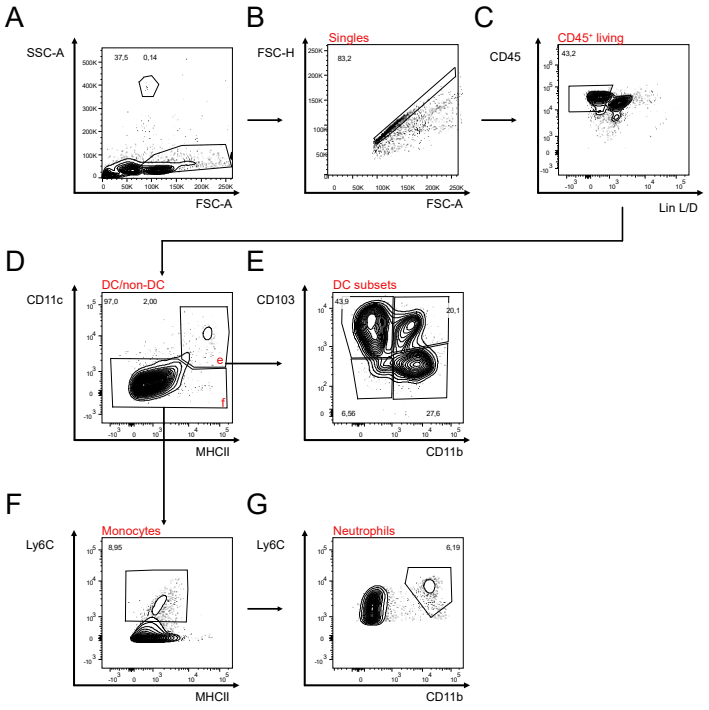

Figure 4.54 | Gating strategy for myeloid cells of mesenteric lymph nodes.
(A-C) Cells were gated on CD45$^+$ lineage$^-$ (CD3$^-$, BB20$^-$) living cells and then divided into CD11c$^+$ MHC II$^+$ cells for DC and non DC (CD11c$^-$) (D). (E) DC were divided into four subsets using CD103 and CD11b expression. (F-G) Non-DC were further divided into monocytes (Ly6C$^+$) and neutrophils (Ly6C^{hi} CD11b$^+$). Gating modified from Scott et al (Scott et al., 2011).

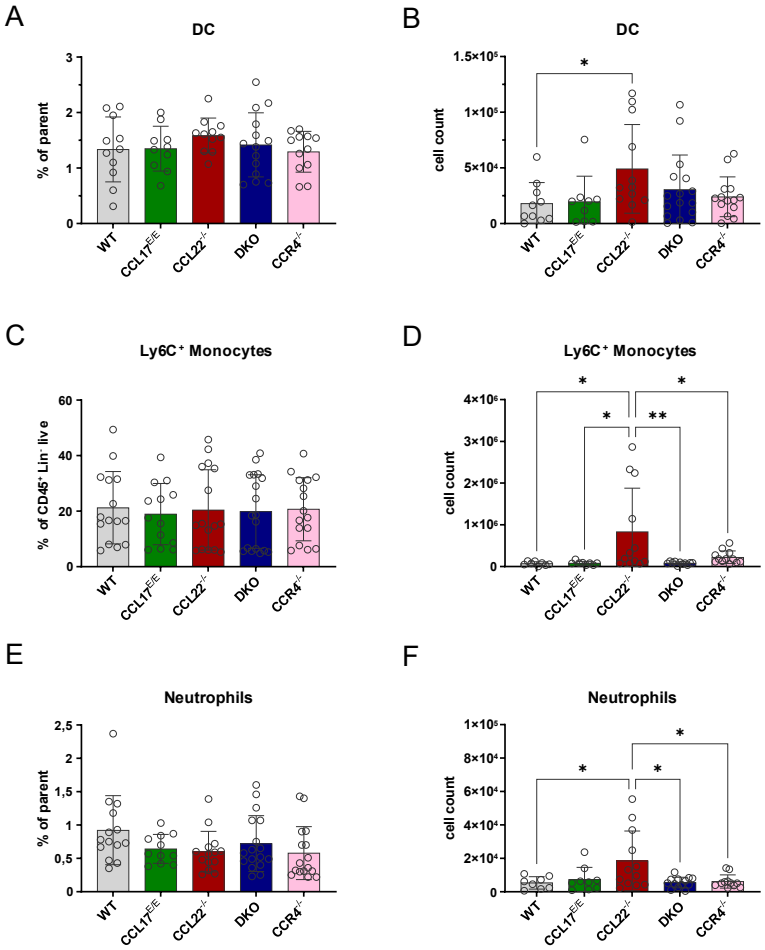

Figure 4.55 |Flow cytometric analysis of DC, monocytes, and neutrophils in the mesenteric lymph nodes of WT, CCL17$^{E/E}$, CCL22$^{-/-}$, DKO and CCR4$^{-/-}$ mice after colitis induction.
Shown are percentages and absolute cell count of (A, B) DC, (C, D) monocytes and (E, F) neutrophils. Statistical significance was tested by ordinary one-way-ANOVA with post-hoc Tukey test (n = 8-17, mean±SD, *p=0.01-0.05, **p=0.001-0.01, ***p<0.001, ****p<0.0001).

The frequencies of DC, monocytes and neutrophils were not altered in the mesenteric lymph nodes between all mouse lines analyzed **(Figure 4.55 A, C, E)**. In contrast, the absolute cell numbers of DC were more than doubled in the CCL22$^{-/-}$ mice compared to WT mice **(Figure 4.55 B)**. The same could also be observed for monocytes and neutrophils **(Figure 4.55 D, F)**. In CCL22$^{-/-}$ mice the monocyte population was increased about tenfold compared to WT mice **(Figure 4.55 D)**. Similarly, the neutrophil subset that accounts for 0.7 % of CD45^{+}, lineage^{-} cells in CCL22$^{-/-}$ mice contained four times more cells than the WT mesenteric lymph nodes. Thus, the numbers of neutrophils were significantly elevated in the CCL22$^{-/-}$ mice **(Figure 4.55 F)**.

Notably, the strong differences in cell count observed here for CCL22$^{-/-}$ mice compared to WT mice were not accompanied by changes in the frequencies of myeloid and neutrophil cell subsets, demonstrating an overall increase in cell numbers without a change in cell composition of the mesenteric lymph nodes. Interestingly, these results match the

observations in the T cell compartment, in which the CCL22$^{-/-}$ mice also contained the highest numbers of cells **(4.3.3)**.

CD11c^{+} DC can be further separated into four DC subsets in the intestine based on CD11b and CD103 expression according to previous findings that differentiate the DC subpopulations by their function (Cerovic et al., 2013; Milling et al., 2010; Scott et al., 2011). Therefore, it was of interest, to investigate whether mice deficient for components of the CCL17/CCL22-CCR4 axis display changes in these DC subpopulations in the mesenteric lymph nodes which may also affect T cell activation during colitis.

Of note, neither frequencies nor absolute cell numbers of all four DC subsets were altered in the gene-deficient mice compared to WT mice **(Figure 4.56)**. For the CD11b^{+} CD103^{+} subsets, CCL22$^{-/-}$ mice demonstrated the highest frequencies and absolute cell numbers that were significantly elevated compared to the CCR4$^{-/-}$ mice **(Figure 4.56 A, B)**. Additionally, as already identified for all DC, CCL22$^{-/-}$ mice had slightly elevated numbers of all four analyzed subsets.

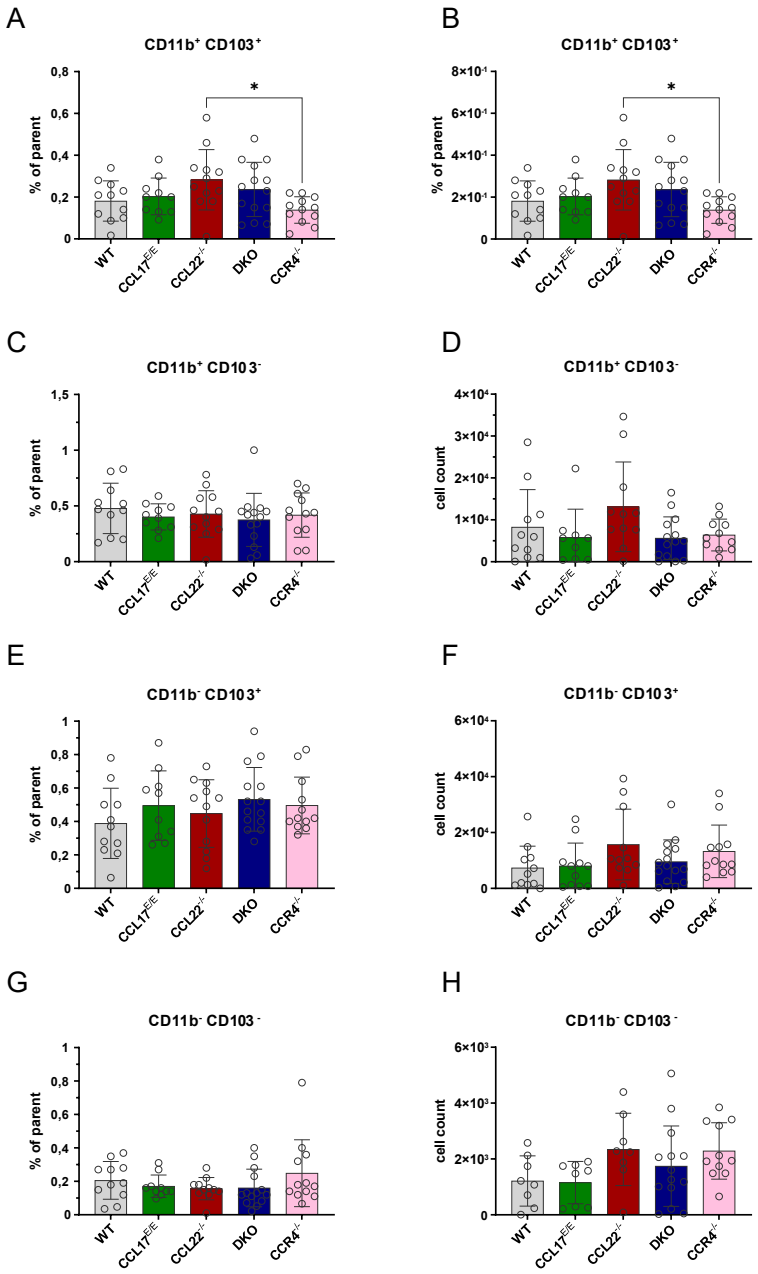

Figure 4.56 | Flow cytometric analysis of DC subsets in the mesenteric lymph nodes of WT, CCL17$^{E/E}$, CCL22$^{-/-}$, DKO and CCR4$^{-/-}$ mice 7 days after colitis induction.
Depicted are percentages and absolute cell counts of (A, B) CD11b^{+} CD103^{+} DC, (C, D) CD11b^{+} CD103^{-} DC, (E, F) CD11b^{-} CD103^{+} DC and (G, H) CD11b^{-} CD103^{-} DC. Statistical significance was tested by ordinary one-way-ANOVA with post-hoc Tukey test (n=8-17 mean±SD, *p=0.01-0.05, **p=0.001-0.01, ***p<0.001, ****p<0.0001).

These results reveal that the numbers of neutrophils, monocytes and DC increased upon DSS-induced colitis in CCL22$^{-/-}$ mice, whereas the composition of the myeloid cell subsets in the mesenteric lymph nodes remained generally unaffected. Although the DC numbers were significantly increased in CCL22$^{-/-}$ mice, different DC subsets were not altered compared to WT mice indicating that no particular DC subset is affected by the loss of CCL22. Furthermore, the effects of the single deficiency of CCL22 are also dominant over CCL17 deficiency or double

deficiency for both chemokines in the myeloid subset, supporting our former hypotheses that CCL22 might have a strong influence on DC-T cell interactions during colitis.

4.3.6. Analysis of cytokine levels in the serum of mice four days after colitis induction might be predictive for the outcome of colitis

In order to understand the disease progression and the involvement of CCL17/CCL22 and CCR4 during DSS-induced colitis concentrations of cytokines in serum of mice four days after colitis induction were analyzed **(Figure 4.57)**. The inflammation panel included the cytokines that are highly associated to colitis severity such as IL-23 or TNF (Sewell & Kaser, 2022; Xiao et al., 2016). Since at day 4 after colitis induction, the severe symptoms of colitis observed on day 7 **(Figure 4.46,Figure 4.47)** were not yet visible, we aimed at analyzing this time point to possibly link cytokine production to the genotype-specific alterations seen at later time point.

Multiplex analysis revealed that the lowest concentration of cytokines was detected in the

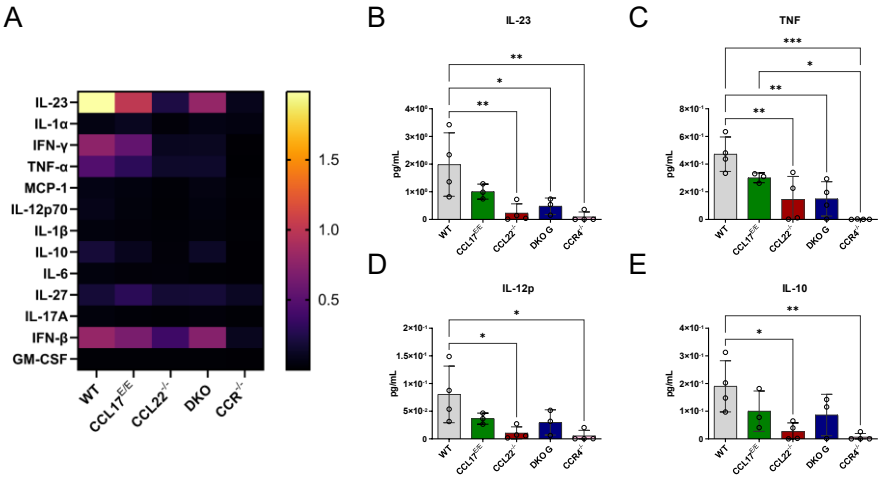

Figure 4.57: Analysis of cytokines in serum 4 days after colitis induction.
(A) Serum levels of different cytokines involved in colitis pathology depicted as a heatmap four days after colitis induction and as bar graphs for (B) IL-23, (C) TNF, (D) IL-12p and (E) IL-10. Statistical significance was tested by ordinary one-way-ANOVA with post-hoc Tukey test (n = 3-4, mean±SD, *p=0.01-0.05, **p=0.001-0.01, ***p<0.001, ****p<0.0001).

serum of CCR4$^{-/-}$ and CCL22$^{-/-}$ mice **(Figure 4.57)**. Here, amongst all 13 cytokines especially IL-23 and Interferon-β (IFNβ) that are increased in WT, CCL17$^{E/E}$ and DKO mice are low to not detectable in CCR4$^{-/-}$ and CCL22$^{-/-}$ mice **(Figure 4.57 A)**. Interestingly, the IFNγ and TNF concentrations in the serum were decreased in CCR4$^{-/-}$, CCL22$^{-/-}$ and DKO mice. Single values showed that differences were significantly lower in IL-23 and TNF in CCL22$^{-/-}$, DKO, CCR4$^{-/-}$ mice compared to WT mice **(Figure 4.57 B, C)**, whereas the IL12p70 levels were significantly decreased in CCL22$^{-/-}$ and CCR4$^{-/-}$ mice only **(Figure 4.57 D)**. In contrast to the elevated levels

of these three proinflammatory cytokines, IL-10, rather known for its suppressive functions and Treg recruitment, was also reduced in CCL22$^{-/-}$ and CCR4$^{-/-}$ mice **(Figure 4.57 E)**.

In summary, in CCL22$^{-/-}$ and CCR4$^{-/-}$ mice the cytokine production four days after colitis induction was lowest which directly correlates with the ameliorated colitis symptoms observed at later time points **(Figure 4.46, Figure 4.47)** and inversely correlates with the altered cell numbers of T cell and myeloid cells on day 7 after colitis induction. Thus, early cytokine responses appear to reflect the outcome of colitis development at later time points.

Conclusively, these results reveal that during the course of DSS-induced colitis the CCL17/CCL22-CCR4-axis does impact the severity of colitis. Especially CCL22$^{-/-}$ mice showed significantly higher numbers of T cells and myeloid cells in the mesenteric lymph nodes, whilst developing least colitis symptoms. Furthermore, the lowest levels of cytokines could be detected in the serum of CCL22$^{-/-}$ mice. DKO and CCR4-deficient mice demonstrated similar alterations in T cell and myeloid cell numbers in the mesenteric lymph nodes but not to the extent of CCL22$^{-/-}$ mice. However, they also exhibited lower cytokine levels in the serum than WT mice. CCL17$^{E/E}$ mice on the other hand were only moderately different from the WT regarding immune cell numbers and frequencies as well as cytokine levels in the serum while they also developed strong colitis symptoms. This indicates that all components of the CCL17/CCL22-CCR4 axis might be involved in the development of colitis symptoms but that in particular CCL22 might be of great importance in disease pathogenesis, T cell trafficking, and possibly DC – T cell interactions during DSS-induced colitis.

5. Discussion

The CCL17/CCL22-CCR4-axis has been associated with different diseases like osteoarthritis, multiple sclerosis, atherosclerosis (Scheu et al., 2017; Shin et al., 2023; C. Weber et al., 2011) but in particular also with allergic and inflammatory diseases that affect barrier organs like lung, skin and gut (Cecilia Berin et al., 2001; Halling et al., 2023; Hao et al., 2016; Jo et al., 2003; Quoc et al., 2022; Shimada et al., 2004; Staples et al., 2012; Wakugawa et al., 2001). Thus, in this thesis the role of CCL22, CCL17 and their receptor CCR4 was investigated in the context of disorders affecting the barrier integrity of the skin and gut, i.e. AD, CHS and DSS-induced colitis.

5.1. Defining the duration of aptamer dependent inhibition and optimal timing of aptamer application

In previous experiments published by Fülle et al. (Fülle, Steiner, et al., 2018), aptamers were applied 1 h before challenge and 12 h post challenge. However, this thesis aimed to investigate how long these aptamers are active *in vivo* by applying them at longer intervals before challenge and if therapeutic administration at a later time point post challenge is effective as well. Additionally, it was tested whether aptamer application can lead to long-term suppression of allergic symptoms. Therefore, effectiveness of symptom amelioration was examined by CCL17 blockade with the CCL17-specific aptamer MF35.47m at different time points during CHS experiments, as for efficient treatment of ACD, a potential therapy should start after first allergic symptoms or as close as possible to the second allergen contact.

5.1.1. Aptamer injection prior the challenge as an indicator for duration of action

To assess the duration of the aptamer-dependent inhibition *in vivo* a comparison of mice that received an injection with the CCL17-specific aptamer MF35m at 48 h, 24 h, 12 h, and 1 h prior to the challenge was performed. As expected, amelioration of allergic symptoms was decreasing with increasing time between aptamer administration and DNFB challenge **(4.1.1.1)**. The strongest effect could be observed in the mice that received the aptamer 1 h prior to the challenge and a less pronounced effect was observed for the mice with aptamer application 24 h prior the challenge. Observed effects were a reduction in ear swelling, as well as decreased immune cell infiltration. In particular, less $CD8^+$ T cells and Treg were detected in the ears of mice of these cohorts. Nevertheless, $CCL17^{E/E}$ mice still demonstrated the strongest effects. Hence, immune cell infiltration might be initiated shortly after DNFB challenge and is also mediated by CCL17. Thus, CCL17 blockade is only effective close to the challenge as it can

then interfere with immune cell recruitment. Since the suppressive effect of aptamer-dependent CCL17 blockade was lost in the cohort in which the aptamer was applied 48 h before challenge, the duration of action of the aptamer is apparently less than two days and likely in the range of 12 h – 24 h. This is in line with the serum stability of MF35m that decreased massively after 24 h when mixed with mouse serum (Fülle, Steiner, et al., 2018). In addition, considering that 48 h before the challenge still falls into the sensitization phase, not only the duration of action might have played a role, but also sensitization could have been disturbed with aptamer injection 48 h before DNFB challenge. Hapten-treated skin cells produce ROS, the release of ATP and other DAMPs that in turn activate inflammasomes and PRRs of the APC that leads to secretion of pro-inflammatory cytokines (Kaplan et al., 2012). Activated DC and LC then migrate to the lymph node to present acquired antigens to T cells in the draining lymph nodes. Interestingly, keratinocytes are able to condition DC in the skin to skew Th2 responses in the lymph nodes by TSLP production (Ebner et al., 2007; Y. J. Liu et al., 2007; Soumelis et al., 2002) and TSLP, in turn, is known to induce CCL17 expression. Thus, CCL17 could be of importance to condition DC and form a type II immune response. Although injection of the aptamer 48 h prior to challenge had no effect on the strength of allergic symptoms, CCL17 could play a role in early sensitization and not in the late sensitization phase as tested here. To investigate in which processes CCL22 is involved and if it facilitates similar or different functions during CHS, CHS experiments including $CCL22^{-/-}$ mice and/or blockade of CCL22 need to be performed. To underpin the influence of the CCL17/CCL22-CCR4-axis in conditioning DC, further experiments in which the sensitization phase of CHS is investigated would be required. Here, especially the early events after DNFB application would be of interest to analyze if TSLP induced production of CCL17 or CCL22 during the sensitization might influence the allergic response.

5.1.2. Involvement of the CCL17/CCL22-CCR4-axis in CHS with repeated challenges

Long-term effectiveness of aptamer application was tested by administration of the CCL17-specific aptamers during the first DNFB challenge, followed by another DNFB challenge on day 6 and analysis of immune cell infiltration in the ear tissues on day 9. Although the CCL17 blockade by aptamers led to the expected amelioration of ear swelling similar as that observed in the $CCL17^{E/E}$ mice, the inhibitory potential of the aptamers was completely lost after the second challenge. Interestingly, a reduction of ear swelling was also not observed for $CCL17^{E/E}$ mice in this setting, indicating that the mechanism leading to an ear swelling response is

different after the second challenge compared to the first one. In the literature, it has been described that after rechallenge of both ears, only the ear that has been previously treated with the hapten but not the vehicle-treated ear showed an immune reaction (Yamashita et al., 1989). This reaction is termed flare-up reaction and proofs the existence of local hapten-specific immune cells (Natsuaki et al., 1993). The immune cell recruitment in the rechallenges might not be CCL17-dependent but may be rather conveyed by local T_{RM} cells. Hence, also in the current experiments a strong ear swelling reaction was observed in the mice that previously demonstrated ameliorated symptoms after aptamer application. Although the allergic reaction was reduced in $CCL17^{E/E}$ mice during the first challenge, enough memory T_{RM} T cells were induced that reacted upon another DNFB challenge and created a flare-up reaction. However, the rechallenge described by Yamashita et al was performed at day 33 post sensitization, i.e. much later compared to the second challenge performed in the present study. Therefore, not the complete long-term T_{RM} population may have been generated yet in the current cohorts at day 6. Interestingly, in the present study an increase in T cell numbers upon DNFB treatment was observed in all cohorts including $CCL17^{E/E}$- and aptamer-treated mice **(Figure 4.5)**, both of which showed reduced T cell infiltration in previous one-challenge CHS experiments (Fülle, Steiner, et al., 2018). Although no differences between cohorts were observed in the two-challenge CHS, the increased numbers of T cells might indicate an enhanced formation of T_{RM} T cells in the cohorts that displayed a reduced immune reaction after the first challenge. In humans, mainly $CD4^+$ T_{RM} cells reside in the dermis facilitating the local memory in ACD, whereas in C57BL/6J mice, numbers of $CD8^+$ T_{RM} cells are increased and predominantly are responsible for the long-lasting memory (Funch et al., 2022; Gamradt et al., 2019; Moed et al., 2004). Furthermore, CCL27 and its receptor CCR10 are hypothesized to play a major role in immune cell recruitment to the skin, suggesting that the T_{RM} generation might be CCL17/CCR4-independent (Moed et al., 2004). Furthermore, a difference in $CD4^+$ and CD8+ T_{RM} cell formation is observed in BALB/c mice compared to C57BL/6J mice. Whereas formation of $CD4^+$ T_{RM} cells in C57BL/6J mice differed with CHS protocols used and likely needs repeated hapten challenges (Gaide et al., 2015; Gamradt et al., 2019), CD8 T_{RM} cell numbers were increased in healed ears after a single challenge and persisted over time and with multiple challenges in the skin of BALB/c mice (Murata & Hayashi, 2020). In the current study, both $CD8^+$ and $CD4^+$ T cell numbers were increased in $CCL17^{E/E}$ and aptamer-treated mice, while all cohorts showed a strong ear swelling reaction during the second challenge. Hence, to further

assess how the CCL17/CCR4-axis is involved in flare-up reactions, more rechallenge CHS experiments with different time points of analysis would be required. Moreover, the kinetics of CCL22 activity in CHS might differ from that of CCL17. Therefore, investigation of CCL22-deficient mice as well as CCL22 blockade in a similar manner could be of interest. Furthermore, an aptamer-aided CCL17 or CCL22 blockade in BALB/c mice could provide additional information about chemokine involvement in local skin memory and formation of $CD4^+$ T_{RM} cells.

In conclusion, the results of this study demonstrate that a single aptamer treatment blocking CCL17 around the time of first challenge is not enough to ensure long-term effectiveness for suppression of the allergic reaction. This could have several reasons. First, administration of one aptamer dose is not enough to suppress local formation of T memory cells in the skin. However, the absence of an amelioration of symptoms in $CCL17^{E/E}$ mice in the same setting argues against that. Second, CCL22 acts different from CCL17 and might rather be involved in formation of T_{RM} cells and long-term memory in CHS. To solve this question, it would be of interest how the CCL22-deficient mice perform after a second challenge in CHS. If $CCL22^{-/-}$ mice also demonstrate a normal ear swelling response after the second challenge, this would indicate that third, the underlying mechanisms of T cell recruitment and activation after secondary challenge differ from the first challenge and are CCL17- and CCL22 independent. Therefore, further investigation of $CCL17^{E/E}$ and $CCL22^{-/-}$ mice as well as mice deficient for both chemokines could shed light on whether the CCL17/CCL22-CCR4-axis is only involved in the first elicitation phase or in chronic stages and flare-ups. In this case, also a comparison between CCL17- and/or CCL22-deficient mice and therapeutic inhibition using the CCL17-specific aptamer MF35.47m and the CCL22-specific aptamer AJ102.29m could give valuable information about the mechanism of action.

5.1.3. Therapeutic use of aptamers post challenge

A comparison of mice that received the CCL17-specific aptamer at the time point of first challenge and 12 h post challenge with mice that received the aptamer 24 h post challenge revealed that aptamer administration and thus blockade of CCL17 can still influence the allergic response 24 h post challenge. Injection of MF35.47m 24 h post challenge was able to reduce the ear swelling reaction, while immune cell infiltration in the ears was similar to non-injected WT control mice **(Figure 4.7)**. Thus, the immune cell recruitment into the skin apparently already occurs early after the challenge and is likely dependent on the

CCL17/CCL22-CCR4-axis. As blockade of CCL17 nevertheless did decrease the ear swelling response, CCL17 could not only influence T cell recruitment but also act on the myeloid compartment and influence recruitment of e.g. neutrophils or mast cells into the skin. The edema formation is therefore not only dependent on T cell-mediated processes but might require CCL17 activity on myeloid cells. As CCL17- and CCL22-deficient mice demonstrated the same phenotype in CHS, i.e. an amelioration of symptoms, it is likely that post challenge CCL22 blockade also prevents ear swelling and immune cell infiltration. Additionally, as a strong increase of CCL22 expression could be measured in ears of mice three days post DNFB challenge **(Figure 4.10)**, CCL22 might also play an important role in later stages of the CHS. Hence, the kinetics of action of both chemokines and the underlying mechanisms of action might differ for CCL17 and CCL22. Therefore, comparing CCL17- and CCL22 blockade 24 h post challenge could reveal if the chemokines act similarly or are involved in different processes during the elicitation phase of CHS.

Taken together, the results of this part suggest that therapeutic aptamer application of a CCL17-specific aptamer is most effective the closer the inhibitory aptamer is applied to the hapten challenge in order to intervene not only with edema formation but also with immune cell recruitment.

5.2. Newly generated CCL22-specific aptamers ameliorate allergic symptoms in CHS

The CCL17/CCL22-CCR4-axis has been closely connected to skin disorders hinting that CCL17- or CCL22-dependent migration contributes to allergy development. Interestingly, in our group we could observe that CCR4 deficiency in mice increases the allergic reaction, in line with similar findings published by others (Lehtimäki et al., 2010; Matsuo et al., 2019; Sato et al., 2023). In contrast, lack of either CCL17 or CCL22 or both chemokines ameliorate CHS associated symptoms **(1.2.3)** (Fülle, Steiner, et al., 2018). In addition, an immense increase of CCL22 was observed in the ear skin of $CCR4^{-/-}$ mice after CHS induction. Thus, it was assumed that CCL22 promotes allergic symptoms in CHS. To test the therapeutic potential of CCL22 blockade in the context of CHS the newly generated CCL22-specific aptamers were tested in this thesis.

Anna Jonczyk (AG Mayer) developed eight different CCL22-specific DNA aptamers, in which three different sequence motifs emerged after the SELEX. These aptamers were tested *in vitro* and the two most promising candidates AJ82 and AJ102 were truncated and modified for

further testing. The truncation of AJ82 with motif 1 and AJ102 with motif 3 was based on the predicted folding structure **(Figure 5.1)**.

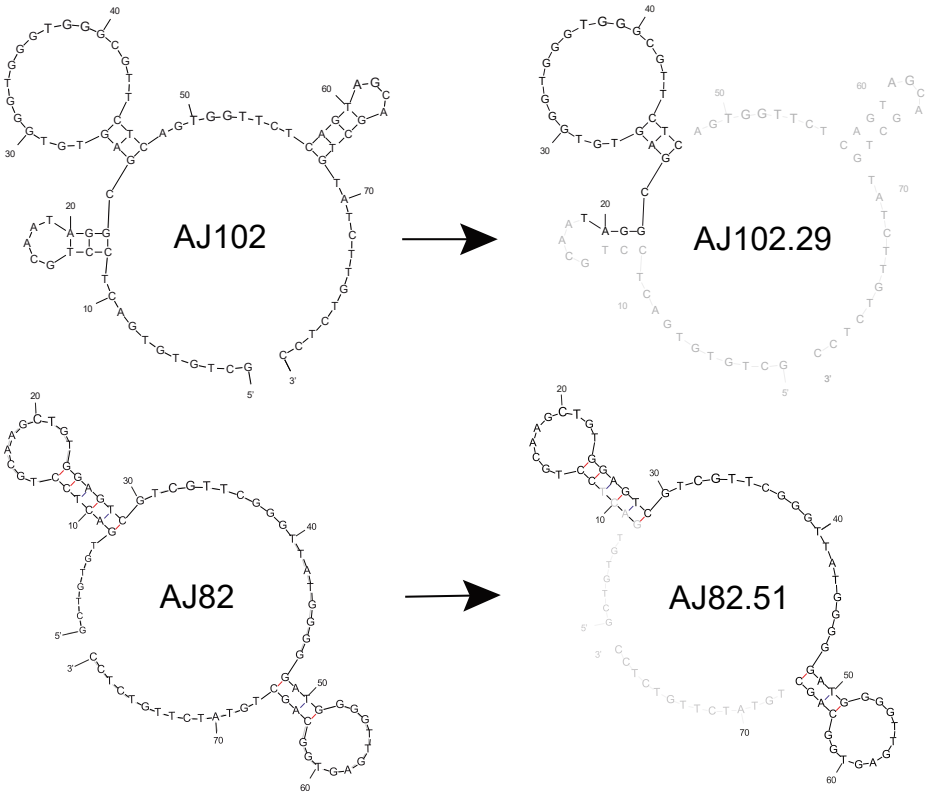

Figure 5.1 | Truncation of parental aptamers based on the predicted structures by Mfold.
Based on the predicted structures of AJ102 (top left) and AJ82 (bottom left) truncated versions were generated. After testing for affinity, specificity and functionality, the truncated versions AJ102.29 (top right) and AJ82.51 (bottom right) were chosen and further analyzed in this study.
Figure was provided by Anna Jonczyk (AG Mayer) using the predicted 3D structures from the Mfold webserver from UNAfold (Zuker, 2003)

Aptamer folding can only be predicted to a certain extent as structural polymorphisms frequently occur and specific structural components like G quadruplexes cannot be predicted in most of the programs that simulate nucleic acid folding. Furthermore, by native polyacrylamide gel electrophoresis analysis it was detected that the truncated aptamer AJ82.51 forms multimers, so that intermolecular structures appear that cannot be depicted by a singular aptamer. This difference between AJ82.51 and AJ102.29 might indicate that the aptamers bind CCL22 at two different sites. Nevertheless, both AJ82.51 and AJ102.29 bind CCL22 effectively and thereby inhibit CCL22-dependent migration. DNA structures can be recognized by PRR and induce an immune response (Dempsey & Bowie, 2015). Consequently, the aptamers were tested for immune recognition as induction of a proinflammatory response during therapeutic use in the context of allergy would be disadvantageous. When testing for immunostimulatory properties, the aptamer AJ82.51 that contains motif 1 exhibited an

adverse activation of the innate immune system thus being non-suitable for therapeutic use **(Figure 4.14)**. Both motifs have a high proportion of guanosine nucleotides and contain cytidine thus possibly exposing CpG sites that could be recognized by TLR-9 (Avci-Adali et al., 2013). Therefore, the formation of AJ82.51 multimers might be responsible for TLR9-dependent immune stimulation as multimerization of synthetic oligonucleotides has been shown to be required for optimal TLR9 activation as it promotes receptor aggregation (Wu et al., 2004). Hence, for the potential development of a therapeutic, it is essential to generate a target-specific aptamer that binds the target with high affinity and blocks its function without immune stimulation.

After confirmation of an inhibitory effect of AJ102.29m on T cell migration *in vitro*, injection of AJ102.29m at the time of the challenge and 12 h post challenge during CHS revealed that *in vivo* use of the aptamer efficiently ameliorated the allergic symptoms. Following aptamer treatment, the reduction in ear swelling as well as the reduction of immune cells in the ears of WT mice that received AJ102.29m was similar but not as strong as in $CCL22^{-/-}$ mice. Thus, the findings demonstrate a potential of aptamer-aided CCL22 blockade as a prospect for ACD treatment.

5.2.1. Topical application of aptamers as a therapeutic option to treat CHS

Although in this study the therapeutic effectiveness of injection of AJ102.29m was shown, a systemic use of CCL22-specific aptamers in human ACD therapy could also exhibit side-effects, such as immunological impairment in addition to the invasive procedure of the injection itself. Systemic administration of AJ102.29m could not only affect allergic reactions, but also act on other organs where CCL22 is of functional importance. For example, T cell homing and migration could possibly be affected in primary and secondary immune organs. Thus, CCL22 blockade might shift the immune synapses towards effector T cell - DC rather than Treg - DC contacts and change Treg recruitment in general (Cecilia Berin et al., 2001; Karlsson et al., 2021; Rapp et al., 2019; Scheu et al., 2017; Thul et al., 2017; Uhlén et al., 2015; Uhlen et al., 2017; D. Wang et al., 2017). Therefore, topical application of AJ102.29m on the ear was used to test whether a local administration as a cream formulation could act directly at the site of the skin allergy without affecting other organs.

Using a Franz diffusion cell, penetration of the skin by AJ102.29 was first tested by microscopic analysis of fluorescently labelled aptamers and by detection of the aptamers by qPCR. Here,

the assay indeed revealed penetration of the epidermis and dermis of the topically applied AJ102.29m **(4.1.5.1)**. The staining pattern of some single dots and clusters of fluorescence signals suggests that the aptamer is localized on cell surfaces or in cells as well as in the interstitial space. Thus, AJ102.29m might bind secreted CCL22 and thereby prevent binding of CCL22 to CCR4. Additionally, the aptamer might bind to CCL22 that is immobilized on the extracellular matrix due to its charge (Yue, 2014). Furthermore, the observation of cell surface bound or internalized aptamer might indicate that AJ102.29 also interacts with CCL22 that is bound to CCR4 on CCR4-expressing cells. Nevertheless, to determine the exact binding mechanism in the skin, additional co-staining with e.g. anti-CCR4, or intracellular vesicle markers are required. However, the analysis of fluorescently stained skin samples showed already that there is an intradermal localization of the aptamer. This is supported by further experiments which show penetration of the aptamer through the whole dermis as the aptamer could be detected in the lower chamber of the Franz diffusion cell. The penetration kinetics of AJ82.51 and AJ102.29 showed a continuous increase of the aptamer concentration within the skin with a plateau at around 14 h. Successful penetration of the aptamers might also be a result of the chemical characteristics of the DAC cream. DAC cream was chosen due to its amphiphilic properties, so that the hydrophilic aptamer is dissolved in the cream, while the lipids contained in the cream enable absorption by the skin (Gloor et al., 2003). Remarkably, aptamer penetration was successful without a drug delivery enhancement strategy like microneedles, thermal ablation, or electroporation as used by others (Jeong et al., 2021; Prausnitz & Langer, 2008). Interestingly, addition of polyethylene glycol (PEG) is also used as a skin penetration enhancer facilitating water lipid emulsions (Amjadi et al., 2017; Mahmoud et al., 2019). For the Franz diffusion cell assay, however, the aptamers were non-PEGylated and instead conjugated to a fluorescent moiety to visualize the aptamer. For *in vivo* applications, the aptamers were PEGylated and, therefore, the skin penetration might even have been enhanced when used in a CHS experiment. Furthermore, as the PEGylation increases the half-life, the aptamer might be available for a longer time when used *in vivo* (Kovacevic et al., 2018). It was recently discovered though, that the use of PEGylated aptamers might evoke immune responses in patients that already have anti-PEG antibodies due to the use of PEG in commercial products that then, in turn, affect the efficiency of the aptamer treatment (Moreno et al., 2019). The fact that a decrease of the allergic reaction as well as a reduction in immune cell infiltration was observed when AJ102.29m was administered

topically, proves the effectiveness of local aptamer-dependent CCL22 blocking to suppress allergic symptoms. In particular, the results presented in this thesis demonstrate that topical blockade of CCL22 by AJ102.29m was successful in decreasing the immune reactions. To further investigate the action and localization of the aptamers, the fluorescently labelled aptamer can be used *in vivo*. In addition, analysis of the ears should be performed at the early days after the challenge to ensure the availability of the aptamer in the skin.

This study clearly showed the potential of topical application for therapeutic nucleic acids for the treatment of skin allergy by intervening with the CCL22-CCR4 Axis. This is an important foundation for development of a formulation based local treatment for ACD patients that could provide non-invasive acute and local mitigation of symptoms with a low risk of adverse effects once aptamers specific for human CCL22 would be available.

5.3. CCL17 and CCL22 as therapeutic targets to treat allergic contact dermatitis

Based on the results presented for the CHS model, CCL17 and CCL22 shall be evaluated as therapeutic targets for ACD in the following chapter.

In this thesis and in line with a previous study from our lab, CCL17-deficiency as well as aptamer-induced inhibition of CCL17 led to reduced allergic reactions during CHS (Fülle, Steiner, et al., 2018). The ear swelling response as well as the immune cell infiltration was decreased in $CCL17^{E/E}$ mice compared to WT mice. In addition, numbers of conventional T cells and $\gamma\delta$ T cells that infiltrated the ear were reduced. Interestingly also DETC numbers were lower in the vehicle and DNFB-treated ears. Also, as shown in this thesis for the first time, $CCL22^{-/-}$ mice demonstrated a decrease in conventional αβ T cell and DETC populations after CHS induction. In addition, less $CD8^+$ and $CD4^+$ T cells were detected in ears of $CCL22^{-/-}$ mice after DNFB challenge. Among the $CD4^+$ T cells, in particular Treg- and Th2 populations were affected. This indicated that a lack of CCL22 decreased T cell immigration into the skin during the effector phase of the CHS. This is in line with literature that found CCL22 to be important for skin homing and recruitment of Treg and Th2 cells (Bonecchi et al., 1998; J. J. Campbell et al., 1999; Colantonio et al., 2002; Faget et al., 2011; Imai et al., 1999; Lloyd et al., 2000; Mariani et al., 2004; Reiss et al., 2001). DNFB application increased the number of CCR4-expressing cells in the skin, suggesting recruitment of CCR4-expressing $CD4^+$ and $CD8^+$ T cells possibly via CCL22. Nevertheless, no significant change in CCR4-expressing T cell numbers was detected in $CCL22^{-/-}$ mice compared with WT mice upon DNFB treatment **(Figure 4.29)**. First, this could

indicate that CCL22 might be able to bind another receptor to recruit non CCR4 expressing T cells, which is blocked in CCL22$^{-/-}$ mice and to a certain degree in aptamer-treated mice. Thus, under CCL22 deficiency these T cells might not be able to enter the skin. Yet CCR4-expressing cells are still recruited by CCL17 in the skin. However, in case of CCL17 deficiency decreased immune cell infiltration could be due to missing CCL17 with a residual migration towards CCL22 of CCR4-expressing cells or cells expressing an unknown CCL22-binding receptor. Of note, however, we could not observe a stronger amelioration of the allergic response or the immune cell infiltration during CHS with DKO mice compared to the single chemokine-deficient mice that would confirm the residual immune cell recruitment in the single deficient mice. In case of the DKO mice, neither of the two CCR4 ligands is present and thus only CCL17- and CCL22-independent migration is possible, which would in addition indicate the presence of another ligand for CCR4. In contrast to this, in case of CCR4 deficiency in mice, an aggravated allergic response was observed in this thesis **(Figure 4.10)** as well as in literature (Lehtimäki et al., 2010). A recent study reinvestigated the role of CCR4 in T cell development (Li et al., 2023). Previously, Cowan et al showed that although the autoimmune regulator (AIRE) regulates CCL17 and CCL22 expression during T cell development in the thymus CCR4 is dispensable for migration and development in the thymus (Cowan et al., 2014). In contrast, Li et al recently confirmed that CCR4 is responsible for medullary accumulation of double-positive CD69^{+} thymocytes (Hu et al., 2015; Li et al., 2023). Thus, CCR4 might be of importance for efficient negative selection thereby regulating central tolerance. The observed exaggerated immune responses in CCR4$^{-/-}$ mice could be due to a higher autoimmunity caused by a defective T cell development in which CCR4-dependent interactions between DC and thymocytes are disturbed that then drive autoimmunity.

If there is another chemokine receptor as well as/or another chemokine involved in the CCL17/CCL22-CCR4-axis redundant roles could explain the complex phenotypes observed **(Figure 5.2)**. Here, a balance in concentrations of the unknown ligand, CCL17 and CCL22 together with the biased agonism might explain the immune cell infiltration behavior in the mice deficient for different components of the CCL17/CCL22-CCR4 axis after CHS induction.

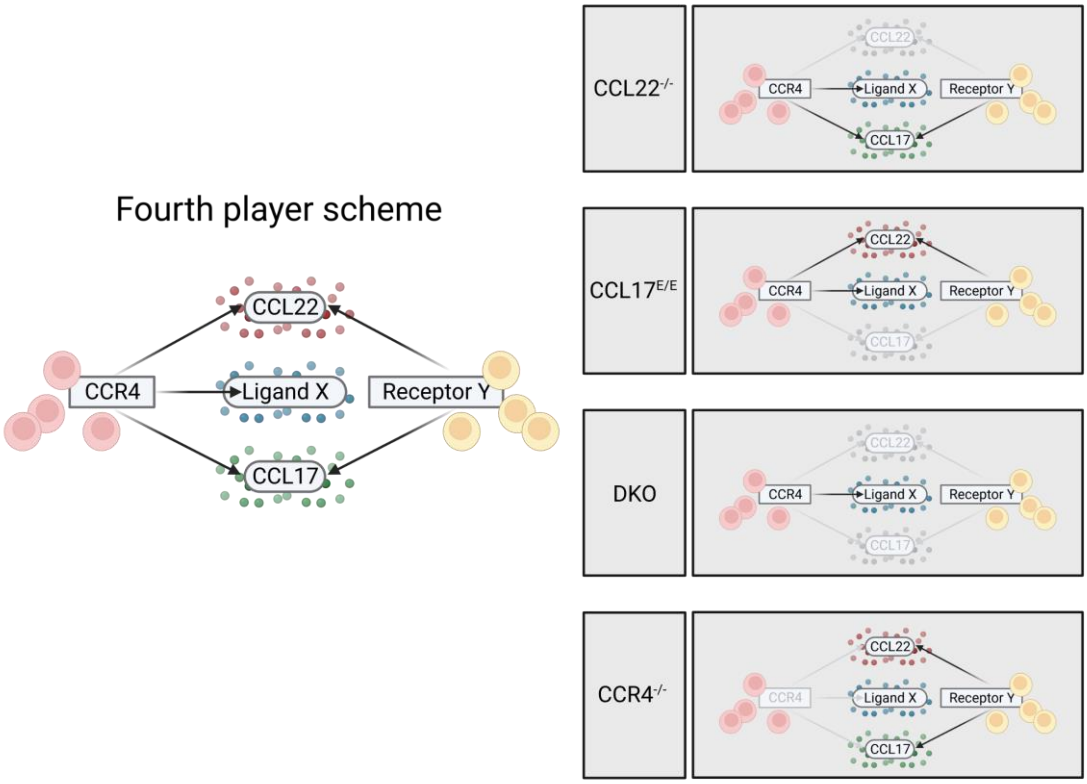

Figure 5.2 | Fourth player scheme for the CCL17/CCL22-CCR4 Axis.
Hypothetical influence of a potential second receptor for CCL17 and CCL22 and/or a third ligand binding CCR4.

Another interesting phenotype observed in CCL22$^{-/-}$ and CCL17$^{E/E}$ mice was a significant reduction of DETC numbers in vehicle- and DNFB-treated skin **(Figure 4.18, Figure 4.25, Figure 4.28, Figure 4.2, Figure 4.3, Figure 4.5, Figure 4.8)**, suggesting a defect in DETC development, homeostasis, or proliferation independent of experimental challenge. A decrease in the frequency of DETC upon DNFB treatment of WT mice occurs upon DETC activation (Gadsbøll et al., 2020). DETC involvement in the CHS response is heavily discussed. On the one hand, DETC are hypothesized to assist conventional αβ T cells in an allergen-unspecific manner and produce IFNγ and IL-17 in mice and humans and thus act pro-inflammatory (Dieli et al., 1998; Dyring-Andersen et al., 2013; Nielsen et al., 2015). On the other hand, studies with TCRγδ-deficient mice and *in vivo* depletion with anti-TCRγδ antibodies demonstrated an

amelioration of the CHS response in an allergen-specific manner (Girardi et al., 2002; Nielsen et al., 2015). However, it could later be shown that the FVB-Tac mice that were used in Girardi et al. have a defect in DETC development and spontaneously develop skin inflammation that could have biased the analysis (Lewis et al., 2006). Consequently, a pro-inflammatory role of DETC during CHS seems to be favored by the literature. The observed reduction in DETC frequency and increase of DETC numbers upon DNFB treatment observed in this thesis, additionally rather underlines a proinflammatory contribution by DETC. Gadsbøll et al. recently examined the decline of DETC percentage and demonstrated that $CD8^+$ T_{RM} displace DETC during CHS likely by metabolically outcompeting DETC. They also demonstrated that the number of $CD8^+$ T_{RM} correlates with severity of CHS symptoms (Gadsbøll et al., 2021). Interestingly, this supports the hypothesis already proposed earlier in this thesis that the increase in DETC numbers observed for the $CCL17^{E/E}$ and CCL17-specific aptamer-treated WT mice during a second challenge might be due to the presence of fewer $CD8^+$ T_{RM} due to the decreased allergic reaction after the first challenge. Thus, in CCL17-deficient mice and in WT mice that received the aptamer, less $CD8^+$ T_{RM} might have been selected and therefore less DETC were displaced by them. Consequently, more DETC would be present during the second challenge. Therefore, blocking of CCL17 or CCL22 could indirectly play a role in induction of skin memory responses. Remarkably, a reduction in epidermal DETC was also seen in $CCR4^{-/-}$ mice confirming the involvement of the CCL17/CCL22-CCR4-axis in DETC maintenance (Nakamura et al., 2013). However, the exact reason for the loss of DETC in $CCR4^{-/-}$ mice could not be determined by the authors as they showed that neither T cell development in the thymus, nor initial seeding of DETC in the skin were affected in $CCR4^{-/-}$ mice. Additionally, the reduced DETC count in the vehicle-treated ears of CCL17- or CCL22-deficient as well as aptamer-treated mice could hint towards a role of CCL17 and CCL22 in DETC maintenance or initial seeding. Furthermore, in another study Jiang et al confirmed CCR4 expression on DETC at embryonic day 15 and the importance of CCR4 for skin homing (Jiang et al., 2010). The strong reduction of DETC in vehicle-treated skin of CCL17- and CCL22-deficient mice indicates that embryonic expression of CCL17 and CCL22 might be of importance for DETC seeding in the skin. Furthermore, similar to the just recently confirmed importance of CCR4 in development of conventional T cells in the thymus (Li et al., 2023), the CCL17/CCL22-CCR4 -axis could also play a role in the development of $\gamma\delta$ T cells.

Taken together, although the underlying mechanisms of the CCL17/CCL22-CCR4-axis in CHS are not fully understood, aptamer-facilitated CCL17- or CCL22 blockade shows a great potential in amelioration of allergic symptoms associated with CHS. However, there are important structural differences between the CCL17-specific aptamer MF35.47m and the CCL22-specific aptamer AJ102.29m. In contrast to the CCL17-specific RNA-aptamer, AJ102.29m has a DNA backbone. The CCL17-specific aptamer is based on 2´fluoro RNA and has an inverted deoxythymidine at the 3´ end, also called cap-structure. This cap is preventing rapid degradation by exonucleases and provides more stability compared to normal RNA (Kratschmer & Levy, 2017). However, DNA aptamers are even more stable and can be more easily stored (Amero et al., 2021; Ni et al., 2017, 2021). Additionally, the production costs are much lower for DNA aptamers compared to RNA aptamers (Kratschmer & Levy, 2017; Ni et al., 2017, 2021). Furthermore, in this study we could demonstrate effective topical application of AJ102.29m, a technique that is non-invasive, has a lower probability of adverse effects, and can be used locally. Thus, this approach could represent a preferable method for therapeutic use when translated to treatment of ACD patients (Sallam et al., 2021).

5.3.1. Prospects of CCL17 or CCL22 blockade in human skin to potentially treat ACD patients

After the demonstration of an effective amelioration of CHS-associated symptoms in mice by systemic or topical application of CCL17- or CCL22-specific aptamers, this thesis aimed to investigate the potential of CCL17- or CCL22 blockade in human T cells, as a first step towards an evaluation of the CCL17/CCL22-CCR4-axis in the therapy of ACD.

For this purpose, a newly generated CCL17-specific aptamer binding to the human CCL17 molecule was tested for inhibition of CCL17-dependent cell migration using a human T cell lymphoma cell line, as well as activated primary human T cells **(4.1.6)**. Although initial assays using the T lymphoma cell line hinted to a possible inhibition of migration, transwell assays with primary T cells failed to confirm an aptamer-dependent inhibition of migration. Nevertheless, based on the successful experiments performed in this thesis using the mouse model, targeting human CCL17 and CCL22 remains a promising approach. Hence, more aptamer candidates of a new SELEX will be tested in the future. Although as a first step the confirmation of the inhibitory capacity of newly isolated aptamers by transwell migration assays needs to be achieved, further experiments are planned to include topical application of the aptamers on freshly excised human skin samples, like shown in a recent publication describing a human skin-penetrating IL-23-specific RNA aptamer (Lenn et al., 2018). In addition

to the methods used in that publication, high resolution microscopy of the *ex vivo* Franz assay experiments established in this thesis, as well as counterstaining with keratinocytes, DC and other skin cells could give information about the localization and penetration of aptamers specific for human CCL17 or CCL22. Furthermore, testing of the *in vivo* functionality of the aptamers by staining of T cell activation markers, analysis of chemokine receptor internalization and determination of T cell migration potential after application of a CCL17- or CCL22-specific aptamer on human skin could shed light on the therapeutic capability. For analysis of aptamer-blocked migration in excised human skin, the *ex vivo* culture system to label and track T cells in fresh skin samples established by Djikgraaf et al. could be employed (Dijkgraaf et al., 2019, 2021). Moreover, PEGylation of the aptamers might be of advantage to enhance skin penetration especially in the thicker human skin.

In conclusion, based on the successful amelioration of allergic symptoms after CCL17/CCL22 blockade in the CHS model in mice, the translation of these findings to application in humans is promising. Next to Pagaptanib, an anti-Vascular Endothelial Growth Factor (VEGF) aptamer used in the treatment of macular degeneration, another aptamer has been approved by the FDA, which is a pegylated RNA aptamer called Avacincaptad Pegol that recognized the C5 molecule of the complement system to treat geographic atrophy – an advanced form of macular degeneration (Mullard, 2023; Ng et al., 2006). Thus, in future additional aptamer-based treatments might evolve based on the results of these studies. In addition, the demonstrated transdermal aptamer delivery could expedite aptamer or nucleic acid administration also in the treatment of other diseases. Remarkably, the CCR4-specific antibody Mogamulizumab that is presently used as a treatment for T-cell lymphoma, Sézary syndrome or Mycosis fungoides leads to severe adverse skin disorders (Duvic et al., 2015; Ogura et al., 2014; Suzuki et al., 2019; Yonekura et al., 2014; Yoshie, 2021). Hence, human CCL17- or human CCL22-blocking aptamers could represent an alternative treatment in the future.

5.4. Influence of the CCL17/CCL22-CCR4-axis on the development of atopic dermatitis-like skin inflammation

Next to contact allergies the involvement of the CCL17/CCL22-CCR4 axis in Type I IgE-mediated hypersensitivity using a mouse model of AD (Abbas et al., 2023) was investigated in this study.

Although the functionality of the experimental model used was successfully shown in WT mice in a pre-experiment **(Figure 4.35)**, no notable differences between allergen-treated and non-treated groups were visible when comparing the mice deficient for different components of the CCL17/CCL22-CCR4-axis **(4.2.2)**. Remarkably, only the combination of OVA and Der.f. resulted in significant increases of IL-13, IgE and mast cell counts. The strong response after Der.f. is in line with the literature as it has been proven that house dust mite allergens induce a strong systemic Type II immune reaction and are immunostimulatory via TLR (Jin et al., 2009; D. Kim et al., 2019; Ogasawara et al., 2022; Trompette et al., 2009). The lack of difference in OVA-treated mice compared with NaCl-treated mice of the same genotype, however, indicated a technical problem during the procedure as repeated epicutaneous exposures to OVA alone is known to induce AD-like skin lesions in mice (Jin et al., 2009; G. Wang et al., 2007). In addition, the previously observed phenotype of suppressed allergic symptoms in CCL17-deficient mice in OVA-induced AD-like lesions could not be reproduced in the current experiment (Stutte et al., 2010). Nevertheless, IgE levels in CCL17- and CCL22-deficient mice were slightly lower than in WT mice, possibly indicating that the allergic reaction induced in this experiment was not potent enough to detect significant differences. Additionally, many experiments using the AD mouse model are performed with mice on a BALB/c genetic background, as these are prone to develop a stronger type II immune response, whereas C57BL/6J mice are biased towards a type I immune response (G. G. Anderson & Cookson, 1999; Spergel et al., 1999). All mice used for the present experiments had a C57BL/6J background. Thus, a possible effect of the genetic deficiencies on the development of AD-like lesions could not be determined properly as the allergic response in this model is generally low in the C57BL/6J genetic background (Abbas et al., 2023) and in the experiments performed in this thesis was even below the threshold of detection for an allergen-specific response. Hence, a possible influence of the components of the CCL17/CCL22-CCR4-axis on development of AD-like symptoms might be more apparent if the mice were available on a BALB/c background. In line with that, it was shown that CCR4 deficiency and the use of a CCR4 antagonist led to amelioration of the allergic response in BALB/c mice but not in C57BL/6J mice (Matsuo et al.,

2018). Alternatively, as the OVA-induced immune reaction was rather weak and could only be boosted in combination with Der.f., the experimental procedure might need to be altered to evoke a more potent immune response. For this, the allergen exposure could be prolonged or the concentration and types of allergens could be enhanced.

Taken together, in contrast to the experiments analyzing the role of the CCL17/CCL22-CCR4-axis in contact dermatitis, no alterations could be observed for the AD model in this thesis. Nevertheless, a connection of the CCL17/CCL22-CCR4-axis in AD cannot be excluded, as the genetic background perhaps prohibited detection of differences between cohorts.

5.5. Role of the CCL17/CCL22-CCR4-axis for development of inflammatory bowel disease

By performing DSS-induced colitis experiments with mice that lack different components of the CCL17/CCL22-CCR4-axis the role of these chemokines and their receptor in IBD development has also been examined in this study.

5.5.1. Role of CCL17 in DSS-induced colitis

In contrast to CCL22-deficient mice, lack of CCL17 expression did not protect from severe symptoms associated with acute colitis. Colon length, weight loss, disease score and histological features of $CCL17^{E/E}$ mice after colitis induction were similar to symptoms of WT mice after colitis induction. Although flow cytometric analysis showed no significant differences between $CCL17^{E/E}$ mice and those of WT mice, a larger number of T cells were detected in mesenteric lymph nodes of $CCL17^{E/E}$ mice. Further, mesenteric lymph nodes of DKO, $CCR4^{-/-}$ and $CCL22^{-/-}$mice contained significantly more T cells than both, WT and $CCL17^{E/E}$ mice. On day 4 of DSS treatment, lower levels of proinflammatory cytokines, such as IL-23, TNF and IL-12 were measured in $CCL17^{E/E}$ mice compared to WT mice indicating minor differences of the immune response after colitis induction when CCL17 is missing. Though it has been published that CCL17 is expressed by $CD103^{+}$ intestinal DC and DC in intestinal lymphoid tissues like Peyers' Patches and mesenteric lymph nodes (Erazo et al., 2021; Metzger et al., 2022), no change in DC subsets could be detected in mice lacking CCL17 compared to WT mice in the DSS colitis model. In Salmonella infection, CCL17-expressing DC take up bacteria and transport them from the gut into the mesenteric lymph node and Peyer's Patches, where CCL17 expression was additionally increased (Erazo et al., 2021). Nevertheless, no major differences in DC numbers or bacterial load were obtained in mice lacking CCL17 in that setting

(Erazo et al., 2021). CCL17 expression in the mesenteric lymph nodes might be further amplified by the micromilieu created by initialization of the immune response as, for example, TNF is known to induce CCL17 production and CCL17 is strongly induced after TLR stimulation (Alferink et al., 2003; Fülle, Offermann, et al., 2018). Moreover, CCL17-expressing DC can produce IL-12 and induce proliferation as well as IFNγ production of T cells (Alferink et al., 2003). Unaffected DC subsets as observed by Erazo et al. are in line with the results of this thesis as frequencies and absolute counts of DC did not differ and T cell numbers were only slightly changed in $CCL17^{E/E}$ mice. Thus, CCL17 expression might rather act as an indicator and amplifier of inflammation reacting to the secreted cytokines and promoting further cytokine production towards a pro-inflammatory response (Bozic et al., 2021). Furthermore, the lower levels of cytokines after 4 days of DSS treatment in $CCL17^{E/E}$ mice would support an amplifying function of CCL17. In our earlier experiments, CCL17 expression was detected at the entry site of antigens in the GALT indicating that CCL17 is involved in facilitating uptake and presentation of luminal antigens in the GALT (Alferink et al., 2003). Hence, although CCL17 might affect DC functionality it has only minor effects on DC numbers as observed in this thesis. In the context of colitis, CCL17 could be influencing T cell responses to a minor extent likely via CCL17-expressing intestinal DC and their attraction into the lymph nodes as observed in Stutte et al. (Stutte et al., 2010). Additionally, CCL17 could also be involved in later stages of the immune response after colitis induction. Therefore, it would be of interest how $CCL17^{E/E}$ mice behave in chronic colitis models. In contrast to the results presented here, Heiseke et al. previously described that $CCL17^{E/E}$ mice lost less weight, had a longer colon length and a lower histological score after acute DSS-induced colitis compared to WT mice (Heiseke et al., 2012). In contrast to the acute colitis model used in this thesis, Heiseke et al. used a colitis model with a higher DSS dose of 4 % for a shorter duration of 5 days. In addition, the polysaccharide DSS differs in its molecular weight that has been shown to influence the severity of colitis and carcinogenic activity immensely (Hirono et al., 1983; Kitajima et al., 2000). An influence of the experimental model or the DSS batch used is supported by the difference in colon length. While the colon length of $CCL17^{E/E}$ was reduced to 5.3 cm after DSS colitis induction in both studies, the reduction of the colon length of WT colons differed between the results shown in this thesis and by Heiseke et al. While the colon length decreased to 5 cm in this thesis **(Figure 4.47)** Heiseke et al. observed a reduction of colon length in WT mice after DSS colitis to 4.5 cm. Thus, the changes between WT and $CCL17^{E/E}$ mice were less striking in the colitis model used in this

thesis, whereas the other genetically deficient mice analyzed displayed a stronger phenotype. Hence, CCL17- and CCL22 single- and double-deficient mice as well as CCR4$^{-/-}$ mice were compared side by side in the current experiments. This allowed a direct comparison of the components of the CCL17/CCL22-CCR4-axis in DSS-induced colitis. Furthermore, Metzger et al uncovered that the housing conditions greatly influence the experimental outcome in colitis-associated tumorigenesis of CCL17$^{E/E}$ mice, indicating that experimental effects of CCL17 deficiency might be different depending on the composition of their microbiome (Metzger et al., 2022).

5.5.2. Role of CCL22 in DSS-induced colitis

One of the main findings of this part of the thesis was that CCL22$^{-/-}$ mice were protected from severe colitis symptoms. DKO- and CCR4-deficient mice were mildly protected, whereas CCL17$^{E/E}$ mice behaved largely like WT mice. Interestingly, Rapp et al observed a deterioration of symptoms in CCL22-deficient mice in a chronic DSS-induced colitis model (Rapp et al., 2019). Although this appears contradictory to our results, the phenotypes likely vary due to the difference in the experimental models employed. The acute colitis model used in this thesis aimed to investigate clinical manifestations of symptoms during an acute colitis episode, such as weight loss, diarrhea, occult blood in stools and anemia. In contrast, in the chronic DSS model used by Rapp et al., mice receive periodic administration of DSS at low concentration for a longer time. This is accompanied by severe infiltration of mononuclear cells and regenerative changes of the epithelium (Chassaing et al., 2014; Okayasu et al., 1990; Perše & Cerar, 2012). In the current work, using an acute colitis model, CCL22$^{-/-}$ mice, lost less weight, had a lower disease score, longer colons, and less severe infiltration of immune cells into the tissue compared to WT mice **(4.3.1)**. Although this relatively strong phenotype in CCL22$^{-/-}$ mice indicates an involvement of the chemokine in intestinal barrier functions, no difference of CCL22 expression between the analyzed cohorts was observed in colonic tissue after DSS colitis **(Figure 4.48)**. CCL22 expression can be found in different parts of the GI tract (Karlsson et al., 2021; Thul et al., 2017; Uhlén et al., 2015; Uhlen et al., 2017). Although local expression after DSS-induced colitis did not differ between CCL22 expressing cohorts, the lack of CCL22 in CCL22$^{-/-}$- and DKO mice might have caused an alteration of immune composition in the intestine already at steady state that in turn affects the immune response during acute DSS-induced colitis. Instead of the colonic intestinal tissue itself, CCL22 could also act on other structures of the GALT. Analyzing the cellular composition of the mesenteric lymph nodes after

DSS-induced colitis, CCL22$^{-/-}$ mice harbored an increased number of T cells. Here, more activated T cells could be detected in the CCL22$^{-/-}$ mice hinting towards a stronger immune response compared to WT mice and to the other cohorts. Interestingly, the importance of CCL22 in mediating T cell - DC contacts by favoring Treg-DC contacts was demonstrated by Rapp et al. (Rapp et al., 2019). Thus, if CCL22 is missing, less Treg-DC interactions might occur during DSS-induced colitis, leading to stronger activation of T cells as indeed observed. Although the Treg counts increased in CCL22$^{-/-}$ mice compared to WT mice after colitis induction the number of activated Treg did not differ between cohorts **(Figure 4.53)** supporting the hypothesis that DSS-induced colitis creates a strong proinflammatory response in the mesenteric lymph nodes of CCL22$^{-/-}$ mice. In contrast to that, CCL22$^{-/-}$ mice demonstrated less severe symptoms of colitis with lower cytokine levels in the serum, less inflammation in the colonic tissue and a generally better disease score. Analyzing the adaptive immune cell populations during acute experimental colitis Hall et al. demonstrated that the number of T cells peaked from day 4 until day 6 in the mesenteric lymph node probably representing the time points where antigen-specific T cells proliferate (Hall et al., 2011; Perše & Cerar, 2012). Hence, the immune response might be delayed in CCL22-deficient mice. Whereas T cells might already migrate to the colon in the other cohorts, T cells in CCL22$^{-/-}$ mice still accumulate in the mesenteric lymph nodes at this time point, because of prolonged expression of CD69 and CD69-dependent retention in the lymph node as Hall et al. also described the involvement of CD69 expression in T cell activation and migration to the colon during DSS-colitis (Hall et al., 2011) . Interestingly, CCL22 mediates T cell - DC contacts by regulating the ratio of DC interacting with conventional T cells and DC interacting with Treg (Rapp et al., 2019). In the absence of CCL22 less Treg - DC contacts occur, and more conventional T cell interact with DC (Rapp et al., 2019). Therefore, the increase in cell numbers observed here might be due to an enhanced ratio of DC interacting with conventional T cells over DC - Treg contacts in CCL22-deficient mice. Furthermore, the throughput of DC cooperating with T cells might be increased in CCL22$^{-/-}$ mice as well thus influencing the expansion of T cells in the mesenteric lymph nodes. This would be supported by the fact that the chronic DSS-induced colitis model leads to deterioration of colitis symptoms in CCL22-deficient mice (Rapp et al., 2019). However, the increased numbers of DC in the mesenteric lymph nodes in CCL22$^{-/-}$ mice cannot be explained by that. Also, some of the effects might be due to residual CCL17 production in CCL22$^{-/-}$ mice. In CCL22 deficiency, the dominant ligand for CCR4 is absent, therefore CCL17 might bind to

CCR4 instead of CCL22 under physiological conditions. Thus, the immune response might be shaped differently due to biased agonism of CCL17 and CCL22. In this case, CCL17 could promote DC maturation and increased migration into the lymph nodes (Alferink et al., 2003; Stutte et al., 2010; Tang & Cyster, 1999).

Remarkably, the DKO mice were not as protected from severe colitis-associated symptoms as the CCL22 single-deficient mice. The DKO mice neither demonstrated the same phenotype as the $CCL22^{-/-}$ nor the $CCL17^{E/E}$ mice, but showed an intermediate colon length, colonic inflammation, disease score and accumulated significantly more T cells in the mesenteric lymph nodes than WT mice after DSS treatment. In $CCL17^{E/E}$ mice expression of the dominant CCR4 ligand CCL22 facilitates major functions in the immune response during colitis, whereas the effects mediated by CCL17 are strengthened in the absence of CCL22. Under physiological conditions CCL17 and CCL22 are known to exert different functions and together orchestrate an effective immune response. But if one component is missing the immune response is tilted. Although it might have an influence on the hosts immunity, taking both ligands out of the equation eliminates the disbalance. This hypothesis would be supported by the fact that the $CCR4^{-/-}$ mice exhibit a similar phenotype compared with the DKO mice during colitis, both representing the complete abolishment of the CCL17/CCL22-CCR4-axis. However, this similarity in phenotypes could not be observed for other experimental models like CHS presented in this thesis. Furthermore, in the DKO, in which neither CCL17 nor CCL22 can bind to CCR4, a third, yet unknown, ligand could bind CCR4. This supports the previously mentioned fourth player hypothesis of another molecule involved in the CCL17/CCL22-CCR4-axis **(Figure 5.2)**.

Atypical chemokine receptors (ACKR) that do not induce signaling pathways upon binding of the ligands have been shown to bind to CCL17 and CCL22 (Bonecchi & Graham, 2016; Melgrati et al., 2023). Thus, ACKR are able to sequester chemokines and reduce chemotactic signals by binding to chemokines that would otherwise bind to a chemokine receptor that induces activation and migration towards a chemokine gradient. While ACKR1 is known to be expressed on erythrocytes and strongly binds to CCL17, ACKR2 can bind both CCL17 and CCL22 with a bias towards CCL22 (Hansell et al., 2011; Santulli-Marotto et al., 2013; Schnabel et al., 2010). Strikingly, it could be shown that ACKR2 is expressed in resting colon and is upregulated upon colitis induction (Bordon et al., 2009). While Bordon et al. observed a reduced susceptibility of ACKR2-deficient mice to colitis symptoms, Vetrano et al. detected that ACKR2-

deficient mice failed to resolve colitis and had significantly higher levels of proinflammatory cytokines (Vetrano et al., 2010). Although these studies show contradictory results in colitis experiments, ACKR2 expression in the colon could change the binding equilibrium of CCL17 and CCL22 to CCR4. Hence, by binding of CCL17 or CCL22 to ACKR chemotaxis of CCR4-expressing T cells might be altered.

5.5.3. Involvement of the CCL17/CCL22-CCR4-axis in mechanisms important for intestinal barrier malfunctions

Taken together, this thesis provides important insights into the influence of the CCL17/CCL22-CCR4-axis on development of IBD by analyzing mice deficient for different components of the CCL17/CCL22-CCR4-axis side by side in an experimental acute colitis model. Based on these experiments, CCL22 appears to play a detrimental role in the formation of acute colitis symptoms, while the role of CCL17 appears to be less dominant. In addition, the results clearly show that the underlying mechanisms are multifactorial. Due to the complexity of the CCL17/CCL22-CCR4-axis, unwrapping of immune mechanisms during colitis likely demands analysis of further players. For that purpose, analysis of the newly generated triple knockout mice (TKO), deficient for CCL17, CCL22 and CCR4 could shed light on the existence of additional chemokine or chemokine receptors involved in this axis. A difference in the outcome of DSS-induced colitis in TKO mice compared with the DKO- and CCR4-deficient mice would confirm the existence of a fourth player in the CCL17/CCL22-CCR4-axis. In that case, the interaction of the fourth player that accounts for residual migratory processes or influences the binding of CCL17/CCL22 to CCR4 in the other cohorts, would be abolished in the TKO. Thus, a deterioration of symptoms during DSS-induced colitis would be expected. Nevertheless, the data show that CCL22 plays an important role in the development of acute colitis symptoms. Here, further investigation of CCL22 expression in different tissues and cell populations as well as T cell proliferation kinetics and tracking of T cell - DC interactions in CCL22-deficient mice could lead to a deeper understanding of IBD development.

6. References

Abbas, M., Moussa, M., & Akel, H. (2023). Type I Hypersensitivity Reaction. *StatPearls*. https://www.ncbi.nlm.nih.gov/books/NBK560561/

Adegbola, S. O., Sahnan, K., Warusavitarne, J., Hart, A., & Tozer, P. (2018). Anti-TNF Therapy in Crohn's Disease. *International Journal of Molecular Sciences*, *19*(8). https://doi.org/10.3390/IJMS19082244

Ahern, P. P., Schiering, C., Buonocore, S., McGeachy, M. J., Cua, D. J., Maloy, K. J., & Powrie, F. (2010). Interleukin-23 drives intestinal inflammation through direct activity on T cells. *Immunity*, *33*(2), 279–288. https://doi.org/10.1016/J.IMMUNI.2010.08.010

Alex, P., Zachos, N. C., Nguyen, T., Gonzales, L., Chen, T. E., Conklin, L. S., Centola, M., & Li, X. (2009). Distinct Cytokine Patterns Identified from Multiplex Profiles of Murine DSS and TNBS-Induced Colitis. *Inflammatory Bowel Diseases*, *15*(3), 341. https://doi.org/10.1002/IBD.20753

Alferink, J., Lieberam, I., Reindl, W., Behrens, A., Weiß, S., Hüser, N., Gerauer, K., Ross, R., Reske-Kunz, A. B., Ahmad-Nejad, P., Wagner, H., & Förster, I. (2003). Compartmentalized production of CCL17 in vivo: Strong inducibility in peripheral dendritic cells contrasts selective absence from the spleen. *Journal of Experimental Medicine*, *197*(5), 585–599. https://doi.org/10.1084/jem.20021859

Alinaghi, F., Bennike, N. H., Egeberg, A., Thyssen, J. P., & Johansen, J. D. (2019). Prevalence of contact allergy in the general population: A systematic review and meta-analysis. *Contact Dermatitis*, *80*(2), 77–85. https://doi.org/10.1111/COD.13119

Amero, P., Lokesh, G. L. R., Chaudhari, R. R., Cardenas-Zuniga, R., Schubert, T., Attia, Y. M., Montalvo-Gonzalez, E., Elsayed, A. M., Ivan, C., Wang, Z., Cristini, V., Franciscis, V. De, Zhang, S., Volk, D. E., Mitra, R., Rodriguez-Aguayo, C., Sood, A. K., & Lopez-Berestein, G. (2021). Conversion of RNA Aptamer into Modified DNA Aptamers Provides for Prolonged Stability and Enhanced Antitumor Activity. *Journal of the American Chemical Society*, *143*(20), 7655–7670. https://doi.org/10.1021/JACS.9B10460

Amjadi, M., Mostaghaci, B., & Sitti, M. (2017). Recent Advances in Skin Penetration Enhancers for Transdermal Gene and Drug Delivery. *Current Gene Therapy*, *17*(2). https://doi.org/10.2174/1566523217666170510151540

Anderson, C. A., Solari, R., & Pease, J. E. (2016). Biased agonism at chemokine receptors: obstacles or opportunities for drug discovery? *Journal of Leukocyte Biology*, *99*(6), 901–909. https://doi.org/10.1189/jlb.2MR0815-392R

Anderson, G. G., & Cookson, W. O. C. M. (1999). Recent advances in the genetics of allergy and asthma. *Molecular Medicine Today*, *5*(6), 264–273. https://doi.org/10.1016/S1357-4310(99)01479-3

Antoni, L., Nuding, S., Wehkamp, J., & Stange, E. F. (2014). Intestinal barrier in inflammatory bowel disease. *World Journal of Gastroenterology : WJG*, *20*(5), 1165. https://doi.org/10.3748/WJG.V20.I5.1165

Antonopoulos, C., Cumberbatch, M., Dearman, R. J., Daniel, R. J., Kimber, I., & Groves, R. W. (2001). Functional caspase-1 is required for Langerhans cell migration and optimal contact sensitization in mice. *Journal of Immunology (Baltimore, Md. : 1950)*, *166*(6), 3672–3677. https://doi.org/10.4049/JIMMUNOL.166.6.3672

Asseman, C., Fowler, S., & Powrie, F. (2012). Control of Experimental Inflammatory Bowel Disease by Regulatory T cells. *Https://Doi.Org/10.1164/Ajrccm.162.Supplement_3.15tac9*, *162*(4 II), 185–189. https://doi.org/10.1164/AJRCCM.162.SUPPLEMENT_3.15TAC9

Atochina, E. N., Beers, M. F., Tomer, Y., Scanlon, S. T., Russo, S. J., Panettieri, R. A., & Haczku, A. (2003). Attenuated allergic airway hyperresponsiveness in C57BL/6 mice is associated with enhanced surfactant protein (SP)-D production following allergic sensitization. *Respiratory Research*, *4*(1), 15. https://doi.org/10.1186/1465-9921-4-15

Auriemma, M., Vianale, G., Amerio, P., & Reale, M. (2013). Cytokines and T cells in atopic dermatitis. *European Cytokine Network*, *24*(1), 37–44. https://doi.org/10.1684/ECN.2013.0333

Avci-Adali, M., Steinle, H., Michel, T., Schlensak, C., & Wendel, H. P. (2013). Potential Capacity of Aptamers to Trigger Immune Activation in Human Blood. *PLoS ONE*, *8*(7). https://doi.org/10.1371/JOURNAL.PONE.0068810

Bain, C. C., Montgomery, J., Scott, C. L., Kel, J. M., Girard-Madoux, M. J. H., Martens, L., Zangerle-Murray, T. F. P., Ober-Blöbaum, J., Lindenbergh-Kortleve, D., Samsom, J. N., Henri, S., Lawrence, T., Saeys, Y., Malissen, B., Dalod, M., Clausen, B. E., & Mowat, A. M. I. (2017). TGFβR signalling controls CD103+CD11b+ dendritic cell development in the intestine. *Nature Communications 2017 8:1*, *8*(1), 1–12. https://doi.org/10.1038/s41467-017-00658-6

Bain, C. C., Scott, C. L., Uronen-Hansson, H., Gudjonsson, S., Jansson, O., Grip, O., Guilliams, M., Malissen, B., Agace, W. W., & Mowat, A. M. I. (2013). Resident and pro-inflammatory macrophages in the colon represent alternative context-dependent fates of the same Ly6Chi monocyte precursors. *Mucosal Immunology*, *6*(3), 498–510. https://doi.org/10.1038/MI.2012.89

Barbarot, S., Auziere, S., Gadkari, A., Girolomoni, G., Puig, L., Simpson, E. L., Margolis, D. J., de Bruin-Weller, M., & Eckert, L. (2018). Epidemiology of atopic dermatitis in adults: Results from an international survey. *Allergy*, *73*(6), 1284–1293. https://doi.org/10.1111/ALL.13401

Bergmann, K.-C., Heinrich, J., & Niemann, H. (2016). Current status of allergy prevalence in Germany. *Allergo Journal International*, *25*(1), 6–10. https://doi.org/10.1007/s40629-016-0092-6

Bevins, C. L., & Salzman, N. H. (2011). Paneth cells, antimicrobial peptides and maintenance of intestinal homeostasis. *Nature Reviews Microbiology 2011 9:5*, *9*(5), 356–368. https://doi.org/10.1038/nrmicro2546

Blair, H. A. (2022). Tralokinumab in Atopic Dermatitis: A Profile of Its Use. *Clinical Drug Investigation*, *42*(4), 365–374. https://doi.org/10.1007/S40261-022-01135-9

Boehm, F., Martin, M., Kesselring, R., Schiechl, G., Geissler, E. K., Schlitt, H. J., & Fichtner-Feigl, S. (2012). Deletion of Foxp3+ regulatory T cells in genetically targeted mice supports development of intestinal inflammation. *BMC Gastroenterology*, *12*(1), 1–11. https://doi.org/10.1186/1471-230X-12-97/FIGURES/5

Bogunovic, M., Ginhoux, F., Helft, J., Shang, L., Hashimoto, D., Greter, M., Liu, K., Jakubzick, C., Ingersoll, M. A., Leboeuf, M., Stanley, E. R., Nussenzweig, M., Lira, S. A., Randolph, G. J., & Merad, M. (2009). Origin of the lamina propria dendritic cell network. *Immunity*, *31*(3), 513–525. https://doi.org/10.1016/J.IMMUNI.2009.08.010

Boirivant, M., Fuss, I. J., Chu, A., & Strober, W. (1998). Oxazolone colitis: A murine model of T helper cell type 2 colitis treatable with antibodies to interleukin 4. *The Journal of Experimental Medicine*, *188*(10), 1929–1939. https://doi.org/10.1084/JEM.188.10.1929

Bollrath, J., & Powrie, F. M. (2013). Controlling the frontier: Regulatory T-cells and intestinal homeostasis. *Seminars in Immunology*, *25*(5), 352–357. https://doi.org/10.1016/J.SMIM.2013.09.002

Bonecchi, R., Bianchi, G., Bordignon, P. P., D'Ambrosio, D., Lang, R., Borsatti, A., Sozzani, S., Allavena, P., Gray, P. A., Mantovani, A., & Sinigaglia, F. (1998). Differential expression of chemokine receptors and chemotactic responsiveness of type 1 T helper cells (Th1s) and Th2s. *The Journal of Experimental Medicine*, *187*(1), 129–134. https://doi.org/10.1084/JEM.187.1.129

Bonecchi, R., & Graham, G. J. (2016). Atypical Chemokine Receptors and Their Roles in the Resolution of the Inflammatory Response. *Frontiers in Immunology*, *7*(JUN), 224. https://doi.org/10.3389/FIMMU.2016.00224

Bordon, Y., Hansell, C. A. H., Sester, D. P., Clarke, M., Mowat, A. McI., & Nibbs, R. J. B. (2009). The atypical chemokine receptor D6 contributes to the development of experimental colitis. *Journal of Immunology (Baltimore, Md. : 1950)*, *182*(8), 5032–5040. https://doi.org/10.4049/JIMMUNOL.0802802

Bouladoux, N., Hennequin, C., Malosse, C., Malissen, B., Belkaid, Y., & Henri, S. (2017). Hapten-Specific T Cell-Mediated Skin Inflammation: Flow Cytometry Analysis of Mouse Skin Inflammatory Infiltrate. *Methods in Molecular Biology (Clifton, N.J.)*, *1559*, 21–36. https://doi.org/10.1007/978-1-4939-6786-5_2

Bozic, T., Sersa, G., Kranjc Brezar, S., Cemazar, M., & Markelc, B. (2021). Gene electrotransfer of proinflammatory chemokines CCL5 and CCL17 as a novel approach of modifying cytokine expression profile in the tumor microenvironment. *Bioelectrochemistry*, *140*, 107795. https://doi.org/10.1016/J.BIOELECHEM.2021.107795

Breuers, S., & Mayer, G. (2023). Automated ssDNA SELEX Using Histidine-Tagged Target Proteins. *Methods in Molecular Biology (Clifton, N.J.)*, *2570*, 3–11. https://doi.org/10.1007/978-1-0716-2695-5_1

Broggi, A., Cigni, C., Zanoni, I., & Granucci, F. (2016). Preparation of Single-cell Suspensions for Cytofluorimetric Analysis from Different Mouse Skin Regions. *Journal of Visualized Experiments : JoVE*, *2016*(110), 52589. https://doi.org/10.3791/52589

Bruckner, R. S., Spalinger, M. R., Barnhoorn, M. C., Feakins, R., Fuerst, A., Jehle, E. C., Rickenbacher, A., Turina, M., Niechcial, A., Lang, S., Hawinkels, L. J. A. C., Van Der Meulen-De Jong, A. E., Verspaget, H. W., Rogler, G., & Scharl, M. (2021). Contribution of CD3+CD8- and CD3+CD8+ T Cells to TNF-α Overexpression in Crohn Disease-Associated Perianal Fistulas and Induction of Epithelial-Mesenchymal Transition in HT-29 Cells. *Inflammatory Bowel Diseases*, *27*(4), 538–549. https://doi.org/10.1093/IBD/IZAA240

Brüggen, M. C., & Stingl, G. (2020). Subcutaneous white adipose tissue: The deepest layer of the cutaneous immune barrier. *Journal Der Deutschen Dermatologischen Gesellschaft = Journal of the German Society of Dermatology : JDDG*, *18*(11), 1225–1227. https://doi.org/10.1111/DDG.14335

Buchmann, K. (2014). Evolution of Innate Immunity: Clues from Invertebrates via Fish to Mammals. *Frontiers in Immunology*, *5*(SEP). https://doi.org/10.3389/FIMMU.2014.00459

Campbell, D. J., & Koch, M. A. (2011). Phenotypical and functional specialization of FOXP3+ regulatory T cells. *Nature Reviews Immunology*, *11*(2), 119–130. https://doi.org/10.1038/nri2916

Campbell, J. J., Haraldsen, G., Pan, J., Rottman, J., Qin, S., Ponath, P., Andrew, D. P., Warnke, R., Ruffing, N., Kassam, N., Wu, L., & Butcher, E. C. (1999). The chemokine receptor CCR4 in vascular recognition by cutaneous but not intestinal memory T cells. *Nature*, *400*(6746), 776–780. https://doi.org/10.1038/23495

Cao, X., Cai, S. F., Fehniger, T. A., Song, J., Collins, L. I., Piwnica-Worms, D. R., & Ley, T. J. (2007). Granzyme B and perforin are important for regulatory T cell-mediated suppression of tumor clearance. *Immunity*, *27*(4), 635–646. https://doi.org/10.1016/J.IMMUNI.2007.08.014

Carty, M., Guy, C., & Bowie, A. G. (2021). Detection of Viral Infections by Innate Immunity. *Biochemical Pharmacology*, *183*, 114316. https://doi.org/10.1016/j.bcp.2020.114316

Caruso, R., Warner, N., Inohara, N., & Núñez, G. (2014). NOD1 and NOD2: signaling, host defense, and inflammatory disease. *Immunity*, *41*(6), 898–908. https://doi.org/10.1016/J.IMMUNI.2014.12.010

Cecilia Berin, M., Dwinell, M. B., Eckmann, L., Kagnoff, M. F., Cecilia, M., & Eck-mann, L. (2001). *Production of MDC/CCL22 by human intestinal epithelial cells*. http://www.ajpgi.org

Cerovic, V., Bain, C. C., Mowat, A. M., & Milling, S. W. F. (2014). Intestinal macrophages and dendritic cells: What's the difference? *Trends in Immunology*, *35*(6), 270–277. https://doi.org/10.1016/j.it.2014.04.003

Cerovic, V., Houston, S. A., Scott, C. L., Aumeunier, A., Yrlid, U., Mowat, A. M., & Milling, S. W. F. (2013). Intestinal CD103(-) dendritic cells migrate in lymph and prime effector T cells. *Mucosal Immunology*, *6*(1), 104–113. https://doi.org/10.1038/MI.2012.53

Chassaing, B., Aitken, J. D., Malleshappa, M., & Vijay-Kumar, M. (2014). Dextran sulfate sodium (DSS)-induced colitis in mice. *Current Protocols in Immunology*, *SUPPL.104*. https://doi.org/10.1002/0471142735.IM1525S104

Chen, W. J., Jin, W., Hardegen, N., Lei, K. J., Li, L., Marinos, N., McGrady, G., & Wahl, S. M. (2003). Conversion of peripheral CD4+CD25- naive T cells to CD4+CD25+ regulatory T cells by TGF-beta induction of transcription factor Foxp3. *The Journal of Experimental Medicine*, *198*(12), 1875–1886. https://doi.org/10.1084/JEM.20030152

Chen, Z., Luo, H., Gubu, A., Yu, S., Zhang, H., Dai, H., Zhang, Y., Zhang, B., Ma, Y., Lu, A., & Zhang, G. (2023). Chemically modified aptamers for improving binding affinity to the target proteins via enhanced non-covalent bonding. *Frontiers in Cell and Developmental Biology*, *11*, 1091809. https://doi.org/10.3389/FCELL.2023.1091809/BIBTEX

Chiba, M., Nakane, K., & Komatsu, M. (2019). Westernized Diet is the Most Ubiquitous Environmental Factor in Inflammatory Bowel Disease. *The Permanente Journal*, *23*(1). https://doi.org/10.7812/TPP/18-107

Chinen, T., Kannan, A. K., Levine, A. G., Fan, X., Klein, U., Zheng, Y., Gasteiger, G., Feng, Y., Fontenot, J. D., & Rudensky, A. Y. (2016). An essential role for the IL-2 receptor in Treg cell function. *Nature Immunology 2016 17:11*, *17*(11), 1322–1333. https://doi.org/10.1038/ni.3540

Chong, B. F., Murphy, J.-E., Kupper, T. S., & Fuhlbrigge, R. C. (2004). E-selectin, thymus- and activation-regulated chemokine/CCL17, and intercellular adhesion molecule-1 are constitutively coexpressed in dermal microvessels: a foundation for a cutaneous immunosurveillance system.

Journal of Immunology (Baltimore, Md. : 1950), *172*(3), 1575–1581. https://doi.org/10.4049/JIMMUNOL.172.3.1575

Chovatiya, R., & Silverberg, J. I. (2022). The Heterogeneity of Atopic Dermatitis. *Journal of Drugs in Dermatology : JDD*, *21*(2), 172. https://doi.org/10.36849/JDD.6408

Chvatchko, Y., Hoogewerf, A. J., Meyer, A., Alouani, S., Juillard, P., Buser, R., Conquet, F., Proudfoot, A. E. I., Wells, T. N. C., & Power, C. A. (2000). A key role for CC chemokine receptor 4 in lipopolysaccharide-induced endotoxic shock. *Journal of Experimental Medicine*, *191*(10), 1755–1763. https://doi.org/10.1084/jem.191.10.1755

Clausen, B. E., & Stoitzner, P. (2015). Functional Specialization of Skin Dendritic Cell Subsets in Regulating T Cell Responses. *Frontiers in Immunology*, *6*(OCT). https://doi.org/10.3389/FIMMU.2015.00534

Colantonio, L., Iellem, A., Sinigaglia, F., & Ambrosio, D. D. *'*. (2002). *Skin-homing CLA + T cells and regulatory CD25 + T cells represent major subsets of human peripheral blood memory T cells migrating in response to CCL1/I-309*. https://doi.org/10.1002/1521-4141

Collin, M., & Milne, P. (2016). Langerhans cell origin and regulation. *Current Opinion in Hematology*, *23*(1), 28–35. https://doi.org/10.1097/MOH.0000000000000202

Coombes, J. L., Siddiqui, K. R. R., Arancibia-Cárcamo, C. V., Hall, J., Sun, C. M., Belkaid, Y., & Powrie, F. (2007). A functionally specialized population of mucosal CD103+ DCs induces Foxp3+ regulatory T cells via a TGF-beta and retinoic acid-dependent mechanism. *The Journal of Experimental Medicine*, *204*(8), 1757–1764. https://doi.org/10.1084/JEM.20070590

Cornick, S., Tawiah, A., & Chadee, K. (2015). Roles and regulation of the mucus barrier in the gut. *Tissue Barriers*, *3*(1–2). https://doi.org/10.4161/21688370.2014.982426

Corridoni, D., Antanaviciute, A., Gupta, T., Fawkner-Corbett, D., Aulicino, A., Jagielowicz, M., Parikh, K., Repapi, E., Taylor, S., Ishikawa, D., Hatano, R., Yamada, T., Xin, W., Slawinski, H., Bowden, R., Napolitani, G., Brain, O., Morimoto, C., Koohy, H., & Simmons, A. (2020). Single-cell atlas of colonic CD8+ T cells in ulcerative colitis. *Nature Medicine*, *26*(9), 1480–1490. https://doi.org/10.1038/S41591-020-1003-4

Cowan, J. E., McCarthy, N. I., Parnell, S. M., White, A. J., Bacon, A., Serge, A., Irla, M., Lane, P. J. L., Jenkinson, E. J., Jenkinson, W. E., & Anderson, G. (2014). Differential requirement for CCR4 and CCR7 during the development of innate and adaptive αβT cells in the adult thymus. *Journal of Immunology (Baltimore, Md. : 1950)*, *193*(3), 1204–1212. https://doi.org/10.4049/JIMMUNOL.1400993

Cox, J. C., & Ellington, A. D. (2001). Automated selection of anti-Protein aptamers. *Bioorganic & Medicinal Chemistry*, *9*(10), 2525–2531. https://doi.org/10.1016/S0968-0896(01)00028-1

Cronshaw, D. G., Kouroumalis, A., Parry, R., Webb, A., Brown, Z., & Ward, S. G. (2006). Evidence that phospholipase C-dependent, calcium-independent mechanisms are required for directional migration of T lymphocytes in response to the CCR4 ligands CCL17 and CCL22. *Journal of Leukocyte Biology*, *79*(6), 1369–1380. https://doi.org/10.1189/JLB.0106035

Danese, S., Rudziński, J., Brandt, W., Dupas, J. L., Peyrin-Biroulet, L., Bouhnik, Y., Kleczkowski, D., Uebel, P., Lukas, M., Knutsson, M., Erlandsson, F., Hansen, M. B., & Keshav, S. (2015). Tralokinumab for moderate-to-severe UC: a randomised, double-blind, placebo-controlled, phase IIa study. *Gut*, *64*(2), 243–249. https://doi.org/10.1136/GUTJNL-2014-308004

Davis, T. H., Morton, C. C., Miller-Cassman, R., Balk, S. P., & Kadin, M. E. (2010). Hodgkin's Disease, Lymphomatoid Papulosis, and Cutaneous T-Cell Lymphoma Derived from a Common T-Cell Clone. *Http://Dx.Doi.Org/10.1056/NEJM199204233261704*, *326*(17), 1115–1122. https://doi.org/10.1056/NEJM199204233261704

Dempsey, A., & Bowie, A. G. (2015). Innate Immune Recognition of DNA: a recent history. *Virology*, *0*, 146. https://doi.org/10.1016/J.VIROL.2015.03.013

D'Haens, G., Panaccione, R., Baert, F., Bossuyt, P., Colombel, J. F., Danese, S., Dubinsky, M., Feagan, B. G., Hisamatsu, T., Lim, A., Lindsay, J. O., Loftus, E. V., Panés, J., Peyrin-Biroulet, L., Ran, Z., Rubin, D. T., Sandborn, W. J., Schreiber, S., Neimark, E., … Ferrante, M. (2022). Risankizumab as induction therapy for Crohn's disease: results from the phase 3 ADVANCE and MOTIVATE induction trials. *Lancet (London, England)*, *399*(10340), 2015–2030. https://doi.org/10.1016/S0140-6736(22)00467-6

Didovic, S., Opitz, F. V., Holzmann, B., Förster, I., & Weighardt, H. (2016). Requirement of MyD88 signaling in keratinocytes for Langerhans cell migration and initiation of atopic dermatitis-like symptoms in mice. *European Journal of Immunology*, *46*(4), 981–992. https://doi.org/10.1002/eji.201545710

Dieli, F., Ptak, W., Sireci, G., Romano, G. C., Potestio, M., Salerno, A., & Asherson, G. L. (1998). Cross-talk between Vβ8+ and γδ+ T lymphocytes in contact sensitivity. *Immunology*, *93*(4), 469–477. https://doi.org/10.1046/J.1365-2567.1998.00435.X

Diepgen, T. L., Ofenloch, R. F., Bruze, M., Bertuccio, P., Cazzaniga, S., Coenraads, P. J., Elsner, P., Goncalo, M., Svensson, & Naldi, L. (2016). Prevalence of contact allergy in the general population in different European regions. *British Journal of Dermatology*, *174*(2), 319–329. https://doi.org/10.1111/BJD.14167

Dijkgraaf, F. E., Matos, T. R., Hoogenboezem, M., Toebes, M., Vredevoogd, D. W., Mertz, M., van den Broek, B., Song, J. Y., Teunissen, M. B. M., Luiten, R. M., Beltman, J. B., & Schumacher, T. N. (2019). Tissue patrol by resident memory CD8+ T cells in human skin. *Nature Immunology*, *20*(6), 756–764. https://doi.org/10.1038/s41590-019-0404-3

Dijkgraaf, F. E., Toebes, M., Hoogenboezem, M., Mertz, M., Vredevoogd, D. W., Matos, T. R., Teunissen, M. B. M., Luiten, R. M., & Schumacher, T. N. (2021). Labeling and tracking of immune cells in ex vivo human skin. *Nature Protocols*, *16*(2), 791–811. https://doi.org/10.1038/S41596-020-00435-8

Dunay, I. R., & Sibley, L. D. (2010). Monocytes mediate mucosal immunity to Toxoplasma gondii. *Current Opinion in Immunology*, *22*(4), 461–466. https://doi.org/10.1016/J.COI.2010.04.008

Duvic, M., Pinter-Brown, L. C., Foss, F. M., Sokol, L., Jorgensen, J. L., Challagundla, P., Dwyer, K. M., Zhang, X., Kurman, M. R., Ballerini, R., Liu, L., & Kim, Y. H. (2015). Phase 1/2 study of mogamulizumab, a defucosylated anti-CCR4 antibody, in previously treated patients with cutaneous T-cell lymphoma. *Blood*, *125*(12), 1883–1889. https://doi.org/10.1182/BLOOD-2014-09-600924

Dyring-Andersen, B., Skov, L., Løvendorf, M. B., Bzorek, M., Søndergaard, K., Lauritsen, J. P. H., Dabelsteen, S., Geisler, C., & Menné Bonefeld, C. (2013). CD4(+) T cells producing interleukin (IL)-17, IL-22 and interferon-γ are major effector T cells in nickel allergy. *Contact Dermatitis*, *68*(6), 339–347. https://doi.org/10.1111/COD.12043

Ebner, S., Nguyen, V. A., Forstner, M., Wang, Y. H., Wolfram, D., Liu, Y. J., & Romani, N. (2007). Thymic stromal lymphopoietin converts human epidermal Langerhans cells into antigen-presenting cells that induce proallergic T cells. *The Journal of Allergy and Clinical Immunology*, *119*(4), 982–990. https://doi.org/10.1016/J.JACI.2007.01.003

Eby, J. M., Kang, H. K., Tully, S. T., Bindeman, W. E., Peiffer, D. S., Chatterjee, S., Mehrotra, S., & Caroline Le Poole, I. (2015). CCL22 to activate treg migration and suppress depigmentation in vitiligo. *Journal of Investigative Dermatology*, *135*(6). https://doi.org/10.1038/jid.2015.26

Egawa, G., & Kabashima, K. (2017). Visualization of the T cell response in contact hypersensitivity. In *Methods in Molecular Biology* (Vol. 1559, pp. 53–62). Humana Press Inc. https://doi.org/10.1007/978-1-4939-6786-5_4

Eiger, D. S., Boldizsar, N., Honeycutt, C. C., Gardner, J., & Rajagopal, S. (2021). Biased Agonism at Chemokine Receptors. *Cellular Signalling*, *78*, 109862. https://doi.org/10.1016/J.CELLSIG.2020.109862

Elson, C. O., Cong, Y., Weaver, C. T., Schoeb, T. R., McClanahan, T. K., Fick, R. B., & Kastelein, R. A. (2007). Monoclonal anti-interleukin 23 reverses active colitis in a T cell-mediated model in mice. *Gastroenterology*, *132*(7), 2359–2370. https://doi.org/10.1053/J.GASTRO.2007.03.104

Erazo, A. B., Wang, N., Standke, L., Semeniuk, A. D., Fülle, L., Cengiz, S. C., Thiem, M., Weighardt, H., Strugnell, R. A., & Förster, I. (2021). CCL17-expressing dendritic cells in the intestine are preferentially infected by Salmonella but CCL17 plays a redundant role in systemic dissemination. *Immunity, Inflammation and Disease*, *9*(3), 891. https://doi.org/10.1002/IID3.445

Esser, P. R., Wölfle, U., Dürr, C., von Loewenich, F. D., Schempp, C. M., Freudenberg, M. A., Jakob, T., & Martin, S. F. (2012). Contact sensitizers induce skin inflammation via ROS production and hyaluronic acid degradation. *PloS One*, *7*(7). https://doi.org/10.1371/JOURNAL.PONE.0041340

Esterházy, D., Loschko, J., London, M., Jove, V., Oliveira, T. Y., & Mucida, D. (2016). Classical dendritic cells are required for dietary antigen-mediated peripheral regulatory T cell and tolerance induction. *Nature Immunology*, *17*(5), 545. https://doi.org/10.1038/NI.3408

Eulberg, D., Buchner, K., Maasch, C., & Klussmann, S. (2005). Development of an automated in vitro selection protocol to obtain RNA-based aptamers: identification of a biostable substance P antagonist. *Nucleic Acids Research*, *33*(4), e45–e45. https://doi.org/10.1093/NAR/GNI044

Facheris, P., Jeffery, J., Del Duca, E., & Guttman-Yassky, E. (2023). The translational revolution in atopic dermatitis: the paradigm shift from pathogenesis to treatment. *Cellular & Molecular Immunology 2023 20:5*, *20*(5), 448–474. https://doi.org/10.1038/s41423-023-00992-4

Faget, J., Biota, C., Bachelot, T., Gobert, M., Treilleux, I., Goutagny, N., Durand, I., León-Goddard, S., Blay, J. Y., Caux, C., & Meńeťrier-Caux, C. (2011). Early detection of tumor cells by innate immune cells leads to T reg recruitment through CCL22 production by tumor cells. *Cancer Research*, *71*(19), 6143–6152. https://doi.org/10.1158/0008-5472.CAN-11-0573

Famulok, M., & Mayer, G. (1999). Aptamers as tools in molecular biology and immunology. *Current Topics in Microbiology and Immunology*, *243*, 123–136. https://doi.org/10.1007/978-3-642-60142-2_7

Ferrer, I. R., West, H. C., Henderson, S., Ushakov, D. S., Sousa, P. S. E., Strid, J., Chakraverty, R., Yates, A. J., & Bennett, C. L. (2019). A wave of monocytes is recruited to replenish the long-term

Langerhans cell network after immune injury. *Science Immunology*, *4*(38). https://doi.org/10.1126/SCIIMMUNOL.AAX8704

Foerster, E. G., Mukherjee, T., Cabral-Fernandes, L., Rocha, J. D. B., Girardin, S. E., & Philpott, D. J. (2022). How autophagy controls the intestinal epithelial barrier. *Autophagy*, *18*(1), 86–103. https://doi.org/10.1080/15548627.2021.1909406

Følsgaard, N. V., Chawes, B. L. K., Bønnelykke, K., Jenmalm, M. C., & Bisgaard, H. (2012). Cord blood Th2-related chemokine CCL22 levels associate with elevated total-IgE during preschool age. *Clinical & Experimental Allergy*, *42*(11), 1596–1603. https://doi.org/10.1111/J.1365-2222.2012.04048.X

Francescone, R., Hou, V., & Grivennikov, S. I. (2015). *Cytokines, IBD, and Colitis-associated Cancer*. https://doi.org/10.1097/MIB.0000000000000236

Franke, A., Balschun, T., Karlsen, T. H., Sventoraityte, J., Nikolaus, S., Mayr, G., Domingues, F. S., Albrecht, M., Nothnagel, M., Ellinghaus, D., Sina, C., Onnie, C. M., Weersma, R. K., Stokkers, P. C. F., Wijmenga, C., Gazouli, M., Strachan, D., McArdle, W. L., Vermeire, S., … Schreiber, S. (2008). Sequence variants in IL10, ARPC2 and multiple other loci contribute to ulcerative colitis susceptibility. *Nature Genetics*, *40*(11), 1319–1323. https://doi.org/10.1038/NG.221

Fülle, L., Offermann, N., Hansen, J. N., Breithausen, B., Erazo, A. B., Schanz, O., Radau, L., Gondorf, F., Knöpper, K., Alferink, J., Abdullah, Z., Neumann, H., Weighardt, H., Henneberger, C., Halle, A., & Förster, I. (2018). CCL17 exerts a neuroimmune modulatory function and is expressed in hippocampal neurons. *GLIA*, *66*(10), 2246–2261. https://doi.org/10.1002/glia.23507

Fülle, L., Steiner, N., Funke, M., Gondorf, F., Pfeiffer, F., Siegl, J., Opitz, F. V, Haßel, S. K., Erazo, A. B., Schanz, O., Stunden, H. J., Blank, M., Gröber, C., Händler, K., Beyer, M., Weighardt, H., Latz, E., Schultze, J. L., Mayer, G., & Förster, I. (2018). RNA Aptamers Recognizing Murine CCL17 Inhibit T Cell Chemotaxis and Reduce Contact Hypersensitivity In Vivo. *Molecular Therapy : The Journal of the American Society of Gene Therapy*, *26*(1), 95–104. https://doi.org/10.1016/j.ymthe.2017.10.005

Funch, A. B., Mraz, V., Gadsbøll, A. S. Ø., Jee, M. H., Weber, J. F., Ødum, N., Woetmann, A., Johansen, J. D., Geisler, C., & Bonefeld, C. M. (2022). CD8+ tissue-resident memory T cells recruit neutrophils that are essential for flare-ups in contact dermatitis. *Allergy: European Journal of Allergy and Clinical Immunology*, *77*(2), 513–524. https://doi.org/10.1111/ALL.14986

Gadsbøll, A. S. Ø., Jee, M. H., Ahlström, M. G., Dyring-Andersen, B., Woetmann, A., Ødum, N., Johansen, J. D., Geisler, C., & Bonefeld, C. M. (2021). Epidermal T cell subsets-Effect of age and antigen exposure in humans and mice. *Contact Dermatitis*, *84*(6), 375–384. https://doi.org/10.1111/COD.13806

Gadsbøll, A. S. Ø., Jee, M. H., Funch, A. B., Alhede, M., Mraz, V., Weber, J. F., Callender, L. A., Carroll, E. C., Bjarnsholt, T., Woetmann, A., Ødum, N., Thomsen, A. R., Johansen, J. D., Henson, S. M., Geisler, C., & Bonefeld, C. M. (2020). Pathogenic CD8+ Epidermis-Resident Memory T Cells Displace Dendritic Epidermal T Cells in Allergic Dermatitis. *The Journal of Investigative Dermatology*, *140*(4), 806-815.e5. https://doi.org/10.1016/J.JID.2019.07.722

Gaffal, E., Cron, M., Glodde, N., Bald, T., Kuner, R., Zimmer, A., Lutz, B., & Tüting, T. (2013). Cannabinoid 1 Receptors in Keratinocytes Modulate Proinflammatory Chemokine Secretion and Attenuate Contact Allergic Inflammation. *The Journal of Immunology*, *190*(10), 4929–4936. https://doi.org/10.4049/JIMMUNOL.1201777

Gaide, O., Emerson, R. O., Jiang, X., Gulati, N., Nizza, S., Desmarais, C., Robins, H., Krueger, J. G., Clark, R. A., & Kupper, T. S. (2015). Common clonal origin of central and resident memory T cells following skin immunization. *Nature Medicine 2015 21:6*, *21*(6), 647–653. https://doi.org/10.1038/nm.3860

Gamradt, P., Laoubi, L., Nosbaum, A., Mutez, V., Lenief, V., Grande, S., Redoulès, D., Schmitt, A. M., Nicolas, J. F., & Vocanson, M. (2019). Inhibitory checkpoint receptors control CD8+ resident memory T cells to prevent skin allergy. *Journal of Allergy and Clinical Immunology*, *143*(6), 2147-2157.e9. https://doi.org/10.1016/j.jaci.2018.11.048

Gao, S., Zheng, X., Jiao, B., & Wang, L. (2016). Post-SELEX optimization of aptamers. *Analytical and Bioanalytical Chemistry*, *408*(17), 4567–4573. https://doi.org/10.1007/S00216-016-9556-2/TABLES/1

Gao, Y., Nish, S. A., Jiang, R., Hou, L., Licona-Limón, P., Weinstein, J. S., Zhao, H., & Medzhitov, R. (2013). Control of T Helper 2 Responses by Transcription Factor IRF4-Dependent Dendritic Cells. *Immunity*, *39*(4), 722–732. https://doi.org/10.1016/J.IMMUNI.2013.08.028

Genaro, L. M., Gomes, L. E. M., Franceschini, A. P. M. de F., Ceccato, H. D., Jesus, R. N. de, Lima, A. P., Nagasako, C. K., Fagundes, J. J., Ayrizono, M. de L. S., & Leal, R. F. (2021). Anti-TNF therapy and immunogenicity in inflammatory bowel diseases: a translational approach. *American Journal of Translational Research*, *13*(12), 13916. /pmc/articles/PMC8748125/

Girardi, M., Lewis, J., Glusac, E., Filler, R. B., Geng, L., Hayday, A. C., & Tigelaar, R. E. (2002). Resident Skin-specific γδ T Cells Provide Local, Nonredundant Regulation of Cutaneous Inflammation. *Journal of Experimental Medicine*, *195*(7), 855–867. https://doi.org/10.1084/JEM.20012000

Giuffrida, P., & Di Sabatino, A. (2020). Targeting T cells in inflammatory bowel disease. *Pharmacological Research*, *159*. https://doi.org/10.1016/J.PHRS.2020.105040

Gloor, M., Hauth, A., & Gehring, W. (2003). *O/W Emulsions compromise the stratum corneum barrier and improvedrug penetration*. 709–715.

Gonsky, R., Deem, R. L., Landers, C. J., Haritunians, T., Yang, S., & Targan, S. R. (2014). IFNG rs1861494 polymorphism is associated with IBD disease severity and functional changes in both IFNG methylation and protein secretion. *Inflammatory Bowel Diseases*, *20*(10), 1794–1801. https://doi.org/10.1097/MIB.0000000000000172

Göringer, H. U., Homann, M., & Lorger, M. (2003). In vitro selection of high-affinity nucleic acid ligands to parasite target molecules. *International Journal for Parasitology*, *33*(12), 1309–1317. https://doi.org/10.1016/S0020-7519(03)00197-8

Gui, Y., Cheng, H., Zhou, J., Xu, H., Han, J., & Zhang, D. (2022). Development and function of natural TCR+ CD8αα+ intraepithelial lymphocytes. *Frontiers in Immunology*, *13*. https://doi.org/10.3389/FIMMU.2022.1059042

Günaltay, S., Kumawat, A. K., Nyhlin, N., Bohr, J., Tysk, C., Hultgren, O., & Hörnquist, E. H. (2015). *Enhanced Levels of Chemokines and Their Receptors in the Colon of Microscopic Colitis Patients Indicate Mixed Immune Cell Recruitment*. https://doi.org/10.1155/2015/132458

Guttman-Yassky, E., Suárez-Fariñas, M., Chiricozzi, A., Nograles, K. E., Shemer, A., Fuentes-Duculan, J., Cardinale, I., Lin, P., Bergman, R., Bowcock, A. M., & Krueger, J. G. (2009). Broad defects in

epidermal cornification in atopic dermatitis identified through genomic analysis. *The Journal of Allergy and Clinical Immunology*, *124*(6). https://doi.org/10.1016/J.JACI.2009.09.031

Hall, L. J., Faivre, E., Quinlan, A., Shanahan, F., Nally, K., & Melgar, S. (2011). Induction and Activation of Adaptive Immune Populations During Acute and Chronic Phases of a Murine Model of Experimental Colitis. *Digestive Diseases and Sciences*, *56*(1), 79–89. https://doi.org/10.1007/s10620-010-1240-3

Halling, A. S., Rinnov, M. R., Ruge, I. F., Gerner, T., Ravn, N. H., Knudgaard, M. H., Trautner, S., Loft, N., Skov, L., Thomsen, S. F., Egeberg, A., Guttman-Yassky, E., Rosted, A. L. L., Petersen, T., Jakasa, I., Kezic, S., & Thyssen, J. P. (2023). Skin TARC/CCL17 increase precedes the development of childhood atopic dermatitis. *Journal of Allergy and Clinical Immunology*, *151*(6), 1550-1557.e6. https://doi.org/10.1016/j.jaci.2022.11.023

Hanauer, S. B., Sandborn, W. J., Rutgeerts, P., Fedorak, R. N., Lukas, M., Macintosh, D., Panaccione, R., Wolf, D., & Pollack, P. (2006). Human anti-tumor necrosis factor monoclonal antibody (adalimumab) in Crohn's disease: the CLASSIC-I trial. *Gastroenterology*, *130*(2), 323–333. https://doi.org/10.1053/J.GASTRO.2005.11.030

Hansell, C. A. H., Hurson, C. E., & Nibbs, R. J. B. (2011). DARC and D6: silent partners in chemokine regulation? *Immunology and Cell Biology*, *89*(2), 197. https://doi.org/10.1038/ICB.2010.147

Hao, S., Han, X., Wang, D., Yang, Y., Li, Q., Li, X., & Qiu, C. (2016). Critical role of CCL22/CCR4 axis in the maintenance of immune homeostasis during apoptotic cell clearance by splenic CD8α(+) CD103(+) dendritic cells. *Immunology*, *148*(2), 174–186. https://doi.org/10.1111/IMM.12596

Haßel, S. K., & Mayer, G. (2019). Aptamers as Therapeutic Agents: Has the Initial Euphoria Subsided? *Molecular Diagnosis and Therapy*, *23*(3), 301–309. https://doi.org/10.1007/s40291-019-00400-6

Hayes, C. L., Dong, J., Galipeau, H. J., Jury, J., McCarville, J., Huang, X., Wang, X. Y., Naidoo, A., Anbazhagan, A. N., Libertucci, J., Sheridan, C., Dudeja, P. K., Bowdish, D. M. E., Surette, M. G., & Verdu, E. F. (2018). Commensal microbiota induces colonic barrier structure and functions that contribute to homeostasis. *Scientific Reports 2018 8:1*, *8*(1), 1–14. https://doi.org/10.1038/s41598-018-32366-6

Healy, J. M., Lewis, S. D., Kurz, M., Boomer, R. M., Thompson, K. M., Wilson, C., & McCauley, T. G. (2004). Pharmacokinetics and biodistribution of novel aptamer compositions. *Pharmaceutical Research*, *21*(12), 2234–2246. https://doi.org/10.1007/S11095-004-7676-4

Heiseke, A. F., Faul, A. C., Lehr, H., Förster, I., Schmid, R. M., Krug, A. B., & Reindl, W. (2012). CCL17 Promotes Intestinal Inflammation in Mice and Counteracts Regulatory T Cell–Mediated Protection From Colitis. *Gastroenterology*, *142*(2), 335–345. https://doi.org/10.1053/J.GASTRO.2011.10.027

Henri, S., Poulin, L. F., Tamoutounour, S., Ardouin, L., Guilliams, M., De Bovis, B., Devilard, E., Viret, C., Azukizawa, H., Kissenpfennig, A., & Malissen, B. (2010). CD207+ CD103+ dermal dendritic cells cross-present keratinocyte-derived antigens irrespective of the presence of Langerhans cells. *The Journal of Experimental Medicine*, *207*(1), 189. https://doi.org/10.1084/JEM.20091964

Hirono, I., Kuhara, K., Yamaji, T., Hosaka, S., & Golberg, L. (1983). Carcinogenicity of dextran sulfate sodium in relation to its molecular weight. *Cancer Letters*, *18*(1), 29–34. https://doi.org/10.1016/0304-3835(83)90114-3

Ho, A. W., & Kupper, T. S. (2019). T cells and the skin: from protective immunity to inflammatory skin disorders. *Nature Reviews Immunology 2019 19:8*, *19*(8), 490–502. https://doi.org/10.1038/s41577-019-0162-3

Hoeffel, G., Chen, J., Lavin, Y., Low, D., Almeida, F. F., See, P., Beaudin, A. E., Lum, J., Low, I., Forsberg, E. C., Poidinger, M., Zolezzi, F., Larbi, A., Ng, L. G., Chan, J. K. Y., Greter, M., Becher, B., Samokhvalov, I. M., Merad, M., & Ginhoux, F. (2015). C-Myb(+) erythro-myeloid progenitor-derived fetal monocytes give rise to adult tissue-resident macrophages. *Immunity*, *42*(4), 665–678. https://doi.org/10.1016/J.IMMUNI.2015.03.011

Holtmeier, W., & Kabelitz, D. (2005). gammadelta T cells link innate and adaptive immune responses. *Chemical Immunology and Allergy*, *86*, 151–183. https://doi.org/10.1159/000086659

Hori, S., Nomura, T., & Sakaguchi, S. (2017). Control of regulatory T cell development by the transcription factor Foxp3. *Journal of Immunology*, *198*(3), 981–985. https://doi.org/10.1126/SCIENCE.1079490/SUPPL_FILE/HORI.SOM.PDF

Horikawa, T., Nakayama, T., Hikita, I., Yamada, H., Fujisawa, R., Bito, T., Harada, S., Fukunaga, A., Chantry, D., Gray, P. W., Morita, A., Suzuki, R., Tezuka, T., Ichihashi, M., & Yoshie, O. (2002). IFN-γ-inducible expression of thymus and activation-regulated chemokine/CCL17 and macrophage-derived chemokine/CCL22 in epidermal keratinocytes and their roles in atopic dermatitis. *International Immunology*, *14*(7), 767–773. https://doi.org/10.1093/INTIMM/DXF044

Hu, Z., Lancaster, J. N., Sasiponganan, C., & Ehrlich, L. I. R. (2015). CCR4 promotes medullary entry and thymocyte–dendritic cell interactions required for central tolerance. *The Journal of Experimental Medicine*, *212*(11). https://doi.org/10.1084/jem.20150178

Huang, C. H., Kuo, I. C., Xu, H., Lee, Y. S., & Chua, K. Y. (2003). Mite allergen induces allergic dermatitis with concomitant neurogenic inflammation in mouse. *Journal of Investigative Dermatology*, *121*(2), 289–293. https://doi.org/10.1046/j.1523-1747.2003.12356.x

Hudcovic, T., Štěpánková, R., Cebra, J., & Tlaskalová-Hogenová, H. (2001). The role of microflora in the development of intestinal inflammation: acute and chronic colitis induced by dextran sulfate in germ-free and conventionally reared immunocompetent and immunodeficient mice. *Folia Microbiologica*, *46*(6), 565–572. https://doi.org/10.1007/BF02818004

Hueber, W., Sands, B. E., Lewitzky, S., Vandemeulebroecke, M., Reinisch, W., Higgins, P. D. R., Wehkamp, J., Feagan, B. G., Yao, M. D., Karczewski, M., Karczewski, J., Pezous, N., Bek, S., Bruin, G., Mellgard, B., Berger, C., Londei, M., Bertolino, A. P., Tougas, G., & Travis, S. P. L. (2012). Secukinumab, a human anti-IL-17A monoclonal antibody, for moderate to severe Crohn's disease: unexpected results of a randomised, double-blind placebo-controlled trial. *Gut*, *61*(12), 1693–1700. https://doi.org/10.1136/GUTJNL-2011-301668

Imai, T., Nagira, M., Takagi, S., Kakizaki, M., Nishimura, M., Wang, J., Gray, P. W., Matsushima, K., & Yoshie, O. (1999). Selective recruitment of CCR4-bearing Th2 cells toward antigen-presenting cells by the CC chemokines thymus and activation-regulated chemokine and macrophage-derived chemokine. *International Immunology*, *11*(1), 81–88. https://doi.org/10.1093/INTIMM/11.1.81

Imam, T., Park, S., Kaplan, M. H., & Olson, M. R. (2018). Effector T helper cell subsets in inflammatory bowel diseases. *Frontiers in Immunology*, *9*(JUN), 369469. https://doi.org/10.3389/FIMMU.2018.01212/BIBTEX

Indra, A. K. (2013). Epidermal TSLP: A trigger factor for pathogenesis of Atopic Dermatitis (AD). *Expert Review of Proteomics*, *10*(4), 309. https://doi.org/10.1586/14789450.2013.814881

Irvine, A. D., McLean, W. H. I., & Leung, D. Y. M. (2011). Filaggrin mutations associated with skin and allergic diseases. *The New England Journal of Medicine*, *365*(14), 1315–1327. https://doi.org/10.1056/NEJMRA1011040

Iwata, M., Hirakiyama, A., Eshima, Y., Kagechika, H., Kato, C., & Song, S. Y. (2004). Retinoic acid imprints gut-homing specificity on T cells. *Immunity*, *21*(4), 527–538. https://doi.org/10.1016/j.immuni.2004.08.011

Jahnz-Rozyk, K., Targowski, T., Paluchowska, E., Owczarek, W., & Kucharczyk, A. (2005). Serum thymus and activation-regulated chemokine, macrophage-derived chemokine and eotaxin as markers of severity of atopic dermatitis. *Allergy: European Journal of Allergy and Clinical Immunology*, *60*(5), 685–688. https://doi.org/10.1111/J.1398-9995.2005.00774.X

Jeong, W. Y., Kwon, M., Choi, H. E., & Kim, K. S. (2021). Recent advances in transdermal drug delivery systems: a review. *Biomaterials Research*, *25*(1), 1–15. https://doi.org/10.1186/S40824-021-00226-6/FIGURES/6

Jiang, X., Campbell, J. J., & Kupper, T. S. (2010). Embryonic trafficking of gammadelta T cells to skin is dependent on E/P selectin ligands and CCR4. *Proceedings of the National Academy of Sciences of the United States of America*, *107*(16), 7443–7448. https://doi.org/10.1073/PNAS.0912943107

Jiang, X., Park, C. O., Sweeney, J. G., Yoo, M. J., Gaide, O., & Kupper, T. S. (2017). Dermal γδ T Cells Do Not Freely Re-Circulate Out of Skin and Produce IL-17 to Promote Neutrophil Infiltration during Primary Contact Hypersensitivity. *PloS One*, *12*(1). https://doi.org/10.1371/JOURNAL.PONE.0169397

Jin, H., He, R., Oyoshi, M., & Geha, R. S. (2009). Animal models of atopic dermatitis. *The Journal of Investigative Dermatology*, *129*(1), 31–40. https://doi.org/10.1038/jid.2008.106

Jinquan, T., & Thestrup-Pedersen, K. (1995). T lymphocyte chemotaxis and skin diseases. In *Experimental Dermatology* (Vol. 4, Issue 5, pp. 281–290). Exp Dermatol. https://doi.org/10.1111/j.1600-0625.1995.tb00206.x

Jo, Y., Matsumoto, T., Yada, S., Fujisawa, K., Esaki, M., Onai, N., Matsushima, K., & Iida, M. (2003). CCR4 is an up-regulated chemokine receptor of peripheral blood memory CD4+ T cells in Crohn's disease. *Clinical and Experimental Immunology*, *132*(2), 332. https://doi.org/10.1046/J.1365-2249.2003.02155.X

Joeris, T., Müller-Luda, K., Agace, W. W., & Mowat, A. M. I. (2017). Diversity and functions of intestinal mononuclear phagocytes. *Mucosal Immunology 2017 10:4*, *10*(4), 845–864. https://doi.org/10.1038/mi.2017.22

Johansson-Lindbom, B., Svensson, M., Pabst, O., Palmqvist, C., Marquez, G., Förster, R., & Agace, W. W. (2005). Functional specialization of gut CD103+ dendritic cells in the regulation of tissue-selective T cell homing. *Journal of Experimental Medicine*, *202*(8), 1063–1073. https://doi.org/10.1084/JEM.20051100

Jugde, F., Alizadeh, M., Boissier, C., Chantry, D., Siproudhis, L., Corbinais, S., Quelvennec, E., Dyard, F., Campion, J. P., Gosselin, M., Bretagne, J. F., Sémana, G., & Heresbach, D. (2001). Quantitation of

chemokines (MDC, TARC) expression in mucosa from crohn's disease and ulcerative colitis. *European Cytokine Network*, *12*(3), 468–477. https://pubmed.ncbi.nlm.nih.gov/11566628/

Kakinuma, T., Nakamura, K., Wakugawa, M., Mitsui, H., Tada, Y., Saeki, H., Torii, H., Asahina, A., Onai, N., Matsushima, K., & Tamaki, K. (2001). Thymus and activation-regulated chemokine in atopic dermatitis: Serum thymus and activation-regulated chemokine level is closely related with disease activity. *The Journal of Allergy and Clinical Immunology*, *107*(3), 535–541. https://doi.org/10.1067/MAI.2001.113237

Kakinuma, T., Nakamura, K., Wakugawa, M., Mitsui, H., Tada, Y., Saeki, H., Torii, H., Komine, M., Asahina, A., & Tamaki, K. (2002). Serum macrophage-derived chemokine (MDC) levels are closely related with the disease activity of atopic dermatitis. *Clinical and Experimental Immunology*, *127*(2), 270–273. https://doi.org/10.1046/J.1365-2249.2002.01727.X

Kamada, N., Hisamatsu, T., Okamoto, S., Chinen, H., Kobayashi, T., Sato, T., Sakuraba, A., Kitazume, M. T., Sugita, A., Koganei, K., Akagawa, K. S., & Hibi, T. (2008). Unique CD14+ intestinal macrophages contribute to the pathogenesis of Crohn disease via IL-23/IFN-γ axis. *The Journal of Clinical Investigation*, *118*(6), 2269. https://doi.org/10.1172/JCI34610

Kanaya, T., Williams, I. R., & Ohno, H. (2020). Intestinal M cells: Tireless samplers of enteric microbiota. *Traffic*, *21*(1), 34–44. https://doi.org/10.1111/TRA.12707/

Kaplan, D. H., Igyártó, B. Z., & Gaspari, A. A. (2012). Early immune events in the induction of allergic contact dermatitis. *Nature Reviews Immunology 2012 12:2*, *12*(2), 114–124. https://doi.org/10.1038/nri3150

Karlsson, M., Zhang, C., Méar, L., Zhong, W., Digre, A., Katona, B., Sjöstedt, E., Butler, L., Odeberg, J., Dusart, P., Edfors, F., Oksvold, P., von Feilitzen, K., Zwahlen, M., Arif, M., Altay, O., Li, X., Ozcan, M., Mardonoglu, A., … Lindskog, C. (2021). A single–cell type transcriptomics map of human tissues. *Science Advances*, *7*(31). https://doi.org/10.1126/SCIADV.ABH2169/SUPPL_FILE/SCIADV.ABH2169_SM.PDF

Kashem, S. W., Haniffa, M., & Kaplan, D. H. (2017). Antigen-Presenting Cells in the Skin. *Annual Review of Immunology*, *35*, 469–499. https://doi.org/10.1146/ANNUREV-IMMUNOL-051116-052215

Katou, F., Ohtani, H., Nakayama, T., Ono, K., Matsushima, K., Saaristo, A., Nagura, H., Yoshie, O., & Motegi, K. (2001). Macrophage-derived chemokine (MDC/CCL22) and CCR4 are involved in the formation of T lymphocyte-dendritic cell clusters in human inflamed skin and secondary lymphoid tissue. *The American Journal of Pathology*, *158*(4), 1263–1270. https://doi.org/10.1016/S0002-9440(10)64077-1

Kaur, H., Bruno, J. G., Kumar, A., & Sharma, T. K. (2018). Aptamers in the therapeutics and diagnostics pipelines. In *Theranostics* (Vol. 8, Issue 15, pp. 4016–4032). Ivyspring International Publisher. https://doi.org/10.7150/thno.25958

Kawada, M., Arihiro, A., & Mizoguchi, E. (2007). Insights from advances in research of chemically induced experimental models of human inflammatory bowel disease. *World Journal of Gastroenterology : WJG*, *13*(42), 5581. https://doi.org/10.3748/WJG.V13.I42.5581

Kelada, S. N. P., Wilson, M. S., Tavarez, U., Kubalanza, K., Borate, B., Whitehead, G. S., Maruoka, S., Roy, M. G., Olive, M., Carpenter, D. E., Brass, D. M., Wynn, T. A., Cook, D. N., Evans, C. M., Schwartz, D. A., & Collins, F. S. (2011). Strain-dependent genomic factors affect allergen-induced

airway hyperresponsiveness in mice. *American Journal of Respiratory Cell and Molecular Biology*, *45*(4), 817–824. https://doi.org/10.1165/RCMB.2010-0315OC

Kiesler, P., Fuss, I. J., & Strober, W. (2015). Experimental Models of Inflammatory Bowel Diseases. *Cellular and Molecular Gastroenterology and Hepatology*, *1*(2), 154–170. https://doi.org/10.1016/J.JCMGH.2015.01.006

Kim, D., Kobayashi, T., & Nagao, K. (2019). Research Techniques Made Simple: Mouse models of atopic dermatitis. *The Journal of Investigative Dermatology*, *139*(5), 984. https://doi.org/10.1016/J.JID.2019.02.014

Kim, J., Kim, B. E., & Leung, D. Y. M. (2019). Pathophysiology of atopic dermatitis: Clinical implications. *Allergy and Asthma Proceedings*, *40*(2), 84–92. https://doi.org/10.2500/AAP.2019.40.4202

Kimball, E. S., Palmer, J. M., D'Andrea, M. R., Hornby, P. J., & Wade, P. R. (2005). Acute colitis induction by oil of mustard results in later development of an IBS-like accelerated upper GI transit in mice. *American Journal of Physiology - Gastrointestinal and Liver Physiology*, *288*(6 51-6), 1266–1273. https://doi.org/10.1152/AJPGI.00444.2004/ASSET/IMAGES/LARGE/ZH30060521130007.JPEG

Kitajima, S., Takuma, S., & Morimoto, M. (2000). Histological analysis of murine colitis induced by dextran sulfate sodium of different molecular weights. *Experimental Animals*, *49*(1), 9–15. https://doi.org/10.1538/EXPANIM.49.9

Koch, S., Kohl, K., Klein, E., Von Bubnoff, D., & Bieber, T. (2006). Skin homing of Langerhans cell precursors: adhesion, chemotaxis, and migration. *The Journal of Allergy and Clinical Immunology*, *117*(1), 163–168. https://doi.org/10.1016/J.JACI.2005.10.003

Kodama, M., Asano, K., Oguma, T., Kagawa, S., Tomomatsu, K., Wakaki, M., Takihara, T., Ueda, S., Ohmori, N., Ogura, H., Miyata, J., Tanaka, K., Kamiishi, N., Fukunaga, K., Sayama, K., Ikeda, E., Miyasho, T., & Ishizaka, A. (2010). Strain-specific phenotypes of airway inflammation and bronchial hyperresponsiveness induced by epicutaneous allergen sensitization in BALB/c and C57BL/6 mice. *International Archives of Allergy and Immunology*, *152 Suppl 1*(SUPPL. 1), 67–74. https://doi.org/10.1159/000312128

Koelink, P. J., Wildenberg, M. E., Stitt, L. W., Feagan, B. G., Koldijk, M., van 't Wout, A. B., Atreya, R., Vieth, M., Brandse, J. F., Duijst, S., te Velde, A. A., D'Haens, G. R. A. M., Levesque, B. G., & van den Brink, G. R. (2018). Development of Reliable, Valid and Responsive Scoring Systems for Endoscopy and Histology in Animal Models for Inflammatory Bowel Disease. *Journal of Crohn's and Colitis*, *12*(7), 794–803. https://doi.org/10.1093/ecco-jcc/jjy035

Kovacevic, K. D., Gilbert, J. C., & Jilma, B. (2018). Pharmacokinetics, pharmacodynamics and safety of aptamers. In *Advanced Drug Delivery Reviews* (Vol. 134, pp. 36–50). Elsevier B.V. https://doi.org/10.1016/j.addr.2018.10.008

Kratschmer, C., & Levy, M. (2017). Effect of Chemical Modifications on Aptamer Stability in Serum. *Nucleic Acid Therapeutics*, *27*(6), 335–344. https://doi.org/10.1089/nat.2017.0680

Kühn, R., Löhler, J., Rennick, D., Rajewsky, K., & Müller, W. (1993). Interleukin-10-deficient mice develop chronic enterocolitis. *Cell*, *75*(2), 263–274. https://doi.org/10.1016/0092-8674(93)80068-P

Kulkarni, N., Pathak, M., & Lal, G. (2017). Role of chemokine receptors and intestinal epithelial cells in the mucosal inflammation and tolerance. *Journal of Leukocyte Biology*, *101*(2), 377–394. https://doi.org/10.1189/jlb.1ru0716-327r

Kusumoto, M., Xu, B., Shi, M., Matsuyama, T., Aoyama, K., & Takeuchi, T. (2007). Expression of chemokine receptor CCR4 and its ligands (CCL17 and CCL22) in murine contact hypersensitivity. *Journal of Interferon & Cytokine Research : The Official Journal of the International Society for Interferon and Cytokine Research*, *27*(11), 901–910. https://doi.org/10.1089/JIR.2006.0064

Lambolez, F., Kronenberg, M., & Cheroutre, H. (2007). Thymic differentiation of TCR alpha beta(+) CD8 alpha alpha(+) IELs. *Immunological Reviews*, *215*(1), 178–188. https://doi.org/10.1111/J.1600-065X.2006.00488.X

Langrish, C. L., Chen, Y., Blumenschein, W. M., Mattson, J., Basham, B., Sedgwick, J. D., McClanahan, T., Kastelein, R. A., & Cua, D. J. (2005). IL-23 drives a pathogenic T cell population that induces autoimmune inflammation. *The Journal of Experimental Medicine*, *201*(2), 233–240. https://doi.org/10.1084/JEM.20041257

Larsen, J. M., Bonefeld, C. M., Poulsen, S. S., Geisler, C., & Skov, L. (2009). IL-23 and T(H)17-mediated inflammation in human allergic contact dermatitis. *The Journal of Allergy and Clinical Immunology*, *123*(2). https://doi.org/10.1016/J.JACI.2008.09.036

Laukova, M., & Glatman Zaretsky, A. (2023). Regulatory T cells as a therapeutic approach for inflammatory bowel disease. *European Journal of Immunology*, *53*(2), 2250007. https://doi.org/10.1002/EJI.202250007

Lehtimäki, S., Tillander, S., Puustinen, A., Matikainen, S., Nyman, T., Fyhrquist, N., Savinko, T., Majuri, M. L., Wolff, H., Alenius, H., & Lauerma, A. (2010). Absence of CCR4 Exacerbates Skin Inflammation in an Oxazolone-Induced Contact Hypersensitivity Model. *Journal of Investigative Dermatology*, *130*(12), 2743–2751. https://doi.org/10.1038/JID.2010.208

Lenn, J. D., Neil, J., Donahue, C., Demock, K., Tibbetts, C. V., Cote-Sierra, J., Smith, S. H., Rubenstein, D., Therrien, J. P., Pendergrast, P. S., Killough, J., Brown, M. B., & Williams, A. C. (2018). RNA Aptamer Delivery through Intact Human Skin. *Journal of Investigative Dermatology*, *138*(2), 282–290. https://doi.org/10.1016/j.jid.2017.07.851

Leung, D. Y. M., Berdyshev, E., & Goleva, E. (2020). Cutaneous barrier dysfunction in allergic diseases. *Journal of Allergy and Clinical Immunology*, *145*(6), 1485–1497. https://doi.org/10.1016/J.JACI.2020.02.021

Lewis, J. M., Girardi, M., Roberts, S. J., Barbee, S. D., Hayday, A. C., & Tigelaar, R. E. (2006). Selection of the cutaneous intraepithelial gammadelta+ T cell repertoire by a thymic stromal determinant. *Nature Immunology*, *7*(8), 843–850. https://doi.org/10.1038/NI1363

Li, Y., Tipan, P. G., Selden, H. J., Srinivasan, J., Hale, L. P., & Ehrlich, L. I. (2023). CCR4 and CCR7 differentially regulate thymocyte localization with distinct outcomes for central tolerance. *ELife*, *12*, 80443. https://doi.org/10.7554/ELIFE.80443

Lieberam, I., & Förster, I. (1999). The murine I-chemokine TARC is expressed by subsets of dendritic cells and attracts primed CD4 + T cells. *Eur J Immunol .*, 2684–2694. https://doi.org/10.1002/(SICI)1521-4141(199909)29:09

Lim, H. D., Robert Lane, J., Canals, M., & Stone, M. J. (2021). Systematic Assessment of Chemokine Signaling at Chemokine Receptors CCR4, CCR7 and CCR10. *International Journal of Molecular Sciences*, *22*(8). https://doi.org/10.3390/IJMS22084232

Lin, R., Choi, Y. H., Zidar, D. A., & Walker, J. K. L. (2018). β-Arrestin-2-Dependent Signaling Promotes CCR4-mediated Chemotaxis of Murine T-Helper Type 2 Cells. *American Journal of Respiratory Cell and Molecular Biology*, *58*(6), 745–755. https://doi.org/10.1165/rcmb.2017-0240OC

Liu, F. T., Goodarzi, H., & Chen, H. Y. (2011). IgE, mast cells, and eosinophils in atopic dermatitis. *Clinical Reviews in Allergy & Immunology*, *41*(3), 298–310. https://doi.org/10.1007/S12016-011-8252-4

Liu, Y. J., Soumelis, V., Watanabe, N., Ito, T., Wang, Y. H., Malefyt, R. D. W., Omori, M., Zhou, B., & Ziegler, S. F. (2007). TSLP: an epithelial cell cytokine that regulates T cell differentiation by conditioning dendritic cell maturation. *Annual Review of Immunology*, *25*, 193–219. https://doi.org/10.1146/ANNUREV.IMMUNOL.25.022106.141718

Lloyd, C. M., Delaney, T., Nguyen, T., Tian, J., Martinez-A, C., Coyle, A. J., & Gutierrez-Ramos, J. C. (2000). CC chemokine receptor (CCR)3/eotaxin is followed by CCR4/monocyte-derived chemokine in mediating pulmonary T helper lymphocyte type 2 recruitment after serial antigen challenge in vivo. *The Journal of Experimental Medicine*, *191*(2), 265–273. https://doi.org/10.1084/JEM.191.2.265

Luciani, C., Hager, F. T., Cerovic, V., & Lelouard, H. (2022). Dendritic cell functions in the inductive and effector sites of intestinal immunity. *Mucosal Immunology*, *15*(1), 40–50. https://doi.org/10.1038/S41385-021-00448-W

Luckheeram, R. V., Zhou, R., Verma, A. D., & Xia, B. (2012). CD4+T Cells: Differentiation and Functions. *Clinical and Developmental Immunology*, *2012*, 12. https://doi.org/10.1155/2012/925135

Luda, K. M., Joeris, T., Persson, E. K., Rivollier, A., Demiri, M., Sitnik, K. M., Pool, L., Holm, J. B., Melo-Gonzalez, F., Richter, L., Lambrecht, B. N., Kristiansen, K., Travis, M. A., Svensson-Frej, M., Kotarsky, K., & Agace, W. W. (2016). IRF8 Transcription-Factor-Dependent Classical Dendritic Cells Are Essential for Intestinal T Cell Homeostasis. *Immunity*, *44*(4), 860–874. https://doi.org/10.1016/J.IMMUNI.2016.02.008

Luís, A., Martins, J. D., Silva, A., Ferreira, I., Cruz, M. T., & Neves, B. M. (2014). Oxidative stress-dependent activation of the eIF2α–ATFr unfolded protein response branch by skin sensitizer 1-fluoro-2,4-dinitrobenzene modulates dendritic-like cell maturation and inflammatory status in a biphasic manner. *Free Radical Biology and Medicine*, *77*, 217–229. https://doi.org/10.1016/J.FREERADBIOMED.2014.09.008

Luu, M., Steinhoff, U., & Visekruna, A. (2017). Functional heterogeneity of gut-resident regulatory T cells. *Clinical & Translational Immunology*, *6*(9), e156. https://doi.org/10.1038/CTI.2017.39

Ma, H., Tao, W., & Zhu, S. (2019). T lymphocytes in the intestinal mucosa: defense and tolerance. *Cellular & Molecular Immunology*. https://doi.org/10.1038/s41423-019-0208-2

MacLeod, A. S., & Havran, W. L. (2011). Functions of skin-resident γδ T cells. *Cellular and Molecular Life Sciences*, *68*(14), 2399–2408. https://doi.org/10.1007/S00018-011-0702-X/FIGURES/1

Mahmoud, N. N., Alhusban, A. A., Ali, J. I., Al-Bakri, A. G., Hamed, R., & Khalil, E. A. (2019). Preferential Accumulation of Phospholipid-PEG and Cholesterol-PEG Decorated Gold Nanorods into Human Skin Layers and Their Photothermal-Based Antibacterial Activity. *Scientific Reports 2019 9:1*, *9*(1), 1–15. https://doi.org/10.1038/s41598-019-42047-7

Maier, K. E., & Levy, M. (2016). From selection hits to clinical leads: progress in aptamer discovery. In *Molecular Therapy - Methods and Clinical Development* (Vol. 3, p. 16014). Elsevier Inc. https://doi.org/10.1038/mtm.2016.14

Malissen, B., Tamoutounour, S., & Henri, S. (2014). The origins and functions of dendritic cells and macrophages in the skin. *Nature Reviews Immunology 2014 14:6*, *14*(6), 417–428. https://doi.org/10.1038/nri3683

Malosse, C., & Henri, S. (2016). Isolation of mouse dendritic cell subsets and macrophages from the skin. *Methods in Molecular Biology*, *1423*, 129–137. https://doi.org/10.1007/978-1-4939-3606-9_9/COVER

Mariani, M., Lang, R., Binda, E., Panina-Bordignon, P., & D'Ambrosio, D. (2004). Dominance of CCL22 over CCL17 in induction of chemokine receptor CCR4 desensitization and internalization on human Th2 cells. *European Journal of Immunology*, *34*(1), 231–240. https://doi.org/10.1002/EJI.200324429

Martínez-Cingolani, C., Grandclaudon, M., Jeanmougin, M., Jouve, M., Zollinger, R., & Soumelis, V. (2014). Human blood BDCA-1 dendritic cells differentiate into Langerhans-like cells with thymic stromal lymphopoietin and TGF-β. *Blood*, *124*(15), 2411–2420. https://doi.org/10.1182/BLOOD-2014-04-568311

Marwa, K., & Kondamudi, N. P. (2023). Type IV Hypersensitivity Reaction. *StatPearls*. https://www.ncbi.nlm.nih.gov/books/NBK562228/

Mason, K. L., Huffnagle, G. B., Noverr, M. C., & Kao, J. Y. (2008). Overview of gut immunology. *Advances in Experimental Medicine and Biology*, *635*, 1–14. https://doi.org/10.1007/978-0-387-09550-9_1/COVER

Matsuo, K., Hatanaka, S., Kimura, Y., Hara, Y., Nishiwaki, K., Quan, Y. S., Kamiyama, F., Oiso, N., Kawada, A., Kabashima, K., & Nakayama, T. (2019). A CCR4 antagonist ameliorates atopic dermatitis-like skin lesions induced by dibutyl phthalate and a hydrogel patch containing ovalbumin. *Biomedicine and Pharmacotherapy*, *109*, 1437–1444. https://doi.org/10.1016/j.biopha.2018.10.194

Matsuo, K., Koizumi, K., Fujita, M., Morikawa, T., Jo, M., Shibahara, N., Saiki, I., Yoshie, O., & Nakayama, T. (2016). Efficient Use of a Crude Drug/Herb Library Reveals Ephedra Herb As a Specific Antagonist for TH2-Specific Chemokine Receptors CCR3, CCR4, and CCR8. *Frontiers in Cell and Developmental Biology*, *4*(JUN), 54. https://doi.org/10.3389/FCELL.2016.00054

Matsuo, K., Nagakubo, D., Komori, Y., Fujisato, S., Takeda, N., Kitamatsu, M., Nishiwaki, K., Quan, Y. S., Kamiyama, F., Oiso, N., Kawada, A., Yoshie, O., & Nakayama, T. (2018). CCR4 Is Critically Involved in Skin Allergic Inflammation of BALB/c Mice. *Journal of Investigative Dermatology*, *138*(8), 1764–1773. https://doi.org/10.1016/j.jid.2018.02.027

Mayer, G. (2009). The chemical biology of aptamers. *Angewandte Chemie - International Edition*, *48*(15), 2672–2689. https://doi.org/10.1002/ANIE.200804643

Mayne, C. G., & Williams, C. B. (2013). Induced and Natural Regulatory T Cells in the Development of Inflammatory Bowel Disease. *Inflammatory Bowel Diseases*, *19*(8), 1772. https://doi.org/10.1097/MIB.0B013E318281F5A3

McDonald, B. D., Dyer, E. C., & Rubin, D. T. (2022). IL-23 Monoclonal Antibodies for IBD: So Many, So Different? *Journal of Crohn's & Colitis*, *16*(Suppl 2), ii42. https://doi.org/10.1093/ECCO-JCC/JJAC038

Melgrati, S., Radice, E., Ameti, R., Hub, E., Thelen, S., Pelczar, P., Jarrossay, D., Rot, A., & Thelen, M. (2023). Atlas of the anatomical localization of atypical chemokine receptors in healthy mice. *PLoS Biology*, *21*(5). https://doi.org/10.1371/JOURNAL.PBIO.3002111

Metzger, R., Winter, L., Bouznad, N., Garzetti, D., von Armansperg, B., Rokavec, M., Lutz, K., Schäfer, Y., Krebs, S., Winheim, E., Friedrich, V., Matzek, D., Öllinger, R., Rad, R., Stecher, B., Hermeking, H., Brocker, T., & Krug, A. B. (2022). CCL17 Promotes Colitis-Associated Tumorigenesis Dependent on the Microbiota. *Journal of Immunology (Baltimore, Md. : 1950)*, *209*(11), 2227–2238. https://doi.org/10.4049/JIMMUNOL.2100867

Milling, S., Yrlid, U., Cerovic, V., & MacPherson, G. (2010). Subsets of migrating intestinal dendritic cells. *Immunological Reviews*, *234*(1), 259–267. https://doi.org/10.1111/J.0105-2896.2009.00866.X

Milne, P., Bigley, V., Gunawan, M., Haniffa, M., & Collin, M. (2015). CD1c+ blood dendritic cells have Langerhans cell potential. *Blood*, *125*(3), 470–473. https://doi.org/10.1182/BLOOD-2014-08-593582

Mizoguchi, A., Mizoguchi, E., & Bhan, A. K. (1999). The critical role of interleukin 4 but not interferon gamma in the pathogenesis of colitis in T-cell receptor alpha mutant mice. *Gastroenterology*, *116*(2), 320–326. https://doi.org/10.1016/S0016-5085(99)70128-9

Moed, H., Boorsma, D. M., Tensen, C. P., Flier, J., Jonker, M. J., Stoof, T. J., von Blomberg, B. M. E., Bruynzeel, D. P., Scheper, R. J., Rustemeyer, T., & Gibbs, S. (2004). Increased CCL27–CCR10 expression in allergic contact dermatitis: implications for local skin memory. *The Journal of Pathology*, *204*(1), 39–46. https://doi.org/10.1002/PATH.1619

Moreno, A., Pitoc, G. A., Ganson, N. J., Layzer, J. M., Hershfield, M. S., Tarantal, A. F., & Sullenger, B. A. (2019). Anti-PEG Antibodies Inhibit the Anticoagulant Activity of PEGylated Aptamers. *Cell Chemical Biology*, *26*(5), 634-644.e3. https://doi.org/10.1016/J.CHEMBIOL.2019.02.001

Mowat, A. M., & Agace, W. W. (2014). Regional specialization within the intestinal immune system. *Nature Reviews Immunology 2014 14:10*, *14*(10), 667–685. https://doi.org/10.1038/nri3738

Mraz, V., Geisler, C., & Bonefeld, C. M. (2020). Dendritic Epidermal T Cells in Allergic Contact Dermatitis. *Frontiers in Immunology*, *11*, 874. https://doi.org/10.3389/FIMMU.2020.00874

Mullard, A. (2023). FDA approves second RNA aptamer. *Nature Reviews Drug Discovery*. https://doi.org/10.1038/D41573-023-00148-Z

Murakami, R., Denda-Nagai, K., Hashimoto, S. ichi, Nagai, S., Hattori, M., & Irimura, T. (2013). A Unique Dermal Dendritic Cell Subset That Skews the Immune Response toward Th2. *PLOS ONE*, *8*(9), e73270. https://doi.org/10.1371/JOURNAL.PONE.0073270

Murata, A., & Hayashi, S. I. (2020). CD4+ Resident Memory T Cells Mediate Long-Term Local Skin Immune Memory of Contact Hypersensitivity in BALB/c Mice. *Frontiers in Immunology*, *11*, 523118. https://doi.org/10.3389/FIMMU.2020.00775/BIBTEX

Murphy, K., & Weaver, C. (2017). *Janeway's Immunobiology, 9th edition*. www.garlandscience.com,

Muzaki, A. R. B. M., Tetlak, P., Sheng, J., Loh, S. C., Setiagani, Y. A., Poidinger, M., Zolezzi, F., Karjalainen, K., & Ruedl, C. (2016). Intestinal CD103(+)CD11b(-) dendritic cells restrain colitis via IFN-γ-induced anti-inflammatory response in epithelial cells. *Mucosal Immunology*, *9*(2), 336–351. https://doi.org/10.1038/MI.2015.64

Nakamura, K., White, A. J., Parnell, S. M., Lane, P. J., Jenkinson, E. J., Jenkinson, W. E., & Anderson, G. (2013). Differential Requirement for CCR4 in the Maintenance but Not Establishment of the Invariant Vγ5+ Dendritic Epidermal T-Cell Pool. *PLoS ONE*, *8*(9). https://doi.org/10.1371/JOURNAL.PONE.0074019

Nakatani, T., Kaburagi, Y., Shimada, Y., Inaoki, M., Takehara, K., Mukaida, N., & Sato, S. (2001). CCR4+ memory CD4+ T lymphocytes are increased in peripheral blood and lesional skin from patients with atopic dermatitis. *Journal of Allergy and Clinical Immunology*, *107*(2), 353–358. https://doi.org/10.1067/mai.2001.112601

Natsuaki, M., Yamashita, N., & Sagami, S. (1993). Reactivity and persistence of local immunological memory on murine contact hypersensitivity. *The Journal of Dermatology*, *20*(3), 138–143. https://doi.org/10.1111/J.1346-8138.1993.TB03848.X

Nava, P., Koch, S., Laukoetter, M. G., Lee, W. Y., Kolegraff, K., Capaldo, C. T., Beeman, N., Addis, C., Gerner-Smidt, K., Neumaier, I., Skerra, A., Li, L., Parkos, C. A., & Nusrat, A. (2010). Interferon-gamma regulates intestinal epithelial homeostasis through converging beta-catenin signaling pathways. *Immunity*, *32*(3), 392–402. https://doi.org/10.1016/J.IMMUNI.2010.03.001

Nell, S., Suerbaum, S., & Josenhans, C. (2010). The impact of the microbiota on the pathogenesis of IBD: lessons from mouse infection models. *Nature Reviews Microbiology 2010 8:8*, *8*(8), 564–577. https://doi.org/10.1038/nrmicro2403

Nemeth, Z. H., Bogdanovski, D. A., Barratt-Stopper, P., Paglinco, S. R., Antonioli, L., & Rolandelli, R. H. (2017). Crohn's Disease and Ulcerative Colitis Show Unique Cytokine Profiles. *Cureus*, *9*(4). https://doi.org/10.7759/CUREUS.1177

Neurath, M. F. (2019). Targeting immune cell circuits and trafficking in inflammatory bowel disease. *Nature Immunology*, *20*(8), 970–979. https://doi.org/10.1038/S41590-019-0415-0

Neurath, M. F., & Chiriac, M. T. (2019). Targeting Immune Cell Wiring in Ulcerative Colitis. *Immunity*, *51*(5), 791–793. https://doi.org/10.1016/j.immuni.2019.10.011

Ng, E. W. M., Shima, D. T., Calias, P., Cunningham, E. T., Guyer, D. R., & Adamis, A. P. (2006). Pegaptanib, a targeted anti-VEGF aptamer for ocular vascular disease. *Nature Reviews. Drug Discovery*, *5*(2), 123–132. https://doi.org/10.1038/NRD1955

Ni, S., Yao, H., Wang, L., Lu, J., Jiang, F., Lu, A., & Zhang, G. (2017). Chemical Modifications of Nucleic Acid Aptamers for Therapeutic Purposes. *International Journal of Molecular Sciences*, *18*(8). https://doi.org/10.3390/IJMS18081683

Ni, S., Zhuo, Z., Pan, Y., Yu, Y., Li, F., Liu, J., Wang, L., Wu, X., Li, D., Wan, Y., Zhang, L., Yang, Z., Zhang, B. T., Lu, A., & Zhang, G. (2021). Recent Progress in Aptamer Discoveries and Modifications for Therapeutic Applications. *ACS Applied Materials and Interfaces*, *13*(8), 9500–9519. https://doi.org/10.1021/ACSAMI.0C05750/ASSET/IMAGES/LARGE/AM0C05750_0017.JPEG

Nielsen, M. M., Dyring-Andersen, B., Schmidt, J. D., Witherden, D., Lovato, P., Woetmann, A., Ødum, N., Poulsen, S. S., Havran, W. L., Geisler, C., & Bonefeld, C. M. (2015). NKG2D-dependent

activation of dendritic epidermal T cells in contact hypersensitivity. *Journal of Investigative Dermatology*, *135*(5), 1311–1319. https://doi.org/10.1038/jid.2015.23

Nielsen, M. M., Lovato, P., MacLeod, A. S., Witherden, D. A., Skov, L., Dyring-Andersen, B., Dabelsteen, S., Woetmann, A., Ødum, N., Havran, W. L., Geisler, C., & Bonefeld, C. M. (2014). IL-1β-dependent activation of dendritic epidermal T cells in contact hypersensitivity. *Journal of Immunology (Baltimore, Md. : 1950)*, *192*(7), 2975. https://doi.org/10.4049/JIMMUNOL.1301689

Nonnecke, E. B., Castillo, P. A., Akahoshi, D. T., Goley, S. M., Bevins, C. L., & Lönnerdal, B. (2022). Characterization of an intelectin-1 (Itln1) knockout mouse model. *Frontiers in Immunology*, *13*. https://doi.org/10.3389/FIMMU.2022.894649

O'Brien, R. L., & Born, W. K. (2015). Dermal γδ T Cells – What Have We Learned? *Cellular Immunology*, *296*(1), 62. https://doi.org/10.1016/J.CELLIMM.2015.01.011

Ogasawara, A., Yuki, T., Katagiri, A., Lai, Y. T., Takahashi, Y., Basketter, D., & Sakaguchi, H. (2022). Proteolytic activity accelerates the TH17/TH22 recall response to an epicutaneous protein allergen-induced TH2 response. *Https://Doi.Org/10.1080/1547691X.2022.2049665*, *19*(1), 27–33. https://doi.org/10.1080/1547691X.2022.2049665

Ogg, G. (2009). Role of T cells in the pathogenesis of atopic dermatitis. *Clinical and Experimental Allergy : Journal of the British Society for Allergy and Clinical Immunology*, *39*(3), 310–316. https://doi.org/10.1111/J.1365-2222.2008.03146.X

Ogura, M., Ishida, T., Inagaki, H., Yamamoto, K., Ueda, R., Hatake, K., Tobinai, K., Akinaga, S., Taniwaki, M., Ando, K., Fujimoto, K., Miyamoto, T., Uike, N., Tamura, K., Tanimoto, M., Tsukasaki, K., Tomonaga, M., Ishizawa, K., & Suzumiya, J. (2014). Multicenter phase II study of mogamulizumab (KW-0761), a defucosylated anti-cc chemokine receptor 4 antibody, in patients with relapsed peripheral T-cell lymphoma and cutaneous T-cell lymphoma. *Journal of Clinical Oncology : Official Journal of the American Society of Clinical Oncology*, *32*(11), 1157–1163. https://doi.org/10.1200/JCO.2013.52.0924

Ohl, L., Mohaupt, M., Czeloth, N., Hintzen, G., Kiafard, Z., Zwirner, J., Blankenstein, T., Henning, G., & Förster, R. (2004). CCR7 governs skin dendritic cell migration under inflammatory and steady-state conditions. *Immunity*, *21*(2), 279–288. https://doi.org/10.1016/J.IMMUNI.2004.06.014

Okayasu, I., Hatakeyama, S., Yamada, M., Ohkusa, T., Inagaki, Y., & Nakaya, R. (1990). A novel method in the induction of reliable experimental acute and chronic ulcerative colitis in mice. *Gastroenterology*, *98*(3), 694–702. https://doi.org/10.1016/0016-5085(90)90290-H

Onoue, A., Kabashima, K., Kobayashi, M., Mori, T., & Tokura, Y. (2009). Induction of eosinophil- and Th2-attracting epidermal chemokines and cutaneous late-phase reaction in tape-stripped skin. *Experimental Dermatology*, *18*(12), 1036–1043. https://doi.org/10.1111/J.1600-0625.2009.00899.X

Ovaere, P., Lippens, S., Vandenabeele, P., & Declercq, W. (2009). The emerging roles of serine protease cascades in the epidermis. *Trends in Biochemical Sciences*, *34*(9), 453–463. https://doi.org/10.1016/J.TIBS.2009.08.001

Pabst, O., Herbrand, H., Worbs, T., Friedrichsen, M., Yan, S., Hoffmann, M. W., Körner, H., Bernhardt, G., Pabst, R., & Förster, R. (2005). Cryptopatches and isolated lymphoid follicles: dynamic lymphoid tissues dispensable for the generation of intraepithelial lymphocytes. *European Journal of Immunology*, *35*(1), 98–107. https://doi.org/10.1002/EJI.200425432

Pabst, O., & Slack, E. (2020). IgA and the intestinal microbiota: the importance of being specific. *Mucosal Immunology*, *13*(1), 12. https://doi.org/10.1038/S41385-019-0227-4

Paller, A. S., Kong, H. H., Seed, P., Naik, S., Scharschmidt, T. C., Gallo, R. L., Luger, T., & Irvine, A. D. (2019). The microbiome in patients with atopic dermatitis. *The Journal of Allergy and Clinical Immunology*, *143*(1), 26–35. https://doi.org/10.1016/J.JACI.2018.11.015

Pasparakis, M., Haase, I., & Nestle, F. O. (2014). Mechanisms regulating skin immunity and inflammation. *Nature Reviews Immunology 2014 14:5*, *14*(5), 289–301. https://doi.org/10.1038/nri3646

Perše, M., & Cerar, A. (2012). Dextran sodium sulphate colitis mouse model: Traps and tricks. *Journal of Biomedicine and Biotechnology*, *2012*. https://doi.org/10.1155/2012/718617

Persson, E. K., Uronen-Hansson, H., Semmrich, M., Rivollier, A., Hägerbrand, K., Marsal, J., Gudjonsson, S., Håkansson, U., Reizis, B., Kotarsky, K., & Agace, W. W. (2013). IRF4 transcription-factor-dependent CD103(+)CD11b(+) dendritic cells drive mucosal T helper 17 cell differentiation. *Immunity*, *38*(5), 958–969. https://doi.org/10.1016/J.IMMUNI.2013.03.009

Poussier, P., Ning, T., Banerjee, D., & Julius, M. (2002). A unique subset of self-specific intraintestinal T cells maintains gut integrity. *The Journal of Experimental Medicine*, *195*(11), 1491–1497. https://doi.org/10.1084/JEM.20011793

Prausnitz, M. R., & Langer, R. (2008). Transdermal drug delivery. *Nature Biotechnology*, *26*(11), 1261. https://doi.org/10.1038/NBT.1504

Proksch, E. (2018). pH in nature, humans and skin. *The Journal of Dermatology*, *45*(9), 1044–1052. https://doi.org/10.1111/1346-8138.14489

Quoc, Q. L., Moon, J. Y., Lee, D. H., Ban, G. Y., Kim, S. H., & Park, H. S. (2022). Role of Thymus and Activation-Regulated Chemokine in Allergic Asthma. *Journal of Asthma and Allergy*, *15*, 157–167. https://doi.org/10.2147/JAA.S351720

Rapp, M., Grassmann, S., Chaloupka, M., Layritz, P., Kruger, S., Ormanns, S., Rataj, F., Janssen, K. P., Endres, S., Anz, D., & Kobold, S. (2016). C-C chemokine receptor type-4 transduction of T cells enhances interaction with dendritic cells, tumor infiltration and therapeutic efficacy of adoptive T cell transfer. *OncoImmunology*, *5*(3). https://doi.org/10.1080/2162402X.2015.1105428

Rapp, M., Wintergerst, M. W. M., Kunz, W. G., Vetter, V. K., Knott, M. M. L., Lisowski, D., Haubner, S., Moder, S., Thaler, R., Eiber, S., Meyer, B., Röhrle, N., Piseddu, I., Grassmann, S., Layritz, P., Kühnemuth, B., Stutte, S., Bourquin, C., von Andrian, U. H., … Anz, D. (2019). CCL22 controls immunity by promoting regulatory T cell communication with dendritic cells in lymph nodes. *The Journal of Experimental Medicine*, jem.20170277. https://doi.org/10.1084/jem.20170277

Reiss, Y., Proudfoot, A. E., Power, C. A., Campbell, J. J., & Butcher, E. C. (2001). CC chemokine receptor (CCR)4 and the CCR10 ligand cutaneous T cell-attracting chemokine (CTACK) in lymphocyte trafficking to inflamed skin. *The Journal of Experimental Medicine*, *194*(10), 1541–1547. https://doi.org/10.1084/JEM.194.10.1541

Reizis, B., Bunin, A., Ghosh, H. S., Lewis, K. L., & Sisirak, V. (2011). Plasmacytoid dendritic cells: recent progress and open questions. *Annual Review of Immunology*, *29*, 163–183. https://doi.org/10.1146/ANNUREV-IMMUNOL-031210-101345

Ribot, J. C., Lopes, N., & Silva-Santos, B. (2020). γδ T cells in tissue physiology and surveillance. *Nature Reviews Immunology 2020 21:4*, *21*(4), 221–232. https://doi.org/10.1038/s41577-020-00452-4

Rimoldi, M., Chieppa, M., Salucci, V., Avogadri, F., Sonzogni, A., Sampietro, G. M., Nespoli, A., Viale, G., Allavena, P., & Rescigno, M. (2005). Intestinal immune homeostasis is regulated by the crosstalk between epithelial cells and dendritic cells. *Nature Immunology 2005 6:5*, *6*(5), 507–514. https://doi.org/10.1038/ni1192

Röhrle, N., Knott, M., & Anz, D. (2020). CCL22 Signaling in the Tumor Environment. *Advances in Experimental Medicine and Biology*, *1231*, 79–96. https://doi.org/10.1007/978-3-030-36667-4_8

Roxo, C., Kotkowiak, W., & Pasternak, A. (2019). G-Quadruplex-Forming Aptamers—Characteristics, Applications, and Perspectives. *Molecules*, *24*(20). https://doi.org/10.3390/MOLECULES24203781

Safinia, N., Scotta, C., Vaikunthanathan, T., Lechler, R. I., & Lombardi, G. (2015). Regulatory T Cells: Serious Contenders in the Promise for Immunological Tolerance in Transplantation. *Frontiers in Immunology*, *6*(AUG). https://doi.org/10.3389/FIMMU.2015.00438

Sakuraba, A., Sato, T., Kamada, N., Kitazume, M., Sugita, A., & Hibi, T. (2009). Th1/Th17 immune response is induced by mesenteric lymph node dendritic cells in Crohn's disease. *Gastroenterology*, *137*(5), 1736–1745. https://doi.org/10.1053/J.GASTRO.2009.07.049

Sallam, M. A., Prakash, S., Kumbhojkar, N., Shields, C. W., & Mitragotri, S. (2021). Formulation-based approaches for dermal delivery of vaccines and therapeutic nucleic acids: Recent advances and future perspectives. *Bioengineering & Translational Medicine*, *6*(3). https://doi.org/10.1002/BTM2.10215

Santulli-Marotto, S., Boakye, K., Lacy, E., Wu, S.-J., Luongo, J., Kavalkovich, K., Coelho, A., Hogaboam, C. M., & Ryan, M. (2013). Engagement of two distinct binding domains on CCL17 is required for signaling through CCR4 and establishment of localized inflammatory conditions in the lung. *PloS One*, *8*(12), e81465. https://doi.org/10.1371/journal.pone.0081465

Santulli-Marotto, S., Wheeler, J., Lacy, E. R., Boakye, K., Luongo, J., Wu, S.-J., & Ryan, M. (2015). CCL22-specific Antibodies Reveal That Engagement of Two Distinct Binding Domains on CCL22 Is Required for CCR4-mediated Function. *Monoclonal Antibodies in Immunodiagnosis and Immunotherapy*, *34*(6), 373–380. https://doi.org/10.1089/mab.2015.0039

Sato, M., Matsuo, K., Susami, Y., Yamashita, A., Hayasaka, H., Hara, Y., Nishiwaki, K., Oiso, N., Kawada, A., Otsuka, A., & Nakayama, T. (2023). A CCR4 antagonist attenuates atopic dermatitis-like skin inflammation by inhibiting the recruitment and expansion of Th2 cells and Th17 cells. *International Immunology*. https://doi.org/10.1093/INTIMM/DXAD019

Savage, P. A., Klawon, D. E. J., & Miller, C. H. (2020). Regulatory T Cell Development. *Annual Review of Immunology*, *38*, 421–453. https://doi.org/10.1146/ANNUREV-IMMUNOL-100219-020937

Scheerens, H., Hessel, E., De Waal-Malefyt, R., Leach, M. W., & Rennick, D. (2001). Characterization of chemokines and chemokine receptors in two murine models of inflammatory bowel disease: IL-10-/- mice and Rag-2-/- mice reconstituted with CD4+CD45RBhigh T cells. *European Journal of Immunology*, *31*(5), 1465–1474. https://doi.org/10.1002/1521-4141(200105)31:5<1465::AID-IMMU1465>3.0.CO;2-E

Scheu, S., Ali, S., Ruland, C., Arolt, V., & Alferink, J. (2017). The C-C Chemokines CCL17 and CCL22 and Their Receptor CCR4 in CNS Autoimmunity. *International Journal of Molecular Sciences*, *18*(11). https://doi.org/10.3390/IJMS18112306

Schlitzer, A., McGovern, N., Teo, P., Zelante, T., Atarashi, K., Low, D., Ho, A. W. S., See, P., Shin, A., Wasan, P. S., Hoeffel, G., Malleret, B., Heiseke, A., Chew, S., Jardine, L., Purvis, H. A., Hilkens, C. M. U., Tam, J., Poidinger, M., … Ginhoux, F. (2013). IRF4 transcription factor-dependent CD11b+ dendritic cells in human and mouse control mucosal IL-17 cytokine responses. *Immunity*, *38*(5), 970–983. https://doi.org/10.1016/J.IMMUNI.2013.04.011

Schmidt, A., Oberle, N., & Krammer, P. H. (2012). Molecular Mechanisms of Treg-Mediated T Cell Suppression. *Frontiers in Immunology*, *3*(MAR). https://doi.org/10.3389/FIMMU.2012.00051

Schnabel, R. B., Baumert, J., Barbalic, M., Dupuis, J., Ellinor, P. T., Durda, P., Dehghan, A., Bis, J. C., Illig, T., Morrison, A. C., Jenny, N. S., Keaney, J. F., Gieger, C., Tilley, C., Yamamoto, J. F., Khuseyinova, N., Heiss, G., Doyle, M., Blankenberg, S., … Tracy, R. P. (2010). Duffy antigen receptor for chemokines (Darc) polymorphism regulates circulating concentrations of monocyte chemoattractant protein-1 and other inflammatory mediators. *Blood*, *115*(26), 5289–5299. https://doi.org/10.1182/BLOOD-2009-05-221382

Scott, C. L., Aumeunier, A. M., & Mowat, A. M. I. (2011). Intestinal CD103 + dendritic cells: Master regulators of tolerance? In *Trends in Immunology*. https://doi.org/10.1016/j.it.2011.06.003

Sebastiani, S., Albanesi, C., De Pità, O., Puddu, P., Cavani, A., & Girolomoni, G. (2002). The role of chemokines in allergic contact dermatitis. *Archives of Dermatological Research*, *293*(11), 552–559. https://doi.org/10.1007/S00403-001-0276-9

Sebastiani, S., Albanesi, C., Nasorri, F., Girolomoni, G., & Cavani, A. (2002). Nickel-specific CD4(+) and CD8(+) T cells display distinct migratory responses to chemokines produced during allergic contact dermatitis. *The Journal of Investigative Dermatology*, *118*(6), 1052–1058. https://doi.org/10.1046/J.1523-1747.2002.01771.X

Seo, S. U., Kuffa, P., Kitamoto, S., Nagao-Kitamoto, H., Rousseau, J., Kim, Y. G., Núñez, G., & Kamada, N. (2015). Intestinal macrophages arising from CCR2(+) monocytes control pathogen infection by activating innate lymphoid cells. *Nature Communications*, *6*. https://doi.org/10.1038/NCOMMS9010

Sewell, G. W., & Kaser, A. (2022). Interleukin-23 in the Pathogenesis of Inflammatory Bowel Disease and Implications for Therapeutic Intervention. *Journal of Crohn's & Colitis*, *16*(Suppl 2), ii3. https://doi.org/10.1093/ECCO-JCC/JJAC034

Shen, C., De Hertogh, G., Bullens, D. M. A., Van Assche, G., Geboes, K., Rutgeerts, P., & Ceuppens, J. L. (2007). Remission-inducing effect of anti-TNF monoclonal antibody in TNBS colitis: mechanisms beyond neutralization? *Inflammatory Bowel Diseases*, *13*(3), 308–316. https://doi.org/10.1002/IBD.20005

Shevach, E. M., & Thornton, A. M. (2014). tTregs, pTregs, and iTregs: Similarities and differences. *Immunological Reviews*, *259*(1), 88–102. https://doi.org/10.1111/imr.12160

Shimada, Y., Takehara, K., & Sato, S. (2004). Both Th2 and Th1 chemokines (TARC/CCL17, MDC/CCL22, and Mig/CXCL9) are elevated in sera from patients with atopic dermatitis. *Journal of Dermatological Science*, *34*(3), 201–208. https://doi.org/10.1016/j.jdermsci.2004.01.001

Shimura, S., Takai, T., Iida, H., Maruyama, N., Ochi, H., Kamijo, S., Nishioka, I., Hara, M., Matsuda, A., Saito, H., Nakae, S., Ogawa, H., Okumura, K., & Ikeda, S. (2016). Epicutaneous Allergic Sensitization by Cooperation between Allergen Protease Activity and Mechanical Skin Barrier Damage in Mice. *The Journal of Investigative Dermatology*, *136*(7), 1408–1417. https://doi.org/10.1016/J.JID.2016.02.810

Shin, H., Prasad, V., Lupancu, T., Malik, S., Achuthan, A., Biondo, M., Kingwell, B. A., Thiem, M., Gottschalk, M., Weighardt, H., Förster, I., Steiger, R. de, Hamilton, J. A., & Lee, K. M.-C. (2023). The GM-CSF/CCL17 pathway in obesity-associated osteoarthritic pain and disease in mice. *Osteoarthritis and Cartilage*, *0*(0). https://doi.org/10.1016/J.JOCA.2023.05.008

Shirley, M. (2017). Dupilumab: First Global Approval. *Drugs*, *77*(10), 1115–1121. https://doi.org/10.1007/S40265-017-0768-3/METRICS

Silverberg, J. I., Barbarot, S., Gadkari, A., Simpson, E. L., Weidinger, S., Mina-Osorio, P., Rossi, A. B., Brignoli, L., Saba, G., Guillemin, I., Fenton, M. C., Auziere, S., & Eckert, L. (2021). Atopic dermatitis in the pediatric population: A cross-sectional, international epidemiologic study. *Annals of Allergy, Asthma & Immunology : Official Publication of the American College of Allergy, Asthma, & Immunology*, *126*(4), 417-428.e2. https://doi.org/10.1016/J.ANAI.2020.12.020

Sølberg, J., Ulrich, N. H., Krustrup, D., Ahlström, M. G., Thyssen, J. P., Menné, T., Bonefeld, C. M., Gadsbøll, A. S. Ø., Balslev, E., & Johansen, J. D. (2019). Skin tape stripping: Which layers of the epidermis are removed? *Contact Dermatitis*, *80*(5), 319–321. https://doi.org/10.1111/COD.13199

Soumelis, V., Reche, P. A., Kanzler, H., Yuan, W., Edward, G., Homey, B., Gilliet, M., Ho, S., Antonenko, S., Lauerma, A., Smith, K., Gorman, D., Zurawski, S., Abrams, J., Menon, S., McClanahan, T., De Waal-Malefyt, R., Bazan, F., Kastelein, R. A., & Liu, Y. J. (2002). Human epithelial cells trigger dendritic cell–mediated allergic inflammation by producing TSLP. *Nature Immunology 2002 3:7*, *3*(7), 673–680. https://doi.org/10.1038/ni805

Spergel, J. M., Mizoguchi, E., Brewer, J. P., Martin, T. R., Bhan, A. K., & Geha, R. S. (1998). Epicutaneous sensitization with protein antigen induces localized allergic dermatitis and hyperresponsiveness to methacholine after single exposure to aerosolized antigen in mice. *Journal of Clinical Investigation*, *101*(8), 1614–1622. https://doi.org/10.1172/JCI1647

Spergel, J. M., Mizoguchi, E., Oettgen, H., Bhan, A. K., & Geha, R. S. (1999). Roles of TH1 and TH2 cytokines in a murine model of allergic dermatitis. *Journal of Clinical Investigation*, *103*(8), 1103. https://doi.org/10.1172/JCI5669

Stagg, A. J. (2018). Intestinal Dendritic Cells in Health and Gut Inflammation. In *Frontiers in immunology*. https://doi.org/10.3389/fimmu.2018.02883

Staples, K. J., Hinks, T. S. C., Ward, J. A., Gunn, V., Smith, C., & Djukanović, R. (2012). Phenotypic characterization of lung macrophages in asthmatic patients: Overexpression of CCL17. *Journal of Allergy and Clinical Immunology*, *130*(6), 1404-1412.e7. https://doi.org/10.1016/j.jaci.2012.07.023

Stillie, R. M., & Stadnyk, A. W. (2009). Role of TNF receptors, TNFR1 and TNFR2, in dextran sodium sulfate-induced colitis. *Inflammatory Bowel Diseases*, *15*(10), 1515–1525. https://doi.org/10.1002/IBD.20951

Stoltenburg, R., Reinemann, C., & Strehlitz, B. (2007). SELEX-A (r)evolutionary method to generate high-affinity nucleic acid ligands. In *Biomolecular Engineering* (Vol. 24, Issue 4, pp. 381–403). https://doi.org/10.1016/j.bioeng.2007.06.001

Strober, W., Fuss, I., & Mannon, P. (2007). The fundamental basis of inflammatory bowel disease. *The Journal of Clinical Investigation*, *117*(3), 514–521. https://doi.org/10.1172/JCI30587

Stutte, S., Quast, T., Gerbitzki, N., Savinko, T., Novak, N., Reifenberger, J., Homey, B., Kolanus, W., Alenius, H., & Förster, I. (2010). Requirement of CCL17 for CCR7- and CXCR4-dependent migration of cutaneous dendritic cells. *Proceedings of the National Academy of Sciences of the United States of America*, *107*(19), 8736–8741. https://doi.org/10.1073/PNAS.0906126107/SUPPL_FILE/SM04.MOV

Su, I. J., Balk, S. P., & Kadin, M. E. (1988). Molecular basis for the aberrant expression of T cell antigens in postthymic T cell malignancies. *The American Journal of Pathology*, *132*(2), 192. /pmc/articles/PMC1880737/?report=abstract

Sugita, K., & Akdis, C. A. (2020). Recent developments and advances in atopic dermatitis and food allergy. *Allergology International*, *69*(2), 204–214. https://doi.org/10.1016/J.ALIT.2019.08.013

Suzuki, Y., Saito, M., Ishii, T., Urakawa, I., Matsumoto, A., Masaki, A., Ito, A., Kusumoto, S., Suzuki, S., Hiura, M., Takahashi, T., Morita, A., Inagaki, H., Iida, S., & Ishida, T. (2019). Mogamulizumab Treatment Elicits Autoantibodies Attacking the Skin in Patients with Adult T-Cell Leukemia-Lymphoma. *Clinical Cancer Research : An Official Journal of the American Association for Cancer Research*, *25*(14), 4388–4399. https://doi.org/10.1158/1078-0432.CCR-18-2575

Tang, H. L., & Cyster, J. G. (1999). Chemokine Up-Regulation and Activated T Cell Attraction by Maturing Dendritic Cells. *Science*, *284*(5415), 819–822. https://doi.org/10.1126/SCIENCE.284.5415.819

Tay, S. S., Roediger, B., Tong, P. L., Tikoo, S., & Weninger, W. (2013). *The Skin-Resident Immune Network*. https://doi.org/10.1007/s13671-013-0063-9

Thelen, F., & Witherden, D. A. (2020). Get in Touch With Dendritic Epithelial T Cells! *Frontiers in Immunology*, *11*, 1656. https://doi.org/10.3389/FIMMU.2020.01656/BIBTEX

Thompson-Chagoyán, O. C., Maldonado, J., & Gil, A. (2005). Aetiology of inflammatory bowel disease (IBD): role of intestinal microbiota and gut-associated lymphoid tissue immune response. *Clinical Nutrition (Edinburgh, Scotland)*, *24*(3), 339–352. https://doi.org/10.1016/J.CLNU.2005.02.009

Thul, P. J., Akesson, L., Wiking, M., Mahdessian, D., Geladaki, A., Ait Blal, H., Alm, T., Asplund, A., Björk, L., Breckels, L. M., Bäckström, A., Danielsson, F., Fagerberg, L., Fall, J., Gatto, L., Gnann, C., Hober, S., Hjelmare, M., Johansson, F., … Lundberg, E. (2017). A subcellular map of the human proteome. *Science*, *356*(6340). https://doi.org/10.1126/SCIENCE.AAL3321/SUPPL_FILE/AAL3321_THUL_SM_TABLE_S9.XLSX

Trompette, A., Divanovic, S., Visintin, A., Blanchard, C., Hegde, R. S., Madan, R., Thorne, P. S., Wills-Karp, M., Gioannini, T. L., Weiss, J. P., & Karp, C. L. (2009). Allergenicity resulting from functional mimicry of a Toll-like receptor complex protein. *Nature*, *457*(7229), 585. https://doi.org/10.1038/NATURE07548

Tsunemi, Y., Saeki, H., Nakamura, K., Nagakubo, D., Nakayama, T., Yoshie, O., Kagami, S., Shimazu, K., Kadono, T., Sugaya, M., Komine, M., Matsushima, K., & Tamaki, K. (2006). CCL17 transgenic mice show an enhanced Th2-type response to both allergic and non-allergic stimuli. *European Journal of Immunology*, *36*(8), 2116–2127. https://doi.org/10.1002/EJI.200535564

Tuerk, C., & Gold, L. (1990). Systematic evolution of ligands by exponential enrichment: RNA ligands to bacteriophage T4 DNA polymerase. *Science (New York, N.Y.)*, *249*(4968), 505–510. https://doi.org/10.1126/SCIENCE.2200121

Uhlén, M., Fagerberg, L., Hallström, B. M., Lindskog, C., Oksvold, P., Mardinoglu, A., Sivertsson, Å., Kampf, C., Sjöstedt, E., Asplund, A., Olsson, I. M., Edlund, K., Lundberg, E., Navani, S., Szigyarto, C. A. K., Odeberg, J., Djureinovic, D., Takanen, J. O., Hober, S., … Pontén, F. (2015). Tissue-based map of the human proteome. *Science*, *347*(6220). https://doi.org/10.1126/SCIENCE.1260419/SUPPL_FILE/1260419_UHLEN.SM.PDF

Uhlen, M., Zhang, C., Lee, S., Sjöstedt, E., Fagerberg, L., Bidkhori, G., Benfeitas, R., Arif, M., Liu, Z., Edfors, F., Sanli, K., Von Feilitzen, K., Oksvold, P., Lundberg, E., Hober, S., Nilsson, P., Mattsson, J., Schwenk, J. M., Brunnström, H., … Ponten, F. (2017). A pathology atlas of the human cancer transcriptome. *Science*, *357*(6352). https://doi.org/10.1126/SCIENCE.AAN2507/SUPPL_FILE/SUPPLEMENTARY-TABLES.ZIP

Varol, C., Vallon-Eberhard, A., Elinav, E., Aychek, T., Shapira, Y., Luche, H., Fehling, H. J., Hardt, W. D., Shakhar, G., & Jung, S. (2009). Intestinal lamina propria dendritic cell subsets have different origin and functions. *Immunity*, *31*(3), 502–512. https://doi.org/10.1016/J.IMMUNI.2009.06.025

Vestergaard, C., Bang, K., Gesser, B., Yoneyama, H., Matsushima, K., & Larsen, C. G. (2000). A Th2 chemokine, TARC, produced by keratinocytes may recruit CLA+CCR4+ lymphocytes into lesional atopic dermatitis skin. *Journal of Investigative Dermatology*, *115*(4), 640–646. https://doi.org/10.1046/j.1523-1747.2000.00115.x

Vetrano, S., Borroni, E. M., Sarukhan, A., Savino, B., Bonecchi, R., Correale, C., Arena, V., Fantini, M., Roncalli, M., Malesci, A., Mantovani, A., Locati, M., & Danese, S. (2010). The lymphatic system controls intestinal inflammation and inflammation-associated Colon Cancer through the chemokine decoy receptor D6. *Gut*, *59*(2), 197–206. https://doi.org/10.1136/GUT.2009.183772

Viney, J. M., Andrew, D. P., Phillips, R. M., Meiser, A., Patel, P., Lennartz-Walker, M., Cousins, D. J., Barton, N. P., Hall, D. A., & Pease, J. E. (2014). Distinct conformations of the chemokine receptor CCR4 with implications for its targeting in allergy. *Journal of Immunology (Baltimore, Md. : 1950)*, *192*(7), 3419–3427. https://doi.org/10.4049/JIMMUNOL.1300232

Vocanson, M., Hennino, A., Chavagnac, C., Saint-Mezard, P., Dubois, B., Kaiserlian, D., & Nicolas, J.-F. (2005). Contribution of CD4+ and CD8+ T-cells in contact hypersensitivity and allergic contact dermatitis. *Expert Rev. Clin. Immunol.*, *1*(1), 75–86. https://doi.org/10.1586/1744666x.1.1.75

Wakugawa, M., Nakamura, K., Kakinuma, T., Onai, N., Matsushima, K., & Tamaki, K. (2001). CC chemokine receptor 4 expression on peripheral blood CD4+ T cells reflects disease activity of atopic dermatitis. *Journal of Investigative Dermatology*, *117*(2), 188–196. https://doi.org/10.1046/j.0022-202x.2001.01430.x

Wallace, K. L., Zheng, L. B., Kanazawa, Y., & Shih, D. Q. (2014). Immunopathology of inflammatory bowel disease. *World Journal of Gastroenterology : WJG*, *20*(1), 6. https://doi.org/10.3748/WJG.V20.I1.6

Wang, B., Fujisawa, H., Zhuang, L., Freed, I., Howell, B. G., Shahid, S., Shivji, G. M., Mak, T. W., & Sauder, D. N. (2000). CD4+ Th1 and CD8+ type 1 cytotoxic T cells both play a crucial role in the full development of contact hypersensitivity. *Journal of Immunology (Baltimore, Md. : 1950)*, *165*(12), 6783–6790. https://doi.org/10.4049/JIMMUNOL.165.12.6783

Wang, D., Li, Q., Yang, Y., Hao, S., Han, X., Song, J., Yin, Y., Li, X., Tanaka, M., & Qiu, C. H. (2017). Macrophage Subset Expressing CD169 in Peritoneal Cavity-Regulated Mucosal Inflammation Together with Lower Levels of CCL22. *Inflammation*, *40*(4), 1191–1203. https://doi.org/10.1007/S10753-017-0562-0

Wang, G., Savinko, T., Wolff, H., Dieu-Nosjean, M. C., Kemeny, L., Homey, B., Lauerma, A. I., & Alenius, H. (2007). Repeated epicutaneous exposures to ovalbumin progressively induce atopic dermatitis-like skin lesions in mice. *Clinical & Experimental Allergy*, *37*(1), 151–161. https://doi.org/10.1111/J.1365-2222.2006.02621.X

Wang, L., Ray, A., Jiang, X., Wang, J. Y., Basu, S., Liu, X., Qian, T., He, R., Dittel, B. N., & Chu, Y. (2015). T regulatory cells and B cells cooperate to form a regulatory loop that maintains gut homeostasis and suppresses dextran sulfate sodium-induced colitis. *Mucosal Immunology 2015 8:6*, *8*(6), 1297–1312. https://doi.org/10.1038/mi.2015.20

Wang, X., Fujita, M., Prado, R., Tousson, A., Hsu, H. C., Schottelius, A., Kelly, D. R., Yang, P. A., Wu, Q., Chen, J., Xu, H., Elmets, C. A., Mountz, J. D., & Edwards, C. K. (2010). Visualizing CD4 T-cell migration into inflamed skin and its inhibition by CCR4/CCR10 blockades using in vivo imaging model. *The British Journal of Dermatology*, *162*(3), 487–496. https://doi.org/10.1111/J.1365-2133.2009.09552.X

Watanabe, N., Kaminuma, O., Kitamura, N., & Hiroi, T. (2016). Induced Treg Cells Augment the Th17-Mediated Intestinal Inflammatory Response in a CTLA4-Dependent Manner. *PLOS ONE*, *11*(3), e0150244. https://doi.org/10.1371/JOURNAL.PONE.0150244

Weber, B., Saurer, L., Schenk, M., Dickgreber, N., & Mueller, C. (2011). CX3CR1 defines functionally distinct intestinal mononuclear phagocyte subsets which maintain their respective functions during homeostatic and inflammatory conditions. *European Journal of Immunology*, *41*(3), 773–779. https://doi.org/10.1002/EJI.201040965

Weber, C., Meiler, S., Döring, Y., Koch, M., Drechsler, M., Megens, R. T. A., Rowinska, Z., Bidzhekov, K., Fecher, C., Ribechini, E., Van Zandvoort, M. A. M. J., Binder, C. J., Jelinek, I., Hristov, M., Boon, L., Jung, S., Korn, T., Lutz, M. B., Förster, I., … Zernecke, A. (2011). CCL17-expressing dendritic cells drive atherosclerosis by restraining regulatory T cell homeostasis in mice. *The Journal of Clinical Investigation*, *121*. https://doi.org/10.1172/JCI44925

Whibley, N., Tucci, A., & Powrie, F. (2019). Regulatory T cell adaptation in the intestine and skin. *Nature Immunology*, *20*(4), 386–396. https://doi.org/10.1038/S41590-019-0351-Z

Whitehead, G. S., Walker, J. K. L., Berman, K. G., Foster, W. M., & Schwartz, D. A. (2003). Allergen-induced airway disease is mouse strain dependent. *American Journal of Physiology. Lung Cellular and Molecular Physiology*, *285*(1). https://doi.org/10.1152/AJPLUNG.00390.2002

Withers, D. R., Hepworth, M. R., Wang, X., Mackley, E. C., Halford, E. E., Dutton, E. E., Marriott, C. L., Brucklacher-Waldert, V., Veldhoen, M., Kelsen, J., Baldassano, R. N., & Sonnenberg, G. F. (2016). Transient inhibition of ROR-γt therapeutically limits intestinal inflammation by reducing TH17 cells and preserving group 3 innate lymphoid cells. *Nature Medicine*, *22*(3), 319–323. https://doi.org/10.1038/NM.4046

Wochner, A., Cech, B., Menger, M., Erdmann, V. A., & Glökler, J. (2007). Semi-automated selection of DNA aptamers using magnetic particle handling. *BioTechniques*, *43*(3), 344–353. https://doi.org/10.2144/000112532/ASSET/IMAGES/LARGE/TABLE3.JPEG

Worthington, J. J., Czajkowska, B. I., Melton, A. C., & Travis, M. A. (2011). Intestinal Dendritic Cells Specialize to Activate Transforming Growth Factor-β and Induce Foxp3+ Regulatory T Cells via Integrin αvβ8. *Gastroenterology*, *141*(5), 1802–1812. https://doi.org/10.1053/J.GASTRO.2011.06.057

Wu, C. C. N., Lee, J., Raz, E., Corr, M., & Carson, D. A. (2004). Necessity of oligonucleotide aggregation for toll-like receptor 9 activation. *Journal of Biological Chemistry*, *279*(32), 33071–33078. https://doi.org/10.1074/jbc.M311662200

Xiao, Y. T., Yan, W. H., Cao, Y., Yan, J. K., & Cai, W. (2016). Neutralization of IL-6 and TNF-α ameliorates intestinal permeability in DSS-induced colitis. *Cytokine*, *83*, 189–192. https://doi.org/10.1016/J.CYTO.2016.04.012

Yadav, M., Stephan, S., & Bluestone, J. A. (2013). Peripherally induced tregs - role in immune homeostasis and autoimmunity. *Frontiers in Immunology*, *4*(AUG). https://doi.org/10.3389/FIMMU.2013.00232

Yamashita, N., Natsuaki, M., & Sagami, S. (1989). Flare-up reaction on murine contact hypersensitivity. I. Description of an experimental model: rechallenge system. *Immunology*, *67*(3), 365. /pmc/articles/PMC1385354/?report=abstract

Yan, J. Bin, Luo, M. M., Chen, Z. Y., & He, B. H. (2020). The Function and Role of the Th17/Treg Cell Balance in Inflammatory Bowel Disease. *Journal of Immunology Research*, *2020*. https://doi.org/10.1155/2020/8813558

Yan, Y., Kolachala, V., Dalmasso, G., Nguyen, H., Laroui, H., Sitaraman, S. V., & Merlin, D. (2009). Temporal and Spatial Analysis of Clinical and Molecular Parameters in Dextran Sodium Sulfate Induced Colitis. *PLOS ONE*, *4*(6), e6073. https://doi.org/10.1371/JOURNAL.PONE.0006073

Yano, C., Saeki, H., Komine, M., Kagami, S., Tsunemi, Y., Ohtsuki, M., & Nakagawa, H. (2015). Mechanism of Macrophage-Derived Chemokine/CCL22 Production by HaCaT Keratinocytes. *Ann Dermatol*, *27*(2). https://doi.org/10.5021/ad.2015.27.2.152

Yonekura, K., Kanzaki, T., Gunshin, K., Kawakami, N., Takatsuka, Y., Nakano, N., Tokunaga, M., Kubota, A., Takeuchi, S., Kanekura, T., & Utsunomiya, A. (2014). Effect of anti-CCR4 monoclonal antibody (mogamulizumab) on adult T-cell leukemia-lymphoma: cutaneous adverse reactions may predict the prognosis. *The Journal of Dermatology*, *41*(3), 239–244. https://doi.org/10.1111/1346-8138.12419

Yoshie, O. (2021). CCR4 as a Therapeutic Target for Cancer Immunotherapy. *Cancers*, *13*(21). https://doi.org/10.3390/CANCERS13215542

Yuan, Q., Bromley, S. K., Means, T. K., Jones, K. J., Hayashi, F., Bhan, A. K., & Luster, A. D. (2007). CCR4-dependent regulatory T cell function in inflammatory bowel disease. *The Journal of Experimental Medicine*, *204*(6), 1327–1334. https://doi.org/10.1084/JEM.20062076

Yuan, X., Cheng, G., & Malek, T. R. (2014). The importance of regulatory T-cell heterogeneity in maintaining self-tolerance. *Immunological Reviews*, *259*(1), 103. https://doi.org/10.1111/IMR.12163

Yue, B. (2014). Biology of the Extracellular Matrix: An Overview. *Journal of Glaucoma*, *23*(8), S20. https://doi.org/10.1097/IJG.0000000000000108

Zemelka-Wiacek, M., Majewska-Szczepanik, M., Gajdanowicz, P., & Szczepanik, M. (2022). Contact Hypersensitivity as a Murine Model of Allergic Contact Dermatitis. *Journal of Visualized Experiments : JoVE*, *2022*(187). https://doi.org/10.3791/64329

Zhang, Y., Lai, B. S., & Juhas, M. (2019). Recent advances in aptamer discovery and applications. In *Molecules* (Vol. 24, Issue 5). MDPI AG. https://doi.org/10.3390/molecules24050941

Zhang, Z., Zheng, M., Bindas, J., Schwarzenberger, P., & Kolls, J. K. (2006). Critical role of IL-17 receptor signaling in acute TNBS-induced colitis. *Inflammatory Bowel Diseases*, *12*(5), 382–388. https://doi.org/10.1097/01.MIB.0000218764.06959.91

Zhao, M., Gönczi, L., Lakatos, P. L., & Burisch, J. (2021). The Burden of Inflammatory Bowel Disease in Europe in 2020. *Journal of Crohn's and Colitis*, *15*(9), 1573–1587. https://doi.org/10.1093/ECCO-JCC/JJAB029

Zlotnik, A., Yoshie, O., & Nomiyama, H. (2006). The chemokine and chemokine receptor superfamilies and their molecular evolution. *Genome Biology 2006 7:12*, *7*(12), 1–11. https://doi.org/10.1186/GB-2006-7-12-243

Zuker, M. (2003). Mfold web server for nucleic acid folding and hybridization prediction. *Nucleic Acids Research*, *31*(13), 3406–3415. https://doi.org/10.1093/NAR/GKG595

7. Acknowledgements

First of all, I want to thank my primary supervisor Prof. Irmgard Förster for offering to perform my thesis in her lab and for the mentorship through my PhD time. She does not only create an open tolerant environment in her group where scientific exchange and progress origins from curiosity and interest, but also always supported and inspired me as a hard-working, wise scientist and successful woman.

I want to thank PD Dr. Heike Weighardt for all her help and guidance. She was always available for practical and theoretical scientific advice, as well as organizational and general problems and often kept us scientifically and morally together.

I also want to thank my secondary supervisor Prof. Günter Mayer, for the great collaboration and his believe in and enthusiasm for our shared project. I hope more scientists take him and his attitude towards science as an example as it greatly inspired me.

Importantly, I am thankful to Anna Jonczyk for working on the CCL22 aptamer project with me. It was a pleasure sharing this project with Anna. In my opinion, she has one of the best scientific minds. Moreover, I know her as a kind, positive, joyful person that I am very thankful for meeting. Special thanks also to Bert.

Furthermore, I want to thank Prof. Waldemar Kolanus for being the chairperson in my doctoral committee and Prof. Anton Bovier for being the fourth committee member.

Certainly, I want to thank all the members of the Förster and Weighardt laboratory. I want to thank Manja, who was my dear lab partner and became such an important friend by living through the long and draining experiments, as well as sharing joy in between lab and non-lab time during the years. I could not have wished for a better PhD companion! Yasmin helped me with so many experiments and is not only kind, but a remarkable scientist. I value her opinion about science and life immensely. I want to thank Philip for his help with lab work, but even more I am thankful that he could overcome my “social aggressiveness” so that a dear friendship developed. With Irina (Iri Iri); I enjoyed the conversations about scandals and our future dream jobs greatly and am happy she looked behind my “never-ending positivity”. I am grateful to Ebby Eberhardt, the last member of the CCL17 club and someone with whom I could enjoy the little pleasures of life like good books or a nice summer day. Thanks to Michelle,

in whose presence one can only feel comfortable, Fred, who could many times relate best, because of similar past experiences in science and Laia who always brings entertainment to the office. A special thanks goes to the extended office crew member Lea Hänschke, who I connected with on the way to the PhD via sharing many stories and emotions as voice messages.

I want to thank past Förster members that participated in creating this kind atmosphere in the group.

Further, thanks to all my friends, with whom I shared so many experiences with along the way, that gave me energy and joy. I want to thank Domnica, for all the deep discussions, we shared over a coffee and who made me feel appreciated. Furthermore, the evenings with my Andoris Helena and Carsten and Max often became the best evenings of the week and let me wind down from work. Thank you all Domnica, Helena, Carsten, Marie, Vanessa, Kerstin, Lena & Valerie for listening, understanding, laughing or being angry together, cheering me up and just being by my side!

From the bottom of my heart, I want to thank Max! For picking me up from late-night experiments at the lab, reassuring me of my strengths, caring for me when I was feeling down, making me feel confident and reminding me of all the things I want and deserve in life. I hope I can give you back all the support and believe you put in me, so that you feel as valued as I do.

Last, but not least I want to thank me for pursuing the PhD until the end, for not giving up, for being honest, for believing in me and becoming more true to myself.